Dissecting the mechanisms of antiplasmodial resistance in *Plasmodium falciparum*

James Muriungi Murithi

Submitted in partial fulfillment of the
requirements for the degree of
Doctor of Philosophy
under the Executive Committee
of the Graduate School of Arts and Sciences

COLUMBIA UNIVERSITY

2021

Abstract

Dissecting the mechanisms of antiplasmodial resistance in *Plasmodium falciparum*

James Muriungi Murithi

The strides made in malaria eradication efforts have been aided by a combination of vector control and chemoprevention. However, *Plasmodium* resistance to first-line artemisinin-based combination therapies (ACTs), and mosquito resistance to insecticides threatens the progress made. Innovative vector control measures, vaccines and antimalarial drugs with novel modes of action are key to disease eradication.

High-throughput phenotypic screening of chemical libraries tested directly against all the stages of the *Plasmodium* lifecycle have been the mainstay of antimalarial drug discovery efforts and have identified compounds that are effective in parasite clearance. Unfortunately, these screens are handicapped in that they are unable to specify the actual compound targets in the *Plasmodium* parasites. As a result, many candidate hits have had to be re-screened in specific assays to determine putative mechanisms of antiplasmodial action. Predictably, this has elevated target-specific screens as the next frontier in drug discovery. This shift has been aided by a number of factors, including the cost effectiveness of these screens and the fact that target-specific screens do not always require specialized access to parasites. When combined with knowledge of the target's structure, where known, target-specific screens have the potential to give lead compounds with impeccable potency and selectivity. This approach has already been

successfully put to use, for example, in the identification of *P. falciparum* p-type ATPase 4 (PfATP4) and *P. falciparum* phosphatidylinositol 4-kinase (PfPI(4)K) inhibitors. The new challenge now is the identification of quality targets. Here, computational biology 'omics' tools have proved to be an invaluable resource. Two of the more commonly used of these tools are genomics and metabolomics.

In-vitro evolution assays followed by whole genome sequencing analysis is a popular genomics approach and helps unveil novel target genes. *Plasmodium* parasites are exposed to sublethal doses of a compound until an upward shift in the half-maximal inhibitory concentration (IC_{50}), indicative of resistant parasites, is observed in the culture. Sequenced genomes of the resistant parasite clones are compared to those of the drug-naive parent to reveal genetic changes, which include both single nucleotide polymorphisms (SNPs) and copy number variations (CNVs). While these genomic changes may point to genes encoding actual drug targets, they often reveal mediators of drug resistance or tolerance. Follow-up assays like SNP validation through gene editing are necessary to distinguish between actual targets, resistance mechanisms and random background mutations. Expectedly, genetic changes in uncharacterized *Plasmodium* genes are the bottle-necks in the identification of novel druggable targets. Even so, this genomics method has uncovered or reconfirmed novel antimalarial drug targets, including the proteasome, aminophospholipid-transporting P-type ATPase (PfAT-Pase2) and cGMP-dependent protein kinase (PfPKG).

Metabolomic profiling and transcriptomics narrows down a compound's mode of action. Here, parasites are treated with a compound of interest and the metabolites extracted and analyzed using liquid chromatography-mass spectrometry (LC-MS). The metabolomics fingerprint or metaprint is then compared to that of untreated parasites. While this method rarely provides the exact drug target, it narrows down the compound's mode of action, which is valuable for target validation and characterization. The issue of non-specific or non-viable phenotype metabolite signals is easily filtered out by treating parasites with various drug concentrations and/or over a period of time. Other areas that limit the effectiveness of this tool and need to be addressed include the analysis of compounds that do not act through metabolic pathway disruption and potential host contamination. Nonetheless, metabolomics are a key player in drug discovery and have successfully been used in the study of pantothenamides (MMV689258) where the observed CoA analog buildup helped identify their mechanism of action in sequestering coenzyme A to block acetyl-CoA anabolism.

Presented herein is a culmination of my graduate research in antimalarial drug discovery. Three independent projects are presented, and they all have either been published or are currently under reviewership. Chapter 1 is an introduction to malaria, a disease that has and continues to claim hundreds of thousands of lives, especially in my home continent of Africa. In chapter 2, I detail the experimental procedures used to generate the data presented in chapters 3-5. Chapter 3 is a detailed susceptibility profiling and metabolomic fingerprinting of *Plasmodium falciparum* asexual blood stages (ABS) to clinical and experimental antimalarials. This work, published in *Cell Chemical Biology (2020)*,

presents to the malaria research community a medium-throughput assay that can be utilized to identify new antimalarial lead compounds and novel assayable targets. Chapter 4 presents a detailed analysis of a novel ATP-binding cassette (ABC) transporter that confers pleiotropic antimalarial drug resistance in *P. falciparum* and that was first identified through *in vitro* evolution assays. This work is currently under review in *Cell Chemical Biology*. Chapter 5 presents work on an promising new preclinical compound, MMV688533, that provides single-dose cure and that was discovered using an innovative orthology-based screen by the Sanofi drug discovery team. In this chapter, I also present in detail the assays performed to better understand this compound's mode of antiplasmodial action and the potential drivers of parasite resistance. This work has been accepted, pending minor textual revisions, in *Science Translational Medicine*. Finally in chapter 6, I summarize chapters 3-5 and share future follow-up work needed to strengthen and contextualize some of the experimental findings presented here.

Table of Contents

List of Figures

List of Tables

Acronyms and Abbreviations

ABCI3: ATP-binding cassette transporter I family member 1

ACT: artemisinin-based combination therapy

ADME: absorption, distribution, metabolism and excretion

AMA1: apical membrane antigen 1

ART: artemisinin

AS: artesunate

AS-AQ: artesunate-amodiaquine

AS-MQ: artesunate-mefloquine

AS-PND: artesunate-pyronaridine

AS-SP: artesunate-sulfadoxine-pyrimethamine

AT: artemether

aTc: anhydrotetracycline

AT-LM: artemether-lumefantrine

ATQ: atovaquone

AQ: amodiaquine

Bip: binding immunoglobulin protein

βH: β-hematin

CETSA: cellular thermal shift assay

cKD: conditional knockdown

CNV: copy number variations

CRISPR: Clustered Regularly Interspaced Short Palindromic Repeats

cryo-EM: cryogenic electron microscopy

CSA: chondroitin sulfate A

CQ: chloroquine

CytBC1: cytochrome bc_1

DDT: dichlorodiphenyltrichloroethane

DHA: dihydroartemisinin

DHA-PPQ: dihydroartemisinin-piperaquine

DHFR: dihydrofolate reductase

DHPS: dihydropteroate synthetase

DV: digestive vacuole

EBL: erythrocyte binding-like protein

eGFP: enhanced Green Fluorescent Protein

ER: endoplasmic reticulum

ERD2: ER lumen protein retaining receptor

FQ: ferroquine

G6PD: glucose-6-phosphate dehydrogenase

gRNA: guide RNA

HA: human influenza hemagglutinin-based tag

Hb: Hemoglobin

Hz: hemozoin crystals

ICAM-1: intercellular adhesion molecule 1

K13: kelch 13 protein

LDH: lactate dehydrogenase

LM: lumefantrine

MalDA: Malaria Drug Accelerator consortium

MMV: Medicines for Malaria Venture

MQ: mefloquine

PDI: protein disulfide isomerase

PfATP4: *P. falciparum* p-type ATPase 4

PfCDPK5: *P. falciparum* plant-like calcium-dependent protein kinase

PfCRT: *P. falciparum* chloroquine resistance transporter

PD: pharmacodynamics

PfACG1: *P. falciparum* acylguanidine 1

PfEHD: *P. falciparum* Eps15 homology domain-containing protein

PfEMP1: *P. falciparum* erythrocyte membrane protein 1

PfHRP2: *P. falciparum* histidine-rich protein 2

PfMDR1: *P. falciparum* multidrug resistance transporter 1

PfPI3K: *P. falciparum* phosphatidylinositol-3-kinase

PfPI(4)K: *P. falciparum* phosphatidylinosi-tol 4-kinase

PfPKG: *P. falciparum* cGMP-dependent protein kinase

PfRhs: *P. falciparum* reticulocyte-binding protein homologs

PK: pharmacokinetics

PMT: phosphoethanolamine N-methyltransferase

PND: pyronaridine

PPQ: piperaquine

PRR: parasite reduction rate

QN: quinine

RDTs: rapid diagnostic tests

RBC: red blood cell

ROS: reactive oxygen species

SAR: structure-activity relationship

SMILES: simplified molecular input line entry system

SNP: single nucleotide polymorphism

SP: sulfadoxine-pyrimethamine

TLR9: Toll-like receptor 9

TNF: tumor necrosis factor

Acknowledgements

I have taken efforts in this endeavor. However, it would not have been possible without the kind support and help of many individuals. I would like to extend my sincere thanks to all of them.

I'll start by thanking my advisor, Dr. David Fidock, whose drive to excel and commitment to his group has been most inspiring. Thank you David for giving me a spot in your lab, for your incredible work ethic that ensures we have all the resources necessary to run our ever-expensive experiments, and for never allowing us to settle. Lastly, thank you for leaving your door open just in case we have questions.

I would also like to express my gratitude to my thesis committee members, Dr. Jonathan Dworkin, Dr. Max Gottesman and Dr. Steven Spitalnik, who have been with me from the very beginning of this long journey. Thank you for your guidance, encouragement and patience. A special thanks to Dr. Chi-Min Ho (Mimi) who graciously agreed to join the team for this last stretch in fulfilment to Integrated Program's thesis defense committee requirements.

I am eternally grateful to the Integrated Program in Cellular, Molecular, and Biomedical Studies, first for accepting me to the program in 2015 and for their continued support since. Thank you to the current co-directors Dr. Ronald (Ron) Liem and Dr. Donna Farber and Ron's former co-director Dr. Lori Sussel for taking a chance on me. It is my sincerest hope that I have made the Program proud. Finally, a big thank you to Zaia Sivo, Integrated' senior program manager. Thank you Zaia for running this ship, for always

putting the student needs first and for the selflessness and grace with which you run your duties. Above all, thank you for your friendship!

I would also like to extend my gratitude to members of the Bill and Melinda Gate's funded Malaria Drug Accelerator (MalDA) consortium, which I've been privileged to be a part of throughout my PhD program. I will always treasure the camaraderie and collaborations with this diverse and driven group of people who are all on a mission to defeat a killer disease, malaria. Special thanks to Dr. Jacquin Niles and Dr. Charisse Pasaje at MIT, who have been outstanding collaborators.

It would be very remiss of me not to thank the big, diverse and functionally dysfunctional Fidock Lab family. To all members, past and present, you made my time here most memorable. It's fair to say that I did not have the smoothest of sails, but your eternal encouragement and support saw me through the worst of times and for that I'll forever be indebted to you. A special thanks to Dr. Manu Vanaerschot and Josefine Striepen whose love and selflessness I'll never be able to repay, and to Mariko Kanai, Ioanna Deni and Dr. Nina Gnadig who always found ways to lift my spirits. Thank you guys for your friendship. Unfortunately for you, I promise to never let go!

Lastly, many thanks to my family. Thank you mom and dad for sacrificing everything to give my siblings and I a shot at a different and hopefully better life. To my siblings, thank you for all the sacrifices you made, the pain you had to bear, and the shots you had to take just so I didn't have to. Anything good in me or that will ever come from me is thanks to your love, kindness and support. For fairness sake, whatever mess I make is your fault as well!

Dedication

To mum and dad,
for everything you gave and lost to get us educated.

Chapter 1. Introduction

1.1. Malaria – overview

1.1.1. History

Malaria is estimated to have claimed between 150 million and 300 million lives, thereby accounting for 2 to 5 percent of all deaths in the 20th century alone [1]. The significant progress made in treatment and prevention efforts has saved countless more lives and has reduced the number of deaths from well over a million per year in the early 2000s to just over 400,000 currently. Still, with the rise and spread of insecticide and antimalarial resistance, and with around half of the global population still living in areas where malaria is transmitted, these gains can be easily lost [2]. By virtue of climate, ecology and poverty, sub-Saharan Africa accounted for over 94% of the world's 229 million malaria cases and 409,000 deaths in 2019.

The history of this killer disease dates back to ancient times and is a testament to malaria's long reign. The deadly periodic fevers described in clay tablets with cuneiform script from Mesopotamia are suggestive of malaria and recently, malaria antigen has been detected in Egyptian remains dating from 3200 and 1304 BC [3]. However, there is perhaps not a better testament to this disease's ancient hold on society than the evidence of the strong selection pressure its exerted on the evolution of the human genome [4,5]. Some hemoglobin-encoding alleles that in homozygous genotypes cause severe blood disorders like thalassemia and sickle cell disease should make these diseases rare as affected individuals are unlikely to survive and reproduce. Yet these alleles have been positively selected in populations living in malaria-endemic areas because heterozygous

genotypes confer strong protection against malaria [6-8]. Indeed, up to 38% of the population in some parts of Africa carry a single copy of the hemoglobin S gene that is associated with sickle cell disease [9].

Genetic polymorphisms that affect red blood cell proteins or cause enzyme deficiencies have also been shown to confer protection against severe disease. For example, genetic inheritance of mutations in a gene that encodes the red blood cell Duffy antigen, a key receptor mediating invasion of the most widespread malaria-causing *Plasmodium* species, *Plasmodium vivax*, is credited with reducing its spread in Africa, although findings of *P. vivax* infections in Duffy antigen-negative individuals complicate these interpretations [10-12]. The deficiency of glucose-6-phosphate dehydrogenase (G6PD) in hemizygous males also provides protection against severe malaria, albeit through an unknown mechanism. Unfortunately, this deficiency also limits the use of primaquine, the only antimalarial currently approved for the treatment of latent (liver-stage) *P. vivax* malaria as it leads to hemolytic anemia in these patients [4,5,13].

Some proposed mechanisms of malaria protection conferred by these varied genetic disorders include: increased phagocytosis and elimination of the infected mutant erythrocytes by the spleen, which reduces parasitemia; reduced parasite invasion of mutant red blood cells; reduced intracellular growth rates; and reduced cytoadherence of infected mutant red blood cells [7]. These mechanisms, in combination or isolation, increase protection against severe malaria, which is the main driver of the aforementioned human evolution over what must have been a long period of time.

1.1.2. Discovery of the malaria parasite

Plasmodium, the single-celled protozoan that cause malaria, was discovered in 1880 by Charles Louis Alphonse Laveran (1845-1922), a French army doctor who while serving in Algeria observed through a microscope crescent-shaped bodies with a small dot of pigment (hemozoin) in the blood of a febrile soldier. Through his extensive examination of another ~200 patients, Laveran recorded both asexual (schizont and trophozoite) and sexual (female and male gametocyte) stages in human blood [14]. Laveran was awarded the Nobel Prize in 1907 in recognition for this work.

1.1.3. Discovery of malaria's mosquito stages

Malaria parasite mosquito stages were discovered by Surgeon-Major Ronald Ross (1857-1932) of the British Indian Medical Service in 1897 when he observed a clear, circular body containing hemozoin in a dapple-winged *Anopheles* mosquito that had previously fed on an infected patient [15]. Using the avian parasite *P. relictum*, Ross observed that *Plasmodium* sporozoites matured in salivary glands leading directly to the proboscis of a mosquito that had previously fed on infected birds [16]. Ross' work was in part guided by his collaboration with his mentor, Sir Patrick Manson, who in 1877 had demonstrated that the filarial worms responsible for lymphatic filariasis were transmitted by mosquitoes [17]. Later, a group of Italian malariologists (Giovanni Battista Grassi, Amico Bignami, Giuseppe Bastianelli, Angelo Celli, Camillo Golgi and Ettore Marchiafava) conclusively demonstrated that the human malaria parasites passed through the same developmental stages in the mosquito as the avian parasites observed by Ross [17]. Like Laveran, Ross was also awarded a Nobel Prize in 1902 for his work on malaria.

1.1.4. Discovery of malaria parasite in human tissue

The question of where sporozoites inoculated by mosquitoes undergo early development in the human host was not solved until 1948 when Henry Shortt, Cyril Garnham and colleagues at the Ross Institute of the London School of Hygiene and Tropical Medicine showed that a phase of division in the liver preceded the development of parasites in the blood [18]. Using the primate malaria species, *P. cynomolgi*, Shortt and Garnham infected rhesus monkeys and were able to detect malaria parasites in their livers a week later [19]. Shortly afterwards Shortt, Garnham and their co-workers found exoerythrocytic forms of *P. vivax* in human volunteers and subsequently in volunteers infected with *P. falciparum* in 1949 and *P. ovale* in 1954 [20-22].

1.2. Epidemiology: Malaria vector, the parasite and the disease

1.2.1. Malaria vector

There are about 40 species of the mosquito genus *Anopheles* that exclusively transmit human malaria parasites [23]. Although malaria-competent *Anopheles* spp. are abundantly distributed all over the globe, their malaria transmission efficacy differs considerably and is highly dependent on the species of the vector. *Anopheles gambiae*, for example, is the dominant and most efficient vector in sub-Saharan Africa [23].

Mosquitoes, just like the *Plasmodium* parasites, have been notoriously hard to eradicate. While the large-scale insecticide campaigns that used dichlorodiphenyltrichloroethane (DDT) for malaria vector control during the first WHO Global Malaria Eradication Program (1955–1969) were effective, their use had to be stopped in part because mosquitoes

started developing resistance to the insecticide. Since then, more selective vector control approaches, including the use of insecticide-treated bed nets and indoor residual spraying, have had their share of success in malaria elimination but mosquito resistance to insecticides continues to be a growing concern. This is best exemplified by the fact that 73 of 82 malaria endemic countries have detected resistance to at least one of the four insecticide classes in use since 2010 [2].

1.2.2. The parasite

Plasmodium spp. are single-celled eukaryotic organisms that belong to the phylum *Apicomplexa*, fittingly named for the apical complex that is involved in host cell invasion [24-26]. There are five human-infective *Plasmodium* spp.; *P. falciparum*, *P. vivax*, *P. malariae*, *P. ovale* and *P. knowlesi*. Of these, *P. falciparum* causes the bulk of malaria-associated morbidity and mortality, especially in sub-Saharan Africa. Outside of this region, *P. vivax* is now often the predominant cause of severe malaria and is found in both tropical and temperate areas including Southeast Asia, Ethiopia and South America [27]. *P. ovale* exists as two sympatric species *P.o. curtisi* and *P.o. wallikeri* and is especially prevalent in West Africa [28]. *P. malariae* can be found worldwide but is also especially prevalent in West Africa and causes the mildest infections. *P. knowlesi* was initially considered as a parasite of non-human primates but is now known to cause malaria in humans [29,30].

1.2.3. The disease

An estimated 229 million cases of malaria occurred in 2019 and sub-Saharan Africa bore the brunt of the burden with 94% of the cases [2]. Other affected regions like South-East Asia, Eastern Mediterranean region and Western Pacific and the Americas recorded 3%, 2% and <1% of the cases, respectively [2]. Children <5 years of age and fetuses of infected pregnant women experience the most morbidity and mortality in areas of continuous malaria transmission. Children >6 months of age are particularly susceptible because they have lost their maternal antibodies but have yet to develop their own protective immunity. Adults and children >5 years of age who live in regions of continuous *P. falciparum* transmission develop a partial protective immunity owing to repeated exposure to the parasite. It is therefore unsurprising that of the total 409,000 malaria deaths recorded in 2019, 67% were of children <5 years old [2]. Expectant women are more susceptible to *Plasmodium* spp. infection because the placenta itself selects for the emergence of parasites that express receptors that recognize the placental vasculature; these receptors are antigens to which pregnant women have not yet become partially immune [31]. This vulnerability not only increases the risk of miscarriage but parasitemia in the placenta can have adverse effects on the fetus as well [32-34]. For disease manifestations and diagnosis please refer to **section 1.5.1.**

Although an estimated 1.5 billion malaria cases and 7.6 million malaria deaths have been averted in the period 2000-2019, the rate of malaria case incidence has stalled since 2015 [2]. This plateauing can be attributed to the emergence of insecticide-resistant mosquitoes,

lack of access to effective medicines and difficulties with achieving higher levels of mosquito control [35].

1.3. *Plasmodium* life cycle

1.3.1. Liver stage

Fewer than 100 *Plasmodium* sporozoites are injected into the dermis during a blood meal by the female *Anopheles* mosquito and can take up to 3 h to exit [36,37]. About 70% of these sporozoites reach and penetrate a blood vessel to enter the blood-stream by gliding motility [38]. While the mechanisms of sporozoite exit from the dermis are not clearly understood, mutant sporozoites lacking Trap-like protein display normal gliding motility but cannot enter the circulation, suggesting an essential role played by this protein in sporozoite entry into the circulating system [37]. The sporozoites that manage to enter the blood stream quickly (within 2 minutes in mice experiments [39]) access the liver through cell traversal. Here, they cross the sinusoidal barrier by forming a transient vacuole (parasitophorous vacuole) using key proteins like the circumsporozoite which bind the sporozoites to liver heparan sulphate proteoglycans [40]. DNA replication begins on day 2 post liver invasion and the parasites remain within the parasitophorous vacuole membrane through late liver stage development, a process that takes up to 10 days. This development culminates in the release of up to 30,000 merozoites per intracellular parasite into the bloodstream through budding of parasite-filled vesicles called merosomes [41,42]. Some parasite species, such as *P. vivax* and *P. ovale*, can also enter a period of latency by forming a non-replicating hypnozoite instead of a schizont. These hypnozoites not only enable long-term survival of the parasite but can also lead to

relapses [43]. Sporozoite multiplication in the liver is not associated with pathology but presents a very appealing target stage for vaccine and prophylaxis because there would be no pathology or disease if the infection was blocked at this stage.

1.3.2. Asexual blood stage

About 10^5-10^6 *Plasmodium* parasites gain entry into the red blood cell through specific ligand-receptor interactions mediated by proteins on the surface of the parasite that interact with receptors on the host erythrocyte or reticulocyte [10,41]. *P. falciparum* can invade and replicate in erythrocytes and reticulocytes but *P. vivax* and other species predominantly invade reticulocytes, which are less abundant [44]. Merozoite red blood cell invasion is a fast and dynamic process and occurs within minutes [45]. The initial interaction between the merozoites and the erythrocytes results in parasite actomyosin motor-driven deformation of the host cell [45]. Little is understood about the molecular details of this period but the merozoite surface protein 1 is a major, albeit non-essential, glycophosphatidyl-inositol-associated protein on the merozoite surface that forms a platform for proteins that bind erythrocytes [46-48]. Some of these proteins, like the erythrocyte binding-like proteins (EBLs) and *P. falciparum* reticulocyte-binding protein homologs (PfRhs), bind specific receptors, like glycophorin A, B and C, on the red blood cell and lay the groundwork for critical signaling activation of subsequent invasion steps leading to, among others, the deformation of the erythrocyte [49]. Active invasion is preceded by the binding of the PfRhs proteins to the essential host receptor basigin, which causes the merozoites to reorientate so that their apical end touches the erythrocyte membrane [50]. An irreversible attachment of merozoites to erythrocytes is then initiated

through the formation of a tight junction between parasite-derived proteins, primarily the apical membrane antigen 1 (AMA1) and the rhoptry neck protein RON complex [51]. Lipid-rich rhoptry contents form the parasitophorous vacuole membrane as the merozoite is propelled into the erythrocyte using force generated by the parasite actomyosin motor [52]. Fusion of membranes at the posterior end of the merozoite to seal the parasite within the parasitophorous vacuole and erythrocyte concludes the active invasion phase [37]. This is then followed by echinocytosis, a process that causes the erythrocyte to shrink and form spiky protrusions, presumably because of the Ca^{2+} influx into the host cell resulting from the PfRhs-basigin complex [45]. The parasites, now inside the red blood cell, export hundreds of proteins into the host cell cytoplasm and cell surface. These modulate the acquisition of nutrients, cell adhesion and sequestration in tissues and pathogenesis [37,53,54]. 48 h after the establishment of erythrocyte infection, multiple rounds of cell division (schizogony) produces as many as 32 merozoites per parasite that egress when fully developed. These are released to access new host cells for invasion by exploding from the host erythrocytes. Merozoite egress is a tightly regulated process involving multiple protein kinases, including the plant-like calcium-dependent protein kinase PfCDPK5 and the cGMP-dependent protein kinase (PfPKG) [55-57].

During symptomatic disease the parasites may replicate exponentially up to 10^{12} parasites per patient [41]. This rapid growth requires sustained pools of amino acids, which the parasites, being auxotrophic for all of the amino acids they need, acquire from hemoglobin (Hb) digestion in the digestive vacuole (DV). This process supplies all amino acids except isoleucine, which is obtained from other host cell components [58]. Nutrient

uptake by the parasite is coupled to the detrimental accumulation of Na^+; however, the parasite expresses an essential plasma membrane Na^+ export pump (the cation ATPase *P. falciparum* p-type ATPase 4 (PfATP4)) that can maintain Na^+ homeostasis [54,59,60]. The remodeling of the plasma membrane to generate daughter merozoites in the late schizont stage requires *P. falciparum* phosphatidylinositol 4-kinase (PfPI(4)K) [61].

1.3.3. Gametocyte development and mosquito stages

During schizogony, a proportion of parasites undergo a developmental switch initiating commitment to sexual development to form male and female gametocytes. The molecular events around this switch are still unclear but the timing of transition occurs at some point in the previous schizogony cycle where daughter merozoites from a single schizont-infected cell are committed to develop into either gametocytes or asexual schizonts [37]. Environmental stimuli, such as high parasitemia (starvation) and exposure to drugs, are associated with increased conversion to gametocyte production. Epigenetic regulation is critical for control of sexual differentiation, and the transcription factor AP2-G has been shown to be a master regulator of gametocytogenesis [62]. While the earliest phases of gametocyte development are morphologically indistinguishable from asexual development, *P. falciparum* gametocytes undergo five morphologically discernible stages over the course of 9-12 days [63]. Stage I gametocytes are morphologically indistinguishable from asexual trophozoites. In stage II, the parasite develops a pointed end. In stage III, one end of the parasite gets elongated while the other flattens and curves so that the parasite resembles the letter ‘D’. In stage IV, the parasite elongates some and resembles the shape of a banana with pointed ends. Stage V gametocytes exhibit a

characteristic crescent shape with rounded ends [64]. Only mature stage V gametocyte stages are present in the blood circulation. All the other stages avoid splenic clearance by sequestering in host tissues, particularly the bone marrow, and emerge into the peripheral circulation only after maturation and for an unknown time until uptake by a feeding mosquito [65]. Because *Plasmodium* parasite transmission from humans to mosquitoes is an essential part of their developmental process, it provides a great intervention point for vaccines or transmission-blocking antimalarials.

Ingestion of gametocytes by a mosquito during a blood meal activates the formation of gametes (gametogenesis) in the mosquito midgut lumen. This is thought to be initiated by several factors, including the drop of temperature by ~5 °C, the presence of the mosquito-derived molecule xanthurenic acid and the increase of extracellular pH from 7.2 to about 8 [66-68]. Each male gametocyte undergo three rounds of mitotic division, forming eight haploid microgametes. These exflagellate and fuse with the female macrogametes, each of which is developed from a single female gametocyte, to form a diploid zygote. Multiple rounds of DNA replication and meiosis follow and result in the formation of a tetraploid ookinete. Through cell traversal, ookinetes cross the midgut epithelium to form oocysts that are lodged under the basal lamina. Finally, oocysts go through multiple rounds of cell division and generate thousands of haploid sporozoites which upon maturation migrate to the mosquito salivary glands and when injected into a new host during the mosquito's next blood meal re-initiate the developmental cycle [69,70].

1.4. *Plasmodium* biology: Asexual blood-stage parasite genomics and hemoglobin catabolism

1.4.1. Genome

The *P. falciparum* genome was sequenced in 2002 and revealed a 23.3 megabase nuclear genome partitioned among 14 chromosomes [25,71]. About 5700 open reading frames have been identified to date. Interestingly, nearly 60% of these lack homologues in other organisms in spite of being conserved in other *Plasmodium* species [71,72]. The nuclear genome is also notoriously AT-rich; >80% throughout the genome and up to 93% in the introns and intergenic regions [71].

Transcriptomic analyses of the asexual and the sexual stages revealed that functionally related genes were transcribed at the same stage of the asexual lifecycle and a subset of genes were specifically expressed in the sexual stages, suggesting a mechanism of coordinated gene regulation and “just-in-time” transcription [73-78]. However, because the nuclear genome is so AT-rich, 5′-untranslated regions of many genes have not yet been accurately defined. It is therefore no wonder that mechanisms of transcriptional regulation in *Plasmodium* are not well understood. Nonetheless, this reduced complexity of the noncoding sequences contains large numbers of poly As and Ts that generate an abundance of variable microsatellite loci that have been explored as genetic markers [79,80]. Besides the nuclear genome, *P. falciparum* also contains a small mitochondrial genome of ~6 kilobases containing three protein-coding genes [81,82] and a significantly larger circular apicoplast genome of ~35 kilobases containing 68 genes [83,84].

But for mitochondria and apicoplast genomes that might be polycistronic [73,74], *P. falciparum* chromosomal gene transcription is thought to be predominantly monocistronic and stage-specific [85]. That said, bicistronic transcription for merozoite apical erythrocyte-binding ligand has been reported [86]. There is no evidence for transposable elements in any *Plasmodium* species genome [87]. In addition, *P. falciparum* genome also lacks non-homologous end joining DNA double-strand break machinery. Nucleotide excision and homologous recombination repair pathways are largely intact however and make gene-editing experiments possible, so long as a template is provided [88].

1.4.2. Hemoglobin catabolism and hemozoin production

Hb degradation in intraerythrocytic malaria parasites is an intense process that occurs in the acidic environment of the DV. The process starts with the invagination of the parasitophorous membrane to form Hb-containing vesicles known as cytostomes that then fuse with the DV membrane and release their cargo therein [89]. In the lumen of the DV, which is acidified by proton pumps on the membrane to a pH ~5.5, Hb is broken down first to oligopeptides and further into dipeptides and amino acids by various aspartic proteases and cysteine proteinases [90,91]. Hb digestion is most active at the late ring and trophozoite stages [92].

In DV's acidic environment, heme iron, which is a major waste product of Hb digestion, is readily oxidized from its Fe^{2+} (ferrous) form to the Fe^{3+} (ferric) form, generating reactive oxygen species (ROS), which, if not detoxified, can cause widespread damage to DNA, lipids, proteins and other biomolecules. *Plasmodium* parasites deal with this toxic waste

by converting it into an insoluble and chemically inert hemozoin crystals, the malaria pigment [93]. While much still remains to be known about the exact mechanism of heme detoxification, histidine-rich proteins 2 and 3 and neutral lipids have been implicated in hemozoin formation [94-96]. An essential heme detoxification protein has also been identified in *Plasmodium* that has been shown to enhance heme-to-hemozoin transformation [97]. Although most of the heme, ~95%, ends in hemozoin crystals, some of it leaves the DV and is degraded by glutathione in the parasite cytosol [98]. Altogether, the parasite digests about 70% of the host cell cytosol but only 16% of the derived amino acids are used for protein synthesis [99,100]. The major purpose of Hb digestion, as determined by model stimulations, is to reduce the colloid-osmotic pressure within the host erythrocyte that is essential to preserve the osmotic stability of the infected cell during the parasite's asexual life cycle [101-103].

1.5. Malarial disease

1.5.1. Clinical presentation and diagnosis

Fever and parasite presence are two key aspects considered by WHO for disease pathology [104]. Parasites can be detected using light microscopic examination of a blood smear or by a rapid diagnostic test. The patient's risk of exposure, including their travel history or if they live in an endemic region can also assist in making the diagnosis. The symptoms of malaria are diverse but belong to one of these four groups: Asymptomatic malaria, uncomplicated malaria, severe (complicated) malaria and placental malaria. As the name suggests, patients with asymptomatic malaria have circulating parasites but lack clinical presentation of an infection. For uncomplicated malaria, the symptoms

include fever, moderate-to-severe shaking chills, profuse sweating, headache, nausea, vomiting, diarrhea and anemia. Both asymptomatic and uncomplicated malaria can be caused by any of the *Plasmodium* spp. Severe or complicated malaria is usually caused by *P. falciparum*, although recently there's been increased observation of cases associated with the other species [105]. Complications include severe anemia and end-organ damage, including coma from cerebral malaria, pulmonary complications like oedema and hyperpnea, and hypoglycemia or acute kidney injury. Severe malaria is often associated with high parasitemias and is associated with increased mortality [104]. In placental malaria, parasites are present in the placenta and this more often than not leads to poor outcomes for the fetus and possibly for the mother as was mentioned earlier.

Patient immune systems are responsible for maintaining malaria parasites at equilibrium levels in asymptomatic carriers, many of who are children and adults in hyperendemic areas. Even so, parasitemia in these carriers can be extremely high, up to 50,000 parasites per μl in one study of asymptomatic pregnant women [106]. Besides the risks associated with malaria infections, asymptomatic individuals are a reservoir for infecting mosquitoes, which leads to continued transmission. Parasitemias in patients with uncomplicated malaria typically range anywhere from 1,000-50,000 parasites per μl of blood although non-immune adults and young children with parasite numbers <1,000 have been known to present with symptoms [107]. Higher parasite numbers are associated with severe malaria but this varies with region. As an example, parasitemias averaged ~4,000 parasites per μl in South America, ~10,000 parasites per μl in Asia and ~20,000 parasites per μl in Africa in pooled analysis of patient data from 61 studies designed to

measure the efficacy of ACTs [107]. The complications of severe malaria are mostly caused by the blocking of blood vessels by infected red blood cells and the severity and symptoms depend on what organ is affected and to what extent. These complications also differ by age. While lung and kidney disease are unusual in children for example, they are quite common in non-immune adults [104].

The limit of parasite detection by thick-smear microscopy is about 50 per μl [108]. WHO-validated rapid diagnostic tests (RDTs) that are based on the immunological detection of parasite antigens like lactate dehydrogenase (LDH) or histidine-rich protein 2 (*pfhrp2*) in the blood can detect 50-1,000 parasites per μl with high specificity but they still lack the sensitivity of PCR-based methods [109]. Data from controlled human infection models where parasite reproduction was monitored by quantitative PCR showed that parasitemias can increase 10-20-fold over a 48-h cycle period, highlighting the importance of detecting low levels of parasitemia in predicting clinical relapses [110].

In clinical studies, parasitemias of asymptomatic carriers can be monitored using PCR-based methods, which detect as few as 22 parasites per μl [111]. More advanced technologies are currently being pursued to detect low-level parasitemia in low-resource settings. An example of this is the development of Loop-mediated isothermal amplification technology, which is a type of PCR that is fast (109-fold amplification in 1 h) and does not require thermal cycling [112,113]. RDTs, which have similar sensitivities to light microscopy examination have the added advantage that they do not require extensive training of the user and that they provide rapid diagnosis at the point-of-care level in resource-limited

settings and have consequently greatly improved malaria control. Unfortunately, false-negative test results, reportedly caused by *pfhrp2* gene deletions in *P. falciparum* strains in South America have been reported [114,115]. This is dangerous because such results could lead to the wrong perception that antimalarial medicines are ineffective, which might misleadingly influence policy. In addition, there's evidence indicating that LDH-targeting RDTs are less sensitive for *P. vivax* than for *P. falciparum* [116]. This is further complicated by the limited information on the sensitivity of these tests for the rarer *P. ovale*, *P. malariae* and *P. Knowlesi*.

1.5.2. Pathogenesis and immunity

Malaria's predominant pathogenic mechanism is the hemolysis of infected red blood cells, which releases both the parasites and malaria endotoxin, a complex of hemozoin and parasite DNA, into the bloodstream. This combination triggers the Toll-like receptor 9 (TLR9), a nucleotide-sensing receptor involved in the host immune response against pathogens, which leads to high levels of tumor necrosis factor (TNF) production and to clinical symptoms such as fever [117-120]. Additionally, membranes of infected red blood cells stiffen, lose their deformability and obstruct capillaries, which is life-threatening in severe malaria cases when vital organs are affected [121].

Disease severity and pathogenesis are linked to surface proteins expressed by the parasite. In *P. falciparum*, the erythrocyte membrane protein 1 (PfEMP1), a major surface antigen encoded by the vast *var* gene family, is involved in cytoadherence and mediates the binding of infected erythrocytes to the endothelial vasculature [31,122-124]. Some of the

well-studied PfEMP1 host ligands include the ubiquitous CD36 that is associated with mild infections, intercellular adhesion molecule 1 (ICAM-1) that is associated with cerebral malaria and chondroitin sulfate A (CSA) that allows parasite adhesion to the epithelial surface of the placenta [125,126]. Disease severity is also predicted by high parasitemia levels and more often than not these correlate with poor outcomes [31,127]. Predictably, circulating levels of *P. falciparum* histidine-rich protein 2 are used as a biomarker of parasitemia to predict the risks for microvascular obstruction and severe disease [128]. *P. vivax* does not express the same family of *var* genes associated with endothelium binding and tissue sequestration. Additionally, *P. vivax* only invades reticulocytes, which are fewer than erythrocytes. The two factors may be the cause of decreased disease severity and lower parasite levels in *P. vivax*-infected patients [31].

Malaria parasites first encounter the host immune system when sporozoites, ~15 per mosquito bite in one study, are injected into the skin [129]. At this stage, the parasites might encounter and be vulnerable to antibodies against *Plasmodium* surface proteins, which might be the first line of the host's acquired immune response against them [130,131]. Consequently, chances of transmission are increased when the host is bitten by mosquitoes carrying larger number of sporozoites, although the diameter of the proximal duct limits the number of sporozoites that can be simultaneously injected into the host [132]. How sporozoites evade all other effectors of the immune system to reach the liver is not well understood. However, sporozoite invasion of hepatocytes is believed to be in part due to their ability to suppress the function of Kupffer cells, the resident macrophages of the liver, and repress the expression of genes that encode MHC class I molecules, which

are molecules that sample peptides generated within the cell and signal the cell's physiological state to the T lymphocytes and natural killer cells [133].

Parasite burden and risk of complicated malaria is dependent on levels of protective immunity acquired by the human host [134-136]. This immunity is thought to result from circulating IgG antibodies against surface proteins on sporozoites and merozoites, which in turn helps block hepatocyte invasion and red blood cell invasion, respectively [134]. In high-transmission areas, adults develop partially protective immunity from repeated infections and young infants (<6 months of age) are also afforded some protection from maternal antibodies [135]. Children between 6 months and 5 years of age have the lowest levels of protective immunity and are therefore the most susceptible to developing life-threatening complications from high parasitemias [137]. In low transmission areas or areas that have seasonal malaria, individuals develop lower levels of protective immunity and typically have worse symptomatic malaria upon infection [136].

The correlation between protective immunity and malaria severity poses a challenge for successful malaria treatment programs because the decrease in the number of infections and transmission rates is coupled with increasing numbers of individuals who lose their protective immunity and become susceptible to severe disease. Given that malaria has been re-introduced in areas that had been malaria-free for many years, this calls for continued well-organized surveillance.

1.5.3. Prophylaxis and treatment

1.5.3.1. Vector control measures

While eradication of mosquitoes is no longer considered an option to eliminate malaria, the use of long-lasting insecticide-treated bed nets and indoor residual spraying are estimated to be responsible for two-thirds of the malaria cases averted in Africa between 2000 and 2015 [138]. More sophisticated fine-mazed, sturdy, long-lasting and wash-proof insecticide-treated bed nets are in use today but their efficacy is threatened by inappropriate use and factors like behavioral changes in mosquitoes, which have increasingly begun biting during the day [139,140]. An even worse problem is the increasing emergence of vector resistance to insecticides, which makes it imperative that new insecticides with different modes of action be developed [140]. Until that happens, technology advances in the deployment of indoor spraying chemicals, including timed release to coincide with seasonal transmission and slow-release polymer-based wall linings will need to play a bigger role in vector control [141-143].

CRISPR-Cas9 gene editing technology has fueled a number of genetic approaches to vector control and offer an exciting area of development for novel insect control strategies. Mosquito population suppression and population alteration are two of the more well-known of these initiatives. In the former, mosquitoes are modified so that the progeny are sterile while in the latter mosquitoes are modified so that the progeny are refractory to *Plasmodium* spp. infection [144]. The initial population suppression approaches that involved releasing sterile male insects have been further improved so male insects now carry a dominant lethal gene that kills their progeny [145-147]. Gene drive systems, which

can be used for both suppression and alteration initiatives using homing endonucleases, are being re-engineered to recognize mosquito genes and will rapidly increase the frequency of desirable traits in a mosquito population [148,149]. Feasibility studies are currently ongoing to determine efficacy [150,151].

The findings that *Aedes aegypti* mosquitoes (vector for Dengue, yellow fever and Zika viruses) infected with bacteria of the *Wolbachia* spp. cannot transmit the Dengue virus to human hosts has inspired new approaches to malaria vector control as well [152]. As a result, symbiont *Wolbachia* spp. that can be modified to make them deleterious to other parasites in *Anopheles* spp. mosquitoes have now been identified [153,154].

While all these approaches are very promising, they are still at very early stages of development. As more progress is made in these technologies, the focus will inevitably shift to environmental uncertainties associated with their widespread distribution and no doubt, there will be complex policy and regulatory requirements that will need to be addressed and overcome.

1.5.3.2. Chemoprotection and chemoprevention

Daily atovaquone-proguanil and daily doxycycline are the WHO-recommended chemoprotection medicines (i.e. medication given at prophylactic doses to temporarily protect individuals entering high endemicity regions) [155].

Chemoprevention is the use of medicines with demonstrated efficacy regularly to large populations at full treatment doses. The major upside to doing this is that some of the individuals treated will inevitably be asymptomatic carriers, who are key to transmission. These campaigns, generally targeting children <5 years of age who are the most vulnerable group have had significant success. An example is the Sahel region where there are seasonal rains and a recurrent threat of malaria. Seasonal malaria chemoprevention with a combination of sulfadoxine-pyrimethamine plus amodiaquine resulted in >80% reduction in the number of malaria cases among children and a >50% reduction in mortality [156-161]. While operationally complex given the required monthly treatments, it is estimated that >20 million children have been protected between 2015 and 2016, at a cost of ~US$1 per treatment. Still, some concern remains about the long-term success of these campaigns. Disease rebound is always a threat and can be caused by among others, interruption by economic difficulties or social unrest and the development of drug resistance.

The issue of drug resistance is especially relevant and has indeed led to a different approach for the rest of sub-Saharan Africa where seasonal chemoprevention trials are monthly 3-day courses of ACTs [160,162]. As an example, dihydroartemisinin (DHA)-piperaquine has been highly efficacious in preventing malaria in high-risk groups [163]. WHO proposes that drugs used for chemoprevention differ from the front-line treatment in use in the same country or region where possible to reduce the potential for the emergence of drug resistance [2]. This highlights the need for the development of multiple, new and diverse antiplasmodial compounds to provide a wider range of options.

1.5.3.3. Vaccines

Natural protective immunity to malaria is lost within 3-5 years in the absence of sustained exposure to malaria, presumably due to clearance of circulating antibodies and the failure of memory B cells to develop into long-lived plasma B cells [164]. That notwithstanding, the fact that adults living in high-transmission areas acquire partial protective immunity indicates that vaccination is a possibility. Unsurprisingly, parasite proteins targeted by natural immunity, like the circumsporozoite protein on sporozoites, proteins expressed by merozoites, and parasite antigens exposed on the surface of infected red blood cells, have been studied for their potential to be used in vaccine programs [165,166]. Unfortunately, this surface protein targeted approach, coupled with the species specificity of experimental malaria vaccines not only restricts their use but also provides room for the emergence of resistance. Still, controlled human infection models have continued to provide more precise understanding of the early cytokine and T cell responses in naive subjects [167-169]. This will inevitably provide a better understanding of the role of regulatory T cells in dampening the response against the parasite, which results in the exhaustion of T cells [170].

The most advanced vaccine candidate is RTS,S, developed by GlaxoSmithKline and the Program for Appropriate Technology in Health Malaria Vaccine Initiative. This vaccine contains a recombinant protein with parts of the *P. falciparum* circumsporozoite protein combined with the hepatitis B virus surface antigen and a proprietary adjuvant and aims to trigger the immune system to defend against the first stages of malaria infection by preventing sporozoite invasion of the liver [171]. RTS,S showed an efficacy of 40% in

children who received four vaccine doses over a 4-year period but that fell to 26% when only three vaccine doses were administered [172]. Furthermore, RTS,S vaccine failed to provide long-term protection. At the request of WHO, more studies are currently underway in different African countries. The other promising vaccine candidate is the whole sporozoite PfSPZ Vaccine made by Sanaria. As the name suggests, this vaccine uses irradiated, and therefore non-infectious, sexual forms of the parasites extracted from mosquito salivary glands [173,174]. In a phase I clinical trial, the efficacy of PfSPZ was highly dependent on prior parasite exposure, with naïve individuals being the most protected [175]. These findings highlight the importance of more extensive clinical testing of both vaccine candidates. While promising, they also show the challenge that lays ahead in developing a highly efficacious vaccine.

Nonetheless, the success of malaria vaccines should not be measured in efficacy terms alone as even with only partial and short-term efficacy they could still be used in the fight against malaria in a more targeted approach. An example would be using vaccines as additional protective measures for the most at risk individuals like pregnant women. Another would be to combined them with chemoprevention to interrupt malaria transmission in low-endemic areas [176]. In the latter case, vaccines that are unable to prevent *Plasmodium* spp. infection could be repurposed to prevent transmission. That said, successful vaccines will inevitably have to include multiple antigens from different stages of the *Plasmodium* life cycle as well as address not only the nature of the immune response in humans but more specifically the factors that lead to diminished T cell responses.

1.5.3.4. Treatment

The choice of antimalarial drugs used for treatment is heavily influenced by the frequencies of drug resistance, with little consideration going into examining the specific differences between the five *Plasmodium* spp. Chloroquine (CQ), with its low cost and excellent safety, is used in most cases of non-*P. falciparum* malaria, where it remains effective, whereas *P. falciparum* malaria requires newer ACT medicines that overcome resistance issues [177]. The persistence of *P. vivax* and *P. ovale* hypnozoites, even after clearance of the stages that cause symptoms, necessitates the use of primaquine, and recently tafenoquine [2].

The mainstay treatments for uncomplicated *P. falciparum* malaria are ACTs, which are fixed-dose combinations of an artemisinin derivative and a quinine derivative [2]. Because it is highly lipophilic, artemisinin itself is not the molecule of choice [178]. Instead, semi synthetic derivatives, namely, DHA (the active metabolite of many artemisinin derivatives), artesunate (AS, a succinate prodrug of DHA that is highly water-soluble) or artemether (AT, a methylether prodrug of DHA) are used in ACTs. The combination partners of choice are 4-aminoquinolines like amodiaquine (AQ), piperaquine (PPQ) and pyronaridine (PND) or amino-alcohols like mefloquine (MQ) and lumefantrine (LM). Currently approved ACTs for clinical use include artemether-lumefantrine (AT-LM), artesunate-amodiaquine (AS-AQ), DHA-piperaquine (DHA-PPQ), artesunate-mefloquine (AS-MQ), artesunate-sulfadoxine-pyrimethamine (AS-SP) and artesunate-pyronaridine (AS-PND) [41]. These combinations have proven extremely effective, are well-tolerated

and are affordable. Importantly, they are stable in tropical climate conditions thanks to effective formulations and packaging [179].

CQ or ACTs are WHO-recommended treatments for uncomplicated *P. vivax* malaria [2]. Although other ACTs are active against *P. vivax*, only AS-PND is approved for the treatment of blood-stage *P. vivax* malaria. Relapses of *P. vivax* malaria are caused by dormant hypnozoites in the liver and present a problem in malaria control. Primaquine is the only clinical antimalarial drug targeting hypnozoites. Tafenoquine, a next-generation 8-aminoquinoline currently completing phase III clinical studies is predicted to have similar levels of efficacy as primaquine at a single dose [180]. As with patients receiving primaquine, patients receiving tafenoquine also require an assessment of their G6PD enzyme activity to ensure safety.

1.6. Antimalarial drugs

1.6.1. Antimalarial drug development and resistance

Along with vector control, chemotherapy has played a big role in the fight against malaria. However, the ability of *Plasmodium* spp. to develop resistance to these treatments has continuously compromised the efficacy of clinical antimalarial compounds. This has in turn necessitated their use as combinations therapies, a nonstop race to develop new compounds and a quest to identify novel parasite targets. This section will mainly focus on common clinical antimalarials in use today, briefly touch on those used in the past and highlight some promising new candidates at various points of development.

1.6.2. Artemisinin and its derivatives

Artemisinin (ART) was first isolated in 1971 by Tu Youyou (winner of the joint Nobel Prize in Physiology or Medicine in 2015) from Chinese sweet worm-wood (*Artemisia annua*) [181,182]. ACTs, which consist of fast-acting semisynthetic derivatives of the endoperoxide ART partnered with slower-acting but longer-lasting drugs, are the current WHO-recommended first-line treatments of uncomplicated malaria [2,183]. ART derivatives, namely AT, AS or DHA, have improved pharmacological properties and when used against ART-sensitive parasites can reduce the parasite biomass by up to 10,000-fold every 48 h thereby providing exceptionally rapid clearance rates [184]. ART semisynthetic derivatives AT and AS are prodrugs which are transformed to the active metabolite DHA. Regrettably, ART derivatives are rapidly metabolized and have half-lives in the range of 1-2 h. As such, they cannot eliminate infections without the added contribution of longer-lasting, albeit slower-acting, partner drugs, which are responsible for eliminating surviving parasites [185].

The exact mode of drug action for ARTs is debated but the most accepted theory is compound activation by heme to generate free radicals that cause alkylation of proteins, lipids and heme, thereby causing oxidative stress and cellular damage [35,186]. Other proposed mechanisms include upregulation of the unfolded protein response pathways which may be linked to decreased parasite development and inhibition of *P. falciparum* phosphatidylinositol-3-kinase (PfPI3K) [187,188].

ART and its derivatives are very effective at killing asexual blood stage rings and trophozoites [189]. The first report of resistance to artemisinin was in western Cambodia in 2008 and manifested in delayed parasite clearance [190]. A decade later, this tolerance phenotype was widespread and was reported in 30 independent cases across Southeast Asia. Alarmingly, this resistance was to DHA-PPQ combination therapy [191]. ART-resistance is now known to be driven by point mutations in propeller domain of *P. falciparum* Kelch 13 (PfK13) [35,192,193].

1.6.3. Quinolines

Quinoline antimalarials are divided into the following categories: 4-aminoquinolines, 8-aminoquinolines and aryl-amino alcohols. The 4-aminoquinolines compounds include CQ, AQ, PPQ, PND and ferroquine (FQ). CQ was developed in the 1940s and was used to treat all forms of malaria with few side effects. It acts by accumulating inside the parasite's DV where it prevents the biomineralization of toxic free heme into inert hemozoin [194]. Resistance is driven primarily by mutations in *P. falciparum* chloroquine resistance transporter (PfCRT). These mutations enable the parasites to efflux CQ out of the DV, thereby preventing drug accumulation at its primary site of action [195].

AQ was first synthesized in 1948 and in combination with AS, is an integral constituent of ACTs as a fixed-dose for the treatment of uncomplicated *P. falciparum* malaria [196,197]. Similar to CQ, AQ is thought to inhibit heme detoxification inside the DV [93]. Reduced parasite sensitivity to AQ has been associated with polymorphisms like N86Y and

D1246Y in *P. falciparum* multidrug resistance transporter 1 (PfMDR1), that have been selected for by AQ therapy in different malaria-endemic settings [198].

PPQ is an important ACT partner drug to DHA and was developed in the 1960s as a part of the Chinese National Malaria Elimination Program as a replacement for CQ as a monotherapy [199]. Resistance was first reported in Cambodia in the early 2010s and is now known to be primarily driven by PfCRT haplotypes [200-203]. PPQ-resistance also appears to be augmented via amplifications in plasmepsins 2 and 3 and these have also been identified, in genome-wide association studies using PPQ-resistant or PPQ-sensitive field isolates, as molecular markers of PPQ resistance [204,205]. These genes, which encode aspartic proteases in the DV, act as hemoglobinases and their amplification is proposed to result in faster rates of Hb digestion. This in turn leads to increased globin-derived peptide and subsequent amino acid availability for protein synthesis, which could help counteract the ability of PPQ to inhibit Hb catabolism and heme detoxification [205-207].

Like PPQ, PND, first synthesized in the 1970s at the Institute of Chinese Parasitic Disease, was also meant to replace CQ [41,208,209]. PND is efficacious against CQ-resistant strains and has yet to succumb to widespread resistance in the over 40 years of use. It's mechanism of action is predicted to be inhibition of β-hematin formation and is an important ACT partner drug to AS [210].

FQ was designed and synthesized in the 1990s by incorporating a ferrocene unit into the basic skeleton of CQ in an effort to develop new antimalarial compounds to counter the

spread of ART-resistance in Southeast Asia [211]. FQ kills parasites by targeting both membrane lipids and inhibiting β-hematin formation in the DV [212]. It is currently going through clinical trials [213].

The two 8-aminoquinoline drugs, primaquine and tafenoquine, can clear dormant hypnozoites in the liver and represent the only likely agents of anti-relapse therapy. Indeed, these are the only two compounds approved for radical cures for *P. vivax* and *P. ovale* malaria [214]. Primaquine requires repeated dosing for up to 15 days but tafenoquine, which was discovered in 1978 at the Walter Reed Army Institute of Research, is about a 100-fold more potent, has a longer half-life and can be used a single dose [215,216]. While thought to be a prodrug, tafenoquine's mechanism of action is not well understood [217].

The three best known aryl-amino alcohols are quinine (QN), LM and MQ. QN is a former frontline antimalarial first isolated from the bark of the cinchona tree in 1820 [218]. Although no longer used as a front-line treatment for malaria, it is currently used to treat uncomplicated *P. falciparum* malaria in pregnant women and provides an alternative to AS for severe malaria [219]. QN has a complex mode of action that includes the inhibition of heme detoxification and parasite mechanism of QN resistance are partially associated with polymorphisms in *pfcrt* and *pfmdr1* [220].

LM was first synthesized in 1976 as part of the Chinese antimalarial research effort "Project 523" which also resulted in the discovery of ART [221]. While it's exact mechanism of action is unknown, studies suggest that it inhibits nucleic acid and protein synthesis

through the inhibition of β-hematin formation by complexation with heme [93]. LM is currently used only in combination with AT [41].

MQ was developed in the 1970s by the United States Army as a replacement for CQ [222]. It has since been used both as a curative and a prophylactic drug and is thought to kill parasites through the disruption of Hb digestion. Resistance was first reported in 1986 and MQ is no longer widely used due to the perception of central nervous system toxicity reported to affect a large number of its users [223,224].

Quinoline compounds are commonly used in combination with a complementary drug to reduce the chance of resistance development.

1.6.4. Other antimalarials

Atovaquone and proguanil

Atovaquone, a naphthoquinone, was first reported in 1991 for the treatment of protozoan infections while proguanil was first reported in 1945 as one of the first antifolate antimalarial drugs [225,226]. The combination of these two (atovaquone-proguanil) since the early 2000s has been very effective in treating malaria due to the synergy resulting from their individual mechanisms of action. Atovaquone acts as a cytochrome bc1 complex inhibitor that blocks mitochondrial electron transport and proguanil, through its metabolite cycloguanil, is a dihydrofolate reductase (DHFR) inhibitor that disrupts deoxythymidylate synthesis [227,228]. Resistance to this drug combination was first reported in the early 2000s [41].

Sulfadoxine and pyrimethamine

Sulfadoxine was developed in the early 1960s and is no longer used as a preventative drug due to high levels of resistance [229]. Pyrimethamine was developed in the early 1950s and was a part of the efforts that won Gertrude Elion and George Hitchings the joint Nobel Prize in Physiology or Medicine in 1988 [230]. The combination of sulfadoxine and pyrimethamine (sulfadoxine-pyrimethamine - SP) was approved for use for the treatment of malaria in 1981. Both drugs are known to target the parasite's folate biosynthesis pathway. Pyrimethamine inhibits dihydrofolate reductase (PfDHFR), while sulfadoxine inhibits dihydropteroate synthetase (PfDHPS). Together, SP interferes with folate biosynthesis, which is essential for DNA synthesis and parasite growth [231]. High-grade SP resistance occurs in mutant parasites harboring the N51I, C59R, and S108N point mutations in PfDHFR and A437G and K540E in PfDHPS [232].

1.6.5. Antimalarial compounds under development

Given the ability of the *Plasmodium* spp. to acquire resistance to chemical material, the bar for new antimalarials must necessarily be high. As such, the attractiveness of new compounds is heavily dependent on a number of factors, including novel modes of action with no cross-resistance to current drugs, single-dose cures, activity against both the disease-causing asexual blood stages and the gametocytes responsible for transmission, chemoprotective ability and the ability to clear *P. vivax* and *P. ovale* hypnozoites from the liver.

Traditionally, antimalarial compounds have been discovered using high-throughput phenotypic or whole-cell assays where a large compound library is screened to identify molecules that are active against *Plasmodium* parasites or actual targets in biochemical assays [233]. This initial screening is then followed by cheminformatic analysis where factors like potency, novelty, ease of synthesis, toxicity and cost are used to help identify promising scaffolds. Additional derivatives of the selected scaffolds are often then synthesized and tested against the whole parasite or against the specific protein target for structure-activity relationship (SAR) analysis, which are in turn used to predict the effect of chemical modifications on the properties of the compound. Iterative SAR analyses help identify lead compound(s) from which candidates are then picked for efficacy testing. The scope and type of assay is usually determined by the number of compounds to be screened and the cost of the operation. High-throughput automation and related technological advances in liquid handling, image analysis and assembly of pure chemical libraries have made it possible to screen millions of compounds [234-237]. While costly, this drug discovery approach has led to the identification of promising compounds like KAE609 and KAF156 that are currently in clinical trials and have the potential to be the next generation antimalarials [238,239]. High-throughput screens have also been developed to identify compounds that act exclusively on the nonreplicating mature gametocytes to prevent their transmission, without exerting selective pressure on asexual blood stage parasites that could generate resistance [240-244].

While the traditional high-throughput screening of compounds is still relevant today, newer and innovative ways are also currently being pursued. There is now a push to

further leverage heme detoxification, to focus on drugs with a pleiotropic array of cellular targets or target processes like parasite-mediated endocytosis of Hb, that involve host proteins.

Towards this end, CQ-like compounds that couple targeting heme with a chemosensitizing component that counteracts mutant PfCRT-mediated CQ resistance are now being designed [245,246]. Our detailed knowledge about drivers of resistance, like PfCRT and PfMDR1, where mutations conferring resistance to one drug can sensitize parasites to other agents has also been harnessed to lay the groundwork for clinical trials (NCT02612545 and NCT02453308) with the triple ACTs AL plus AQ or DHA-PPQ plus MQ to test whether these combinations can successfully eliminate resistant and sensitive infections, and, potentially, block the emergence of parasites resistant to all three agents. Lastly, some potential target host factors required for intraerythrocytic parasite growth have been identified. These include the human ferrochelatase which is imported into parasites and seems to contribute to heme biosynthesis and a host tyrosine kinase that seems to be co-opted to assist with erythrocyte membrane destabilization and parasite egress [247-250].

Another promising strategy is the repurposing of existing drugs that are used to treat other diseases but are efficacious against malaria parasites. The advantage of this method is that the said compounds may already have good biological properties and hence require less optimization and may also reveal novel antiplasmodial mechanisms of action. Some examples of repurposed compounds include: methylene blue, which is a drug for the

treatment of methaemoglobinemia in clinical trials (NCT02851108) as a combination with primaquine; fosmidomycin, an antibiotic in clinical trials (NCT02198807) as a combination with PPQ; rosiglitazone, an antidiabetic drug that in clinical trials as an adjunctive therapy for severe malaria (NCT02694874); imatinib, a cancer therapy drug currently in clinical trials (NCT03697668) as a triple combination with DHA-PPQ; and sevuparin, a drug for the treatment of sickle cell disease in clinical trials (NCT01442168) as a combination with atovaquone-proguanil.

Table 1.1. below list some of the other promising compounds in clinical and preclinical development.

Table 1. 1. | Select antiplasmodial compounds identified by recent drug discovery efforts.

Compound	Compound class	Stage in development	Target/MoA	Reference
M5717	quinoline-4-carboxamide	Phase I (NCT03261401)	PfeEF2	251,252
DM1157	"reversed chloroquine"	Phase I (NCT03490162)	inhibition of β-hemozoin	253,254
P218	2,4-diaminopyrimidine	Phase I (NCT02885506)	PfDHFR	255
(+)-SJ733	tetrahydroisoquinolone carboxanilide	Phase I (NCT02661373)	PfATP4	238,256
ACT-451840	Piperazine	Phase I (NCT02223871)	Unknown	257,258
OZ439	trioxolane	Phase IIb (NCT02497612)	Oxidative stress	259,260
KAF156	imidazolopiperazine	Phase IIb (NCT03167242)	PfCARL, UDP-galactose Acetyl-CoA	261,262
KAE609	spiroazepineindole	Phase IIb (NCT03334747)	PfATP4	263,264
DSM265	triazolopyrimidine	Phase IIa (NCT02123290)	PfDHODH	265,266
MMV048	3,5-dia-ryl-2-aminopyridine	Phase IIa	PfPI4K	61,267
Bortezomib	peptidyl boronic acid	Pre-clinical	β5 *P. falciparum* 20S proteasome	268
WLL, WLW	peptide vinyl sulfones	Pre-clinical	β2, β5 (WLL), β2 (WLW) *P. falciparum* 20S proteasome	269,270
GNF-Pf-5640	Hexahydroquinoline	Pre-clinical	--	271
MB14	4-cyano-3-methylisoquinoline	Pre-clinical	PfATP4	272
MMV030084	trisubstituted imidazole	Pre-clinical	PfPKG	57
AN13762	benzoxaborole	Preclinical	PfCPSF3	273,274
MMV253	triaminopyrimidine	Lead development	PfATP4 inhibition	275
SC83288	amicarbalide	--	PfATP6 and PfMDR2	276,277
UCT943	2-aminopyrazine	--	PfPI4K	278,279

MoA: Mechanism of Action; PfeEF2: *P. falciparum* elongation factor 2; PfDHFR: *P. falciparum* dihydrofolate reductase; PfATP4: *P. falciparum* P-type cation-transporter ATPase; PfCARL: *P. falciparum* cyclic amine resistance locus; UDP: Uridine diphosphate galactose; PfDHODH: *P. falciparum* dihydroorotate dehydrogenase; PfPI4K: *P. falciparum* phosphatidylinositol 4-kinase; PfPKG: *P. falciparum* cGMP-dependent protein kinase; PfCPSF3: *P. falciparum* cleavage and polyadenylation specificity factor; PfATP6: *P. falciparum* Ca^{2+}-ATPase; PfMDR2: *P. falciparum* multidrug resistance protein 2; --: unknown.

1.6.6. Antimalarial drug targets

This section briefly describes some of the targets listed in **Table 1.1.** above.

Translational elongation factor 2 (PfeEF2): PfeEF2 is an essential factor for eukaryotic protein synthesis and catalyzes the translocation of tRNA and mRNA [280]. It is currently a target by the antiplasmodial compound M5717 [281].

P-type ATPase 4 (PfATP4): The malaria parasite must maintain a low intracellular Na^+ concentration to survive, especially in the presence of the high concentration of extracellular sodium ions. The parasite's influx of Na^+ is regulated by using PfATP4 that shuttles sodium ions out of the cell. Inhibition of this transporter by compounds like (+)-SJ733, KAE609 and MB14 results in a buildup of Na^+ inside the parasite and leads to cell death [238,263,272].

V-type H+-ATPase: H^+ are imported through the same pathway regulating its Na^+ concentration. To maintain an intracellular pH of ~7.3, the parasite effluxes H^+ using a complementary V-type ATPase transporter [282]. Inhibition of this transporter by compounds like bafilomycin A and concanamycin A leads to cell death [283].

Phosphatidylinositol 4-kinase (PfPI4K): PfPI4K phosphorylates lipids, allowing them to regulate intracellular signaling and trafficking [61]. Inhibition of the ATP-binding pocket of PI4K by compounds like MMV048 and UCT943 leads to disruption of the intracellular distribution of PI4-phosphate (PI4P), which in turn results in decreased late-stage parasite development.

Dihydroorotate dehydrogenase (PfDHODH): *Plasmodium* parasites are unable to use endogenous host pyrimidines and must synthesize them *de novo*. A key step in the biosynthesis of pyrimidines is the oxidation of dihydroorotate to produce orotate, a reaction that is catalyzed by the enzyme dihydroorotate dehydrogenase (DHODH) [284]. Compounds like DSM265 inhibit this enzyme so that the malaria parasite can no longer obtain the required metabolites to survive, and is killed [285].

Dihydrofolate reductase (PfDHFR): Malaria parasites also require folates in order to maintain their high rate of replication. Unlike the pyrimidines, the parasites are able to scavenge folates or synthesize them *de novo*. Dihydrofolate reductase (DHFR) catalyzes a step required for folate recycling, which in turn are used in the synthesis of thymidylate, purines and methionine. The inhibition of this enzyme by compounds like P218 kills the parasites by depriving them of these essential molecules [286].

1.7. The rise and spread of multidrug resistance

The prior combination of AS-MQ has been largely replaced by DHA-PPQ in Asia as a consequence of *P. falciparum* multidrug resistance-1 transporter (pfmdr1) amplifications in Southeast Asian parasites. *pfmdr1* encodes a DV membrane-bound ATP-binding cassette (ABC) transporter whose amplifications or polymorphisms constitute a major

determinant of parasite resistance to MQ and LM [287,288]. PPQ is generally effective against parasites that evolved resistance to CQ through specific sets of point mutations in PfCRT, which is also present on the DV membrane [289,290]. However, the rapid increase in mutant K13 parasite strains in Southeast Asia has resulted in greater numbers of parasites being exposed to the ACT partner drugs as monotherapy agents, once the short-lived ART component has dropped to sub-therapeutic levels. As a consequence of this increased selection pressure, resistance to the partner drug PPQ has now emerged, is spreading quickly in Southeast Asia and is rendering DHA-PPQ treatment increasingly inefficacious [291-293]. PPQ resistance is also driven by gain of individual PfCRT mutations, including the H97Y, M343L, G353V and F145I, which confer varying levels of fitness costs that ultimately influences their relative abundance within parasite populations [207,294]. Alarmingly, novel mutant K13 parasite strains have recently been identified in Africa [295].

As has been mentioned, MQ or LM treatment in Southeast Asia selects for parasites with increased *pfmdr1* copy number [288,296,297]. Luckily, *pfmdr1* copy-number variants are exceedingly rare in Africa and LM continues to be an important ACT partner drug to AT [41,298]. Why the aryl-amino alcohols select for gene amplifications in the parasites of one continent and not another is not quite clear but a possible explanation is that Africa's combination of lower drug pressure coupled with more frequent mixed infections exacerbates the fitness cost resulting from *pfmdr1* overexpression, which in turn results in the predominance of single-copy *pfmdr1* parasites.

Distinct PfMDR1 haplotypes can modulate the efficacy of several antimalarials. A good example is the N86Y mutation that has been shown to confer partial resistance to the active metabolite of AQ (monodesethyl-AQ) as well as augment the level of CQ resistance imparted by mutations in PfCRT. Surprisingly, this mutation is counter-selected by LM, ARTs and MQ, which shows the interconnectedness of many of the clinical antimalarials and/or the parasite's mechanisms of resistance [297,299]. Disturbingly, multiple new mutations in PfMDR1 and PfCRT have been documented across Asia and Africa, suggesting that the widespread use of ACTs is selecting for novel variants of these multi-drug resistance transporters [300].

The fear of imminent spread of multidrug resistance to Africa is merited and is backed by history. Southeast Asia is the original source of parasite resistance to the former first-line drugs CQ and SP [301]. From there, resistance spread to Africa where it caused a dramatic worsening of the malaria situation until ACTs were deployed. In Senegal for example, the emergence of CQ resistance was estimated to have caused up to a six-fold increase in mortality rates in children with malaria [302]. There is therefore a valid concern that resistance mechanisms originating in Southeast Asia could once again spread into Africa, with potentially devastating consequences [303].

Why Southeast Asia in general, Cambodia in particular, is *P. falciparum*'s favored region for the emergence of multi-drug resistance is still debated but could be as a result of any or a combination of the following: 1) the frequent choice to ACTs and issues of incomplete patient compliance coupled with substandard drugs [304]; 2) Asian parasites, being in a low

transmission region, are largely monoclonal and this might lessen any resistance-associated fitness cost, thereby allowing parasites to optimize resistance mechanisms and enable their successful dissemination. In contrast, parasite infections in high transmission Africa are frequently polyclonal and any resistance-associated fitness cost would compromise the parasite's ability to compete [183]; 3) host immunity, which plays an important role in the clearance of resistant *P. falciparum* infections, is typically lower in Asian settings because of the reduced frequency of human exposure to malaria parasites. Consequently, little if any, natural clearance of drug-resistant infections in Asia allows these parasites to thrive [305].

Chapter 2. Experimental Procedures

2.1. Experimental Procedures for Chapter 3

2.1.1. Experimental model and subject details.

The *P. falciparum* parasites used in this study were cultured in human O^+ blood (sex of donor unknown) at 3% hematocrit in RPMI-1640 media supplemented with 50 µM hypoxanthine, 2 g L^{-1} sodium bicarbonate, 2 mM L-glutamine, 25 mM HEPES, 0.5% AlbuMAXII (Invitrogen) and 10 µg mL^{-1} gentamycin in 5% O_2, 5% CO_2 and 90% N_2 at 37 °C. The 3D7-A10 *P. falciparum* line is a clone of the 3D7 line received from the Goldberg lab at Washington State University in St. Louis. The 3D7-MR4 line was obtained from the Malaria Research and Reference Reagent Resource Center (MR4, Cat#MRA-102). The Dd2-B2 *P. falciparum* line is a clone obtained by limited dilution from the Dd2 line provided by Dr. Thomas Wellems (NIAID, NIH).

2.1.2. Stage specificity assay.

Standard asexual blood stage susceptibility results were collected by exposing asynchronous 3D7-A10 parasite cultures to 10 different concentrations plus no-compound controls for 72 h. To determine the specific asexual blood stage at which the compounds are active, schizonts were magnetically purified using MACS LD columns (Miltenyi Biotec) from cultures that had been repeatedly synchronized with 5% sorbitol. After a 3h incubation at 2% hematocrit to allow re-invasion, cultures were again sorbitol-synchronized to obtain a pure ring-stage culture (time = 0 h). These parasites were then plated in five 96-well plates and exposed to compounds as early rings (0-8 h), late rings

(8-16 h), early trophozoites (16-24 h), late trophozoites (24-32 h) or schizonts (32-40 h). Incubation times were adjusted to the 40 h asexual blood stage cycle of the 3D7-A10 parasite line. Synchronicity of the cultures was confirmed by imaging on average 83 parasites per time point in control conditions. Compounds were removed through three rounds of washing including two plate changes in 37°C prewarmed culture media after each exposure. All pipetting steps to expose and wash parasites were performed using a Tecan Freedom Evo 100 for increased throughput and accuracy. Each group of plates per timepoint were placed in a separate humidified chamber to avoid any delay in growth rate due to temperature variations. For the stage specificity assay, growth inhibition was assessed at the 60 h time point at which parasites had expanded, reinvaded new RBCs, and developed into the trophozoite stage that allows straight-forward quantification by flow cytometry. This is very similar to the standard 72 h assay in which parasites are not synchronized, but also allowed to reinvade and develop further for another half life cycle. Parasite survival for both the 72 h and stage-specific 8 h exposures was assessed by SYBR Green and MitoTracker Deep Red FM staining (Life Technologies) and subsequent flow-cytometric analysis (Accuri C6, BD Biosciences) [306]. IC_{50} values were derived from growth inhibition data using nonlinear regression (Prism 7, GraphPad). All asexual blood stage assays were repeated on at least three independent occasions with two technical replicates.

2.1.3. Culturing for Metabolomics.

3D7-MR4 parasites were cultured at 50 ml volumes and 2% hematocrit as described elsewhere [260]. Cultures were kept at the appropriate temperature and gas mixture in

incubators between media exchange, culture division, and synchronization. Synchronization was achieved via 5% sorbitol. All reagents and experimental spaces were mycoplasma-free, and reagents passed through 0.2 µm liquid filters when possible prior to use.

2.1.4. Metabolomics.

Hydrophilic metabolite changes in response to compound exposure were profiled as previously described [260]. Treatments were performed on 1×10^8 MACS-purified, synchronized trophozoite parasite-infected RBCs (24-36 h post invasion) in 5 mL RPMI. Compounds were added at a concentration of $10\times IC_{50}^{72h}$ and incubated for 2.5 h. All treatment conditions were performed as technical triplicates and included an untreated control. Subsequently, PBS washes were performed, and infected RBCs were extracted with 90% methanol containing 0.5 µM $^{13}C^{15}N$-labelled aspartate as an internal standard, then dried under nitrogen and stored at -80°C. Process blanks were generated at the time of extraction in technical triplicates. Samples were then resuspended in high-performance liquid chromatography (HPLC) grade water containing 1 µM chlorpropamide as an additional internal standard and analyzed by ultra-high-performance liquid chromatography mass spectrometry UHPLC-MS as described [260].

2.1.5. Targeted Analysis.

Following negative ionization analysis of hydrophilic extracts on a Thermo Exactive Plus Orbitrap, sample data were converted and transferred for analysis. Targeted peak picking from a curated list of 298 metabolites was achieved using el-MAVEN software

(https://elucidatainc.github.io/ElMaven/ [307]), followed by normalization and analysis via RStudio (http://www.rstudio.com/) and Metaboanalyst (https://www.metaboanalyst.ca/ [308]). Data were visualized using the Hyperspec (http://hyperspec.r-forge.r-project.org) and Suprahex R (Fang et al., 2014) scripting packages in RStudio. Hierarchical clustering of the metabolic profiles to identify related metabolic signatures was performed using the Ward method, based on the Pearson correlation coefficients, by the Hyperspec R integrated heatmap function.

2.1.6. Resistance selections.

Attempts to obtain parasites resistant to MMV030666, MMV000787 and MMV021735 were performed using either single step (continuous) or ramping selection protocols as described elsewhere [233]. For single step selections, parasites are continuously exposed to relatively high concentrations of the compound of interest (usually $3\times IC_{50}$) with culture media and RBCs being regularly refreshed until actively growing parasites are again observed. Cultures were monitored for minimum 70 days after start of exposure. For ramping selections, parasites are exposed at low compound concentrations (usually $1\times IC_{50}$ or lower) and parasite growth is continuously monitored. When parasites seem to have adapted to the pressure, compound concentrations are gradually increased to adapt parasites to even higher levels of compound. Standard IC_{50}^{72h} assays were performed on recrudesced parasites from single step selections, if any, and on parasites resulting from ramping selections.

2.1.7. Solubility assay.

The aqueous solubility of MMV007181, MMV000442 and MMV006455 was determined at a single concentration of 500 µM because of compound scarcity. The protocol used was adapted from Millipore Corporation's "MultiScreen® Solubility Filter Plate" application note. Dihydroartemisinin, chloroquine and piperaquine were used as controls. Briefly, compounds were first dissolved in DMSO at 10 mM. They were then added to 1× PBS (pH 7.4) at a 1:20 ratio in 1.5 ml tubes and mixed on a shaker (100 rpm) at room temperature for 1.5 h. They were then filtered using Target2 regenerated cellulose 0.2 µM filters (Thermal Scientific, part number F2500-8) to remove any precipitate. 160 µl of the filtrate was dispensed into flat-bottomed 96-well culture plates and diluted with 40 µl/well acetonitrile. The plate was then placed on a shaker (100 rpm) at room temperature for 10 min. After mixing, the filtrate was analyzed using a Spectramax 340PC (Molecular Devices) at 280, 300, 320, 340, 360 and 800 nm. Standards were made by adding compounds into standards buffer (80:20 1× PBS: acetonitrile, pH 7.4) at a 1:25 ratio. The mixtures were allowed to mix on a shaker (100 rpm) for 10 min at room temperature and analyzed at the same six wavelengths as mentioned above. The aqueous solubility of compounds was then determined by calculating the ratio of absorbances between the filtrate and the standard using the formula below:

$$\frac{(\sum \text{AU at } 280, 300, 320, 340, 360 \text{ nm}) - (\text{AU at } 800 \text{ nm})\ \text{Filtrate}}{(\sum \text{AU at } 280, 300, 320, 340, 360 \text{ nm}) - (\text{AU at } 800 \text{ nm})\ \text{Standard}}$$

If the ratio is ≈ 1, a compound's aqueous solubility is ≥ 500 µM. Ratios < 1.0 and > 0.5 indicate a solubility between 100 µM and 500 µM, while ratios ≤ 0.5 indicate a solubility ≤ 100 µM.

2.2. Experimental Procedures for Chapter 4

2.2.1. Experimental model and subject details.

Asexual blood stage *P. falciparum* parasites used in this study were cultured at 3% hematocrit in O^+ human erythrocytes in RPMI-1640 medium supplemented with 50 μM hypoxanthine, 2.1 g/L $NaHCO_3$, 2 mM L-glutamine, 25 mM HEPES, 0.5% (w/v) AlbuMAXII (Invitrogen) and 10 μg/mL gentamycin at 37°C in flasks gassed with 5% CO_2/5% O_2/90% N_2. The 3D7-A10 Dd2-B2 and NF54 *P. falciparum* parasites lines used here have been previously reported [189,309]. Dd2 ^{Dd2} and Dd2 ^{3D7} isogenic *pfcrt*-edited lines were reported in [310]. The human biological samples were sourced ethically and their research use was in accordance with terms of informed consent under an IRB/EC approved protocol.

2.2.2. Compounds, resistance selections and *in vitro* drug susceptibility assays.

Compounds **2-5** were kindly provided by the Medicines for Malaria Venture (Geneva, Switzerland), and **1** and **6** were synthesized at the Drug Discovery and Development Centre (H3D) at the University of Cape Town in South Africa as part of the SoftFocusKinase 59 (SFK59) library [311,312]. Parasites resistant to compound **1** were obtained from single-step selections where 10^7 3D7-A10 parasites in triplicate were cultured continuous at 3□IC_{50} drug pressure. For the SNP-selecting **3** and **4**, single-step selections were run on 10^9 3D7-A10 parasites. The same numbers of parasites and selection methods were used on Dd2-B2 selections using compound **5**. Resistant clones were obtained from bulk cultures by limiting dilution. For the susceptibility experiments, compounds were assayed using 2-fold dilutions with inhibition measured after 72 h. Parasite viability was determined by staining the parasites with SYBR Green and MitoTracker Deep Red (Life Technologies) followed by

flow cytometry (Accuri C6, BD Biosciences or iQue Plus, Sartorius) [306]. IC_{50} values were derived by nonlinear regression (Prism 7, GraphPad).

2.2.3. Whole-genome sequencing analysis.

Sequencing of *P. falciparum* clones resistant to compounds **2-4** was performed by the Winzeler lab, using methodology reported in [313]. For **1** and **5**, resistant clones were sequenced by the Fidock lab, using methods reported in [57,314]. Paired-end libraries were sequenced on Illumina HiSeq or MiSeq instruments.

In the Winzeler lab, the Nextera XT kit (Illumina) was used to prepare DNA libraries from samples for whole-genome sequencing using the dual index protocol [313]. The libraries were run on the Illumina HiSeq 2500 in rapid run mode with 100-bp paired-end reads. The reads were aligned to the *P. falciparum* 3D7 reference genome (PlasmoDB v. 13.0) as described previously [315]. Single nucleotide polymorphisms (SNPs) and indels were called with the Genome Analysis Toolkit's (GATK) HaplotypeCaller. Variants were filtered by quality scores and sequencing bias statistics based on GATK's default filtering parameters. SNPs were filtered out if they met any of the following criteria: quality depth (QD), <2.0; mapping quality (MQ), <50.0, Phred-scaled P value using Fisher's exact test to detect strand bias (FS), >60.0; symmetric odds ratio (SOR), >4.0; Z-score from Wilcoxon rank sum test of alternative versus reference read mapping qualities (MQRankSum), less than 12.5; ReadPosRankSum (RPRS) parameter, less than 8.0. Indels were filtered out if they met any of the following criteria: QD, <2.0; RPRS, less than 20.0; FS, >200.0. Variants were

annotated using snpeff (version 4.2). Custom scripts were used to compare the variants between the parent sequence and the resistant clones.

In the Fidock lab, whole-genome sequencing of genomic DNA from parental and resistant clones employed an Illumina TruSeq DNA PCR-Free library preparation protocol and a MiSeq sequencing platform. Briefly, 2 mg of genomic DNA were sheared to a mean length of 550bp, end-repaired, adenylated on their 3' ends and ligated to indexed adaptors. Samples were pooled and sequenced on Illumina MiSeq flow cells to obtain 300 bp paired-end reads. Sequence data were aligned to the *P. falciparum* 3D7 genome (PlasmoDB version 48) using BWA (Burrow-Wheeler Alignment). We used Samtools and Picard to remove PCR duplicates and reads that did not map to the reference genome. Reads were realigned around indels using GATK RealignerTargetCreator and base quality scores were recalibrated using GATK Table-Recalibration. GATK HaplotypeCaller (version 4.1.8; Min Base quality score ≥ 18) was used with the clones to identify all possible variants, which were filtered based on quality scores (variant quality as function of depth QD > 1.5, mapping quality > 40) and read depth (depth of read > 5) to obtain high-quality SNPs. These SNPs were annotated using snpEFF. The list of variants from the resistant clones were compared against the 3D7-A10 parent to obtain homozygous SNPs that were present exclusively in the resistant clones. IGV was used to confirm the SNPs present in the resistant clones. BicSeq was used to discover copy number variants (CNVs) against the 3D7-A10.

2.2.4. Genome editing.

L690I mutation in ABCI3 was validated by engineering it into 3D7-A10 parent using a two-plasmid CRISPR/Cas9 system. The Cas9 was derived from *Streptococcus pyogenes* and was fused to the selection marker yDHODH that confers resistance to DSM1 [316]. Both Cas9 and the selection marker were expressed from the *P. falciparum* calmodulin promoter. The Cas9 plasmid also contained a guide RNA that was expressed from the U6 promoter. Guide RNA sequences were selected using ChopChop, an online gRNA design tool, and were based on their proximity to the mutation of interest, GC content, and absence of poly A/T tracks (http://chopchop.cbu.uib.no). The donor plasmid contained the *abci3* fragment with the L690I mutation and blasticidin-S deaminase (*bsd*), a selection marker that protects against blasticidin (Sigma-Aldrich). Plasmid transfections were conducted using an Amaxa nucleofector [317]. Briefly, a cell pellet of 7×10^8 highly synchronized and magnet-purified 3D7-A10 mature schizonts were first re-suspended in 100 µl of Nucleofector Solution 2 (with the supplement added) that had been pre-warmed to room temperature. This was then mixed with 10 µg of plasmid DNA in a volume of 5 µl deionized water. The sample was then transferred into an Amaxa certified cuvette and electroporation done using the Amaxa U-033 program. The parasite were allowed to re-invade fresh red blood cells in complete media that had been pre-warmed to 37^{o}C. Parasite uptake of the donor plasmid was selected with 2 mg/ml BSD for six days starting one day after the transfections, and parasites were maintained thereafter in complete media until recrudescence. Gene editing was assessed via Sanger sequencing of PCR products amplified from bulk cultures. Edited parasite clones were obtained by limiting dilution. Parasites were assayed for drug susceptibility by flow cytometry [306].

3´Flag and 3´HA tagging of ABCI3 was achieved by transfecting highly sorbitol-synchronized 3D7-A10 ring-stage parasites with an all-in-one CRISPR/Cas9 plasmid. The *P. falciparum* codon-optimized Cas9 endonuclease was derived from *Streptococcus pyogenes* and was expressed under a calmodulin promoter. The plasmid also carried a human DHFR (hDHFR) selectable marker (that confers resistance to WR99210) under a *P. chabaudi dhft-ts* promoter and the guide RNA (gRNA) sequence under a U6 promoter. Guide RNAs were selected using the online tool ChopChop 9 https://chopchop.cbu.uib.no). 10^8 parasites were electroporated with purified circular plasmid DNA as described [318]. Briefly, a 5 mL culture of 3D7-A10 (≥ 10% rings) was washed and resuspended in 220 μL 1× Cytomix. This mixture was then added to 50 μg of plasmid DNA and electroporated at a voltage of 0.31 kV and capacitance of 950 μF using a Gene-Pulser (Bio-Rad) [319]. Starting on the day after the transfections, the cultures were maintained in 2.5 nM WR99210 until recrudescence [320]. Successful gene editing was assessed via Sanger sequencing of products PCR amplified from bulk cultures. Edited parasite clones were obtained by limiting dilution. Successful gene tagging was confirmed via PCR, Sanger sequencing immunofluorescence and immune-EM assays. Oligonucleotide primers used in this study are listed in **Table 2.1** below.

Table 2. 1. | Oligonucleotides used in this study.

Experiment	Nucleotide Sequence (5' to 3')	Description	Lab name
L690I validation in 3D7-A10 (related to **Fig. 2C**)	GGGAAATAACTATGGAATATAAAAAAACAG	ABCI3 L690I donor fragment fwd	p6417
	GTTGTGTCGAAGAGGTATCATGGG	ABCI3 L690I donor fragment rev	p6418
	GTTTCGATATAAATAAAGAG	ABCI3 L690I guide RNA	p6387/p6388
F689C and S696Y validation in Dd2-B2 (related to **Fig. S1A**)	GACAAACAAAATGACGAATG	ABCI3 F689C guide RNA (1)	p8159/p8160
	GTTTCGATATAAATAAAGAG	ABCI3 F689C guide RNA (2)	p8165/p8166
	GAGGTACCGAGCTCGaattcCAGATGAAAAGGAGTATCAGG	ABCI3 F689C/S696Y donor fragment fwd (In-Fusion)	p8161
	GAAAAGTGCCACCTGacgtcCAATCCTTAAACACATTTGAC	ABCI3 F689C/S696Y donor fragment rev (In-Fusion)	p8162
cKD in NF54^{pCRISPR} line (related to **Fig. S3**)	GTACGGTACAAACCCGGAATTCGAGCTCGGAGAAATTGCTTTAATGAGTTACATGGG	ABCI3 RHR forward	--
	GGGTATTAGACCTAGGGATAACAGGGTAATGGAAAAATATAAAAAATGAAACTACACC	ABCI3 RHR reverse	--
	GTTTAACGACAAAGATATCG	sgRNA target site	--
ABCI3 3×Flag and 3×HA tagging in 3D7-A10 (related to **Fig. S5**)	ATTGCTTTAATGAGTTACAT	ABCI3 3' tagging guide RNA	p7421/p7422
	AGAGGTACCGAGCTCGaattcCTCATCTCACCAGAAGATATG	ABCI3 3' donor fragment fwd	p7423
	CGAAAAGTGCCACCTGacgtcTCTACAACTATATAAGAAACTCC	ABCI3 3' donor fragment rev	p7424
	GCAGAAAATTTATATTTTCAAAGTGGAGATTATAAAGATCATGATGGAGATTATAAAGATCATGATATAGATTATAAAGATGATGATGATAAAtaa	TEV + 3×Flag tag fragment	--
	TACCCATACGATGTTCCTGACTATGCTGGTTATCCTTATGACGTGCCTGACTATGCAGGATCCTATCCATATGACGTTCCAGATTACGCT	3×HA tag fragment	--

--: No oligonucleotides

2.2.5. Generation of cKD parasite lines.

We utilized CRISPR-Cas9 to modify the native PfABCI3 (PF3D7_0319700) locus and install the linearized pSN054 donor vector [321], which incorporates a 10× aptamer array and the TetR-DOZI expression cassette containing the blasticidin S-deaminase gene, the reporter gene Renilla luciferase (RLuc), and the fusion proteins TetR-DOZI [322]. The right homology region (RHR; 264 bp) was PCR amplified and inserted into the pSN054 vector using the I-SceI restriction site. Fragments corresponding to the left homology region (LHR; 426 bp) fused to the re-codonized 3'-end of the gene (bp 9991-10092) without the stop codon as well as the target-specifying guide RNA sequence were synthesized using the BioXP™ 3200 System (SGI-DNA) and cloned into the pSN054 vector using restriction sites FseI/AsisI and AflII, respectively. Donor vector generation was carried out via Gibson assembly, and the final construct was confirmed by restriction digests and Sanger sequencing. Transfection into Cas9- and T7 RNA polymerase-expressing NF54 parasites was carried out by preloading erythrocytes with the donor vector as described previously [323]. Cultures were maintained in 500 nM anhydrotetracycline (aTc; Sigma-Aldrich 37919) and the selectable drug 2.5 mg/mL of Blasticidin (RPI Corp B12150-0.1), and recovered parasites were monitored via Giemsa smears and RLuc measurements.

2.2.6. Parasite growth assays.

To assess the effect of knocking down the expression of the ABCI3 protein on the viability of parasites, synchronous ring-stage parasites were cultured in the presence (50 nM) and absence of aTc and set up in triplicate in a 96-well U-bottom plate (Corning 62406-121). Luminescence was measured at 0, 72, and 120 h post-invasion using the Renilla-Glo(R)

Luciferase Assay System (Promega, E2750) and the GloMax Discover Multimode Microplate Reader (Promega). The luminescence values were normalized to CQ-treated (200 nM) samples and results were visualized on a scatter plot using GraphPad Prism (version 8; GraphPad Software).

2.2.7. Compound susceptibility assays.

Compound susceptibility of the cKD parasites was assessed as described above. Compounds were assayed using 2-fold dilutions with inhibition measured after 56 h. Parasite viability was determined by staining the parasites with SYBR Green and MitoTracker Deep Red (Life Technologies) followed by flow cytometry (Accuri C6, BD Biosciences) [306]. IC_{50} values were derived by nonlinear regression (Prism 7, GraphPad).

2.2.8. Immunofluorescence assays.

Indirect Immunofluorescence assays (IFAs) were performed in suspension as described [193]. Briefly, parasites were fixed in 4% (v/v) formaldehyde (Thermo Fisher Scientific) for 1 h at room temperature. This was followed by a second fixation step that supplemented the 4% formaldehyde solution with 1 mM cysteine and $CaCl_2$ followed by an overnight incubation at 4°C. Cells were then permeabilized on ice using 0.05% Triton X-100 in 1×PBS for 5 min. Autofluorescence was quenched using a 50 mM glycine treatment for 10 min. After two washes in 1× PBS the cells were resuspended in 1% (w/v) bovine serum albumin (BSA) in 1×PBS blocking buffer and incubated with the appropriate dilution for each primary antibody used: 1:200 for rabbit or mouse anti-Flag (Genscript), rabbit anti-

ERD2 (BEI Recourses), rabbit anti-BiP (kindly provided by Min Zhang), 1:50 for rat anti-Rab5B and Rab7 (kindly provided by Gordon Langsley) and 1:200 for anti-PfCRT antibodies. This was followed by incubation with the corresponding species-specific secondary antibodies (Alexa Fluor 488-, 594- or 647- conjugated goat anti mouse or rabbit antibodies; Thermo Fisher) diluted 1:2000 in 1% BSA in 1× PBS. Thin blood smears of stained RBCs were prepared on microscope slides and mounted with cover slips using Prolong Diamond Antifade Mount with DAPI (Thermo Fisher). Parasites were imaged using a Nikon Eclipse Ti-E wide-field microscope equipped with a sCMOS camera (Andor) and a Plan-apochromate oil immersion objective with 100× magnification (1.4 numerical aperture). A minimum of 27 Z stacks (0.2 µm step size) were photographed for each parasitized RBC. NIS-Elements imaging software (Version 5.02, Nikon) was used to control the microscope and camera as well as to deconvolve the images (using 25 iterations of the Richardson-Lucy algorithm for each image). ImageJ (Fiji) (version 2.0.0-rc-68/1.52 h) was used to crop the images, adjust brightness and intensity, overlay channels and prepare montages.

2.2.9. Measurement of drug cellular accumulation using the inoculum effect analysis.

In the absence of radioactively labelled compounds, we measured the drug cellular accumulation using the inoculum effect [324]. Briefly, highly synchronized 3D7-A10, ABCI3 $^{3\ copies}$ (resistant to **1)** and ABCI3 $^{L690I\ ed.}$ (resistant to **4**) parasite lines were exposed to serially diluted MMV compounds or CQ at parasitemia ranging from 0.25% - 4%. The inoculum size, which ranged from 0.75 - 6 was calculated as the parasitemia × hematocrit

[324]. The measure of absolute drug potency was achieved by extrapolating the linear relationship between the increasing inoculum size and IC_{50} to an inoculum size of zero from the following equation: IC_{50} measured = IC_{50} absolute + (IC_{50} absolute $\times$ accumulation ratio $\times$ fractional volume of parasitized erythrocytes, PRBCs) [324]. The mathematical relationship for the determination of the cellular drug accumulation ratio (CAR): CAR = (IC_{50} measured − IC_{50} absolute)/(IC_{50} absolute $\times$ fractional volume of PRBCs) has been previously reported [325]. This ratio represents the amount of drug in the infected cell pellet to the amount of drug in a similar volume of medium.

2.2.10. Immuno-electron microscopy.

To immunolocalize HA-tagged ABCI3, *P. falciparum* cultures were fixed in 4% paraformaldehyde (Polysciences Inc., Warrington, PA) in 100 mM PIPES/0.5 mM $MgCl_2$, pH 7.2 for 1 h at 4°C. Samples were then embedded in 10% gelatin and infiltrated overnight with 2.3 M sucrose/20% polyvinyl pyrrolidone in PIPES/$MgCl_2$ at 4°C. Samples were trimmed, frozen in liquid nitrogen, and sectioned with a Leica Ultracut UCT7 cryo-ultramicrotome (Leica Microsystems Inc., Bannockburn, IL). 50 nm sections were blocked with 5% fetal bovine serum (FBS)/5% normal goat serum (NGS) for 30 min and subsequently incubated with rabbit anti-HA antibody (Sigma, St. Louis, MO) at 1:100 for 1 h, followed by secondary anti-rabbit IgG antibody conjugated to 18 nm colloidal gold (Jackson ImmunoResearch Laboratories, Inc., West Grove, PA) for 1 h. Sections were stained with uranyl acetate and lead citrate, and viewed on a JEOL 1200 EX transmission electron microscope (JEOL USA Inc., Peabody, MA) equipped with an AMT 8 megapixel digital camera and AMT Image Capture Engine V602 software (Advanced Microscopy

Techniques, Woburn, MA). All labeling experiments were conducted in parallel with controls omitting the primary antibody. These controls were consistently negative at the concentration of colloidal gold conjugated secondary antibodies used in these studies.

2.2.11. Detergent-based β-hematin Inhibition Assay (βHIA).

A solution containing water + 305.5 μM Nonidet P-40 (NP-40) + DMSO at a v/v ratio of 70% + 20% + 10%, respectively, was prepared and 100 μL added to all wells in columns 1-11 in a flat-bottomed 96-well plate. Working stocks of test compounds and controls were constituted to 10 mM from which 20 μL of each was added to wells in the final column (column 12) together with distilled water (140 μL) and 305.5 μM NP-40 detergent (40 μL). This effectively lowered the final drug concentration to 1mM. Serial dilution of each compound (100 μL) from column 12 to column 2 was carried out (column 1 served as a blank). A 25 mM hematin stock solution was prepared by sonicating hemin in DMSO for 3 mins and 178.8 μL of this suspended in 20 mL acetate buffer (1 M, pH 4.8) and thoroughly mixed. The homogenous suspension (100 μL) was then added to all wells to give final hematin concentrations of 100 mM and final drug concentration of 0.5 mM in column 12. Plates were covered and incubated at 37 °C for 5 h after which 32 μL of 50% pyridine solution (20% (v/v) H2O, 20% (v/v) acetone and 2 M HEPES buffer (pH 7.4) and 50% pyridine) was added to each well to give a final pyridine concentration of 5% (v/v). Acetone (60 μL) was then added to assist with hematin dispersion. The UV-vis absorbance of the plate wells was read at 405 nm on a SpectraMax P340 plate reader. The βH inhibitory IC_{50} values for each compound were computed from the blank-

corrected absorbance values at 405 nm using a sigmoidal dose-response curve fitting analysis on GraphPad Prism software (GraphPad Prism 9, La Jolla, USA).

2.2.12. Cellular heme fractionation assays.

Baseline NF54 parasite sensitivity to compounds **1**, **3**, **4**, **5**, CQ and pyrimethamine was determined using a standard 72 h SYBR Green chemosensitivity assay. The IC_{50} values were used to set up the heme fractionation experiment as described elsewhere [93,326]. Briefly, ring-stage NF54 parasites were synchronized by treating them for two cycles using 5% sorbitol. The ~3-5 h old parasites were then incubated in a gradient of IC_{50} concentrations (based on the 72 h chemosensitivity assay) ranging from 0.5-4× at 5% parasitemia and 2% hematocrit. A no-drug control was included. After 28 h, late trophozoites were harvested by lysis of the red blood cells with 0.05% saponin followed by multiple washes with 1× PBS (pH 7.5) to remove traces of RBC Hb. Pellets were then resuspended in 1× PBS (pH 7.5) and an aliquot of the trophozoite suspension used to quantify the total number of trophozoites isolated using flow cytometry with parasites stained with 1´ SYBR Green and 100 nM MitoTracker Deep Red. Contents of the remaining trophozoite pellet were then released by hypotonic lysis and sonication. The fractions corresponding to digested Hb, free heme and Hz were then carefully recovered through centrifugation and treatment with HEPES buffer (pH 7.4), 4% SDS, 25% pyridine solution, 0.3M HCl and 0.3M NaOH. The UV−visible spectrum of each heme fraction as an Fe(III)heme−pyridine complex was measured using a multi-well SpectraMax P340 plate reader. The total amount of each heme species was quantified using a heme standard curve where the mass of each heme-Fe species per trophozoite (fg/cell) was

calculated by dividing the total amount of each heme species by the corresponding number of parasites in that fraction, as determined by flow cytometry. Statistical comparisons and analyses for trends were made using prism (Prism 9, GraphPad) using Students' t-test with Welch correction.

2.3. Experimental Procedures for Chapter 5

2.3.1. Synthesis of MMV688533.

Step 1. $Pd(PPh_3)_2Cl_2$ (4.96 g, 7.07 mmol) and cuprous iodide (1.34 g, 7.06 mmol) were added to a degassed solution of methyl 3-bromo-5-(trifluoromethyl)benzoate (20.0 g, 70.67 mmol) and trimethylsilylacetylene (17.4 g, 176.67 mmol) in 100 mL of acetonitrile in a sealed tube. The tube was degassed again and heated at 70 °C for 2 h. The reaction mixture was cooled and filtered through a celite bed. The filtrate was concentrated in vacuum and the residue purified through silica gel (60-120 mesh) column chromatography using petroleum ether to generate a 3-Trifluoromethyl-5-trimethylsilanylethynyl-benzoic acid methyl ester (14 g, yield 66 %) as yellow liquid.

Step 2. Potassium carbonate (0.58 g 4.2 mmol) was added to a solution of 3-Trifluoromethyl-5-trimethylsilanylethynyl-benzoic acid 2-methyl ester (14.0 g, 46.60 mmol) in 50 mL methanol and stirred at room temperature for 20 minutes. The reaction mixture was concentrated under reduced pressure. The residue was diluted with 100 mL ethyl acetate, washed with water and brine and dried over anhydrous sodium sulphate and concentrated to yield 3-Ethynyl-5-trifluoromethyl-benzoic acid methyl ester (11 g, yield 61%) as a brown liquid.

Step 3. Lithium hydroxide (6.0 g, 144.10 mmol) was added to an ice cooled solution of 3-Ethynyl-5-trifluoromethyl-benzoic acid methyl ester (11.0 g, 48.03 mmol) in 50 mL tetrahydrofuran and 25 mL water and stirred at room temperature for 3 h. The reaction mixture was concentrated and acidified with aqueous citric acid solution. The precipitated solid was filtered, washed with water and dried to generate 3-Ethynyl-5-trifluoromethyl-benzoic acid (9.2 g, yield 78%) as pale brown solid.

Step 4. Dicyclohexylcarbodiimide (13.28 g, 64.48 mmol) and pentafluorophenol (11.8 g, 64.48 mmol) in 50 mL tetrahydrofuran was added to a solution of 3-Ethynyl-5-trifluoromethyl-benzoic acid (9.2 g, 42.99 mmol) and stirred at room temperature for 3 h. Upon the completion of the reaction, the mixture was cooled in an ice bath and the precipitated dicyclohexylurea removed by filtration. The filtrate was concentrated and purified using a silica gel (60-120 mesh) column chromatography using ethyl acetate in petroleum ether, producing 3-Ethynyl-5-trifluoromethyl-benzoic acid pentafluorophenyl ester (13.6 g, yield 83%) as an off-white solid.

Step 5. Monobocguanidine (6.82 g, 42.94 mmol) was added to a solution of 3-Ethynyl-5-trifluoromethyl-benzoic acid pentafluorophenyl ester (13.6 g, 35.78 mmol) in 50 mL tetrahydrofuran and stirred at room temperature for 4 h. After the completion of the reaction, the mixture was evaporated and purified through silica gel (60-120 mesh) column chromatography using ethyl acetate in petroleum ether to generate tert-butylN-[N-[3-ethynyl-5-(trifluoromethyl)benzoyl] carbami-midoyl]carbamate (8.2 g, yield 64 %) as an off white solid.

Step 6: 10 mL of concentrated H_2SO_4 was added dropwise to a solution of 5-bromo-2-iodobenzoic acid (100 g, 305.89 mmol) in 800 mL MeOH. The mixture was refluxed for 16

h and then concentrated. The residue was dissolved in 1 L ethyl acetate. The organic layer was washed with saturated $NaHCO_3$ and 3 × 200 mL brine, dried over Na_2SO_4, filtered and concentrated to generate 5-Bromo-2-iodo-benzoic acid methyl ester (101.4 g, yield 90%) as yellow solid.

Step 7. Copper (I) bromide (1.21g, 8.45 mmol) was added to a solution of 5-Bromo-2-iodo-benzoic acid methyl ester (24 g, 70.4 mmol) and methyl 2,2-difluoro-2-(fluorosulfonyl)acetate (13.5 mL, 105.6 mmol) in 80 mL N-methyl-2-pyrrolidinone. The reaction mixture was stirred at 100 °C for 5 h. The reaction was filtered and partitioned between ethyl acetate and brine. The aqueous layer was extracted with ethyl acetate, and the organic layers were combined and dried over Na_2SO_4. After filtration, the solvent was removed *in vacuo*. The residue was purified by silica gel column (0-4% Ethyl acetate in Petroleum ether) to give the 5-Bromo-2-trifluoromethyl-benzoic acid methyl ester (119.2 g, yield 96%) as yellow oil.

Step 8. Lithium hydroxide (4.4 g, 104.76 mmol) was added to an ice cooled solution of 5-Bromo-2-trifluoromethyl-benzoic acid methyl ester (9.1 g, 35.68 mmol) in 20 mL tetrahydrofuran and 10 mL water and stirred at room temperature for 3 h. The reaction mixture was concentrated and acidified with aqueous citric acid solution. The precipitated solid was filtered, washed with water and dried to produce 5-Bromo-2-trifluoromethyl-benzoic acid (8 g, yield 95%) as pale yellow solid.

Step 9. 5-Bromo-2-trifluoromethyl-benzoic acid (8.0 g, 29.74 mmol) in 40 mL thionyl chloride solution was heated to reflux for 3 h. The completion of reaction (conversion of acid chloride to methyl ester) was observed by thin layer chromatography (TLC). Thionyl chloride was evaporated and the residue added to the reaction mixture containing 2-amino pyridine (3.2

g, 32.71 mmol), triethyl amine (12.44 mL, 89.21 mmol) in dry 80 mL ethyl acetate at 0 ºC. The reaction mixture was stirred at room temperature for 12h. Reaction completion was observed by TLC. The reaction mixture was then added to 200 mL water and extracted with 2 × 200 mL ethyl acetate. The combined organic layer was washed with 2 × 100 mL water, brine, dried over sodium sulphate and evaporated. The crude material was purified by column chromatography using ethyl acetate in petroleum ether to generate 5-Bromo-N-pyridin-2-yl-2-trifluoromethyl-benzamide (5.1 g, yield 49%) as off white solid.

Step 10. 5-Bromo-N-pyridin-2-yl-2-trifluoromethyl-benzamide intermediate (0.690 kg, 2 mol.), CuI (0.019 kg, 0.1 mol.), $Pd(PPh_3)2Cl_2$ (0.140 kg, 0.2 mol.) and acetonitrile were mixed in a 6 L reactor under nitrogen. Tert-butyl N-[N-[3-ethynyl-5-(trifluoromethyl)benzoyl]carbamimidoyl]carbamate intermediate (0.924 kg, 2.6 mol) was added in 5 min on the suspension while stirring at 25 °C. The mixture was degassed under nitrogen bubbling for an additional 30 min while still stirring. Triethylamine (0.605 kg, 5.98 mol) was added in 17 min at 25 °C. An exotherm of + 6 °C was observed. The dropping funnel was washed with 0.5 L acetonitrile. The reaction mixture was heated at 45 °C and maintained for 2 h until tert-butyl N-[N-[3-ethynyl-5-(trifluoromethyl)benzoyl]-carbamimidoyl]carbamate was < 1%. The suspension was then cooled to 10 °C at the rate of – 20 °C/h and maintained for 1 h. The expected intermediate tert-butyl N-[N-[3-[2-[3-(2-pyridyl-carbamoyl)-4-(trifluoromethyl)phenyl]ethynyl]-5-(trifluoromethyl)benzoyl]-carba-mimidoyl] carbamate was filtered and the cake was washed with 1.4 L acetonitrile followed by 0.7 L water. After drying by nitrogen flux overnight at 0.3 bar, tert-butyl N-[N-[3-[2-[3-(2-pyridylcarbamoyl)-4-(trifluoromethyl)phenyl]ethynyl]-5-(trifluoromethyl)benzoyl]carbamimidoyl]-carbamate was isolated (0.745 kg, yield 60%).

Step 11. A suspension of tert-butyl N-[N-[3-[2-[3-(2-pyridylcarbamoyl)-4-(trifluoromethyl) phenyl]-ethynyl]-5-trifluoromethyl)benzoyl]carbamimidoyl]carbamate (1.5 kg, 2.42 mol) in 14.5 L ethyl acetate was heated at 70 °C while stirring. Trifluoroacetic acid (2.2 kg, 19.30 mol) was added in 30 min at 70 °C. The dropping funnel was washed with 0.75 L ethyl. The reaction mixture was maintained for 22 h at 70 °C until tert-butyl N-[N-[3-[2-[3-(2-pyridylcarbamoyl)-4-(trifluoromethyl)-phenyl]ethynyl]-5-(trifluoromethyl)benzoyl]carbamimidoyl]carbamate was < 1%. After cooling at 20 °C the mixture was basified by addition of a solution of 28% NH_4OH in 1 h until pH was between 9-10. After an additional 15 min stirring, 11.3 L water were added and the phases separated. The organic layer was diluted with 45 L, 30 vol ethyl acetate and washed successively with an aqueous solution of sodium metabisulfite ($Na_2S_2O_5$ 0.15 kg in 15 L water) and 15 L water. An additional treatment with charcoal (Darco S51) was done. 56.37 kg of ethyl acetate solution was used for the next salification step.

Step 12. A part of the previous acetate solution of 5-((3-(carbamimidoylcarbamoyl)-5-(trifluoro-methyl)phenyl)ethynyl)-N-(pyridin-2-yl)-2-(trifluoromethyl)benzamide (0.958 kg, 1.844 mol,), which was estimated to be pure, was concentrated under a reduced pressure of 100 mbars and at 50 °C into 10 vol of ethyl acetate. An additional azeotropic drying was realized with 15 vol ethyl acetate. The obtained 10 vol solution was heated at 50 °C, and then a seeding with 2% of 5-((3-(carbamimidoylcarbamoyl)-5-(trifluoromethyl)phenyl)ethynyl)-N-(pyridin-2-yl)-2-(trifluorom-ethyl)-benzamide malonic acid was done. A solution of malonic acid (0.192 kg, 1.144 mol.) in 2.8 L ethyl acetate was added in 30 min at 50 °C. The dropping funnel was washed with 0.4 L ethyl acetate and crystallization was observed during the addition of the acid. Stirring was maintained for 1 h

at 50 °C and cooled to 10 °C at the rate of -20 °C/h. 5-((3-(carbamimidoylcarbamoyl)-5-(trifluoromethyl) phenyl)ethynyl)-N-(pyridin-2-yl)-2-(trifluoromethyl) benzamide malonic acid was isolated by a fast filtration and the cake was washed twice with 1 L ethyl acetate. The product was dried under nitrogen flux overnight to generate 5-((3-(carbamimidoylcarbamoyl)-5-(trifluoromethyl) phenyl)ethynyl)-N-(pyridin-2-yl)-2-(trifluoromethyl)benzamide malonic acid compound (1.096 kg, yield of 95.3%).

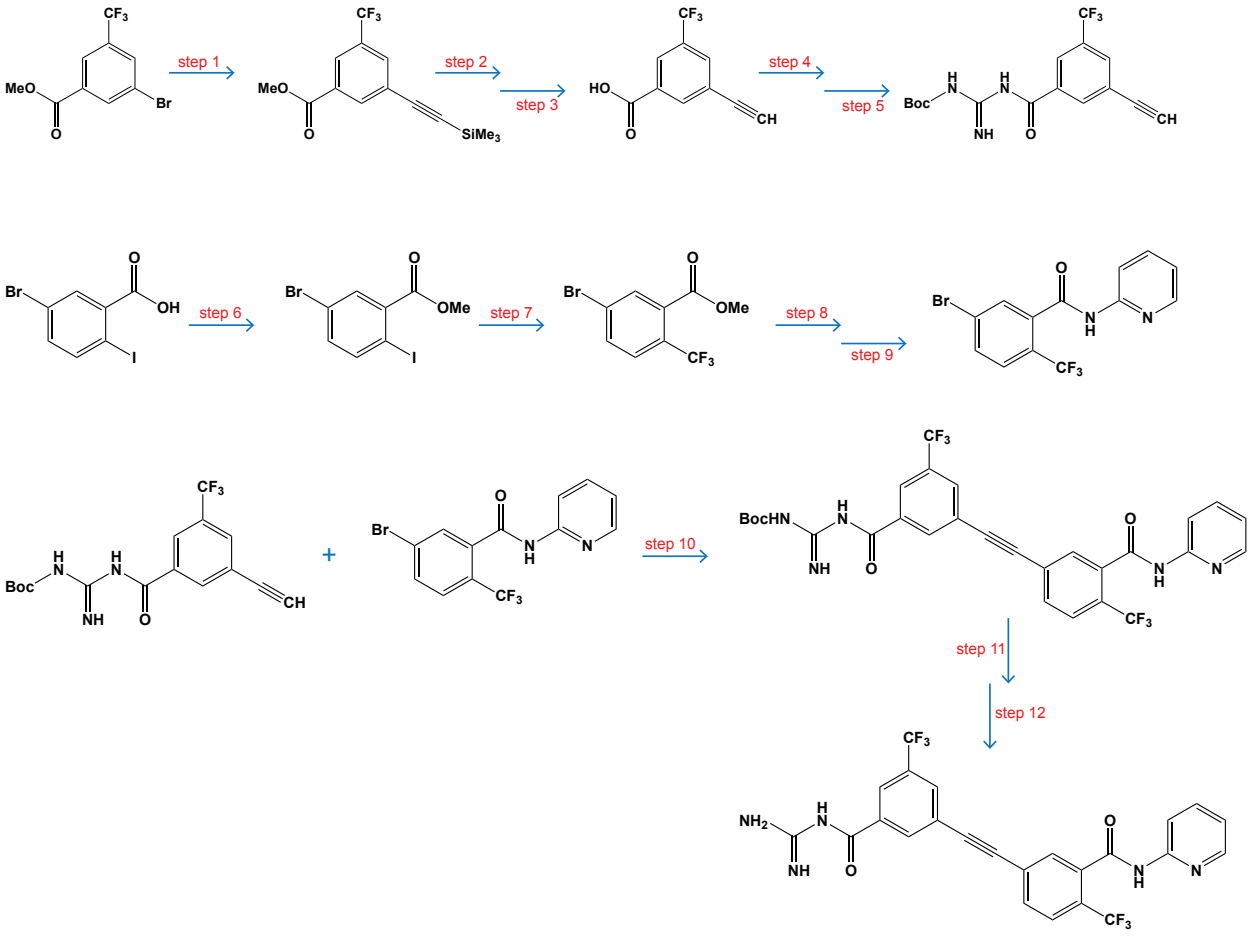

Fig. 2. 1. | Illustration of MMV688533 synthesis.

2.3.1.1. Nuclear magnetic resonance (NMR) and mass spectrometry (MS) analysis.

^{1}H NMR and ^{13}C NMR data were recorded on a Bruker 400MHz AVANCE series or Bruker300 MHz DPX Spectrometer with $CDCl_3$ or DMSO-d6 or CD3OD as solvent. ^{1}H chemical shifts were referenced at 7.26 ppm for $CDCl_3$, 2.5 ppm for DMSO-d6 and 3.3 ppm for CD3OD. ^{13}C chemical shifts were referenced at 77 ppm for $CDCl_3$, 39 ppm for DMSO-d6 and 44 ppm for CD3OD, and obtained with ^{1}H decoupling. Multiplicities are abbreviated as follows: singlet (s), doublet (d), triplet (t), quartet (q), doublet-doublet (dd), quintet (quint), sextet (sextet), septet (septet), multiplet (m), and broad (br).

MS data were measured on Agilent 1200/1260 Series LC/MSD mass spectrometer with the following settings. Column: Zorbax XDB C18 (50 × 4.6) mm, 5µm or Acquity BEH C18 (50 × 2,1 mm; 1.7 µm). Mobile phase: Solvent A: 0.1% Formic Acid in Milli-Q water (or) 0.1% Trifluoroacetic acid in Milli-Q-water. Solvent B: Acetonitrile. Flow rate: 1.5 mL/min. Injection Volume: 2 µL. Wavelength: Maximum chromatogram (210-400nm). Run time: 6.0 min. Ionization source: Multi-mode (ESI and APCI). Purity was measured on an Agilent 1200/1260 Series HPLC spectrometer. Column: C18 (250 × 4.6) mm, 5µm (or) C18 (150 × 4.6) mm, 5µm. Mobile phase: Solvent A: 10 mM ammonium acetate in Milli-Q water (or) 0.1% Trifluoroacetic acid in Milli-Q-water; Solvent B: Acetonitrile. Flow rate: 1.0mL/min. Injection Volume: 2 µL. Wavelength: Maximum chromatogram (210-400 nm). Run time: 30 min.

For compound 1c, MS data were measured with UPLC-SQD (Simple Quad, from Waters). Column: Acquity BEH C18 (50 × 2,1 mm; 1.7 µm). Mobile phase: Solvent A: H_2O+0.05%

TFA; Solvent B: CH_3CN+0.035% TFA. Flow rate; 1 mL/min. UV Detection: l = 220 nm. MS detection (Simple Quad) ionization: ESI + Electrospray First / Last Mass (uma) FS: 160 / 1200 uma. Capillary voltage (KV): 3.5.Cone. (V): 20. Source Temperature: 150°C. Desolvation temperature: 500°C. Desolvation gas flow (L/h): 1200. Cone gas flow (L/h): 100. LM 1 resolution: 13.00. HM1 resolution: 13.00. Ion energy1: 0.20.

For the intermediate 5-Bromo-2-iodo-benzoic acid methyl ester (step 6), LC-MS was measured as follows: Column: XBridge C18,4.6*50mm, 3.5 µm Mobile phase: 10 mM NH_4HCO_3 (A) / acetonitrile (B). Elution program: Gradient from 5 to 95% of B in 1.6 min at 1.8 mL/min. Temperature: 50ºC. Detection: UV (214, 4 nm). MS: ESI, Positve mode, 110 to 1000 amu.

2.3.2. Compound potency against *P. falciparum* and *P. vivax* parasites.

Antimalarial activity against resistant culture-adapted strains of *P. falciparum* and clinical field isolates was performed with the modified [^{3}H]-hypoxanthine incorporation assay, as previously reported [327]. MMV688533 (Sanofi, Toulouse, France) and the reference antimalarial drugs chloroquine, piperaquine, mefloquine, and artesunate (provided by the WWARN QA/QC Reference Material Programme), were prepared as 1 mg/mL stock solutions in dimethyl sulfoxide (DMSO) or H_2O according to the manufacturers' instructions. Drug plates were pre-dosed by diluting the compounds in 50% methanol followed by lyophilization and storage at 4 °C.

2.3.2.1. Field location and sample collection.

In Papua Indonesia, *Plasmodium* isolates were collected from patients attending malaria clinics in Timika, a region endemic for multidrug-resistant strains of *P. vivax* and *P. falciparum* [328,329]. Patients with symptomatic malaria were recruited into the study if singly infected with *P. falciparum* or *P. vivax*, with a parasitemia of between 2,000 and 80,000 parasites per µL, and a majority (>60%) of parasites present as rings. Venous blood (5 mL) was collected by venipuncture and host white blood cells were removed with Plasmodipur filters (EuroProxima B.V., The Netherlands). Packed infected RBCs were then used for *ex vivo* drug susceptibility assays. In Uganda, *Plasmodium* isolates were collected from patients aged 6 months or older presenting to the Tororo District Hospital, Tororo District, or Masafu Hospital in the Busia District, with a clinical syndrome suggestive of malaria and *Plasmodium falciparum* parasites identified in blood by microscopy. Informed consent was obtained from patients and/or primary care givers (depending on age).

2.3.2.2. *Ex vivo* drug susceptibility assays.

In Papua Indonesia, drug susceptibility was measured in *P. vivax* and *P. falciparum* isolates using a protocol modified from the WHO microtest [254,329,330]. In brief, 200 µL of a 2% hematocrit of blood media mixture, consisting of RPMI 1640 medium plus 10% AB^+ human serum for *P. falciparum* or McCoy's 5A medium plus 20% AB^+ human serum for *P. vivax* was added to each well of pre-dosed drug plates containing 11 serial concentrations (2-fold dilutions) of the test antimalarials (maximum concentration shown in brackets) chloroquine (2,993 nM), piperaquine (1,029 nM), mefloquine (338 nM), artesunate (49 nM), and MMV688533 (237 nM). A candle jar was used to mature the parasites at 37 °C for 35-56 h.

Incubations were stopped when >40% of the ring-stage parasites had reached the mature schizont stage in the drug-free control wells, as determined by light microscopy. Parasite growth was quantified by nucleic acid staining and parasitemias were measured using flow cytometry. Parasite growth was quantified for each drug concentration and normalized to the control well. The dose-response data were analyzed using nonlinear regression analysis and the half-maximal inhibition of growth (IC_{50}) values derived using an inhibitory sigmoid E_{max} model (*In Vitro* Analysis and Reporting Tool; IVART7). *Ex vivo* IC_{50} data were only used from predicted curves where the E_{max} and E_0 were within 15% of 100 and 1, respectively. The drug plate quality was assured by running schizont maturation assays with the *P. falciparum* chloroquine-resistant strain K1 and the chloroquine-sensitive strain FC27. For data quality control, raw flow cytometry values were analyzed by two independent operators and compared. If the raw dose-response data derived by the two operators led to a dramatic shift in IC_{50} estimates for any of the drugs, they were reviewed and adjusted by a third operator. Ethical approval for this study was obtained from the Eijkman Institute Research Ethics Commission of the Eijkman Institute for Molecular Biology, Jakarta, Indonesia; the Human Research Ethics Committee of the Northern Territory Department of Health & Families; and the Menzies School of Health Research, Darwin, Australia.

In Africa, drug susceptibility was measured in *P. vivax* and *P. falciparum* isolates using a protocol summarized as follows: All MMV compounds were dissolved in DMSO to a final concentration of 0.5-10 mM and stored at -20°C. On the day of assay, 2 µL of DMSO stocks drug were diluted in 498 µL complete RPMI media (RPMI 1640 medium

supplemented with 25 mM HEPES, 0.2% NaHCO3, 0.1 mM hypoxanthine, 100 µg/mL gentamicin, and 0.5% Albumax I [Invitrogen]). Diluted drugs were not stored for longer than 24 h. Drugs were serially diluted 3-fold in 96-well assay plates in complete media containing 0.4% DMSO, to a final volume of 50 µL, in columns 1-10. Column 11 contained drug-free controls while column 12 contained uninfected RBC controls. Parasitized whole blood samples were washed 3 times with RPMI (w/o Albumax) media at 37 °C and then resuspended in fresh RPMI media to a final hematocrit of 2%. 150 µL of the parasite culture was added to each well into the assay plate for final parameters of 0.2% parasitemia and 2% hematocrit. Plates were incubated for 72 h in a humidified modular incubator under a tri-gas mixture (5% O_2, 5% CO_2, 90% N_2) at 37 °C. Plates were then stained with SYBR Green I and fluorescence determined using a BMG Fluostar Optima plate reader at excitation 485 nm / emission 530 nm [331]. Fluorescence data were curve fitted to estimate IC_{50} values (GraphPad Prism 7). For each isolate, a Z' factor was calculated from drug-free positive and negative controls (8 parasitized RBC wells and 8 uninfected RBC wells, respectively).

2.3.3. Determination of the in vitro rate of killing (parasite reduction ratio, PRR).

As described in [332], the compound IC_{50} was determined via [^{3}H]-hypoxanthine incorporation. For PRR assays, 10^5 3D7A parasites cultures were exposed to MMV688533 at 10×IC_{50} for 120 h. Drug treatment was renewed every 24 h over the entire period. Parasite aliquots were taken from the treated cultures every 24 h, with drug washout, throughout the 5-day treatment period. Fresh RBC and new media were then added to the drug-free parasites, which were serially diluted in quadruplicate into 96 well plates. Growth in individual wells

was detected after 3 and 4 weeks using [^{3}H]-hypoxanthine incorporation. The number of viable parasites was determined by the dilution down to which growth was observed. The rate of killing was represented by the log of viable parasites as a function of treatment duration. PRR was defined as the log-linear reduction of viable parasites over 48 h.

2.3.4. Determination of efficacy and pharmacokinetic profiles in the *P. falciparum* SCID mouse model.

Immunodeficient female NSG or NOG mice were engrafted with a minimum of 40% human erythrocytes circulating in peripheral blood during the entire experiment. Each mouse was inoculated with a 50%-75% hematocrit erythrocyte suspension (Basque Center of Transfusion and Human Tissues, Galdakao, Spain and Bank of Blood and Tissues, Barcelona, Spain) in RPMI1640 medium, 25% (vol/vol) decomplemented human serum, 3.1 mM hypoxanthine. Intraperitoneal (i.p.) and/or intravenous (i.v., via tail lateral vein) injections were done once daily until the end of the drug administration period. Humanized NSG or NOG mice were infected with peripheral blood from CO_2-euthanized donor mice harboring 5-10% parasitemia. The humanized mice of the efficacy study were infected by inoculation of 0.3 mL of the infected-erythrocyte suspension by the lateral vein of the tail. For treatment, drug was administered at Day 1 (~1% patent parasitemia) (P0) by oral gavage (volume p.o. is 10 mL/kg body weight). To measure the therapeutic response, 2 µL peripheral tail blood from *P. falciparum*-infected mice were stained with TER-119-Phycoerythrine (marker of murine erythrocytes) and SYTO-16 (nucleic acid dye) and analyzed by flow cytometry (Attune NxT Acoustic Focusing Flow Cytometer, Invitrogen).

Drug effect on circulating *P. falciparum* Pf3D70087/N9 parasites was assessed by microscopy (Giemsa-stained blood smears; 2 µL blood samples taken at 48 h and 96 h).

To assess the drug concentrations in mice, 25 µL samples of peripheral blood were taken at different times (usually 0.5, 1, 2, 4, 6 or 8 h and 23 h after the first dosing), mixed with 25 µL of MilliQ H_2O and immediately frozen on a thermal block at -80º C. The treated mice that reached the limit of detection by standard flow cytometry (<0.01% from total circulating erythrocytes) were maintained until day 60 of the assay with a chimerism >50% of total circulating erythrocytes by regular injection of human erythrocytes every 3 or 4 days. During the follow up period, 2 µL blood samples were taken every 2 or 3 days and analyzed by flow cytometry with a limit of quantification of 0.1%. The first day of parasitemia detection was recorded. The mice were deemed cured (free of detectable parasite) if no recrudescence was detected by day 60.

As biological controls; a) parasite growth in untreated and/or vehicle-treated individuals was evaluated from day 1 to 5; b) the parasite burden was measured from day 1 to 5 of the assay in individuals treated with a fixed dose of a standard antimalarial; and c) the distribution of parasitemia at day 1 of the assay for all individual mice tested in the assay was compared to parasitemia distributions in previous experiments.

For data analysis, ED_{90} and AUC_{ED90} were defined and calculated according to [333]. ED_{90} is the effective dose in mg/kg that reduced parasitemia by 90% at day 5 compared to vehicle-treated mice. AUC_{ED90} is the average estimated daily exposure that reduced parasitemia

from peripheral blood at day 5 of the assay by 90% compared to vehicle-treated mice. The ED_{90} was calculated by fitting the variable Y= $\log_{10}$ [parasitemia at day 5 of the assay] and the variable X= $\log_{10}$ [dose level in mg/kg] defined as an ordered pair for every individual of the study. The AUC_{ED90} was calculated by fitting the variable Y= $\log_{10}$ [parasitemia at day 5 of the assay] and the variable X= $\log_{10}$ [AUC of compound during the first 23 h after the first drug administration, in ng·h/mL] defined as an ordered pair for every individual of the study. The equation used to fit the data is Y=Bottom + (Top-Bottom)/(1+10((LogED_{50}-X)×Hill Slope)). The ED_{90} and AUC_{ED90} were calculated by interpolation of the X value that corresponded to antilog10 [Y= "Top"-1] in each respective best fitted curve [333].

The time in days (te) and the average concentration in blood (C, in ng/mL) for killing all *P. falciparum* parasites in mice were interpolated from a multivariate logistic regression. The fitted function links the dichotomic response variable Therapeutic response (Tr), which takes Tri=0 if an individual shows recrudescence and Tri=1 if no recrudescence was detected at day 60 of the assay, and the explanatory variables te and C. These parameters offered direct empirical estimates of the time of exposure and concentration in blood to at least kill a defined number of circulating parasites, which was typically 10^8 per mouse. The regression formular is as follows: (Tr=1|te,)= 11+ $e-(\alpha+\beta 1te+\beta 2C)$.

Data analysis was performed using GraphPad Prism 7.0 (GraphPad Software), Excel 2016 (Microsoft) and R free software (https://www.r-project.org). Phoenix WinNonlin vers.7.0 (Certara) was used for PK Non-Compartmental Analysis. Animal experiments performed at TAD were approved by The Art of Discovery Institutional Animal Care and

Use Committee (TAD-IACUC). The Committee is certified by the Biscay County Government (Bizkaiko Foru Aldundia, Basque Country, Spain) to evaluate animal research projects from Spanish institutions according to point 43.3 from Royal Decree 53/2013, from the 1st of February (BOE-A-2013-1337). All experiments were carried out in accordance with European Directive 2010/63/EU. The results from the animal experiments are reported following ARRIVE guidelines. (https://www.nc3rs.org.uk/arrive-guidelines) except for disclosure of business trade confidential information.

2.3.4.1. Prediction of the efficacious dose in humans based on P. falciparum SCID mouse PK/PD.

The prediction of the first efficacious dose in human was based on: 1) minimum parasiticidal concentration (MPC) as evaluated from a population-based PK/PD modeling of experimental data from SCID mouse studies. At team at MMV used a NonMem software and another at Sanofi used a Monolix software to build a PK/PD model. Both teams reached a similar median estimate value of 20 ng/mL as the MPC; 2) K_{kill} of the compound as deduced from *in vitro* logPRR (5 in 48 h). However, a conservative approach was recommended by MMV to use a capped value of 3 based on values observed for endoperoxides when tested in human; 3) predicted human PK parameters as determined by an allometric approach. For the allometric scaling of clearance from animal data, two methods, Mahmood rules and Fixed exponent method, were used. These led to the prediction of a low to a very low MMV688533 clearance in humans 3.6 and 1.4 L/h respectively, that corresponded to a total clearance of < 5% of hepatic blood flow. This in turn corresponded to a predicted half-life of 103 h and 277 h respectively in

humans. The volume of distribution (Vdss) relying on allometry method with an exponent of 1, was predicted to be as large as 540 L for 70 kg human; 4) biopharmaceutical model (GastroPlus) used to estimate Fa% vs dose in human and verified on Rat & Dog PK data.

2.3.5. *P. falciparum* lines used for selections, drug assays and transfections.

Asexual blood-stage parasites were cultured at 3% hematocrit in O^+ human erythrocytes in RPMI-1640 medium supplemented with 50 µM hypoxanthine, 2.25 g/L $NaHCO_3$, 2 mM L-glutamine, 25 mM HEPES, 0.5% (w/v) AlbuMAXII (Invitrogen) and 10 µg/mL gentamycin at 37 °C in flasks gassed with 5% O_2/5% CO_2/90% N_2. The *P. falciparum* 3D7-A10 and Dd2-B2 clones used for the selections and drug assays, and the NF54attB line used to express *pfacg1*-eGFP and *pfehd*-3×HA, have been previously reported [189,271,334].

2.3.5.1. Parasite stage-specificity assays.

In vitro IC_{50} values were determined by incubating parasites for 72 h across a range of 10 different concentrations of antimalarial compounds plus two no-compound controls. Stage-specificity assays used a modified protocol with tightly-synchronized parasites tested at different starting stages of the ABS cycle [189].

2.3.5.2. *P. falciparum* resistance selections.

Single-step selections for MMV688533 resistance employed triplicate flasks of 2×10^9 Dd2-B2 parasites exposed to 5-14× the IC_{50} (25–80 nM) of MMV688533. Selections were

terminated after 60 days as resistant parasites had not emerged. Ramping selections used triplicate flasks of 2×10^8 3D7-A10 parasites exposed to MMV688533 at concentrations that increased gradually from 1-10× the IC_{50} (5.5–60 nM) over a six-month period. Resistant clones were obtained from the bulk cultures of the ramping selections by limiting dilution, and four clones were selected for whole-genome sequencing. MMV688533 growth inhibition was determined by staining the parasites with SYBR Green and MitoTracker Deep Red (Life Technologies) followed by flow cytometry (Accuri C6, BD Biosciences) [306]. IC_{50} values were derived from growth inhibition data using nonlinear regression (Prism 7, GraphPad). Unless stated otherwise, all drug assays were performed on at least four separate occasions (as biological repeats) with two technical replicates.

2.3.5.3. Genome editing.

Mutations in PfACG1 and PfEHD that were identified from the *in vitro* selections were validated by engineering them into the parental 3D7-A10 line using an “all-in-one” pDC2-based CRISPR/Cas9 plasmid ([335]). The Cas9 in this plasmid is derived from *Streptococcus pyogenes,* has been codon optimized for *P. falciparum,* and is under the expression of a calmodulin promoter. The plasmid also contains a human *dhfr* (h*dhfr*) selectable marker (that confers resistance to WR99210) under a PcDT promoter, and the sequence encoding the guide RNA (gRNA) under a U6 promoter. Guide RNAs were selected using the online tool ChopChop based on their proximity to the mutation of interest, GC content, and absence of poly A/T tracks (http://chopchop.cbu.uib.no). The gRNA primers were annealed with BbsI overhangs using PCR and cloned into a BbsI-linearized pDC2 CRISPR/Cas9 vector. The donor templates, also supplied on the same

plasmid, had >300bp of homology flanking the mutation of interest. These fragments were first amplified by PCR and cloned into pGEM-T vectors to introduce shield mutations by site-directed mutagenesis. Shielded donor fragments were then amplified by PCR and cloned into the EcoRI/AatII-linearized pDC2 CRISPR/Cas9 vector by In-Fusion cloning (Takara). Finally, the plasmids were midi-prepped for transfections.

Parasites were electroporated with purified circular plasmid DNA as described [318]. Briefly, a 2.5 mL culture of 3D7-A10 or sel. 533-CL1 (≥ 5% rings) was washed and resuspended in 220 μL 1× Cytomix. This mixture was then added to 50 μg of plasmid DNA and electroporated at a voltage of 0.31 kV and capacitance of 950 μF inside 2 mm gap cuvettes (Bio-Rad) using a Gene-Pulser (Bio-Rad) [319]. Starting one day after the transfections, the cultures were selected for six days with 2.5 nM WR99210 [320] and maintained thereafter in complete media until recrudescence. Gene editing was assessed via Sanger sequencing of blood PCR (Bioline) from bulk cultures. Edited parasite clones were obtained by limiting dilution. The parasites were then assayed for resistance to MMV688533 using flow cytometry.

Both the mycobacteriophage Bxb1 serine integrase system [319] and CRISPR/Cas9 gene editing tools were used to generate the doubly-tagged parasite line expressing PfACG1-eGFP and PfEHD-3×HA fusion proteins. Briefly, NF54attB parasites [334] were first co-transfected with an integrase-expressing plasmid pINT and a donor attP-containing plasmid pDC2-*pfacg1*-eGFP. This donor plasmid also contained a blasticidin S-deaminase (BSD) selectable marker that confers resistance to blasticidin hydrochloride [336]. The integrase plasmid pINT contained a Neomycin selectable marker that confers

resistance to geneticin (G418; [337]. Transfections were done as described above and the cultures maintained in 250 µg/mL G418 + 2 µg/mL BSD media for six days post-transfection, followed by 2µg/mL BSD media until recrudescence. Sorbitol-synchronized eGFP-tagged ring-stage clonal parasites obtained by limiting dilution were then transfected with the codon-optimized all-in-one plasmid containing a 1.1kb *pfehd* donor fragment consisting of two 3' homology sequences flanking the 3×HA tag. These transfections were selected with 2.5 nM WR99210 until recrudescence. Successful gene tagging was confirmed via PCR, Sanger sequencing and immunofluorescence assays.

2.3.6. Conditional knock-down (cKD) parasite studies.

2.3.6.1. Generation of cKD parasite lines.

To investigate the interaction between MMV688533 and PfACG1 and PfEHD genes, we utilized CRISPR/Cas9 to generate parasite cell lines stably expressing the TetR-DOZI-RNA aptamer module for conditional regulation of target gene expression. These transgenic lines also contained the reporter construct *Renilla* luciferase (RLuc), the selection marker Blasticidin-S deaminase, and a C-terminal 2×HA epitope tag [322]. To construct the donor plasmids, PCR-amplified right homology regions (RHR) and BioXP3200 System-synthesized DNA fragments corresponding to the left homology regions (LHR) fused to the re-codonized 3'-end of each target genes, as well as the target specifying guide RNA sequences, were cloned via Gibson assembly into the pSN054 linear vector [321]. The final constructs were confirmed by restriction digests and Sanger sequencing. Transfections into Cas9- and T7 RNA polymerase-expressing NF54 parasites were carried out by preloading erythrocytes with the donor plasmids as

described previously [323]. Cultures were maintained in 500 nM anhydrotetracycline (aTc; Sigma-Aldrich 37919) and 2.5 μg/mL of Blasticidin-S (RPI Corp B12150-0.1). Parasite cell lines stably integrating the donor plasmids were monitored via Giemsa smears and RLuc measurements.

2.3.6.2. Western blotting of cKD parasite lines.

PfACG1 and PfEHD cKD parasites were cultured with 50 nM aTc or without aTc to maintain and downregulated protein expression, respectively. Proteins were then extracted after 72 h via saponin lysis and resuspended in lysis buffer that consists of 4% SDS and 0.5% Triton X-114 in 1×PBS. Proteins were separated on Mini-PROTEAN TGX precast gels (4-15% gradient) in tris-glycine buffer, transferred to a polyvinylidene fluoride (PVDF) membrane using the Mini Trans-Blot Electrophoretic Transfer Cell system, and blocked with 100 mg/mL skim milk in TBS/Tween. Membrane-bound proteins were probed with mouse anti-HA (1:3000; Sigma H3663) and rabbit anti-GAPDH (1:5000; Abcam AB9485) primary antibodies, and anti-mouse (1:5000; Thermo Fisher Scientific 62-6520) and anti-rabbit (1:5000; Cell signaling 7074S) horseradish peroxidase (HRP)-conjugated secondary antibodies. Following incubation in SuperSignal West Pico Chemiluminescent substrate (Thermo Fisher Scientific PI34080), protein blots were imaged and analyzed using the ChemiDoc MP System and Image Lab 5.2.0 (Bio-Rad).

2.3.6.3. cKD proliferation assays.

To assess the effect of conditionally perturbing PfACG1 and PfEHD expression on parasite growth, synchronous ring-stage parasites cultured in the presence (50 and 3 nM) or absence of aTc were cultured in triplicate in a 96-well U-bottom plate (Corning 62406-121). Luminescence signals were taken at 0, 72, and 120 h post-invasion using the Renilla-Glo(R) Luciferase Assay System (Promega E2750) and the GloMax Discover Multimode Microplate Reader (Promega). The luminescence values in the knockdown conditions were normalized to aTc-treated (100% growth) and chloroquine-treated (200 nM) samples (no growth) as controls and results were analyzed using GraphPad Prism (version 8; GraphPad Software).

2.3.6.4. Compound susceptibility assays with cKD parasite lines.

A stock solution of MMV688533 was dispensed into 96-well U-bottom plates and serially diluted in complete medium to yield final concentrations ranging from 0.3-160 nM. Synchronous ring-stage PfACG1 and PfEHD cKD parasite lines as well as a control cell line expressing an aptamer-regulatable fluorescent protein were maintained in the presence (500 nM) or absence of aTc and were distributed into the drug plates. DMSO- and chloroquine-treated samples (200 nM) served as reference controls. Luminescence was measured after 72 h as described above and EC_{50} values were obtained from corrected dose-response curves using GraphPad Prism.

2.3.7. Whole-genome sequencing analysis.

The 3D7-A10 parent and MMV688533-resistant clones were subjected to whole-genome sequencing using an Illumina TruSeq DNA PCR-Free library preparation protocol and a MiSeq sequencing platform, as described [57].

2.3.8. Immunofluorescence assays.

Indirect IFA studies were performed in suspension. Cells were fixed in 4% (v/v) formaldehyde (Thermo Fisher Scientific) for 1 h at room temperature. followed by a second fixation step supplementing the 4% formaldehyde solution with 1 mM cysteine and $CaCl_2$ and subsequent incubation overnight at 4 °C. Cells were then permeabilized on ice using 0.05% Triton X-100 in 1×PBS for 5 min. Autofluorescence was quenched using a 50 mM glycine treatment for 10 min. After two washes in 1× PBS the cells were resuspended in 1% (w/v) bovine serum albumin (BSA) in 1×PBS blocking buffer and were then incubated with the appropriate dilution for each primary antibody used (1:200 for rabbit anti-ERD2 (BEI Recourses), anti-PMT (kindly provided by Choukri Ben Mamoun), anti-PDI (mouse anti-PDI (1D3), Enzo Life Sciences), rabbit or mouse anti-GFP (Takara (Clontech), Roche), rabbit anti-HA antibodies (Sigma), 1:50 for rabbit anti-Rab5A, Rab5C, or Rab11A, rat anti-Rab5B or Rab7 (kindly provided by Gordon Langsley), 1:200 for anti-coronin (kindly provided by Jake Baum), 1:200 for anti-ACP (kindly provided by Geoffrey McFadden), 1:200 for anti-K13 [193], 1:200 for anti-PfCRT antibodies [41] followed by incubation with corresponding species-specific secondary antibodies (Alexa Fluor 488-, 594- or 647- conjugated goat anti mouse or rabbit antibodies; Thermo Fisher) diluted 1:2000 in 1% BSA in 1× PBS. MitoTracker Red CMXRos (Thermo Fisher) was used to

stain mitochondria. HCS LipidTOX Deep Red Neutral Lipid Stain and Nile Red (Invitrogen) were used to stain neutral lipid bodies according to the protocol provided by the manufacturer. Thin blood smears of stained RBCs were prepared on microscope slides and mounted with cover slips using Prolong Diamond Antifade Mountant with DAPI (Thermo Fisher). Parasites were imaged using a Nikon Eclipse Ti-E wide-field microscope equipped with a sCMOS camera (Andor) and a Plan-apochromate oil immersion objective with 100× magnification (1.4 numerical aperture). A minimum of 27 Z stacks (0.2 µm step size) were photographed for each parasitized RBC. NIS-Elements imaging software (Version 5.02, Nikon) was used to control the microscope and camera as well as to deconvolve the images (using 25 iterations of the Richardson-Lucy algorithm for each image) and perform 3D reconstructions [193]. ImageJ (Fiji) (version 2.0.0-rc-68/1.52 h) was used to crop the images, adjust brightness and intensity, overlay channels and prepare montages.

2.3.9. Evaluation of genotoxicity.

Salmonella typhimurium test strains including the mixed strains TA7001 and TA7006 for detection of base-pair substitutions and TA98 strain for detection of frameshift mutations were used for genotoxicity testing (Ames test). MMV688533 was cytotoxic starting at 300 µg/mL in mixed and TA98 strains in the absence of metabolic activation. Cytotoxicity was also noted in the presence of metabolic activation starting from 100 µg/mL in TA98 strain and from 1000 µg/mL in mixed strains. Under the conditions of the test, MMV688533 was classified as non-mutagenic.

L5178Y and TK6 cells were used for *in vitro* micronucleus test to investigate the clastogenicity/aneugenicity potential of MMV688533. There was no statistically significant increase in the number of micronuclei as compared to the solvent control with or without metabolic activation. MMV688533 was therefore deemed non-clastogenic/aneugenic.

2.3.10. Pharmacokinetic studies in mice, rats and dogs.

Pharmacokinetic studies in mice were performed following a single intravenous (3 mg/kg) or oral (3.5, 10 and 30 mg/kg) administration of MMV688533 to male Swiss mice (3 dosed intravenous (i.v.) and 3 per os (p.o.)). Feeding was performed *ad libitum*. Vehicles / Formulations were at 0.6 mg/mL in PEG200/Solutol/G5% (20%/5%/75%) for i.v. solution and at 0.3, 1 and 3 mg/mL in Methylcellulose /Tween 80 (0.6%/0.5%) for p.o. suspensions in water. Administration modes were i.v. 3 mg/kg, 5 mL/kg and p.o. 3.5, 10 and 30 mg/kg,10 mL/kg. Matrix and Sampling times were for i.v. plasma and lung / 0.083, 0.5, 1, 2, 4, 6, 8 and 24 h and for p.o plasma (only at 10 mg/kg), blood, liver and lung / 0.25, 0.5, 1, 2, 4, 6, 8 and 24 h. The analytical method was LC-MS/MS with a lower limit(s) of quantification 2 ng/mL for plasma, 5 ng/mL for blood and 6 ng/g for tissues. PK analysis were performed using non-compartmental models (Plasma, IV bolus and Plasma, Extravascular) Phoenix (WinNonLin version 6.4)

In rats, the PK studies were performed following a single intravenous (3 mg/kg) or oral (10 mg/kg) administration to male Sprague-Dawley rats. The procedure was as described above but for the following exception: The rats were not fasted and the oral volume of administration of 10 mg/kg was 10 mL/kg Matrix. The sampling times for i.v. blood were

0.083, 0.25, 0.5, 1, 2, 4, 7, 24 and 48 h and for p.o. blood 0.5, 1, 2, 4, 7, 24 and 48 h. PK analysis was performed using a the 200-202, IV bolus and Extravascular non-compartmental models.

In dogs, the PK of MMV688533 was performed following a single 2 mg/kg intravenous administration of the compound to female Beagle dogs that were fasted overnight. The vehicle / formulation solution was at 2 mg/mL PEG400/Ethanol/Solutol HS15/G5 % (20/5/5/70) pH 3. For administration, i.v. was the preferred route (2 mg/kg, 1 mL/kg). Matrix and sampling times were blood at 0.083, 0.25, 0.5, 1, 2, 4, 6, 8, 24, 30, 48 and 72 h. The limit of quantification was 1 ng/mL. MMV688533 following a single oral dose of 0.5 mg/kg was also administered as malonate salt in a capsule or oral solution to male Beagle pentagastrin-dogs weighing 8.6 to 10.8 kg. 3 males per dose were dosed p.o, and serial sampling was applied. Feeding conditions were fasted overnight and fed 4 h post dosing. Vehicles / Formulations were capsule (MMV688533/microcrystalline cellulose/ croscarmellose sodium (5/91.67/3.33) followed by 50 mL of water. Solution at 0.25 mg/mL in PEG400/Ethanol/Solutol/G5% (20/5/7.5/67.5). Administration mode was p.o. 0.5 mg/kg (active compound), 2 mL/kg for solution. Matrix and sampling times were blood at 0.25, 0.5, 1, 2, 4, 6, 24, 48, 72 and 168 h. Limit of quantification was 0.833 ng/mL for MMV688533.

2.3.11. Safety pharmacology profiling.

2.3.11.1. Preliminary non-clinical toxicology studies in rats.

Two-week toxicity studies in rats were conducted to evaluate the potential toxicity of MMV688533 (malonate form) when administered once daily for 15 days to Sprague Dawley rats by the oral route (gavage). Four study groups, each composed of 5 male and 5 female Sprague Dawley rats, were given MMV688533 at 12.5, 25 or 50 mg/kg/day or vehicle alone [0.5% (w/w) Polysorbate 80 and 0.6% (w/w) methylcellulose in water], once daily for 15 consecutive days, under a dose-volume of 5 mL/kg. In addition, 3 satellite rats/sex/group were included in the study. These rats received the test item in the same conditions as principal animals and were used for toxicokinetic studies. Parameters evaluated included mortality, clinical signs, body weight, and food consumption. Blood samples for hematology, coagulation and clinical chemistry were collected from all principal animals on day 3 and at necropsy. Blood samples for toxicokinetic determinations were obtained from satellite animals at 1, 2, 4, 7 and 24 h after dosing on day 1, as well as 1, 2, 4, 7, 24, 48 and 96 h after dosing on day 14. Control animals were sampled at 4 and 24 h after dosing on both days. At necropsy, all study animals were observed for any macroscopic post-mortem examinations, and weights of selected organs were recorded. Representative tissue samples at 50 mg/kg/day and in controls were histologically examined. Tissues with suspected compound-related microscopic findings were also evaluated microscopically for rats in the lower dose groups.

2.3.11.2. Preliminary non-clinical toxicology studies in dogs.

Two male and two female beagle dogs were given MMV688533 (malonate form) at 10, 30 or 100 mg/kg/day, or the vehicle alone [0.5% (w/w) Polysorbate 80 and 0.6% (w/w) methylcellulose in water], once a day for 15 consecutive days, under a dose-volume of 5 mL/kg. Animals of all groups were treated for 15 days, except for those at 100 mg/kg/day, which were euthanized prematurely after 11 and 10 administrations, respectively for males and females, for ethical reasons. Parameters evaluated included mortality, clinical signs, body weights and food consumption. Blood samples for hematology, coagulation and clinical chemistry analyses were collected once during the pretest period and on Days 3 and 8 (all animals), and on Day 14 (groups 1, 2 and 3). Urine samples for chemistry analyses were collected once during the pretest period (all animals) and on Day 14 (groups 1, 2 and 3). At necropsy [Day 10 (group 4 females) or 11 (group 4 males), or Day 16 for group 1, 2 and 3 animals], all study animals were observed for any macroscopic post-mortem examinations, and weights of selected organs were recorded and representative tissue samples were examined. In addition, the toxicokinetic profiles of MMV688533 and its main metabolite MMV893023 were determined from blood samples collected on Day 1 (all animals) and on Day 15 (groups 1, 2 and 3) at 1, 2, 4, 7 and 24 hours post-dosing. For group 4 animals, blood samples for TK determinations were collected on Day 11 for the males or on Day 10 for the females, before dosing, and 1 and 2 hours post-dosing.

2.3.11.3. *Ex vivo* rabbit Purkinje fibers cardiovascular study.

This study was designed to evaluate the cardiac cellular electrophysiological effects of MMV688533 on the action potential parameters in isolated rabbit Purkinje fibers.

MMV688533 was tested at 0.1, 1.4, 4.9 and 6.4 µmol/L corresponding to 0.05, 0.7, 2.5 and 3.3 µg/mL of active ingredient, respectively. The effects of the active MMV688533 metabolite RA11263363A on resting membrane potential and action potential parameters recorded from isolated rabbit Purkinje fibers (male, New Zealand rabbits; 1.3 to 1.5 kg; 7-10 weeks of age) were evaluated through a microelectrode technique. The following parameters were measured: resting potential (RP in mV), amplitude (APA in mV), maximal rate of rise of action potential (Vmax in V/s) and the action potential duration at 50 and 90% of repolarization (APD50 and APD90 in ms). The fibers were superfused with an oxygenated physiological solution containing 120 mM NaCl; 4 mM KCl; 1 mM $MgCl_2$; 1.8 mM NaH_2PO_4; 25 mM $NaHCO_3$; 11 mM glucose; 1.8 mM $CaCl_2$; pH = 7.4, at 36±1°C. RA11263363A (592.3 g/mol, salt form and 519.4 g/mol, base form, batch CLT.CBN1.039.1) was first dissolved into DMSO to obtain a 12 mM stock solution. This solution was further diluted with 100% DMSO to obtain solutions at 4, 1.2 and 0.12 mM. These four solutions (0.12, 1.2, 4 and 12 mM) were added into the physiological solution to obtain the appropriate nominal concentrations of 0.3, 3, 10 and 30 µM, which corresponded to 0.2, 1.6, 5.2 and 15.6 µg/mL of active ingredient respectively. The final concentration of DMSO in the test formulation was kept constant at 0.25% (v/v) in the physiological solution. Purkinje fibers (n=3) were first superfused by the physiological solution. After a 30-minute control period, test compound was evaluated at increasing concentrations sequentially applied, every 30 minutes. For each tested concentration, the fibers were stimulated at the basal rate of 1 pulse per second (1 Hz). In addition, stimulation rate was decreased from 1 pulse per second (1 Hz) to 1 pulse every 4 seconds (0.25 Hz) for 3 minutes, increased again to 1 pulse per second for 1 minute and finally increased to 3 pulses per second (3 Hz) for 2

additional minutes (between the 19th and the 25th minute). The low stimulation rate was used to favor the occurrence of abnormal electrical events during the repolarization phase of the action potential and to facilitate the development of Early After Depolarization's (EADs). The high stimulation rate was used to evaluate the use-dependent sodium channel blockade. After the highest concentration, the physiological solution was superfused again to evaluate the reversibility of the drug effect (washout).

2.3.11.4. *In vivo* anaesthetized guinea pig cardiovascular study.

The purpose of this study was to assess the potential effects on cardiovascular parameters of continuous intravenous (IV) administration of MMV688533 chlorhydrate to anesthetized guinea pigs, when tested at cumulative doses of 10, 20 and 30 mg/kg. Each dose was successively administered as a 15-min infusion/dose. Blood concentrations of MMV688533 were also assessed. An aqueous solution of ethanol/solutol/NaCl (10% / 5% / 85%, v/v/v) was used for the study. Cardiovascular functions were evaluated by measuring hemodynamic parameters like arterial blood pressure (BP) and heart rate (HR), and electrocardiographic (ECG) parameters.

Animals were premedicated with buprenorphine (0.05 mg/kg intramuscular) ~30 min prior to surgery and anesthesia maintained under isoflurane (2-5%) and constant O_2 flux (0.7 – 1.3 mL/min). Under deep anesthesia, lidocaine was injected subcutaneously at sites of the tracheotomy and insertion of electrocardiogram needles, and a tracheotomy performed to allow mechanical ventilation followed by carotid (arterial measurements) and jugular (infusion of control article or test article) catheterizations. Administration of Ringer lactate

solution (5 mL/ kg intraperitoneal), heated to body temperature to compensate for the hydric loss inherent to anesthesia, was performed at the discretion of the study director according to major bleeding surgery or signal instability (information documented in study records). BP and ECG parameters were recorded in anesthetized guinea pigs placed on a heating pad. Systemic BP was recorded using an independent catheter pressure transducer (MillarTM equipment) introduced into the carotid artery. The standard ECG (one lead derivation among L1 or L2 or L3) was recorded using four subcutaneously-placed needle electrodes to provide an optimal separation of T wave from P wave of the next complex. Once satisfactory in terms of their quality and stability, the signals were recorded for 15 minutes (corresponding to the stability period). Thereafter a set of animals (group T2) received a NaCl infusion (starting at T0 min) followed by RA11263363A at cumulative doses of 10, 20 and 30 mg/kg. Each infusion was delivered every 15 minutes at a rate of 0.3 mL/kg/min, with the last infusion followed by a period of recovery.

At the end of the recovery period (T75 min) one single arterial blood sample (~0.2 mL) was collected from the abdominal artery. A second set of animals (group T1) was infused with the control article in the same experimental conditions without the terminal blood sampling. A last set (group T3) was dedicated to evaluating pharmacokinetic (PK) parameters in which animals fitted with a jugular catheter (for RA11263363A infusion) and a carotid catheter (arterial blood sampling) were treated in the same experimental conditions as those described for the group T2. At the end of each 15-min period of infusion a blood sample (~0.2 mL) was collected. This was also done during the recovery period at 5, 10 and 75 min. Each volume of blood collected was immediately replaced by an equivalent volume of

Ringer lactate solution. Of note, in group T3, at the end of the recovery period (T75 min) arterial blood (~0.2 mL) was sampled and was compared to the corresponding sample in group T2. All blood samples (0.2 mL) were collected with sodium heparinate as anticoagulant and placed on wet ice immediately after collection. Then all samples were stored at -20°C until analysis. Thereafter the animals were euthanized by IV or intra-cardiac overdose of sodium pentobarbital.

2.3.12. Patch Clamp electrophysiological hERG assay.

2.3.12.1. Cell culture procedure.

HEK293 cells were stably transfected with hERG cDNA. Stable transfectants were selected by co-expression with the Geneticin (G418)-resistance gene incorporated into the expression plasmid. Selection pressure was maintained by including G418 in the culture medium. Cells were cultured in Dulbecco's Modified Eagle Medium / Nutrient Mixture F-12 (D-MEM/F-12) supplemented with 10% fetal bovine serum, 100 U/mL penicillin G sodium, 100 µg/mL streptomycin sulfate and 500 µg/mL G418.

2.3.12.2. Electrophysiological Procedures.

Cells were transferred to the recording chamber and superfused with vehicle control solution. Micropipette solution for whole cell patch clamp recordings was composed of: 130 mM potassium aspartate; 5mM $MgCl_2$; 5mM EGTA; 4mM ATP; 10mM HEPES. The pH was adjusted to 7.2 with KOH. Micropipette solution was prepared in batches, aliquoted, frozen for storage and a fresh aliquot thawed each day. The recording was performed at a temperature of 33-35 ºC using a combination of in-line solution pre-heater, chamber heater

and feedback temperature controller. Temperature was measured using a thermistor probe in the recording chamber. Micropipettes for patch clamp recording were made from glass capillary tubing using a P-97 (Sutter Instruments, Novato, CA) or PC-10 (Narshige, Amityville, NY) micropipette puller. A commercial patch clamp amplifier (PC-505B from Warner Instruments, Hamden CT) was used for whole cell recordings. Before digitization, current records were low-pass filtered at one-fifth of the sampling frequency.

2.3.12.3. Experimental Procedures.

Cells stably expressing hERG were held at -80 mV. Onset and steady state inhibition of hERG potassium current due to MMV688533 were measured using a pulse pattern with fixed amplitudes (conditioning prepulse +20 mV for 1 s; repolarizing test ramp to -80 mV (-0.5 V/s) repeated at 5 s intervals). Each recording ended with a final application of a supramaximal concentration of the reference substance (E-4031, 500 nM) to assess the contribution of endogenous currents. The remaining uninhibited current was subtracted off-line digitally from the data to determine the potency of the test substance for hERG inhibition. MMV688533 was tested at 1 μM in three cells (n = 3). Inhibitory effects on hERG potassium current amplitude of 17.9, 11.5 and 12.4% were observed. Based on these results and the solubility limit of the test article in the vehicle, additional nominal concentrations (0.3 and 3 μM; Protocol Amendment No. 1) were selected to evaluate the concentration-response relationship. One or more test article concentrations were applied sequentially (without washout between test substance concentrations) in ascending order, to each cell (n ≥ 3). Peak current was measured during the test ramp. A steady state was

maintained for at least 20 s before applying test article or positive control. Peak current was measured until a new steady state was achieved.

Chapter 3. Combining stage specificity and metabolomic profiling to advance antimalarial drug discovery

James M. Murithi[1], Edward S. Owen[2], Eva S. Istvan[3], Marcus C.S. Lee[4], Sabine Otillie[5], Kelly Chibale[6,7], Daniel E. Goldberg[3], Elizabeth A. Winzeler[5], Manuel Llinás[2,8,9], David A. Fidock[1,10,¶], Manu Vanaerschot[1]

[1]Department of Microbiology and Immunology, Columbia University Irving Medical Center, New York, NY 10032, USA. [2]Department of Biochemistry and Molecular Biology, Pennsylvania State University, University Park, PA 16802, USA. [3]Department of Medicine, Division of Infectious Diseases, and Department of Molecular Microbiology, Washington University School of Medicine, Saint Louis 63130, USA. [4]Parasites and Microbes Programme, Wellcome Sanger Institute, Wellcome Genome Campus, Hinxton, Cambridgeshire CB10 1SA, UK. [5]School of Medicine, University of California San Diego (UCSD), La Jolla, CA 92093, USA. [6]Drug Discovery and Development Centre (H3D), University of Cape Town, Rondebosch 7701, South Africa. [7]South African Medical Research Council Drug Discovery and Development Research Unit, Department of Chemistry & Institute of Infectious Disease and Molecular Medicine, University of Cape Town, Rondebosch 7701, South Africa. [8]Department of Chemistry, Pennsylvania State University, University Park, PA 16802, USA. [9]Huck Center for Malaria Research, Pennsylvania State University, University Park, PA 16802, USA. [10]Division of Infectious Diseases, Department of Medicine, Columbia University Irving Medical Center, New York, NY 10032, USA.

Author contributions

J.M.M. and M.V. designed and performed stage-specificity assays and analyzed the results. E.S.O. and M.L. designed metabolomic experiments, which were performed by E.S.O. and analyzed by E.S.O. and M.L. E.S.I. and M.C.S.L. performed resistance selections. S.O. sourced the compounds. J.M.M., M.V., E.S.O., M.L. and D.A.F. integrated the different datasets. M.V., D.A.F., E.A.W., D.E.G. and M.L. coordinated

individual lab efforts. J.M.M., M.V., E.S.O. and D.A.F. wrote the manuscript, which was approved by all authors.

Note: This chapter is reproduced and adapted from: **James M. Murithi**, Edward S. Owen, Eva S. Istvan, Marcus C.S. Lee, Sabine Otillie, Kelly Chibale, Daniel E. Goldberg, Elizabeth A. Winzeler, Manuel Llinás, David A. Fidock, Manu Vanaerschot "Combining Stage Specificity and Metabolomic Profiling to Advance Antimalarial Drug Discovery" (2020) ***Cell Chemical Biology*** (Vol. 27, Issue 2, Pages 158-171).

I generated: **50%** of the data in **Figs. 3.1-3.6, 3.10** and **Tables 3.1-3.2**; **100%** of the data in **Fig. 3.11** and **Table 3.3**. Data in Fig. 3.7 were generated by colleagues at Pennsylvania State University.

3.1. Abstract

We report detailed susceptibility profiling of asexual blood stages of the malaria parasite *Plasmodium falciparum* to clinical and experimental antimalarials, combined with metabolomic fingerprinting. Results revealed a variety of stage-specific and metabolic profiles that differentiated the modes of action of clinical antimalarials including chloroquine, piperaquine, lumefantrine and mefloquine, and identified late trophozoite-specific peak activity and stage-specific biphasic dose-responses for the mitochondrial inhibitors DSM265 and atovaquone. We also identified experimental antimalarials hitting previously unexplored druggable pathways as reflected by their unique stage-specificity and/or metabolic profiles. These included several ring-active compounds, ones affecting hemoglobin catabolism through distinct pathways, and mitochondrial inhibitors with lower propensities for resistance than either DSM265 or atovaquone. This approach, also applicable to other microbes that undergo multiple differentiation steps, provides an effective tool to prioritize compounds for further development within the context of combination therapies.

3.2. Introduction

Malaria caused by the protozoan parasite *Plasmodium falciparum* remains a major public health menace, especially in young children in sub-Saharan Africa [338]. When an individual is bitten by a *Plasmodium*-infected mosquito, the parasite first replicates in hepatocytes and then initiates ~48 h cycles of red blood cell (RBC) infection. In these RBCs, the parasite develops inside a parasitophorous vacuole, progressing from a ring into a highly metabolically active trophozoite and then a multinucleated schizont that yields 8-24

merozoites generated through asexual replication. Upon egress from the lysed host RBC, these merozoites infect new RBCs, with parasites capable of infecting up to 10-20% of RBCs in an immunologically naïve host [339].

Chemotherapy remains a major pillar in the fight against malaria, alongside vector control, diagnosis and access to treatment. The former first-line antimalarials chloroquine and sulfadoxine-pyrimethamine mainly affected trophozoites by inhibiting the hemoglobin catabolism pathway that provides nutrients for the parasite and the folate biosynthesis pathway that delivers the building blocks for DNA synthesis, respectively [41]. KAI407, a phosphatidylinositol 4-kinase (PI4K) inhibitor, is one of the more recent candidate antimalarials that specifically inhibit schizont development [61]. These drugs mostly target trophozoites and schizonts, which sequester in the microvasculature [340]. Compounds targeting ring stages, which circulate throughout the blood stream, are desirable to prevent further vasculature blockage. Artemisinins were the first clinical antimalarials with ring-stage activity and artemisinin-based combination therapies have proven effective in reducing the malaria death and case load [338]. However, parasites resistant to artemisinins and their partner drugs have emerged and are now undermining malaria control [294,341]. The discovery of antimalarials that hit novel targets and are active against multiple asexual blood stages, including rings, is thus of paramount importance.

Thousands of antimalarials with submicromolar potency have been identified in high-throughput whole-cell screens [234-236,342-345], but target identification forms a major bottleneck for their further development into leads with increased target binding,

selectivity, and whole-cell activity [346]. Metabolomic analysis of biochemical pathways affected upon compound exposure recently identified the mode of action of various candidate antimalarials from the Medicines for Malaria Venture Malaria Box [260], and is a valuable tool to interrogate new screening hits. Combining this approach with other phenotypic assays can help explore the activity profile and therapeutic potential of candidate antimalarials.

The Malaria Drug Accelerator (MalDA) consortium aims to identify new antimalarial leads through *in vitro* phenotypic screens and the identification of novel assayable targets [233,343]. Within this context, we developed an assay that compares the stage-specific susceptibility of *P. falciparum* asexual blood stage parasites and combined this with metabolomic profiling.

3.3. Results

We designed a medium-throughput *in vitro* assay to quantitatively assess the susceptibility of the distinct stages of *P. falciparum* intra-erythrocytic development. Highly-synchronized 3D7-A10 parasites (that have an accelerated 40 h asexual blood stage cycle) were exposed to a range of compound concentrations for 8 h during the early ring, late ring, early trophozoite, late trophozoite, and schizont stages (**Fig. 3.1A**). Assays were performed in 96 well plates, with a maximum in-well DMSO concentration of 0.35%. Cultures were continued to allow parasites to further develop in the absence of compound, extending through to invasion of new RBCs and development until the trophozoite stage. The total assay duration was 60 h. Parasites were stained with SYBR

Green and Mitotracker Deep Red and quantified by flow cytometry. Half-maximal inhibitory concentrations (IC_{50}) were derived by non-linear regression analyses of the dose-response data. The IC_{50} value based on these 8 h exposures at specific asexual blood stages is referred to as the IC_{50}^{8h}, while the IC_{50} calculated from the standard 72 h exposure assay is the IC_{50}^{72h}.

Light microscopy confirmed that the different periods of exposure corresponded to the different developmental stages and showed that the 32-40 h timepoint spanned schizont development, parasite egress and reinvasion (**Fig. 3.1A**), indicating that all asexual blood stages were profiled. The assay was further validated by the stage-specific susceptibility profiles of dihydroartemisinin, chloroquine and KAI407 that showed the expected peak activity on early rings, rings and trophozoites, and schizonts, respectively [41,347] (**Fig. 3.1B**). The 35-fold difference in IC_{50}^{8h} between schizonts and late trophozoites for KAI407 (**Table 3.1**) highlighted the tight synchronization of parasites that is crucial for this assay.

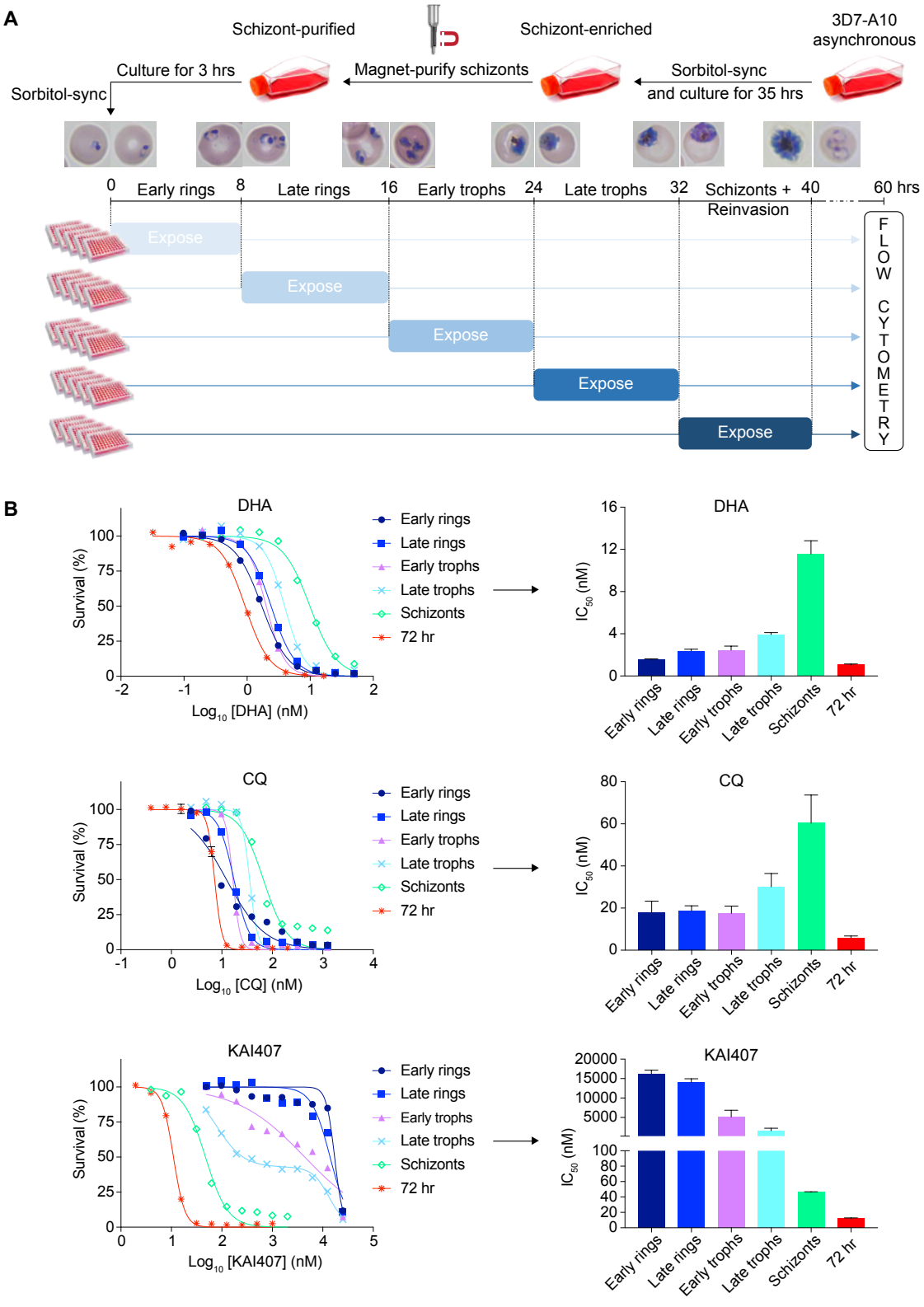

Fig. 3. 1. | Experimental design for asexual blood stage specificity profiling of antimalarials and profiles of reference drugs.

(**A**) Synchronized parasites were exposed for 8 h at the stages indicated. Survival at 60 h post-invasion was assessed by flow cytometry. (**B**) Unique stage-specificity profiles of chloroquine, dihydroartemisinin and KAI407. Bar plots indicate the IC_{50}^{8h} when parasites were exposed only during the early ring, late ring, early trophozoite, late trophozoite or schizont stage, with error bars showing the standard error of the mean based on at least three independent repeats. All data are available in **Table 3.1.**

The asexual blood stage susceptibility profile was determined for a set of 36 compounds that included licensed drugs, candidate antimalarials, compounds with a known target, and various screening hits (profiles of compounds are shown in **Fig. 3.2-3.5,** simplified molecular input line entry system **(**SMILES) for compounds are listed in **Table 3.2**, and structures of compounds are displayed in **Fig. 3.1-3.2**). Hits were selected from screens previously performed by the MalDA consortium (see **Table 3.2** references) and prioritized based on their potency, chemical diversity and unknown mode of action. Licensed antimalarial drugs and additional previously published preclinical compounds were included to provide more insights into their mode of action or to serve as a reference.

First, compounds were classified based on their timing of peak activity, defined as the asexual blood stage at which the compounds showed the lowest IC_{50}^{8h} values. This identified compounds with peak activity during (i) all rings and trophozoites, (ii) all rings, (iii) all trophozoites, (iv) all trophozoites and schizonts, (v) late trophozoites, and (vi) schizonts (**Fig. 3.6**). When compounds were classified by their overall activity profile based on identifying the specific stages that showed IC_{50}^{8h} values < 1 μM (**Fig. 3.10**; **Table 3.1**), seven active classes were identified: compounds active on (i) all asexual blood stages, (ii) all rings and trophozoites, (iii) late rings and all trophozoites, (iv) all

trophozoites and schizonts, (v) late trophozoites and schizonts, (vi) only late trophozoites, and (vii) only schizonts. Fosmidomycin, a moderately potent inhibitor of *P. falciparum* isoprenoid biosynthesis [348], as well as the hit compounds MMV000787, MMV019017, MMV020746, MMV022478 and MMV665939 showed IC_{50}^{8h} values > 1 μM at all tested stages and therefore did not match any of these groups (**Table 3.1**).

The clinical antimalarials dihydroartemisinin, chloroquine, piperaquine and lumefantrine showed little variation in IC_{50}^{8h} values throughout the ring and trophozoite stages, and were consequently classified in the group with peak activity at ring and trophozoite stages. While chloroquine, piperaquine and lumefantrine IC_{50}^{8h} values were similar for ring and trophozoite stages, survival curves for early rings were less steep than those for late rings and trophozoites (**Fig. 3.1, Fig. 3.2**). DSM265 and atovaquone, which are inhibitors of pyrimidine synthesis and the mitochondrial electron transport chain, respectively (**Fig. 3.5A**), showed peak activity specifically during late trophozoite stages (**Fig. 3.5B, Fig. 3.6**). These mitochondrial inhibitors also displayed a biphasic survival curve at the early trophozoite and schizont stages that was not observed at other stages (**Fig. 3.5B**; **Table 3.1**).

MMV000442, MMV006455, MMV007181 and MMV665971 showed incomplete killing at all asexual blood stages, with evidence of initial growth inhibition at lower concentrations followed by demonstrably better growth at higher concentrations in the early and late ring stages (**Fig. 3.3, Fig. 3.4**). This incomplete killing was not observed in the 72 h exposure survival curves for these compounds (**Fig. 3.3, Fig. 3.4**). Aqueous solubility experiments

for MMV000442, MMV006455 and MMV007181 indicated a solubility >100 μM (**Table 3.3**), well above the highest concentration used in the stage specificity assay.

Peak activity on all rings

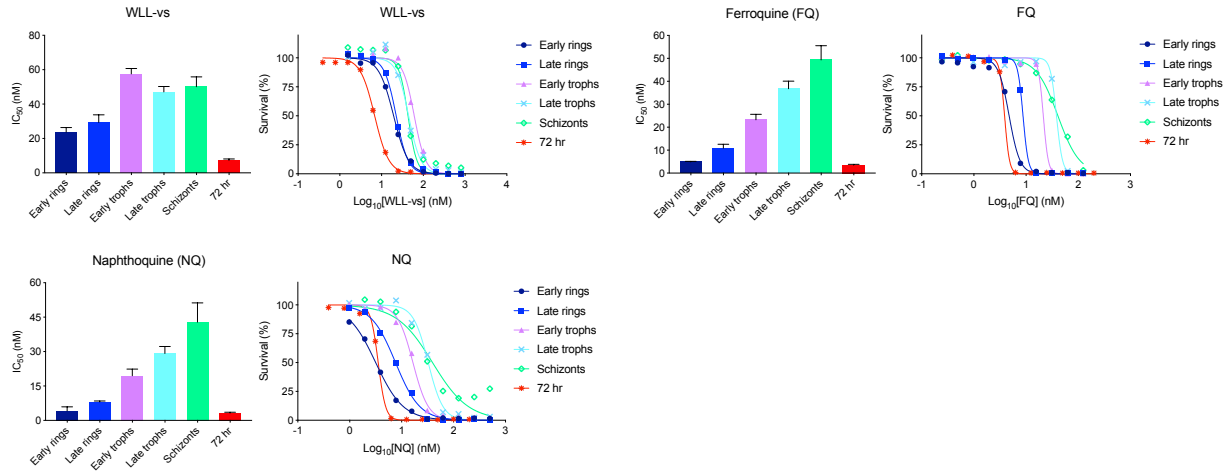

Peak activity on all rings and trophozoites

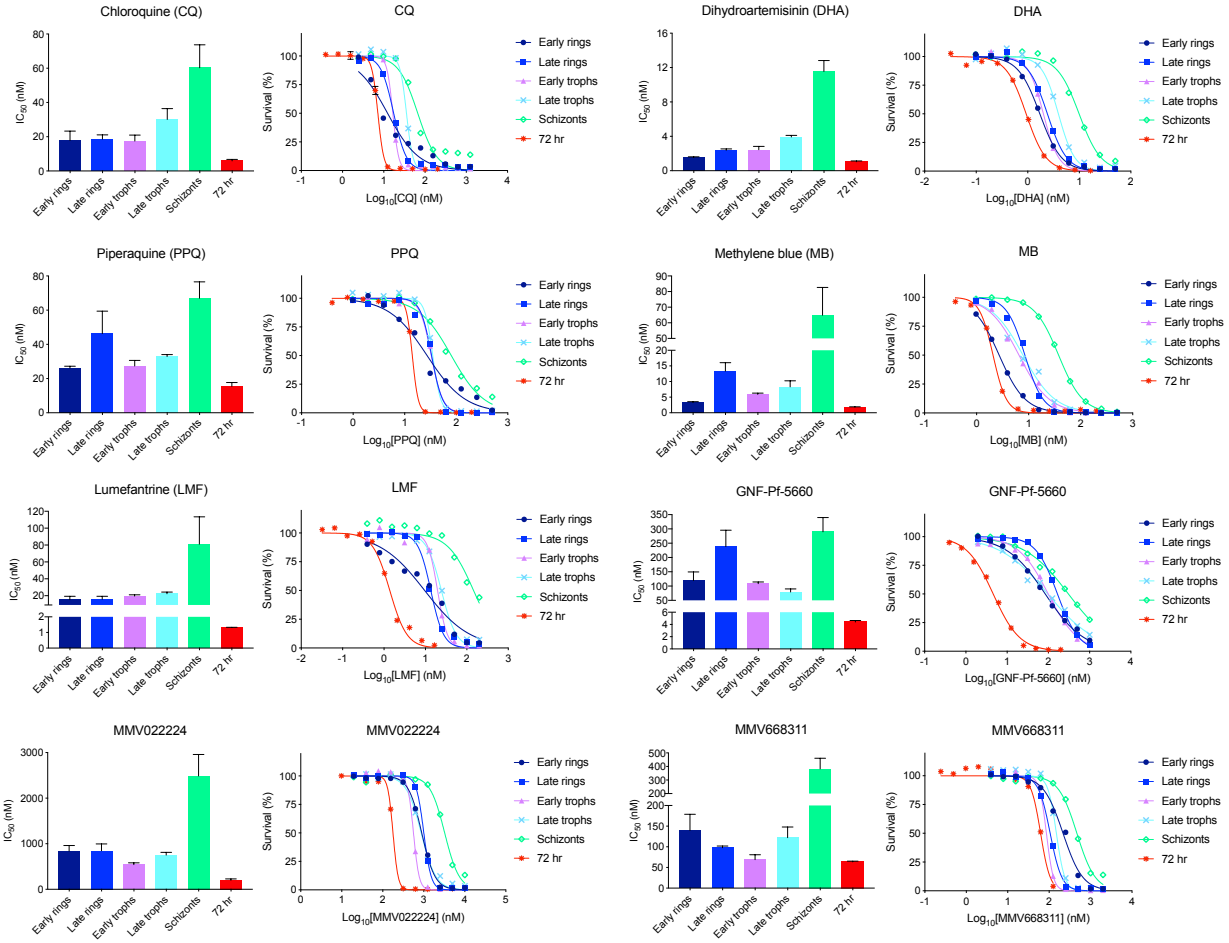

Fig. 3. 2. | Detailed Asexual Blood Stage Susceptibility Profiles for Antimalarials with Peak Activity on All Rings or All Rings and Trophozoites.

Data for chloroquine and dihydroartemisinin can be found in **Fig. 3.1**. Bar graphs indicate mean IC_{50}^{8h} values, whereas survival graphs show the most representative curves from independent repeats. Error bars indicate the standard error of the mean based on >3 independent repeats. Data are summarized in **Table 3.1**.

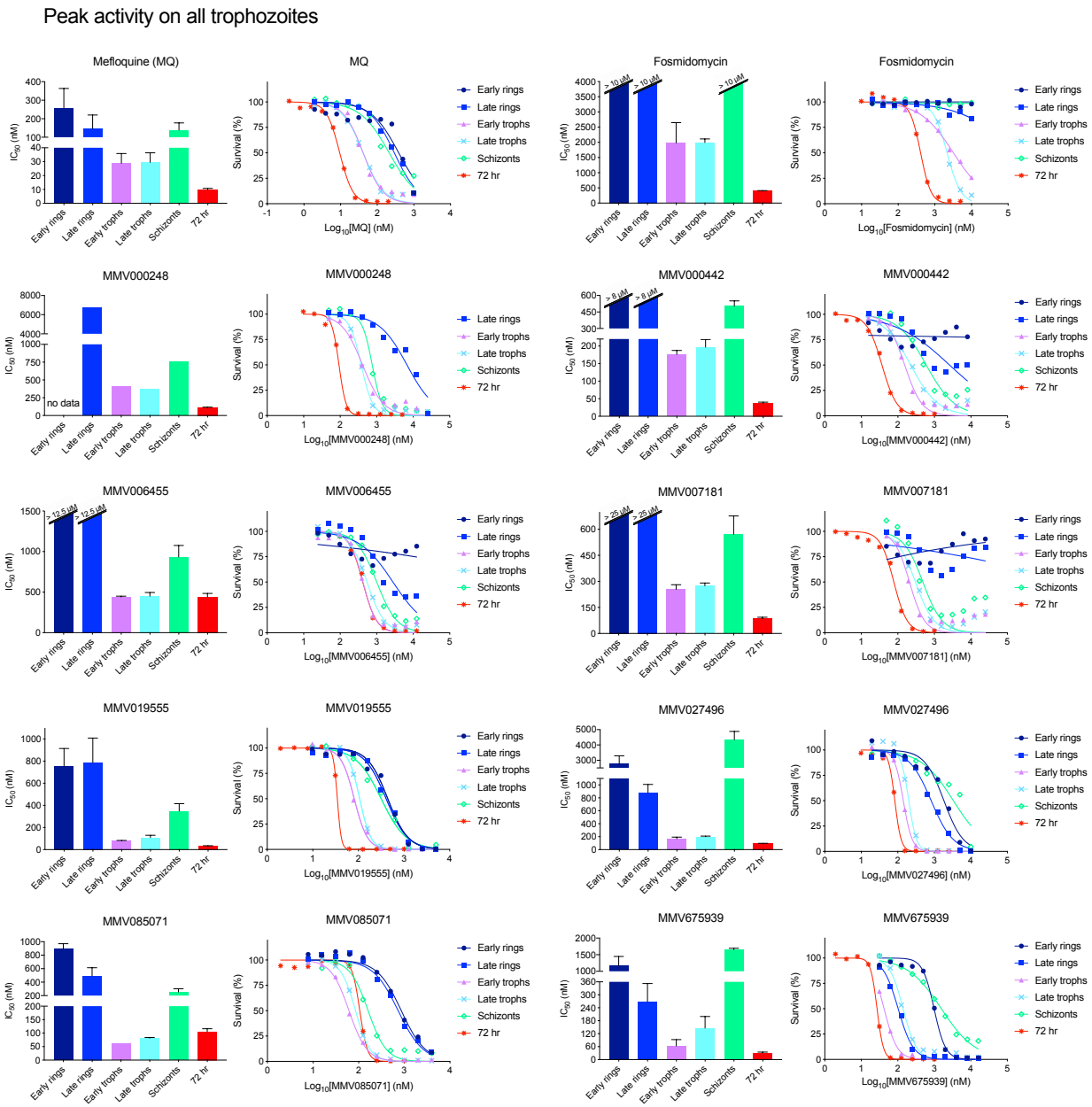

Fig. 3. 3. | Detailed Asexual Blood Stage Susceptibility Profiles for Antimalarials with Peak Activity on All Trophozoites.

Bar graphs indicate mean IC_{50}^{8h} values, whereas survival graphs show the most representative curves from independent repeats. Error bars indicate the standard error of the mean based on >3 independent repeats. Data are summarized in **Table 3.1**.

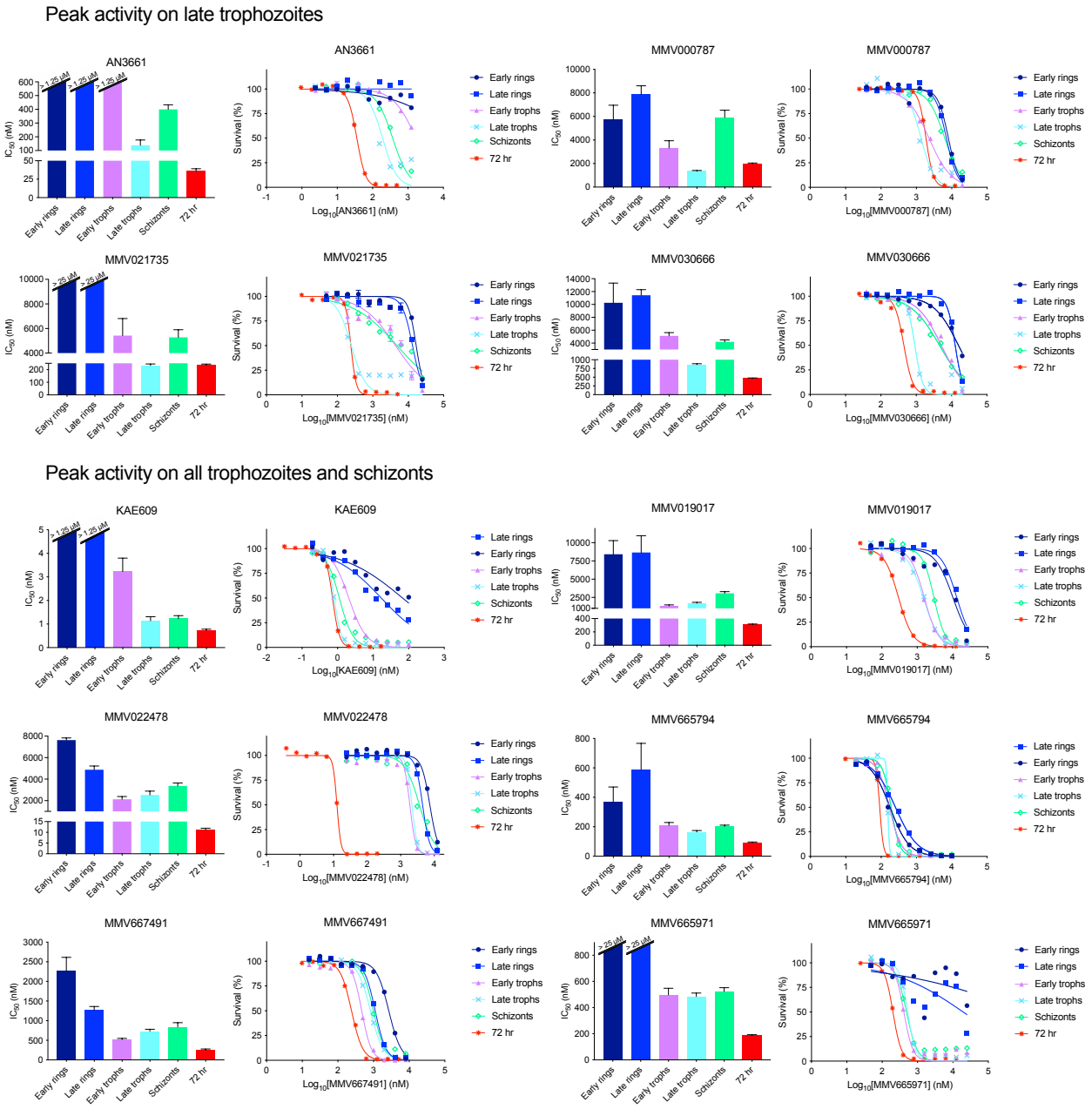

Fig. 3. 4. | Detailed Asexual Blood Stage Susceptibility Profiles for Antimalarials with Peak Activity on Late Trophozoites, or on All Trophozoites and Schizonts.

Data for DSM265 and atovaquone, both compounds with peak activity at the late trophozoite stage, can be found in **Fig. 3.5**. Bar graphs indicate mean IC_{50}^{8h} values,

whereas survival graphs show the most representative curves from independent repeats. Error bars indicate the standard error of the mean based on >3 independent repeats. Data are summarized in **Table 3.1.**

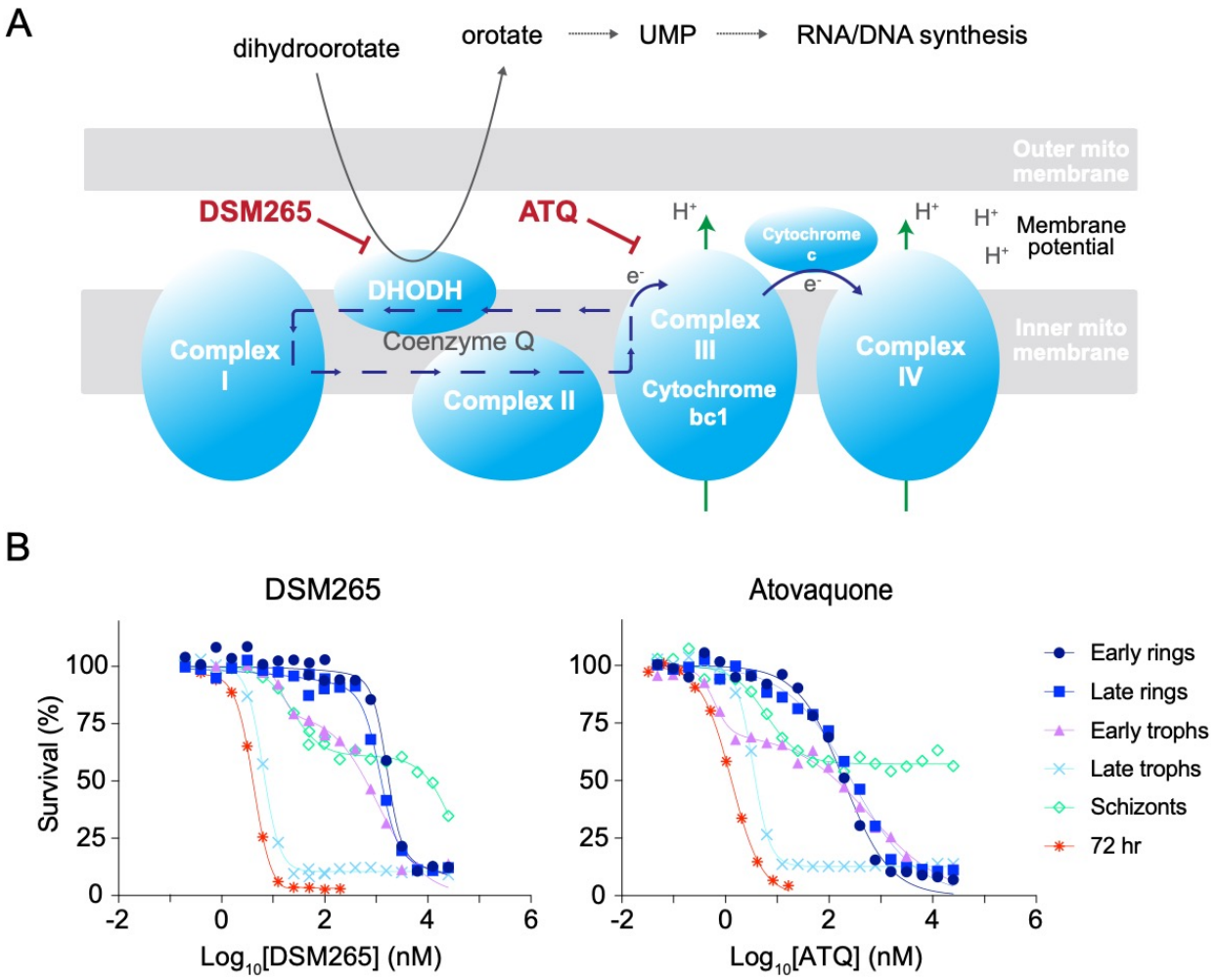

Fig. 3. 5. | Late trophozoites are the most susceptible stage to DSM265 and atovaquone that inhibit pyrimidine biosynthesis and the mitochondrial electron transport chain, respectively.

(**A**) Overview of the pyrimidine biosynthesis and the mitochondrial electron transport chain pathways. DSM265 inhibits DHODH, whereas atovaquone inhibits cytochrome bc1 (Goodman et al., 2017). (B) Stage specificity profiles for DSM265 and atovaquone. IC_{50}^{8h} values for (**B**) are available in **Table 3.1**.

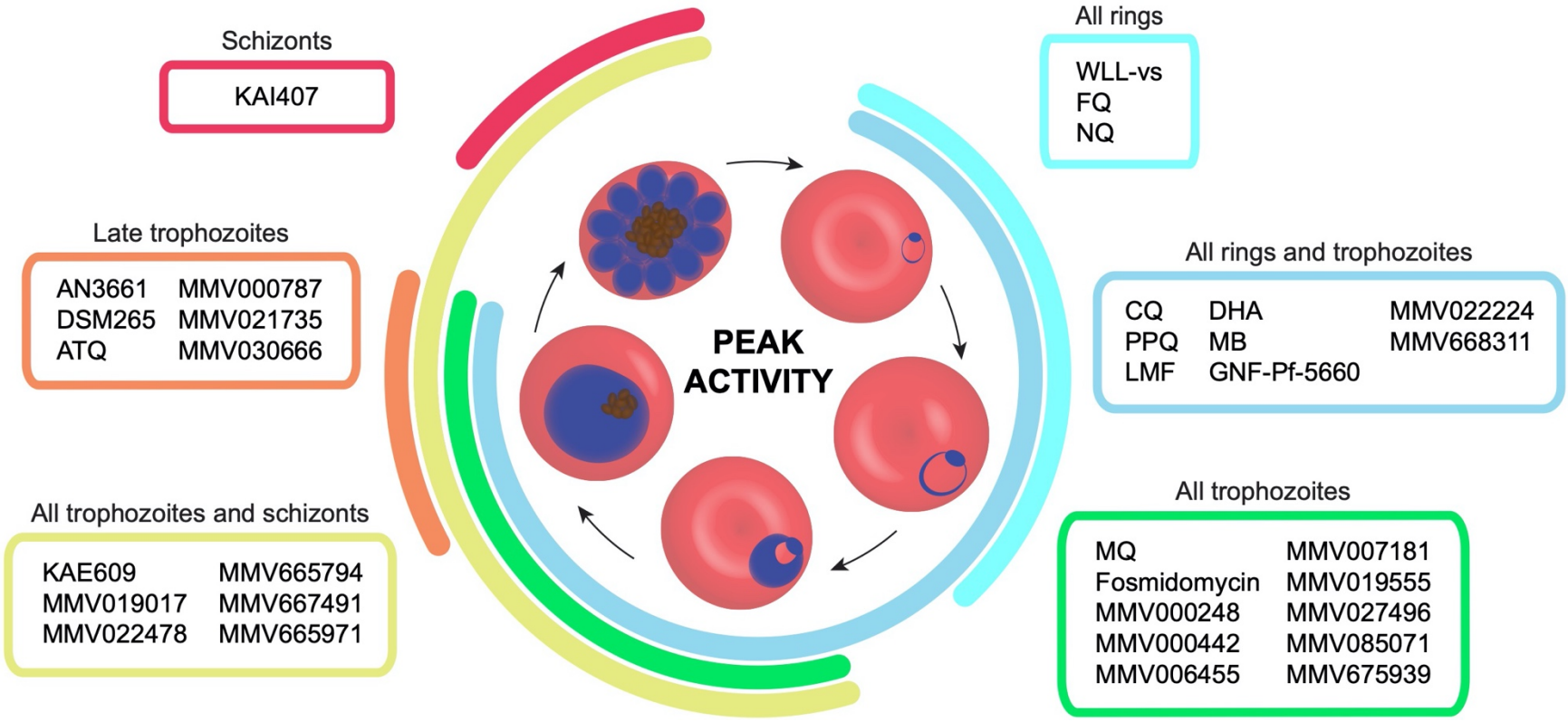

Fig. 3. 6. | Stage of peak activity for clinical and experimental antimalarials.
Peak activity illustrates the period when the parasite was most susceptible to the tested compounds. MMV020746 and MMV665939 were omitted as their IC_{50}^{8h} values were >10 mM. All data are available in **Table 3.1** and **Fig. 3.1-3.5**. ATQ, atovaquone; CQ, chloroquine; DHA, dihydroartemisinin; FQ, ferroquine; LMF, lumefantrine; MB, methylene blue; MQ, mefloquine; NQ, naphthoquine; PPQ, piperaquine.

To further examine whether the compound stage-specificity profiles that we identified correlated with their mode of action, we examined the metabolic profile of 33 compounds (**Fig. 3.7**). These consisted of 27 newly assayed compounds, plus another six (chloroquine, DSM265, MMV000248, MMV006455, MMV019017 and KAE609) for which data were already available [260]. In these experiments, we exposed trophozoite-infected RBCs to $10\times IC_{50}^{72h}$ concentrations and then subjected parasite extracts to mass spectrometry-based metabolomic profiling [260].

Across all 33 compounds, we obtained quantitative data for 195 metabolites that represent major metabolic pathways, including but not limited to pyrimidine and purine synthesis, hemoglobin catabolism, folate biosynthesis, central carbon metabolism, glycolysis, and redox metabolism. Based on these metabolic profiles, compounds were hierarchically clustered via Ward clustering based on Pearson correlation coefficients to identify related metabolic signatures (**Fig. 3.7**).

Several established metabolic signatures were observed among the analyzed compounds. Mitochondrial electron transport chain disruption is linked to inhibition of dihydroorotate dehydrogenase (DHODH) and cytochrome bc_1 (CytBC1), leading to increases in the pyrimidine precursors dihydroorotate and N-carbamoyl-L-aspartate [260]. This metabolic signature was observed for DSM265 and ATQ, which respectively inhibit DHODH and CytBC1, as well as MMV000787, MMV021735, and MMV030666 for which the mode of action was previously unknown (**Fig. 3.7**).

We performed resistance selections with MMV021735, MMV030666 and MMV000787 to compare their propensity for resistance to that of DSM265 and atovaquone, which have a relatively low minimum inoculum for resistance of 2×10^6 and 2×10^7parasites, respectively, when using $3\times IC_{50}^{72h}$ drug concentrations [339]. Selections involving continuous exposure of 1×10^9 Dd2-B2 parasites to a $3.5\times IC_{50}^{72h}$ concentration of MMV000787, or intermittent drug pulsing in which parasites were exposed for several days at a time to $6\times IC_{50}^{72h}$ concentrations of MMV000787 for 5 months, did not result in MMV000787-resistant parasites. For MMV021735, exposing 5×10^8 3D7-A10 parasites to $3\times IC_{50}^{72h}$ concentrations in triplicate failed to yield resistant parasites. Exposing 5×10^8 3D7-A10 or Dd2-B2 parasites to $3\times IC_{50}^{72h}$ concentrations of MMV030666 also failed to yield resistance. A ramping selection with 3D7-A10 parasites starting at $1\times IC_{50}^{72h}$ and gradually increasing to $1.8\times IC_{50}^{72h}$ over the course of 3 months also did not produce resistance. These data indicate that MMV000787, MMV21735 and MMV030666 have minimum inocula of resistance well above 5×10^8 parasites.

Peptide decreases commonly linked with inhibition of hemoglobin endocytosis and/or catabolism within the digestive vacuole were also observed across multiple antimalarial compounds (**Fig. 3.7**). This metabolic signature of decreased peptide levels (HVDD, PVNF, PEEK, PEE, DLS, SDL, SID, DLH, LD, PE, PD, SD, VD, and EV) was particularly pronounced for the compounds MMV022478, MMV019555, MMV667491, MMV030666, MMV000248, MMV006455, MMV007181, MMV020746, MMV000442, GNF-Pf-5660, KAE609 and MMV019017. Of these, MMV006455, MMV019017 and KAE609 also possessed increased levels of the deoxyribonucleotides dAMP and dTMP and decreased

levels of cAMP. KAE609 and MMV019017 additionally showed decreased nucleoside di- and triphosphates levels (GDP, UDP, GTP, dATP, dGTP/ATP, dUTP), which have previously been identified as a signature of inhibiting the Na^+/H^+-dependent ATPase PfATP4 [260]. The hemozoin inhibitor chloroquine did not show the expected strong hemoglobin catabolism signature, but instead showed a more modest decrease in peptide levels and clustered with the PFATP4-inhibitor KAE609.

Interestingly, the metabolic profile for MMV030666 indicated perturbation of both the mitochondrial electron transport chain and Hb catabolism. MMV022224 induced increased levels of peptides, a profile that has not been observed before. Due to the peculiar profiles of these compounds, they were selected for an additional study in which synchronized parasites were exposed to 3× the IC_{50}^{8h} of the most sensitive life stage at 8 h intervals, similar to the stage specificity assay, and cell morphology was assessed by microscopy at the end of each interval (**Fig. 3.11**). This showed MMV030666-exposed parasites to be most susceptible during the late trophozoite stage, as evidenced by their bloated digestive vacuoles. This phenotype is characteristic of Hb catabolism perturbation [201], and is consistent with the metabolomics data. MMV022224-exposed parasites proved to be affected mostly during early and late trophozoite stages, without displaying swollen vacuoles. The health of ring-stage parasites, which showed similar IC_{50}^{8h} values as trophozoites for MMV022224, was harder to microscopically evaluate due to their smaller size.

Mefloquine, naphthoquine, piperaquine, methylene blue, MMV675939, dihydroartemisinin, WLL-vs, MMV668311, ferroquine, MMV085071 did not induce major changes within the set of metabolites detected in our study and therefore clustered in the low fold change group (**Fig. 3.7**).

Hemoglobin catabolism
Cellular homeostasis
Low fold change
mETC/ pyrimidine synthesis
MMV022478
MMV019555
MMV667491
MMV030666
MMV027496
MMV000248
MMV006455
MMV007181
MMV020746
MMV665939
MMV000442
GNF-Pf-5660
LMF
MMV665794
KAI407
KAE609
MMV019017
CQ
MQ
NQ
PPQ
MB
MMV675939
DHA
WLL-vs
MMV668311
FQ
MMV022224
MMV085071
MMV021735
ATQ
DSM265
MMV000787
Log2 fold change
-4
0
4
Cmpd Peak Activity: Rings Rings &Trophozoites Trophozoites Late Trophozoites Trophozoites & Schizonts Schizonts Not Classified

Fig. 3. 7. | Metabolic profiling of compounds identified cellular processes targeted by compounds.
Compounds were clustered based on hydrophilic metabolite response to all measured metabolites. Compounds are listed only if they showed a >2-fold change ($log_2 > 1$) in metabolite levels compared with untreated controls in at least one of the treated samples. Compounds are color-coded based on peak activity as shown in **Fig. 3.6**. Metabolite data for chloroquine, DSM265, MMV000248, MMV006455, MMV019017, and KAE609 were sourced from (Allman et al., 2016). Data for all other 27 compounds were generated in this study. ATQ, atovaquone; Cmpd, compound; CQ, chloroquine; DHA, dihydroartemisinin; FQ, ferroquine; LMF, lumefantrine; MB, methylene blue; mETC, mitochondrial electron transport chain; MQ, mefloquine; NQ, naphthoquine; PPQ, piperaquine.

Table 3. 1. | Asexual blood stage-specific IC_{50}^{8h} data in nM for the tested antimalarials.

Compound	Early rings			Late rings			Early trophozoites			Late trophozoites			Schizonts			Overall (72hr assay)			Peak Activity	Ratio lowest $IC_{50}^{8hr}/IC_{50}^{72hr}$
	Mean IC_{50}	SEM	n	Mean IC_{50}	SEM	n	Mean IC_{50}	SEM	n	Mean IC_{50}	SEM	n	Mean IC_{50}	SEM	n	Mean IC_{50}	SEM	n		
Dihydroartemisinin	1.5	0.1	3	2.4	0.1	3	2.4	0.4	3	3.9	0.2	3	11.6	1.3	3	1.0	0.1	4	Rings + Trophs	1.5
Chloroquine	17.8	5.5	4	18.6	2.5	3	17.4	3.5	3	30.1	6.3	3	60.3	13.4	3	5.9	0.8	3	Rings + Trophs	2.9
Mefloquine	258	106	3	147	74	3	28.8	7.0	3	29.5	6.9	3	138	39	3	9.8	1.0	3	Trophs	3.0
Lumefantrine	15.4	4.0	3	15.8	3.5	3	19.54	1.6	3	22.3	2.0	3	81.0	32.5	3	1.3	0.0	3	Rings + Trophs	11.6
Piperaquine	26.2	1.1	3	46.3	13.1	3	27.4	3.3	3	32.9	1.1	3	67.0	9.6	3	15.4	2.3	4	Rings + Trophs	1.7
Ferroquine	4.9	0.3	3	10.9	1.7	3	23.2	2.4	3	36.8	3.3	3	49.3	6.2	3	3.5	0.4	4	Rings	1.4
Methylene blue	3.2	0.3	3	13.3	2.7	3	5.9	0.4	3	8.3	2.0	3	64.8	17.8	3	1.8	0.1	4	Rings + Trophs	1.8
KAI407 - shift 1	-	-	-	-	-	-	-	-	-	161	44.0	3	-	-	-	-	-	-	-	3.9
KAI407 - shift 2	16263	904	2	14021	923	3	5139	1727	3	13386	354	2	46.2	0.6	3	11.8	1.0	3	Schizonts	-
AN3661	> 1.25 µM	-	3	> 1.25 µM	-	3	> 1.25 µM	-	3	138	39	3	400	34	3	35.6	3.6	3	Late Trophs	3.9
KAE609	> 1.25 µM	-	3	> 1.25 µM	-	3	3.2	0.6	3	1.1	0.2	3	1.2	0.1	3	0.73	0.05	4	Trophs + Schizonts	1.5
WLL-vs	23.7	2.6	3	29.4	4.4	3	57.6	3.1	3	47.1	3.1	3	50.1	5.7	3	7.2	0.8	3	Rings	3.3
DSM265 - shift 1	-	-	-	-	-	-	10.2	2.2	3	7.7	0.9	3	19.2	2.3	3	3.8	0.1	3	Late Trophs	2.0
DSM265 - shift 2	4821	1605	3	1493	308	3	1481	240	3	-	-	-	> 25 µM	-	-	-	-	-	-	-
Atovaquone - shift 1	-	-	-	-	-	-	0.68	0.06	3	3.7	0.2	3	7.4	1.3	3	1.1	0.1	3	Late Trophs	3.3
Atovaquone - shift 2	553	228	3	324	45	3	619	132	3	-	-	3	> 25 µM	-	3	-	-	-	-	-
Fosmidomycin	> 10 µM	-	3	> 10 µM	-	3	1983	665	3	1993	117	3	> 10 µM	-	3	405	8	3	Trophs	4.9
GNF-Pf-5660	119	30	3	238	57	3	108	6	3	79.3	10.8	3	290	50	3	4.4	0.2	3	Rings + Trophs	18.0
MMV665794	369	101	3	590	177	3	210	20	3	165	10	3	203	8	3	91.3	5.2	4	Trophs + Schizonts	1.8
Naphtoquine	4.2	1.8	3	8.1	0.4	3	19.5	2.9	3	29.2	3.1	3	42.8	8.4	3	3.2	0.4	4	Rings	1.3
MMV000442	> 8 µM	-	3	> 8 µM	-	3	176	11	3	197	22	3	503	48	3	37.2	3.1	3	Trophs	4.7
MMV675939	1170	277	3	268	84	3	62.9	29.9	3	146	54	3	1647	45	3	30.8	4.4	5	Trophs	2.0
MMV085071	893	78	3	492	122	3	61.1	0.1	3	81.4	2.8	3	254	47	3	105	11	3	Trophs	0.6
MMV668311	140	39	3	97.7	4.3	3	68.9	11.9	3	122	26	3	382	79	3	63.5	1.7	3	Rings + Trophs	1.1
MMV020746	> 25 µM	-	2	> 25 µM	-	2	12587	1681	2	> 25 µM	-	2	> 25 µM	-	2	56.8	6.6	4	All stages > 10 µM	221.5
MMV667491	2264	349	3	1270	92	3	521	28	3	731	50	3	842	108	3	243	35	4	Trophs + Schizonts	2.1
MMV006455	> 12.5 µM	-	3	> 12.5 µM	-	3	441	10	3	450	46	3	933	142	3	439	46	4	Trophs	1.0
MMV022478	7628	202	2	4870	353	2	2132	252	2	2529	353	2	3370	269	2	11.1	0.8	3	Trophs + Schizonts	192.4
MMV007181	> 25 µM	-	3	> 25 µM	-	3	253	27	3	274	16	3	570	107	3	84.9	8.9	3	Trophs	3.0
MMV665971	> 25 µM	-	3	> 25 µM	-	3	496	51	3	485	26	3	523	29	3	185	9	3	Trophs + Schizonts	2.6
MMV665939	17011	2420	3	22853	5330	3	13476	4752	3	39017	13066	3	54384	14265	3	478	49	4	All stages > 10 µM	28.2
MMV019017	8418	1862	2	8663	2298	3	1338	133	3	1708	116	3	3060	229	3	306	12	3	Trophs + Schizonts	4.4
MMV000248	n.d.	n.d.	0	6744	-	1	411	-	1	376	-	1	754	-	1	103	14	4	Trophs	3.7
MMV021735	> 25 µM	-	3	> 25 µM	-	3	5422	1392	3	234	12	3	5281	622	3	232	11	4	Late Trophs	1.0
MMV022224	838	123	3	845	152	3	542	39	3	752	58	3	2486	472	3	199	31	5	Rings + Trophs	2.7
MMV027496	2760	529	3	878	130	3	168	26	3	199	9	3	4339	545	3	89.7	7.9	3	Trophs	1.9
MMV019555	755	159	3	788	221	3	81.4	1.6	3	110	20	3	349	66	3	33.3	1.8	3	Trophs	2.4
MMV030666	10264	3053	3	11440	861	3	5124	506	3	858	29	3	4191	307	3	462	18	4	Late Trophs	1.9
MMV000787	5737	1215	3	7870	731	3	3312	629	3	1354	57	3	5912	617	3	1960	83	3	Late Trophs	0.7

Shift 1 and shift 2 indicate the two half-maximal inhibitory concentrations for biphasic dose response curves. SEM: standard error of the mean; n: number of biological repeats; - : no data; IC_{50}^{8h}: IC_{50} based on 8-h exposure; IC_{50}^{72h}: IC_{50} based on 72-h exposure.

Table 3. 2. | SMILES and suspected mode of action (if known) of the tested antimalarials.

Compound	SMILES	Suspected mode of action	Origin candidate antimalarials	Alternative name
Dihydroartemisinin (DHA)	C[C@@H]1CC[C@H]2[C@H]([C@H](O[C@H]3[C@@]24[C@H]1CCC(O3)(OO4)C)O)C	-	-	-
Chloroquine (CQ)	CCN(CC)CCCC(C)NC1=C2C=CC(=CC2=NC=C1)Cl	β-hematin[a]	-	-
Mefloquine (MFQ)	c1cc2c(cc(nc2c(c1)C(F)(F)F)C(F)(F)F)[C@@H]([C@H]3CCCCN3)O	-	-	-
Lumefantrine (LMF)	CCCCN(CCCC)CC(C1=C2C3=C(C=C(C=C3)Cl)C(=CC4=CC=C(C=C4)Cl)C2=CC(=C1)Cl)O	-	-	-
Piperaquine (PPQ)	c1cc2c(ccnc2cc1Cl)N3CCN(CC3)CCCN4CCN(CC4)c5ccnc6c5ccc(c6)Cl	β-hematin[b]	-	-
Ferroquine (FQ)	CN(C)CC1=C(C=[C-]C1)CNC2=C3C=CC(=CC3=NC=C2)Cl.C1C=CC=[C-]1.[Fe+2]	β-hematin[c,d]	-	-
Methylene blue (MB)	CN(C)C1=CC2=C(C=C1)N=C3C=CC(=[N+](C)C)C=C3S2.[Cl-]	β-hematin[e]	-	-
KAI407	O=C(N(C)C1=CC=C(C=C1)C#N)C2=CN3C(C=N2)=NC=C3C4=CC=C(C=C4)C(F)(F)F	PI4K[f]	-	-
AN3661	OB1C2=C(CCC(O)=O)C=CC=C2CO1	CPSF[g]	-	-
KAE609	ClC1=C(F)C=C2C(NC3=C2C[C@H](C)N[C@@]34C(CC5=C4C=C(Cl)C=C5)=O)=C1	ATP4[h]	-	-
WLL-vs	CC(C)C[C@@H](/C=C/S(=O)(=O)CNC(=O)[C@H](CC(C)C)NC(=O)[C@H](CC1=CNC2=CC=CC=C21)NC(=O)CN3CCOCC3	Proteasome[i,j]	-	-
DSM265	FS(F)(F)(F)C1=CC=C(NC2=CC(C)=NC3=NC(C(F)(F)C)=NN23)C=C1)F	DHODH[k]	-	-
Atovaquone (ATQ)	O=C1C([C@@H]2CC[C@@H](C3=CC=C(Cl)C=C3)CC2)=C(O)C(C4=CC=CC=C41)=O	CYTB[l]	-	-
Fosmidomycin	C(CN(C=O)O)CP(=O)(O)O	DXR[m]	-	-
GNF-Pf-5660	CCOC(=O)C1=C(C)NC2=C(C1C3=CC=CC=C3Cl)C(=O)CC(C2)C4=CC=C(OC)C(OC)=C4	*[n]	-	-
Naphthoquine (NQ)	CC(C)(C)NCc1cc(c2c(c1O)CCCC2)Nc3ccnc4c3ccc(c4)Cl	-	-	MMV000017
MMV665794	FC(F)(F)C1=CC(NC2=C(NC3=CC(=CC=C3)C(F)(F)F)N=C3C=CC=CC3=N2)=CC=C1	-	MMV Malaria Box	-
MMV000442	CC(C)(C)c1ccc2OCN(Cc3ccc(Cl)cc3)Cc2c1	-	MMV Malaria Box	-
MMV675939	FC(F)(F)C1=CC=C(NC2=CC(NC(C3=CC(C(F)(F)F)=CC=C3)=N4)=C4C=N2)N=C1	-	Literature[o]	-
MMV085071	COc1cncc(c1)-c1cncc(n1)N1CCN(CC1)c1ccncc1	-	MMV Pathogen Box	-
MMV668311	CNc1nc(NCCCN(C)C)c2sc(cc2n1)c3cccc(c3)C(F)(F)F	-	Literature[p]	-
MMV020746	Cc1ccc(Oc2ncccc2C(=O)Nc2cccc3cccnc23)c(C)c1	-	Literature[p]	TCMDC-125499
MMV667491	CN(C)CCCn1cnc2c(c1=N)C(c3ccc4ccccc4c3O2)c5ccc(cc5)OC	-	MMV Malaria Box	-
MMV006455	CCCN(CCC)CC(O)COC1=C(C=CC=C1)C(=O)NC1=CC=CC=C1	-	MMV Malaria Box	-
MMV022478	Clc1cccc(c1)-c1cnn2ccc(nc12)C(=O)Nc1ccc(cc1)N1CCNCC1.OC(C(F)(F)F)=O	-	MMV Pathogen Box	-
MMV007181	CC1=C2C=CC(O)=CC2=NC(NC2=CC=C(OCC3=CC=CC=C3)C=C2)=C1	-	MMV Malaria Box	-
MMV665971	CCOC(=O)C1=C(C)N=c2s\c(=C/c3cc(Cl)ccc3O)c(=O)n2C1c1ccc(OC)cc1	-	MMV Malaria Box	-
MMV665939	FC1=CC=C(C=C1)C(=O)NC1=C(SC=C1)C(=O)NC1CCCCC1	-	MMV Malaria Box	-
MMV019017	COCCNCC(O)CN1C2=CC=C(Cl)C=C2C2=C1C=CC(Cl)=C2	-	MMV Malaria Box	-
MMV000248	Cl.CCN(CC)CCn1c2ccccc2n(CC(O)c2ccc(Cl)c(Cl)c2)c1=N	-	MMV Malaria Box	-
MMV021735	CCCCCCCN(CC1=CC=C(OC(C)(C)C(=O)OCC)C=C1)C(=O)NC1=CC=C(Cl)C=C1OCC	-	Literature[p]	TCMDC-131919
MMV022224	[O-]C(=O)C(F)(F)F.CN(C)CC1=CC=C(C=C1)C1=CC2=C(N1)N=CC=C2C1=CC=C(CN(C)C)C=C1	-	Literature[p]	TCMDC-132409
MMV027496	COC1=C(OCCN(C)C)C=CC(=C1)C1=NC(=C(N1)C1=CC=CC=C1)C1=CC=CC=C1	-	Literature[p]	TCMDC-137716
MMV019555	Cl.C(CCCNc1c2CCCCc2nc2ccccc12)CCNc1c2CCCCc2nc2ccccc12	-	MMV Malaria Box	TCMDC-124183
MMV030666	CC(C)(C)OC(=O)N1CCN(CC1)C1=CC=CC=C1NC(=O)C1=C(OC2=CC=C(F)C=C2)C(=CC=C1)C(F)(F)F	-	Literature[p]	TCMDC-140951
MMV000787	CCCOCC1=C2C=CC=NC2=C(O)C(CN2CCN(CC2)C2=CC(Cl)=CC=C2)=C1	-	MMV Malaria Box	-

PI4K: Phosphatidylinositol-4-OH kinase, CPSF: Cleavage and polyadenylation specificity factor, ATP4: P-type cation translocating ATPase, DHODH: Dihydroorotate dehydrogenase, CYTB: Cytochrome B, DXR: 1-deoxy-D-xylulose-5-phosphate reductoisomerase; SMILES: simplified molecular line entry system.

[a]Slater, A.F., and Cerami, A. (1992). Inhibition by chloroquine of a novel haem polymerase enzyme activity in malaria trophozoites. Nature *355* , 167-169.

[b]Raynes, K., Foley, M., Tilley, L., and Deady, L.W. (1996). Novel bisquinoline antimalarials. Synthesis, antimalarial activity, and inhibition of haem polymerisation. Biochemical Pharmacology *52* , 551-559.

[c]Biot, C., Taramelli, D., Forfar-Bares, I., Maciejewski, L.A., Boyce, M., Nowogrocki, G., Brocard, J.S., Basilico, N., Olliaro, P., and Egan, T.J. (2005). Insights into the mechanism of action of ferroquine. Relationship between physicochemical properties and antiplasmodial activity. Molecular Pharmaceutics *2* , 185-193.

[d]Dubar, F., Egan, T.J., Pradines, B., Kuter, D., Ncokazi, K.K., Forge, D., Paul, J.F., Pierrot, C., Kalamou, H., Khalife, J., et al. (2011). The antimalarial ferroquine: role of the metal and intramolecular hydrogen bond in activity and resistance. ACS Chemical Biology *6* , 275-287.

[e]Atamna, H., Krugliak, M., Shalmiev, G., Deharo, E., Pescarmona, G., and Ginsburg, H. (1996). Mode of antimalarial effect of methylene blue and some of its analogues on Plasmodium falciparum in culture and their inhibition of P. vinckei petteri and P. yoelii nigeriensis in vivo. Biochemical Pharmacology *51* , 693-700.

[f]McNamara, C.W., Lee, M.C., Lim, C.S., Lim, S.H., Roland, J., Simon, O., Yeung, B.K., Chatterjee, A.K., McCormack, S.L., Manary, M.J., et al. (2013). Targeting Plasmodium PI(4)K to eliminate malaria. Nature *504* , 248-253.

[g]Sonoiki, E., Ng, C.L., Lee, M.C., Guo, D., Zhang, Y.K., Zhou, Y., Alley, M.R., Ahyong, V., Sanz, L.M., Lafuente-Monasterio, M.J., et al. (2017). A potent antimalarial benzoxaborole targets a Plasmodium falciparum cleavage and polyadenylation specificity factor homologue. Nature Communications *8* , 14574.

[h]Spillman, N.J., Allen, R.J., McNamara, C.W., Yeung, B.K., Winzeler, E.A., Diagana, T.T., and Kirk, K. (2013). Na(+) regulation in the malaria parasite Plasmodium falciparum involves the cation ATPase PfATP4 and is a target of the spiroindolone antimalarials. Cell Host Microbe *13* , 227-237.

[i]Stokes, B.H., Yoo, E., Murithi, J.M., Luth, M.R., Afanasyev, P., da Fonseca, P.C.A., Winzeler, E.A., Ng, C.L., Bogyo, M., and Fidock, D.A. (2019). Covalent Plasmodium falciparum-selective proteasome inhibitors exhibit a low propensity for generating resistance in vitro and synergize with multiple antimalarial agents. PLoS Pathog. 15, e1007722.

[j]Li, H., O'Donoghue, A.J., van der Linden, W.A., Xie, S.C., Yoo, E., Foe, I.T., Tilley, L., Craik, C.S., da Fonseca, P.C., and Bogyo, M. (2016). Structure- and function-based design of Plasmodium-selective proteasome inhibitors. Nature *530* , 233-236.

[k]Coteron, J.M., Marco, M., Esquivias, J., Deng, X., White, K.L., White, J., Koltun, M., El Mazouni, F., Kokkonda, S., Katneni, K., et al. (2011). Structure-guided lead optimization of triazolopyrimidine-ring substituents identifies potent Plasmodium falciparum dihydroorotate dehydrogenase inhibitors with clinical candidate potential. Journal of Medicinal Chemistry *54* , 5540-5561.

[l]Fry, M., and Pudney, M. (1992). Site of action of the antimalarial hydroxynaphthoquinone, 2-[trans-4-(4'-chlorophenyl) cyclohexyl]-3-hydroxy-1,4-naphthoquinone (566C80). Biochemical Pharmacology *43* , 1545-1553.

[m]Armstrong, C.M., Meyers, D.J., Imlay, L.S., Freel Meyers, C., and Odom, A.R. (2015). Resistance to the antimicrobial agent fosmidomycin and an FR900098 prodrug through mutations in the deoxyxylulose phosphate reductoisomerase gene (dxr). Antimicrobial Agents and Chemotherapy *59* , 5511-5519.

[n]Vanaerschot, M., Lucantoni, L., Li, T., Combrinck, J.M., Ruecker, A., Kumar, T.R.S., Rubiano, K., Ferreira, P.E., Siciliano, G., Gulati, S., et al. (2017). Hexahydroquinolines are antimalarial candidates with potent blood-stage and transmission-blocking activity. Nature Microbiology *2* , 1403-1414.

[o]Nchinda, A.T., Le Manach, C., Paquet, T., Gonzalez Cabrera, D., Wicht, K.J., Brunschwig C., Njoroge, M., Abay, E., Taylor, D., Lawrence, N., et al. (2018). Identification of fast-acting 2,6-disubstituted imidazopyridines that are efficacious in the in vivo humanized Plasmodium falciparum NODscidIL2Rγ^{null} mouse model of Malaria. Journal of Medicineal Chemistry *61* , 4213-4227.

[p]Corey, V.C., Lukens, A.K., Istvan, E.S., Lee, M.C.S., Franco, V., Magistrado, P., Coburn-Flynn, O., Sakata-Kato, T., Gnadig, N., et al. (2016). A broad analysis of resistance development in the malaria parasite. Nature Communications *15* , 11901.

Table 3. 3. | Assessment of compound solubility by UV/vis spectroscopy.

Compound	Wavelength						Ratio fil./std.	Solubility
	280	300	320	340	360	800		
	Absorbance (AU)							
DHA fil.	2.351	0.462	0.250	0.179	0.124	0.041	1.02	≥ 500 µM
DHA std.	2.314	0.456	0.244	0.173	0.120	0.042		
Chloroquine fil.	2.637	1.170	2.155	2.075	0.203	0.042	0.91	≥ 100 µM and ≤ 500 µM
Chloroquine std.	2.747	1.331	2.562	2.178	0.204	0.041		
Piperaquine fil.	2.322	0.473	0.269	0.189	0.129	0.041	0.69	≥ 100 µM and ≤ 500 µM
Piperaquine std.	2.694	0.822	0.646	0.555	0.462	0.304		
MMV007181 fil.	2.346	0.470	0.259	0.194	0.139	0.042	0.69	≥ 100 µM and ≤ 500 µM
MMV007181 std.	2.677	0.754	0.534	0.551	0.508	0.131		
MMV000442 fil.	2.517	0.606	0.380	0.310	0.248	0.086	0.74	≥ 100 µM and ≤ 500 µM
MMV000442 std.	2.754	0.898	0.711	0.660	0.619	0.274		
MMV006455 fil.	2.810	0.904	0.336	0.186	0.130	0.041	1.00	≥ 500 µM
MMV006455 std.	2.826	0.928	0.329	0.175	0.120	0.041		

Fil.: filtered; std: standard.

3.4. Discussion

Herein we report the results of *P. falciparum* asexual blood stage susceptibility assays that compared the susceptibility of early rings, late rings, early trophozoites, late trophozoites and schizonts, for a set of 36 clinical and experimental antimalarials. These studies, which exposed each tightly-synchronized stage for 8 h and assessed growth stage at the same 60 h timepoint (**Fig. 3.1A**), extend earlier experimental designs that assessed activity on a subset of stages or did not include wash-offs to restrict exposure to each stage [349,350]. Since compounds are washed out after each exposure moment and parasites are allowed to continue to grow in absence of compound until the end of the assay, the stage specificity assay quantifies the cytotoxic (killing) effect of compounds. The IC_{50}^{8h} values are therefore in essence stage-specific half-maximal lethal doses (LD_{50}) [351]. This contrasts with the IC_{50}^{72h} values that are determined in assays that expose parasites continuously to compounds and measure the cytostatic (growth inhibitory) effect of compounds. Our results were combined with metabolomic profiling of the cellular pathway perturbations caused by these compounds, as an exploratory approach to identify common or unique profiles among the tested antimalarials. Classification of compounds according to the timing of their peak activity revealed a remarkable variety of profiles among both clinical and the experimental compounds (**Fig. 3.6**). As examples, the inhibitors DSM265 and atovaquone (which target DHODH and CytBC1 respectively) showed activity against late trophozoites only, and the PI4K inhibitor KAI407 showed activity against only schizonts, in good agreement with earlier studies [61,352,353] (**Fig. 3.1; Fig. 3.5; Table 3.1**).

Compounds with different chemical scaffolds that are known to target the same or related pathways showed similar stage specificity and metabolic profiles. This was especially apparent for atovaquone and DSM265 that act on related mitochondrial processes (**Fig. 3.5A**). These agents also shared similar killing dynamics, with a monophasic survival curve for the highly sensitive late trophozoites and biphasic curves for early trophozoites and schizonts (**Fig. 3.5B**). Of note, when parasite survival was assessed using only the SYBR Green signal, and not the Mitotracker signal, we observed the same killing dynamics for atovaquone and DSM265. This likely reflects a dual purpose of the mitochondria of maintaining its membrane potential through the mitochondrial electron transport chain, required for the production of ATP, and enabling pyrimidine biosynthesis through DHODH (**Fig. 3.5A**). Inhibition of DHODH by DSM265 will not only affect pyrimidine biosynthesis but also the recycling of ubiquinone that is crucial for the parasite to maintain its mitochondrial membrane potential. Likewise, inhibition of CytB by atovaquone will not only directly affect the mitochondrial membrane potential, but also the recycling of ubiquinone and therefore the function of DHODH. DHODH and CytB are thus two distinct drug targets that are functionally linked. In accordance, DSM265 and atovaquone show the same stage specificity profile. Pyrimidines are most needed in late trophozoites when DNA synthesis peaks, allowing the production of daughter merozoites during schizogony [354]. Without pyrimidines, late trophozoites would not be able to develop into functional schizonts, resulting in a low IC_{50}^{8h} and a smooth monophasic killing curve in late trophozoites (**Fig. 3.5B**). In early trophozoites and schizonts, the dependency on pyrimidines is lower but a functional mitochondrial membrane potential would still appear to be vital for the many ongoing biological processes, leading to a biphasic response in

which the first shift relates to pyrimidine biosynthesis and a second shift relates to the mitochondrial membrane potential. Early and late rings showed a monophasic response with high IC_{50}^{8h} values, reflecting a parasite growth phase when pyrimidine biosynthesis and mitochondrial activity appear to be minimal. Atovaquone inhibition through membrane potential disruption was relatively ineffective in our 8 h exposure model, illustrating the need for longer compound exposure for mitochondrial electron transport chain inhibitors [352,355]. Importantly, incomplete killing by atovaquone and DSM265 was observed in all stages, matching previous data from recrudescence-based assays that showed atovaquone to be a slow and incomplete killer [332,356].

Of note, the late trophozoite stage specificity profiles for ATQ and DSM265 are consistent with the timing of expression of their targets: *cytb* expression peaks during the late trophozoite stage, whereas maximal expression of *dhodh* spans early to late trophozoite stages [357]. The same holds true for KAE609 that targets PfATP4: transcription of *pfatp4* peaks at the early trophozoite stage [357], consistent with KAE609 being inactive against rings yet active against early trophozoites and later stages. Interestingly, *pi4k*, which encodes the target of KAI407, is transcribed at fairly stable levels without showing a clear peak at any stage [357]. The schizont-specific activity profile of KAI407 may be determined by the availability of substrates that interact at this stage with PI4K.

These assays also differentiated the mode of action of chloroquine, piperaquine, and mefloquine, which share a core 4-aminoquinoline ring structure. Piperaquine essentially consists of two molecules of chloroquine connected by a central linker. Chloroquine and

piperaquine are generally thought to act at the highly metabolically active trophozoite stage by inhibiting the biomineralization of free heme, released during hemoglobin digestion, into hemozoin, thereby causing a buildup of toxic free heme or heme-drug adducts [41]. Both chloroquine and piperaquine showed a similar stage specificity profile when the error margin is taken into account, and exerted potent growth inhibition in early ring stages. This would suggest that hemoglobin catabolism begins even in early rings, prior to the formation of the digestive vacuole inside which the bulk of hemozoin is generated. This inference is supported by a previous report [347] and studies that detected hemoglobin uptake [358] and activity of falcipains (required for hemoglobin digestion [359]) in very early rings. Notably, early rings showed a flatter slope of the dose-dependent curve than late rings and trophozoites, indicating different growth inhibitory dynamics (**Fig. 3.1, Fig. 3.2**). Metabolic perturbation profiles, nonetheless, revealed a strikingly different profile for chloroquine and piperaquine (**Fig. 3.7**). Chloroquine induced various perturbations that were not observed under piperaquine pressure, such as >2-fold increased levels of dAMP, dUTP, cytidine, xanthosine and N-acetyl-lysine, decreased *p*-hydroxybenzoate levels, and decreased peptide levels that are characteristic for hemoglobin catabolism inhibition. Some of these metabolic changes in chloroquine-exposed parasites, such as the increased dAMP levels, caused chloroquine to metabolically cluster with the PfATP4 inhibitor KAE609 and other compounds that cause an overall disturbance in cellular homeostasis. This clustering, however, is based on rather modest changes and should be interpreted with caution. Piperaquine metabolically clustered with other compounds that induced an overall low differential fold change (**Fig. 3.7**). The only notable changes were $\geq$2-fold decreased levels of dCDP, dTMP, guanosine

and guanine. This suggests that piperaquine might have an additional mode of action beyond inhibition of hemozoin formation that perturbs purine and pyrimidine metabolism.

Mefloquine, an arylamino alcohol that also shares a quinoline ring, was earlier reported to inhibit hemozoin formation in parasites at a lower level than chloroquine [93], possibly because of reduced mefloquine accumulation in the digestive vacuole. Earlier studies examining mefloquine and its relationship to the primary resistance determinant PfMDR1 (located on the membrane of the digestive vacuole) suggested that mefloquine acts primarily outside the digestive vacuole [297]. The difference in mode of action between mefloquine and chloroquine is also reflected in their stage specificity and metabolomics profiles, with mefloquine showing peak activity only in trophozoites and clustering separately from other compounds affecting hemoglobin catabolism (**Fig. 3.7**). These data further support the notion that the target of mefloquine is presumably located outside of the digestive vacuole, affecting the parasite in ways that could not be detected by our metabolomics study.

The clinical antimalarial lumefantrine displayed peak activity during both rings and trophozoites, similar to chloroquine and piperaquine but different from the trophozoite-only peak activity of mefloquine. Metabolically, lumefantrine induced minor peptide increases and clustered with GNF-Pf-5660 that is known to affect hemoglobin uptake without directly targeting hemozoin formation [271]. The different stage specificity and metabolic profiles between lumefantrine and mefloquine suggest distinct mode of actions, despite PfMDR1 being a determinant of low-level resistance to both [183].

Methylene blue is known to act as a redox cycler and is used clinically to treat methemoglobinemia via its reduction of Fe^{3+} to Fe^{2+} [360]. Methylene blue also binds hematin (a precursor of hemozoin crystals) at low micromolar concentrations *in vitro* [360]. Our finding of similar stage-specificity and metabolomic profiles between methylene blue and piperaquine suggest that both could impact heme detoxification and hemozoin formation, albeit via different mechanisms. Methylene blue potentially causes a reduction of Fe^{3+} whereas piperaquine is presumed to bind Fe^{3+}-heme and prevent its incorporation into chemically inert hemozoin [206]. Methylene blue, in contrast to piperaquine, is also potent against mature gametocytes that are not thought to degrade hemoglobin [334], implying an additional mode of action for methylene blue that might affect additional redox cycling agents such as NADPH levels [240].

Interestingly, ferroquine and naphthoquine, which are both chloroquine derivatives that are currently part of artemisinin-based combination therapies under clinical trials [361,362], shared a unique stage-specificity profile showing peak activity during early rings and a gradual increase of IC_{50}^{8h} values through to schizonts (**Fig. 3.2**). Ferroquine has hemozoin inhibitory activity similar to chloroquine and has been shown to induce the formation of hydroxyl radicals via the Fenton reaction, leading to lipid peroxidation and exacerbating oxidative stress in the parasite [363-365]. This additional mode of action might contribute to the unique stage-specific profile of ferroquine action. The mode of action of naphthoquine is less understood. Even though parasites exposed to naphthoquine and ferroquine did not reveal major changes in the levels of detected metabolites thus causing

them to cluster in the low fold change metabolic group (**Fig. 3.7**), their shared and distinctive stage-specificity profiles suggest a common target or pathway.

Compounds with peak activity during ring stages are highly desired. In our assays, naphthoquine, ferroquine and WLL-vs showed peak activity specifically during ring stages, whereas chloroquine, piperaquine, methylene blue, dihydroartemisinin, lumefantrine, GNF-Pf-5660, MMV022224 and MMV668311 showed peak activity in rings and trophozoites. This diversity among ring-active compounds suggests the presence of multiple druggable processes in rings, despite this stage being considered less metabolically active [260] than trophozoites. One such process involves the proteasome, since the ring-active compound WLL-vs specifically binds to and inhibits the β2 and β5 subunits of the *P. falciparum* 26S proteasome [269,270]. Other processes that appear to begin early in rings include hemoglobin endocytosis and catabolism [271,358,359].

We note that WLL-vs, included in our study, is a covalent binder of the *P. falciparum* 26S proteasome inhibitor, meaning that wash-out protocols would have little effect on its irreversible mode of action. Previous studies on *Plasmodium* have shown that mRNA transcripts are produced in a “just-in-time” fashion, i.e. when they are needed for the parasite’s development [357]. This would suggest that the chances of falsely detecting early stage activity are minimal. However, a lingering effect after drug wash-out could theoretically result in overestimating compound activity during later stages. For this reason, we have included five different time points at which compound exposure was started, followed by drug wash-outs, in order to minimize compound carry over. This

approach was validated with our WLL-vs data, which showed lower IC_{50}^{8h} values in rings compared to trophozoites and schizonts (**Fig. 3.2**).

An established high-priority mode of action is inhibition of mitochondrial functions, targeting either DHODH (DSM265) or CytBC1 (atovaquone) [366] (**Fig. 3.5A**). Both, however, yield resistance at low inocula, which in patients translates into an increased risk of treatment failure using these classes of inhibitors [367,368]. The experimental compounds MMV000787, MMV021735 and MMV030666 showed peak activity in late trophozoites, albeit with incomplete killing, and shared the same distinct metabolic profile of increased dihydroorotate and N-carbamoyl-L-aspartate levels and decreased orotidine 5-P levels (**Fig. 3.7**) that is characteristic for DHODH and CytBC1 inhibition [260]. Interestingly, selections with these former compounds failed to yield resistant parasites, even at high inocula of 5×10^8 parasites. They also did not show the biphasic curves observed for atovaquone and DSM265. These data raise the possibility that inhibition of mitochondrial pathways might be achievable through mode of actions that are distinct from DHODH and CytBC1 and that are less prone to resistance acquisition. In addition to the metabolic signature of mitochondrial inhibition, MMV030666 also induced decreased peptide levels, causing it to metabolically cluster with compounds inhibiting hemoglobin catabolism (**Fig. 3.7**). However, MMV030666 still maintained a late trophozoite stage-specific activity profile similar to that of DSM265 and atovaquone but distinct from the overall trophozoite or ring plus trophozoite peak activity profiles usually observed for the majority of compounds with a hemoglobin catabolism metabolic signature (**Fig. 3.4**, **Fig. 3.5, Fig. 3.7**). Cell morphological analysis of MMV030666-exposed parasites (**Fig. 3.11**)

identified late trophozoites as the most sensitive intra-erythrocytic stage, consistent with mitochondrial inhibition, but also showed a bloated digestive vacuole that is characteristic for inhibitors of Hb catabolism [201].

Most hits that clustered within the hemoglobin catabolism group, characterized by decreased peptide levels [260], showed peak activity in trophozoites (MMV027496, MMV019555, MMV000248, MMV006455, MMV007181 and MMV000442). The exception was GNF-Pf-5660 [271], lumefantrine and MMV665794 that showed peak activity against rings and trophozoites. This observation, plus additional metabolic changes induced by MMV019555, highlights the potential diversity in mode of actions among compounds showing hemoglobin catabolism perturbation.

Among all compounds tested, MMV022224 was unique both in its metabolomic fingerprint and its stage specificity. Exposure to MMV022224 caused increased peptide levels and only this compound showed activity exclusively in rings and trophozoites but not in schizonts. Peptide accumulation may suggest a metabolic disruption further downstream in the hemoglobin catabolism pathway, possibly of an aminopeptidase or transporter. These unique profiles highlight MMV022224 as an attractive hit from a discovery and development perspective.

It is important to note that the metabolomics experiments in this study were exploratory in nature, involving one to two biological replicates to screen for known and novel candidate mode of actions within a large set of compounds. Once compounds are

selected and prioritized for further discovery or development studies, these metabolomics data should be complemented with targeted in-depth follow-up studies to validate candidate targets and mode of actions as demonstrated recently for a new class of pantothenamides [369].

The asexual blood stage susceptibility profiles of compounds may also help determine whether a protein is a target or solely a resistance mechanism. Resistance selections with MMV675939, MMV665939 and MMV020746 all identified single nucleotide polymorphisms or copy number variations in the ABC transporter I family member 1, also known as ABCI3 (PF3D7_0319700) [233]. MMV675939 was most active on early and late trophozoites with IC_{50}^{8h} values that were only 2-fold higher than the IC_{50}^{72h} value, while MMV020746 and MMV665939 showed IC_{50}^{8h} values that were >28-fold higher than the IC_{50}^{72h} (**Table 3.1**). This contrast between the timing of peak activity for MMV675939 and the two other compounds suggests that they have different mode of actions and that ABCI3 is solely a resistance mediator and not the target.

Asexual blood stage susceptibility profiling may also help prioritize screening hits. Compounds with potent IC_{50}^{8h} values across all stages are of particular interest for further development as such activity profiles might compensate for a faster clearance or other pharmacokinetic-related issues that reduce *in vivo* exposure time. Dihydroartemisinin and piperaquine, two first-line antimalarial drugs, showed activity on all stages with IC_{50}^{8h} values at the most susceptible stages that were within 2-fold of their IC_{50}^{72h} values (**Table 3.1**). Chloroquine, mefloquine and lumefantrine showed larger IC_{50}^{8h} over IC_{50}^{72h} ratios,

but with IC_{50}^{8h} values still <300 nM (**Table 3.1**). Based on these parameters, ferroquine, WLL-vs, and GNF-PF-5660 represent promising antimalarial scaffolds. WLL-vs is of particular interest given its selectivity for the parasite proteasome and the fact that resistance is rare and low-grade [269,270,370]. Ferroquine has shown promising efficacy in phase II trials [361] and our assays indicated a unique ring-active profile that underscores its potential. With GNF-Pf-5660, chemical derivatization efforts are underway to improve its partial *in vivo* efficacy, established in rodent malaria models [271].

Compounds that show IC_{50}^{8h} values orders of magnitude larger than IC_{50}^{72h} values are potentially of less interest as these may have multiple mode of actions throughout intra-erythrocytic development and/or require longer exposures to achieve full killing. In addition, such a profile indicates that the short exposures usually applied for metabolomics will likely yield a less informative response. None of the current clinical or advanced candidate antimalarials showed this profile, suggesting that this is indeed a good de-prioritization criterion for further development. Examples of experimental compounds with such an unfavorable profile in our dataset were MMV022478 and MMV019017 (**Fig. 3.4**), and MMV665939 and MMV020746 that showed IC_{50}^{8h} values > 10 µM at all stages (data not shown) **(Table 3.1)**.

MMV000442, MMV006455, MMV007181 and MMV665971 showed a peculiar profile in early and late ring stages, with initial growth inhibition at lower compound concentrations that reverses to less inhibition at higher concentrations (**Fig. 3.3, Fig. 3.4**). Solubility assays with MMV0004442, MMV006455 and MMV665791 indicated that these

compounds have an aqueous solubility >100 μM, indicating that these survival curves are not due to solubility issues. This phenomenon has been observed in other chemical series and can at times be overcome through lead optimization [311]. Despite their undesirable dose-response curves, these compounds might still prove valuable as starting points for drug discovery efforts.

The asexual blood stage specificity profiles can also inform the selection of partner drugs for combination therapies. Ideally, combinations would target all different asexual blood stages. As an example, schizont-specific compounds could be partnered with compounds that target rings and trophozoites. These profiles can also be used to devise strategies to delay the emergence of resistance. For example, the late trophozoite-active compound DSM265 could be combined with another compound with a broader activity profile including late trophozoite in order to delay the emergence of DSM265 resistance [367].

In summary, integrating investigations into antimalarial stage-specific mode of actions including metabolic perturbations into drug discovery and development programs should benefit ongoing efforts to develop new medicines to counter the spread of antimalarial multidrug resistance, as part of the mission to eliminate this disease.

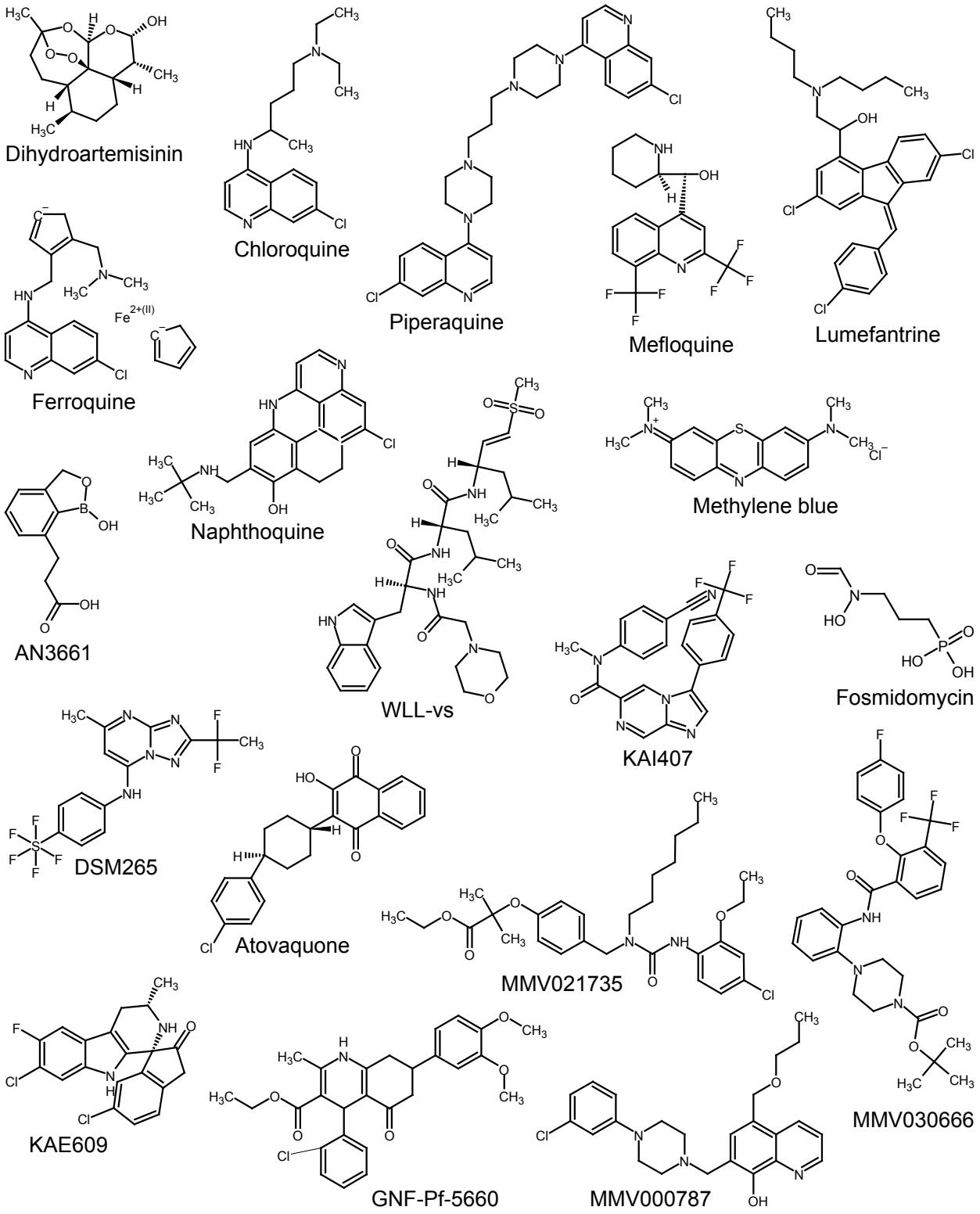

Fig. 3. 8. | Structures of the tested antimalarials, part 1. References on mode of action can be found in Table 3.2.

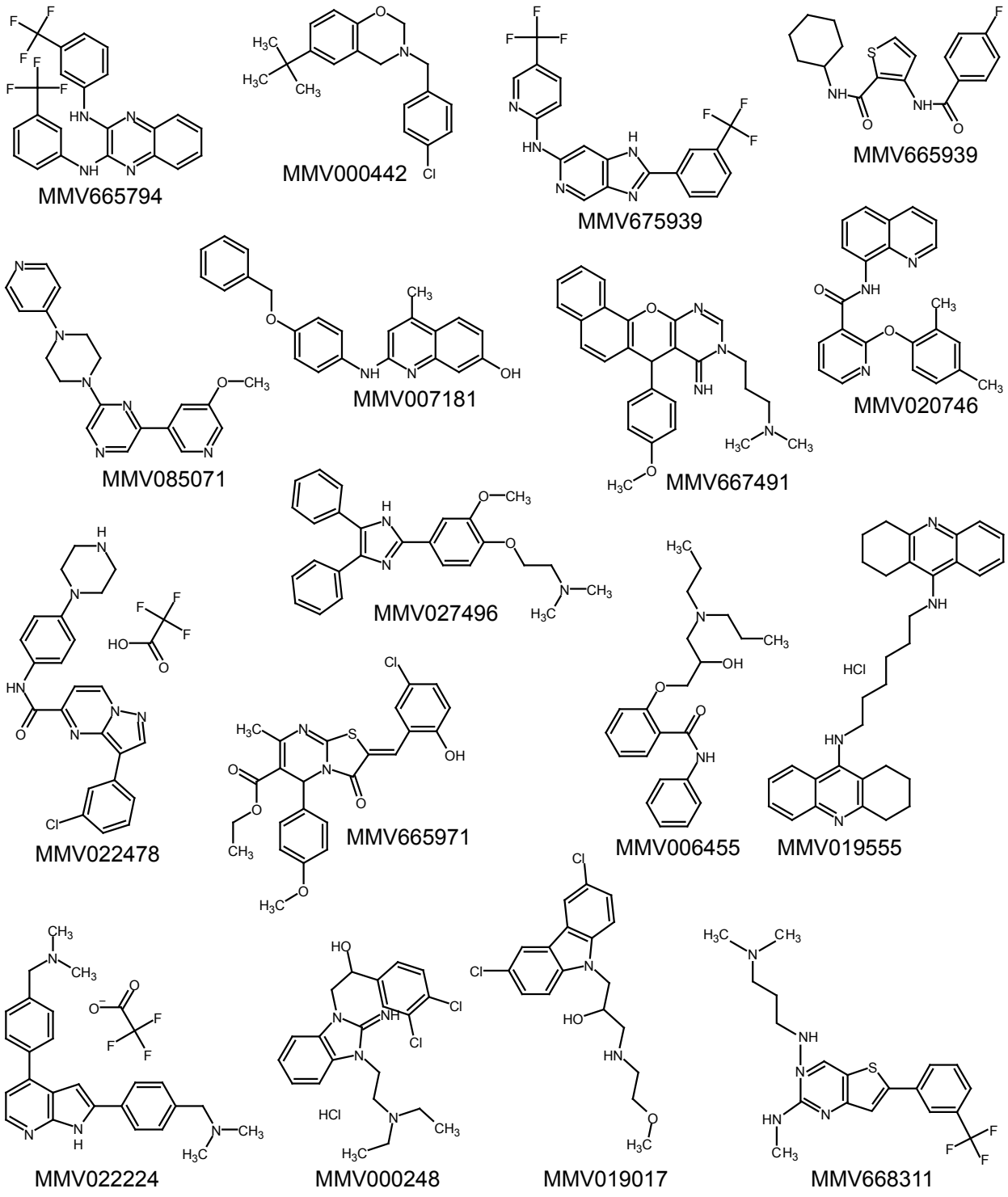

Fig. 3. 9. | Structures of the tested antimalarials, part 2. References on mode of action can be found in Table 3.2.

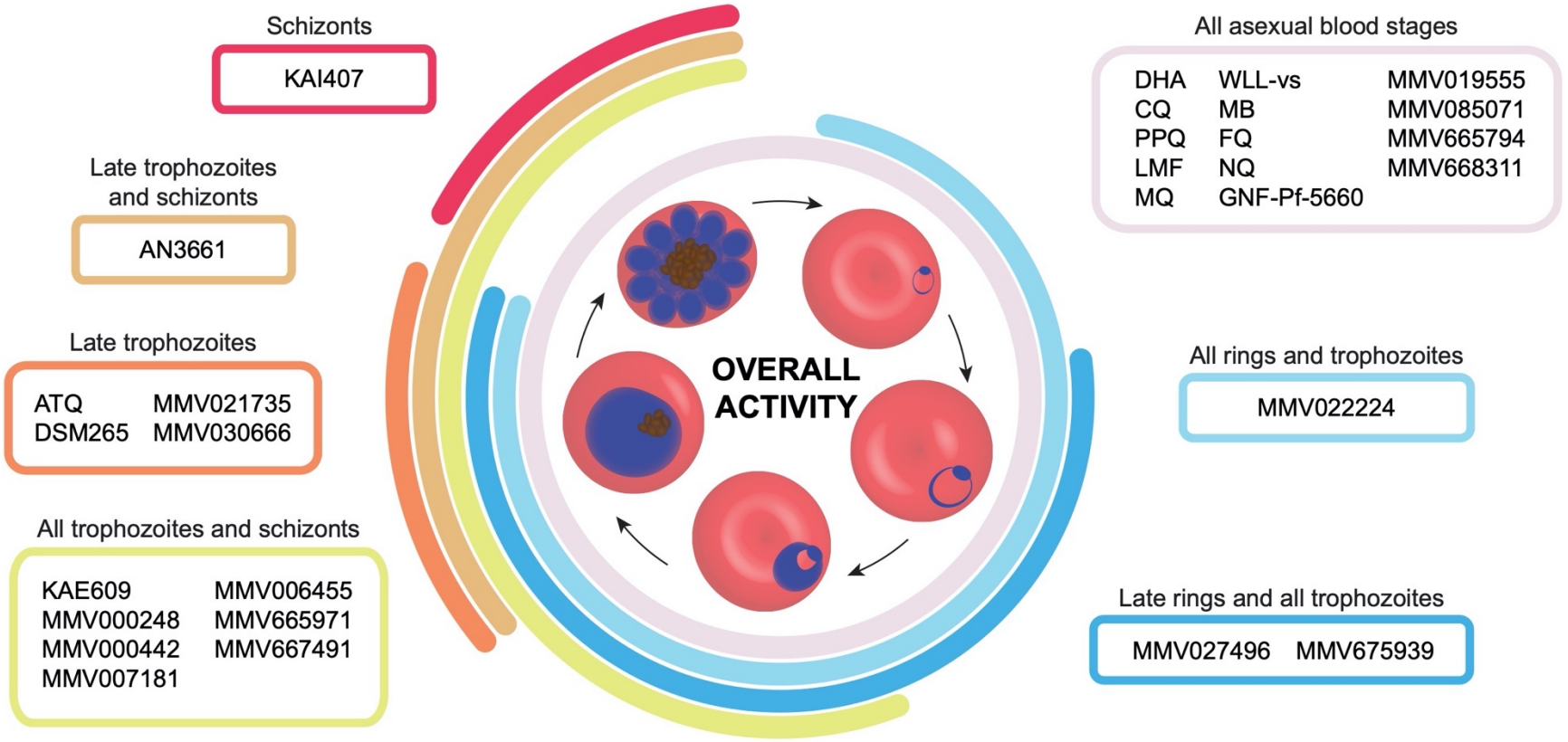

Fig. 3. 10. | Overall activity profile of compounds.

Overall activity is defined as the stages with IC_{50}^{8h} values <1 µM. Fosmidomycin, MMV000787, MMV019017, MMV020746, MMV022478 and MMV665939 are not depicted, as all stages showed IC_{50}^{8h} values >1 µM. MMV006455, MMV000442, MMV007181 and MMV665971 are omitted from panel A due to incomplete killing at individual stages. DHA: dihydroartemisinin; CQ: chloroquine; PPQ: piperaquine; LMF: lumefantrine; MQ: mefloquine; MB: methylene blue; FQ: ferroquine; NQ: naphthoquine; ATQ: atovaquone.

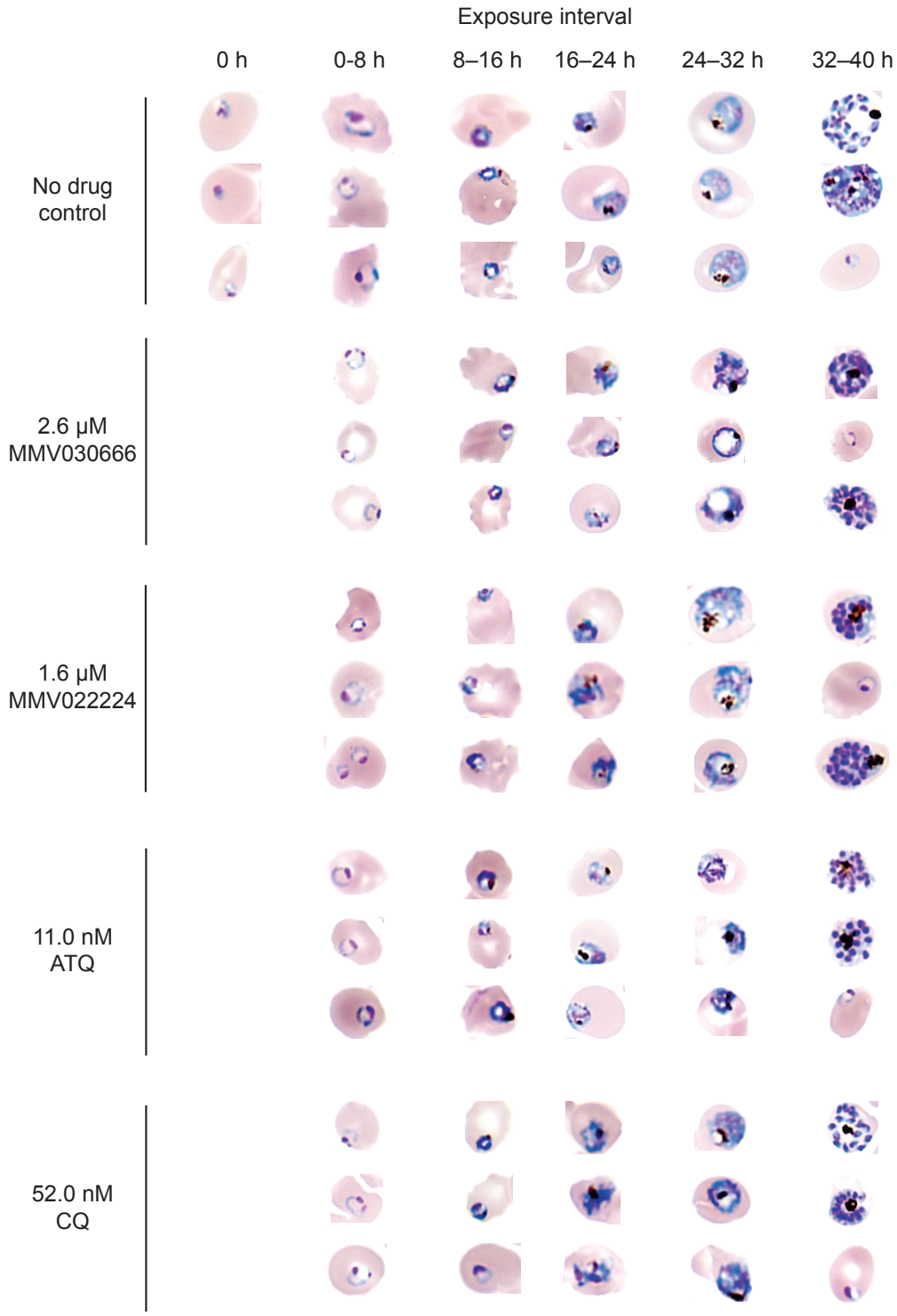

Fig. 3. 11. | Microscopical studies confirm the stage specificity profiles of MMV030666 and MMV022224, using ATQ and CQ as controls.

Synchronized parasites were exposed to 3× their lowest IC_{50}^{8h} at the indicated life stages, and were assessed at the end of each exposure. ATQ: atovaquone, CQ: chloroquine.

Chapter 4. The *Plasmodium falciparum* ABC Transporter ABCI3 Confers Parasite Strain-Dependent Pleiotropic Antimalarial Drug Resistance

James M. Murithi[1], Ioanna Deni[1], Charisse Flerida A. Pasaje[2], John Okombo[1], Jessica L. Bridgford[1], Nina F. Gnädig[1], Rachel L. Edwards[3], Tomas Yeo[1], Sachel Mok[1], Anna Y. Burkhard[1], Olivia Coburn-Flynn[1], Eva S. Istvan[4], Tomoyo Sakata-Kato[5], Maria G. Gomez-Lorenzo[6], Annie N. Cowell[7], Kathryn J. Wicht[8], Claire Le Manach[8], Gavreel F. Kalantarov[9], Sumanta Dey[2], Maëlle Duffey[10], Benoît Laleu[10], Amanda K. Lukens[5], Sabine Ottilie[7], Manu Vanaerschot[1], Ilya N. Trakht[9], Francisco-Javier Gamo[6], Dyann F. Wirth[5], Daniel E. Goldberg[4], Audrey R. Odom John[11], Kelly Chibale[8], Elizabeth A. Winzeler[7], Jacquin C. Niles[2], David A. Fidock[1,12]

[1]Department of Microbiology and Immunology, Columbia University Irving Medical Center, New York, NY 10032, USA. [2]Department of Biological Engineering, Massachusetts Institute of Technology, Cambridge, MA 02139, USA. [3]Division of Infectious Diseases, Allergy and Immunology, Center for Vaccine Development, Saint Louis University, Saint Louis, MO 63104, USA. [4]Department of Medicine, Division of Infectious Diseases, and Department of Molecular Microbiology, Washington University School of Medicine, Saint Louis, MO 63110, USA. [5]Department of Immunology and Infectious Diseases, Harvard T.H. Chan School of Public Health, Boston, MA 02115, USA; Infectious Disease and Microbiome Program, Broad Institute, Cambridge, MA 02142, USA. [6]Global Health Pharma Research Unit, GlaxoSmithKline, 28760 Tres Cantos, Madrid, Spain. [7]School of Medicine, University of California San Diego (UCSD), La Jolla, CA 92093, USA. [8]Drug Discovery and Development Center (H3D) and South African Medical Research Council Drug Discovery and Development Research Unit, Department of Chemistry and Institute of Infectious Diseases and Molecular Medicine, University of Cape Town, Rondebosch 7701, South Africa. [9]Division of Experimental Therapeutics, Department of Medicine, Columbia University Irving Medical Center, New York, NY 10032, USA. [10]Medicines for Malaria Venture, 1215 Geneva, Switzerland.

[11]Children's Hospital of Philadelphia, Philadelphia, PA 19104, USA. [12]Division of Infectious Diseases, Department of Medicine, Columbia University Irving Medical Center, New York, NY 10032, USA.

Author contributions

K.J.W. and C.L.M. synthesized compounds **1** and **6.** B.L. designed and optimized compound **5**. I.D., O.C-F., E.S.I., T.S-K. and M.G.G-L performed resistance selections. J.M.M. and I.D performed CRISPR/Cas9 SNP validation experiments. T.Y., S.M. and A.N.C. prepared and analyzed WGS data. J.M.M., I.D., J.L.B. and A.Y.B. performed asexual blood stage assays. C.F.A.P. and S.D. generated ABCI3 cKD parasites. J.M.M. and N.F.G. performed immunofluorescence assays. R.L.E. performed immuno-electron microscopy assays. J.O. generated the heme fractionation data. G.F.K. produced PfCRT antibodies. A.K.L., S.O., M.V., I.N.T., F-J.G., D.F.W., D.E.G., A.R.O.J., J.C.N., K.C., E.A.W. and D.A.F. supervised individual lab efforts and for several along with M.D. and B.L. provided funding and expertise. J.M.M., I.D. and D.A.F. wrote the manuscript, with input from all authors. All authors approved the final manuscript.

Note: This chapter is reproduced and adapted from: **James M. Murithi**, Ioanna Deni, Charisse Flerida A. Pasaje, John Okombo, Jessica L. Bridgford, Nina F. Gnädig, Rachel L. Edwards, Tomas Yeo, Sachel Mok, Anna Y. Burkhard *et al*. “The *Plasmodium falciparum* ABC Transporter ABCI3 Confers Parasite Strain-Dependent Pleiotropic Antimalarial Drug Resistance” 2021. Under review in ***Cell Chemical Biology***.

I generated: **100%** of the data in **Figs. 4.2, 4.10** and **Tables 4.1, 4.3, 4.6**; **90%** of the data in **Figs. 4.5, 4.9**; **80%** in **Fig. 4.7** and **Table 4.5**; **70%** in **Fig. 4.4** and **30%** in **Fig. 4.11**. All other data were generated by colleagues in the Fidock Lab.

4.1. Abstract

Widespread *Plasmodium falciparum* resistance to first-line antimalarials underscores the vital need to develop compounds with novel modes of action and identify new druggable targets. Here, we profiled five compounds that potently inhibit *P. falciparum* asexual blood stages. Resistance selection studies with three carboxamide-containing compounds, confirmed by gene editing and conditional knockdowns, identified point mutations in the parasite transporter ABCI3 as the primary mediator of resistance. Selection studies with imidazopyridine or quinoline-carboxamide compounds also yielded changes in ABCI3, this time through gene amplification. The mode of action of the imidazopyridine was attributed to inhibition of heme detoxification, as evidenced by cellular accumulation and heme fractionation assays. For the copy number variation-selecting compounds, we found that resistance, manifesting as a biphasic concentration-response curve, could independently be mediated by mutations in the chloroquine resistance transporter PfCRT. These studies reveal the interconnectedness of *P. falciparum* transporters in overcoming drug pressure in different parasite strains.

4.2. Introduction

An estimated 1.5 billion malaria cases and 7.6 million deaths have been averted since 2000 as a result of chemotherapy, vector control, diagnosis and access to treatment [2]. Despite this extraordinary success, 229 million new cases and 409,000 deaths were reported in 2019 alone [2], underscoring the difficult path to malaria eradication. The onset of wide-spread antimalarial parasite resistance, dating back to quinine resistance in 1910 and chloroquine (CQ) resistance in the 1950s [41], has been a major obstacle in malaria

drug discovery and development efforts and has continuously compromised the important role played by chemotherapy in saving lives. Recently, *P. falciparum* resistance to first-line Artemisinin-based Combination Therapies (ACTs) has been spreading across Southeast Asia and is now threatening sub-Saharan Africa [371-373]. This makes it imperative that we identify new druggable targets in malaria parasites using compounds that have novel modes of antiplasmodial action.

The Malaria Drug Accelerator (MalDA) consortium is a target-guided drug discovery platform that applies *in vitro* blood stage, liver stage and gametocyte screening of compounds to identify novel assayable targets [233,343,374]. Similar whole-cell screens have been used to identify antiplasmodial compounds with sub-micromolar potencies by other groups [234-236,342-345] but the lack of target identification has stalled the development of many of these compounds into candidates for clinical application [346]. We describe here a series of experiments including *in vitro* resistance selections and CRISPR/Cas9 genetic validation, drug susceptibility, conditional knock-down (cKD), drug cellular accumulation, protein localization and heme fractionation assays to characterize culture-adapted *P. falciparum* resistance to five chemically distinct compounds studied by MalDA. These data highlight an important role for the ATP-binding cassette (ABC) transporter ABCI3 (PF3D7_0319700) as a pleiotropic drug resistance determinant in *P. falciparum*.

4.3. Results

4.3.1. *In vitro* selection studies on *Plasmodium falciparum* asexual blood stage parasites select for ABCI3 point mutations or gene amplifications.

We identified possible *P. falciparum* resistance mechanisms to five chemically distinct compounds (**Fig 4.1**) by performing *in vitro* single-step resistance selections [375]. 10^7-10^9 wild-type cloned 3D7-A10 or Dd2-B2 parasites were exposed to 3× the half maximal growth inhibitory concentrations (IC_{50}) of each compound, tested in triplicate. Resistance was obtained for all five compounds and clones were recovered by limiting dilution. Whole-genome sequencing results of these clones segregated the compounds into two distinct categories: A) those that generated copy number variations (CNVs) (compounds **1** and **2**); and B) those that generated single nucleotide polymorphisms (SNPs) (compounds **3**, **4** and **5**) in ABCI3 (**Fig 4.1**). Specifically, compound **3** generated resistant parasites harboring either the ABCI3 Y2079C or R2180P mutations, compound **4** the L690I or R2180G mutations, and compound **5** the F689C or S696Y mutations (**Fig 4.2A**).

The CNV clones selected using compounds **1** and **2** all had three copies of ABCI3, compared to a single copy in the parental 3D7-A10 line, and generated biphasic dose-response curves against both compounds. These biphasic curves yielded two IC_{50} values, termed IC_{50} shift 1 and shift 2. The IC_{50} shift 1 and 2 for the CNV line against compound **1** was 106±8 nM and 1249±79 nM respectively relative to the parental IC_{50} of 47±0.8 nM (**Table 4.1**). For compound **2**, IC_{50} shifts 1 and 2 were 265±34 nM and 4054±69, respectively, compared to the parental IC_{50} of 281±19 nM. The Y2079C and R2180P SNPs that were generated from 3D7-A10 parasite selections with compound **3** resulted in a ~3×

shift in IC_{50} (2746±89 nM and 3029±141 nM respectively, compared to the parental value of 1012±64 nM). For compound **4**, the ABCI3 L690I and R2180G mutants were ~9-16× resistant to the compound (2300±217 nM and 1268±55 nM respectively compared to the 3D7-A10 parental value of 140±14 nM). Selections using compound **5** were performed on a Dd2-B2 background, yielding ABCI3 F689C and S696Y mutations that caused a ~11-180× increase in IC_{50}, i.e. 89±4 nM and 1433±24 nM compared to the parental Dd2-B2 IC_{50} of 8.0±0.9 nM (**Table 4.2**).

To test the causal role of ABCI3 SNPs in *P. falciparum* resistance to these compounds, we developed a CRISPR/Cas9 gene editing strategy to edit the L690I mutation into wild-type 3D7-A10 parasites (**Fig 4.2B**). Results with the edited (ed.) line (ABCI3 $^{L690I\ ed.}$) confirmed similar levels of resistance to the selection compound **4** as observed with the drug-pressured line (ABCI3 ^{L690I}) (20-fold vs 22-fold IC_{50} increases relative to the parent for edited vs selected mutants; **Fig 4.2C; Table 4.3**). Additionally, this mutation conferred a modest (2- to 2.3-fold) level of cross-resistance to another SNP-selecting compound **3** (that selected for Y2079C and R2180P). The L690I mutants showed no significant difference in susceptibility to the CNV-selecting compound **1** (**Fig 4.2C; Table 4.3**).

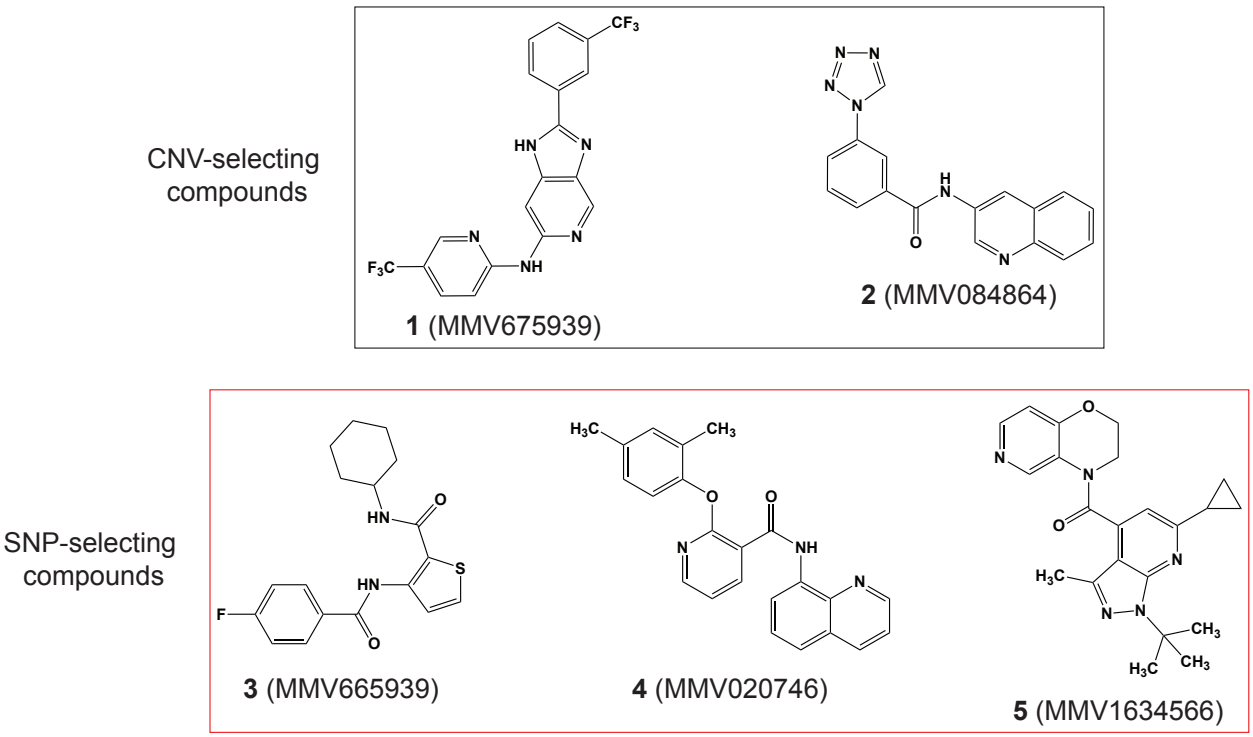

Fig. 4. 1. | Chemical structures of MMV compounds used in this study.
Compounds **1 (**MMV675939) and **2** (MMV084864) selected for CNVs in ABCI3 whereas **3** (MMV665939), **4** (MMV020746) and **5** (MMV1634566) selected for SNPs in this gene. **1** is a 2,6-disubstituted imidazopyridine (2-(3-(trifluoromethyl)phenyl)-6-*N*-(5-(trifluoromethyl)pyridin-2-yl)-1*H*-imidazo[4,5-*c*]pyridine); **2** is a quinoline tetrazole carboxamide (*N*-quinolin-3-yl-3-tetrazol-1-yl-benzamide); **3** is a thiophene carboxamide (*N*-cyclohexyl-3-[(4-fluoro-benzoyl)amino]-2-thiophenecarboxamide); **4** is an 8-aminoquinoline pyridine carboxamide (2-(2,4-dimethylphenoxy)-*N*-8-quinolinyl-3-pyridinecarboxamide); and **5** is a pyrazolopyridine carboxamide ((1-(*tert*-butyl)-6-cyclopropyl-3-methyl-1*H*-pyrazolo[3,4-*b*]pyridin-4-yl)(2,3-dihydro-4*H*-pyrido[4,3-*b*][1,4]aoxazin-4-yl)methanone).

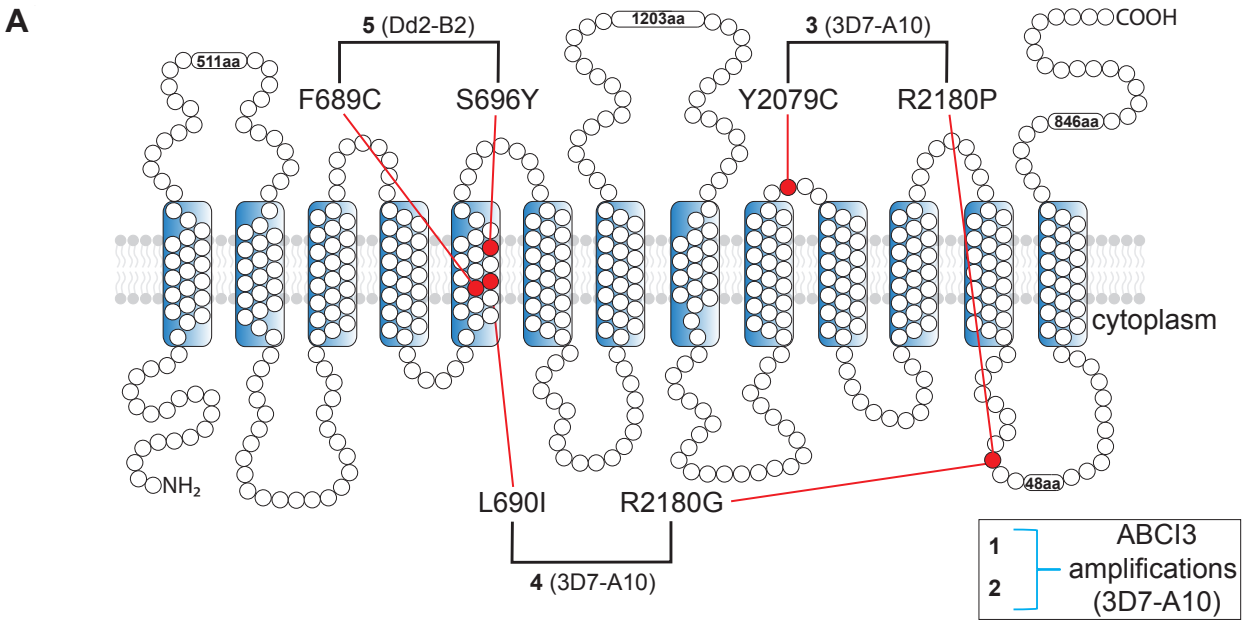
A
5 (Dd2-B2)
1203aa
3 (3D7-A10)
COOH
511aa
F689C
S696Y
Y2079C
R2180P
846aa
cytoplasm
NH2
48aa
L690I
R2180G
4 (3D7-A10)
1
2
ABCI3 amplifications (3D7-A10)

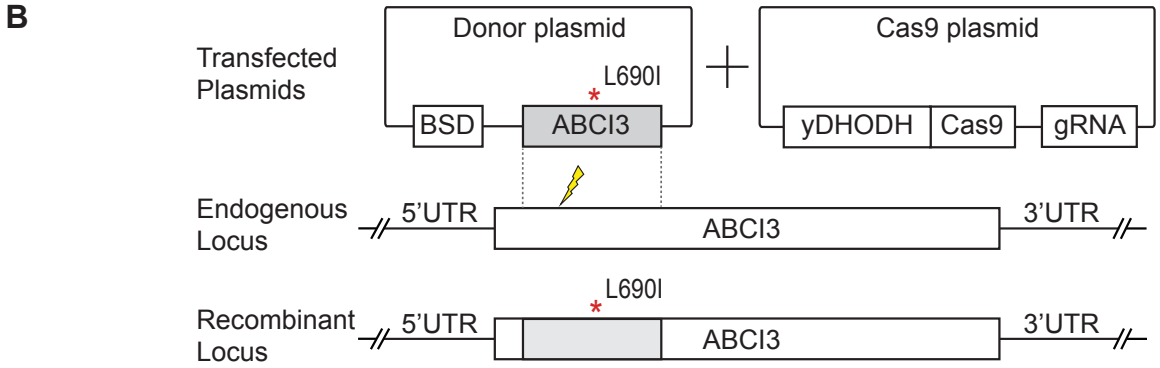
B
Transfected Plasmids
Donor plasmid
L690I
BSD
ABCI3
Cas9 plasmid
yDHODH
Cas9
gRNA
Endogenous Locus
5'UTR
ABCI3
3'UTR
Recombinant Locus
L690I
5'UTR
ABCI3
3'UTR

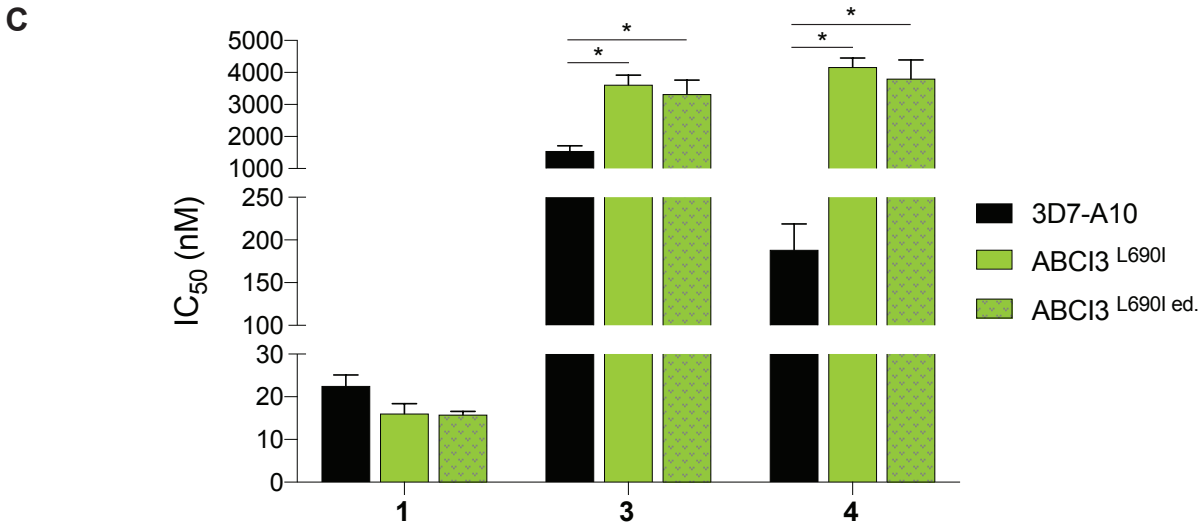
C
IC50 (nM)
5000
4000
3000
2000
1000
250
200
150
100
30
20
10
0
1
3
4
3D7-A10
ABCI3 L690I
ABCI3 L690I ed.

Fig. 4. 2. | ABCI3 L690I mutation confers resistance to compounds 3 and 4.
(**A**) Topology of ABCI3 protein based on the TMHMM, InterPro and Uniprot structural algorithms. SNP-selecting compounds (**3-5**) generated the mutations indicated in red, whereas CNV-selecting compounds are boxed. (**B**) The ABCI3 L690I point mutation was introduced into parental 3D7-A10 parasites using a two-plasmid CRISPR/Cas9 approach with the nearby double stranded break site indicated with a thunderbolt. Transfected parasites were selected using blasticidin-S deaminase (BSD). gRNA: guide RNA; yDHODH: yeast dihydroorotate dehydrogenase; UTR: untranslated region. (**C**) Parasites Cas9-edited to express the ABCI3 L690I mutation (ABCI3 $^{L690I\ ed.}$) phenocopied the gain of resistance observed in **4**-pressured parasites harboring this same mutation (ABCI3 ^{L690I}). L690I conferred cross resistance to **3** but not the CNV-selecting compound **1**. Bar graphs indicate mean±SEM IC_{50} values of 72 h dose-response assays with asynchronous parasites. N, n = 5, 2; * $p<0.05$, as defined using Mann-Whitney *U* tests of mutants vs. parental 3D7-A10.

Table 4. 1. | *Plasmodium falciparum* asexual blood stage IC_{50} data in nM for the tested antimalarials.

	3D7-A10			ABCI3 $^{3\ copies}$				ABCI3 ^{Y2079C}				ABCI3 ^{R2180P}				ABCI3 ^{R2180G}				ABCI3 ^{L690I}			
Antimalarials	Mean IC_{50}	SEM	N	Mean IC_{50}	SEM	N	*P* value	Mean IC_{50}	SEM	N	*P* value	Mean IC_{50}	SEM	N	*P* value	Mean IC_{50}	SEM	N	*P* value	Mean IC_{50}	SEM	N	*P* value
1	47.0	0.8	8	106 (1249)	8.0 (79.0)	15	0.0003 (<0.0001)	48.0	0.8	14	0.71	58.0	2.0	14	0.0001	56.0	2.0	5	0.0062	45.0	1.0	7	0.23
2	281	19.0	6	265 (4054)	34.0 (69.0)	4	0.48 (0.0095)	252	13.0	6	0.24	275	12.0	6	0.94	260	14.0	6	0.48	208	11.0	6	0.0043
3	1012	64.0	11	2890	246	5	0.0005	2746	89.0	15	<0.0001	3029	141	15	<0.0001	2784	196	8	<0.0001	2511	225	8	<0.0001
4	140	14.0	10	500	47.0	15	<0.0001	1241	34.0	8	<0.0001	1918	61.0	7	0.0001	1268	55.0	4	0.002	2300	217	5	0.0007
5*	2.0	0.1	10	25.0	0.9	11	<0.0001	8.0	0.7	6	0.0002	29.0	1.7	6	0.0002	21.0	1.0	6	0.0002	2.0	0.3	9	0.36
6	16.0	2.0	11	32.0	3.0	15	0.0001	20.0	1.0	10	0.11	25.0	1.0	10	0.0015	23.0	1.0	8	0.01	17.0	0.7	8	0.54
Dihydroartemisinin	0.4	0.1	6	0.3	0.0	6	0.13	0.4	0.1	6	0.39	0.6	0.1	6	0.24	0.4	0.1	6	0.59	0.4	0.1	6	0.31
Chloroquine	5.0	0.5	4	4.9	0.4	5	0.91	5.1	0.6	5	0.90	6.4	0.6	6	0.17	4.8	0.3	5	0.56	5.3	0.4	5	0.73
Piperaquine	8.5	0.6	5	8.0	1.1	5	0.84	9.5	1.2	5	0.31	10.0	1.6	5	0.55	8.7	1.0	5	0.42	8.2	0.9	5	0.84
md-amodiaquine	10.6	0.2	6	6.6	0.8	6	0.002	7.6	0.9	6	0.04	11.3	0.4	5	0.25	11.7	1.4	4	>0.9999	10.7	0.5	5	>0.9999
Quinine	13.9	0.7	6	11.5	0.7	4	0.11	12.8	0.8	5	0.33	16.1	0.7	6	0.06	12.2	0.8	4	0.11	12.1	0.7	4	0.19
Lumefantrine	0.8	0.2	4	1.4	0.3	4	0.34	1.1	0.2	4	0.49	1.4	0.2	5	0.11	0.8	0.3	5	0.90	0.9	0.3	5	0.90
Mefloquine	4.2	0.6	5	4.0	0.5	5	0.84	4.6	0.6	6	0.66	5.7	0.7	6	0.18	5.6	0.7	5	0.22	5.2	0.5	5	0.31

SEM: standard error of the mean; N: number of biological repeats (with technical duplicates); () the IC_{50} and SEM of the second shift of the biphasic curve. * Selections with compound **5** were run on a Dd2-B2 parental background (IC_{50} = 8nM). *P* values were determined by comparison between the variant lines and parental 3D7-A10 using Mann-Whitney *U* tests.

Table 4. 2. | *Plasmodium falciparum* asexual blood stage IC_{50} data in nM for the tested antiplasmodial compounds.

	Dd2-B2			ABCI3 $^{F689C\ ed.}$				ABCI3 $^{S696Y\ ed.}$			
Antimalarials	Mean IC_{50}	SEM	N	Mean IC_{50}	SEM	N	*P* value	Mean IC_{50}	SEM	N	*P* value
1	27.0(1404)	3.0(343)	4	30.0	3.0	6	--	34.0	2.0	6	--
2	265(3542)	14.0(465)	5	257	26.0	7	--	279	26.0	7	--
3	1546	95.0	7	956	112	7	0.0041	>5 mM		4	0.0061
4	246	20.0	7	36.0	4.0	7	0.0006	>10 mM		4	0.0061
5*	8.0	0.9	6	89.0	4.0	6	0.0022	1433	24.0	7	0.0012

SEM: standard error of the mean; N: number of biological repeats (with technical duplicates); () the IC_{50} and SEM of the second shift of the biphasic curve. * Selections with compound **5** were run on a Dd2-B2 parental background. *P* values were determined by comparison between the variant lines and parental Dd2-B2 using Mann-Whitney *U* tests. -- not determined.

Table 4. 3. | *Plasmodium falciparum* asexual blood stage IC_{50} data in nM for compounds 1, 3 and 4 against 3D7-A10 parent, drug-selected, and gene-edited L690I parasite lines.

	3D7-A10			ABCI3 ^{L690I}				ABCI3 $^{L690I\ ed.}$			
Compounds	Mean IC_{50}	SEM	N	Mean IC_{50}	SEM	N	*P* value	Mean IC_{50}	SEM	N	*P* value
1	23.0	2.6	6	16.0	2.4	4	0.11	16.0	0.8	4	0.11
3	1548	161	4	3616	299	4	0.03	3327	436	4	0.03
4	188	30.0	4	4168	286	4	0.03	3805	585	4	0.03

SEM: standard error of the mean; N: number of biological repeats (with technical duplicates). ABCI3 ^{L690I}: *P. falciparum* line generated from selections with compound 4. ABCI3 $^{L690I\ ed.}$: *P. falciparum* line generated by introducing the ABCI3 L690I mutation into parental 3D7-A10 using CRISPR/Cas9. *P* values were determined by comparison between the variant lines and parental 3D7-A10 using Mann-Whitney *U* tests.

We also validated the ABCI3 F689C and S696Y mutations by introducing them into parental Dd2-B2 parasites using a separate “all in one” CRISPR/Cas9 strategy (**Fig. 4.3**). The edited (ABCI3 $^{F689C\ ed.}$ and ABCI3 $^{S696Y\ ed.}$) and original drug-selected lines (ABCI3 ^{F689C} and ABCI3 ^{S696Y}) displayed similar gains of resistance to compound **5** (11-fold vs 12-fold increase in IC_{50} for F689C selected vs edited clones, and 179-fold vs 203-fold IC_{50} increase for the S696Y selected vs edited clones, respectively; **Fig. 4.3; Table 4.4**). These data confirm that the L690I, F689C and S696Y mutations in ABCI3 are drivers of parasite resistance to compounds **4** and **5**.

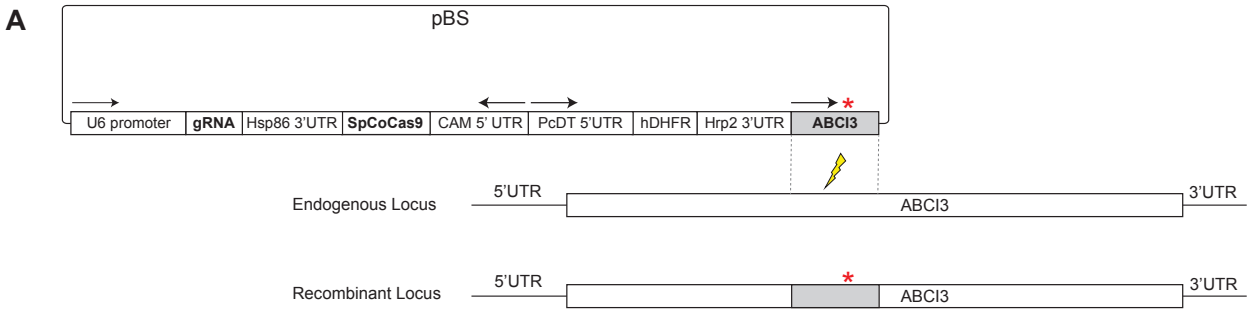

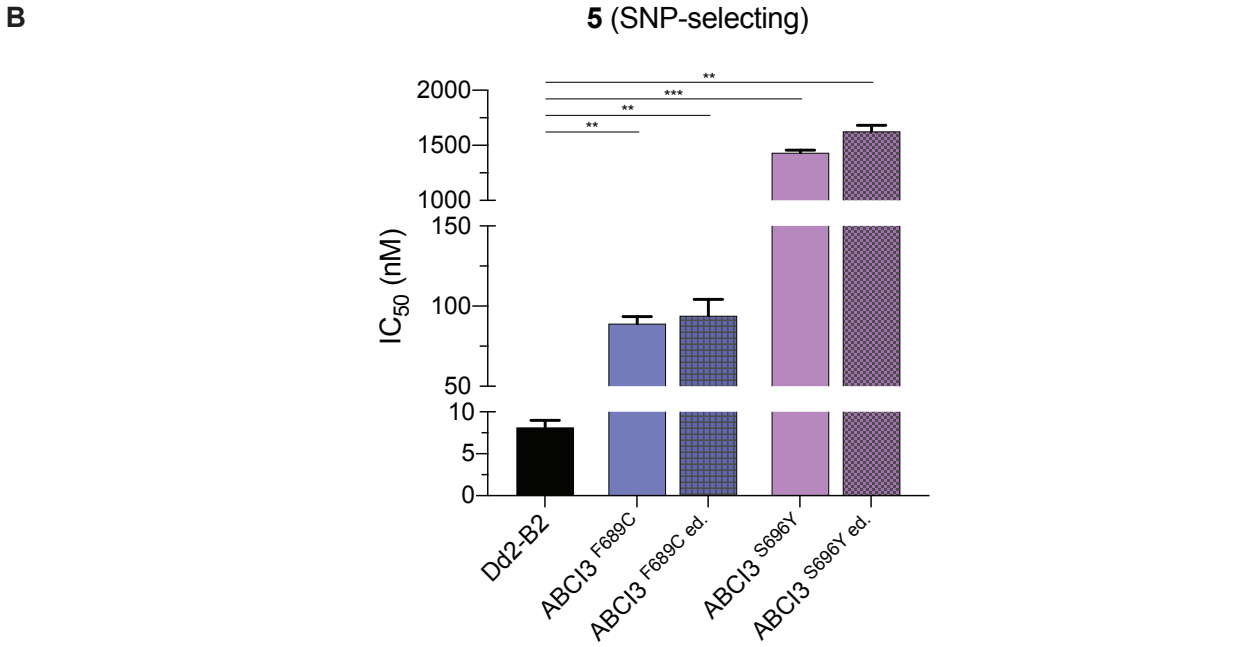

Fig. 4. 3. | ABCI3 F689C and S696Y mutations are the drivers of parasite resistance to compound 5.

(**A**) CRISPR/Cas9 strategy to introduce ABCI3 point mutations into the wild-type Dd2-B2 parasite line. The plasmid contains a human dihydrofolate reductase (hDHFR) selectable marker and a sequence encoding the guide RNA (gRNA), expressed from a PcDT and a U6 promoter, respectively. (**B**) F689C- and S696Y-edited parasites have comparable levels of resistance to compound **5** as do the selected clones. pBS: BlueScript plasmid; Hrp2: histidine-rich protein 2; Hsp86: Heat shock protein 86; SpCoCas9: *Streptococcus pyogenes-Plasmodium falciparum* codon-optimized Cas9; CAM: Calmodulin; PcDT: *Plasmodium chabaudi* dihydrofolate reductase-thymidylate synthase; UTR: Untranslated region. Mean ± SEM; N≥4,n=2. Mann-Whitney *U* tests compared the edited and selected lines to the parent Dd2-B2. **p<0.01.

Table 4. 4. | *Plasmodium falciparum* asexual blood stage IC_{50} data in nM for compound 5 against Dd2-B2 parent, selected and edited ABCI3 F689C and S696Y cell lines respectively.

	Dd2-B2			ABCI3 ^{F689C}				ABCI3 $^{F689C\ ed.}$				ABCI3 ^{S696Y}				ABCI3 $^{S696Y\ ed.}$			
Compound	Mean IC_{50}	SEM	N	Mean IC_{50}	SEM	N	*P* value	Mean IC_{50}	SEM	N	*P* value	Mean IC_{50}	SEM	N	*P* value	Mean IC_{50}	SEM	N	*P* value
5	8.0	0.9	6	89.0	4.0	6	0.0022	94.0	10.0	6	0.0022	1433	24.0	7	0.0006	1626	56.0	7	0.0012

SEM: standard error of the mean; N: number of biological repeats (with technical duplicates). ABCI3 ^{F689C}/ ABCI3 ^{S696Y}: *P. falciparum* lines generated from selections with compound 5. ABCI3 $^{F689C\ ed.}$/ ABCI3 $^{S696Y\ ed.}$: *P. falciparum* lines generated by introducing ABCI3 F689C and S696Y mutations into parental Dd2-B2 using CRISPR/Cas9. *P* values were determined by comparing the shift in IC_{50} between the variant lines and parental Dd2-B2 using Mann-Whitney *U* tests.

We conducted 72 h susceptibility assays using asynchronous 3D7-A10 or Dd2-B2 parental lines and their corresponding drug-resistant clones to investigate levels of resistance conferred by CNVs of ABCI3 to the SNP-selecting compounds and vice versa. Results from these experiments showed that CNVs of ABCI3 not only conferred parasite resistance to the CNV-selecting compounds **1** and **2** but also to the three SNP-selecting compounds (~3-fold increase in IC_{50} for compound **3**, ~3.6-fold for compound **4** and ~12.5-fold for compound **5**; **Table 4.1**). In addition, the 3D7-A10-based CNV clone with three copies of ABCI3 and the Dd2-B2 parental line displayed biphasic dose-response curves when tested against compounds **1** and **2** (**Fig. 4.4A, C**).

We observed that the effect of mutations in ABCI3 was compound-specific and sometimes sensitized parasites to the SNP-selecting compounds. For example, ABCI3 F689C mutation conferred parasite sensitivity to both compounds **3** and **4** (~2× and 7× decrease in IC_{50} respectively) despite conferring parasite resistance to compound **5** (~11× increase in IC_{50}; **Fig. 4.4C; Table 4.2**). With the exception of the L690I mutation that does not confer parasite resistance to compound **5**, the other profiled mutations in ABCI3 (Y2079C, R2180P, R2180G and S696Y) conferred parasite resistance to the three SNP-selecting compounds (**Fig. 4.4B-C; Table 4.2**). However, none of the profiled SNPs in ABCI3 conferred resistance to the two CNV-selecting compounds **1** and **2** (**Fig. 4.4A, C; Table 4.2**). Interestingly, the L690I mutant parasites (selected with compound **4**) showed no shift in susceptibility to compound **5** even though that compound selected for an adjacent ABCI3 F689C mutation (**Fig. 4.2A, 4.4B**).

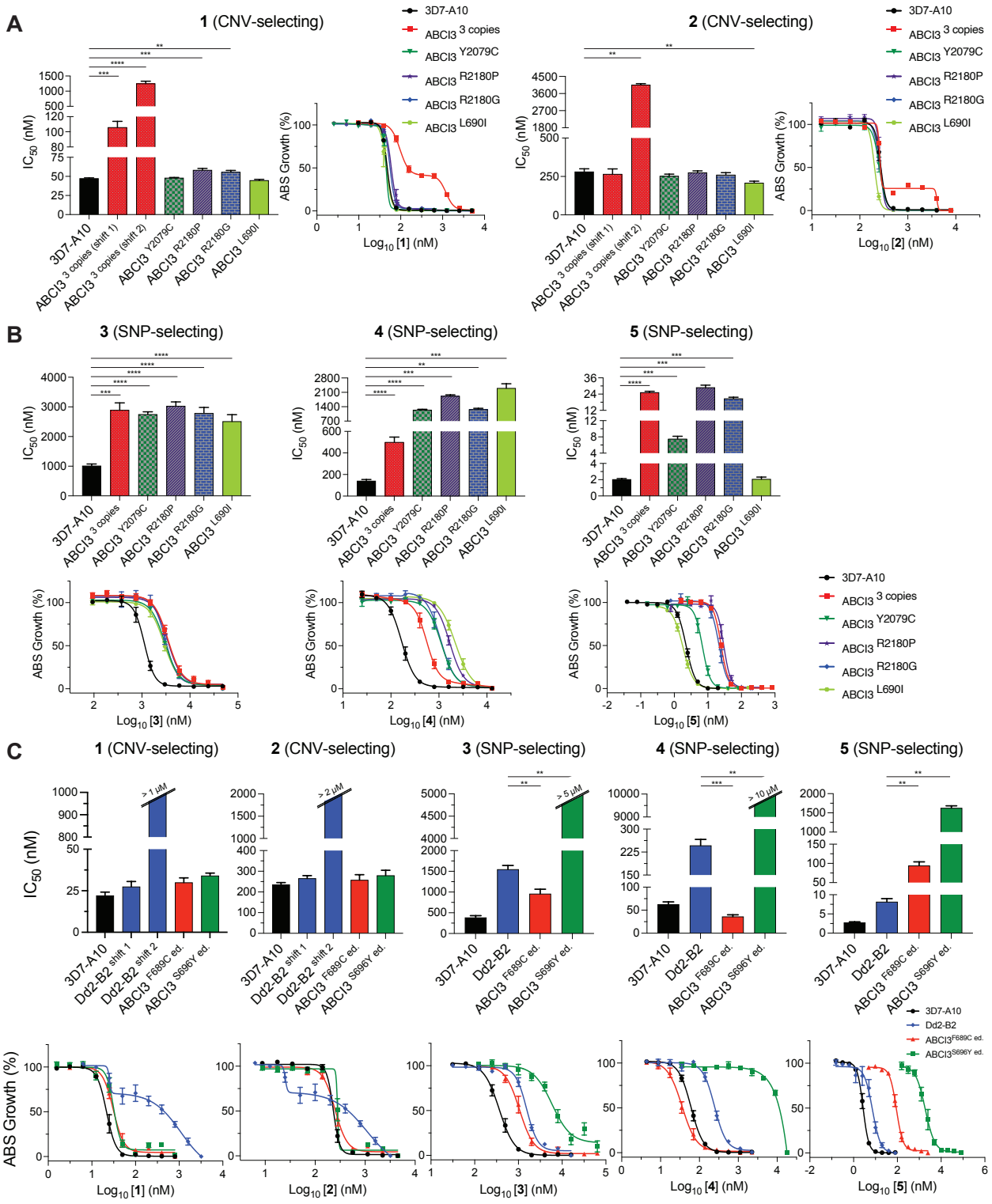
A
1 (CNV-selecting)
2 (CNV-selecting)
IC50 (nM)
ABS Growth (%)
3D7-A10
ABCI3 3 copies
ABCI3 Y2079C
ABCI3 R2180P
ABCI3 R2180G
ABCI3 L690I
3D7-A10
ABCI3 3 copies (shift 1)
ABCI3 3 copies (shift 2)
ABCI3 Y2079C
ABCI3 R2180P
ABCI3 R2180G
ABCI3 L690I
Log10 [1] (nM)
Log10 [2] (nM)
B
3 (SNP-selecting)
4 (SNP-selecting)
5 (SNP-selecting)
Log10 [3] (nM)
Log10 [4] (nM)
Log10 [5] (nM)
C
1 (CNV-selecting)
2 (CNV-selecting)
3 (SNP-selecting)
4 (SNP-selecting)
5 (SNP-selecting)
> 1 µM
> 2 µM
> 5 µM
> 10 µM
3D7-A10
Dd2-B2 shift 1
Dd2-B2 shift 2
Dd2-B2
ABCI3 F689C ed.
ABCI3 S696Y ed.
Dd2-B2
ABCI3F689C ed.
ABCI3S696Y ed.

Fig. 4. 4. | CNVs of ABCI3 confer resistance across all tested chemotypes while SNPs confer compound-specific resistance or hypersensitization.
(**A**) ABCI3 amplification in 3D7-A10 parasites mediates a biphasic gain of resistance to **1** and **2**, whose activities are unaffected by SNPs in this gene. (**B**) ABCI3 CNVs and most selected SNPs confer resistance in 3D7-A10 parasites to the three SNP-selecting compounds **3-5**. The L690I mutation, however, does not impact the potency of compound **5**. (**C**) The F689C and S696Y ABCI3 SNPs edited into Dd2 parasites eliminate the biphasic dose-response observed with **1** and **2** tested against the Dd2 parent. These mutations afford compound-specific gains of resistance or hypersensitization to the SNP-selecting compounds **3-5**. Mean ± SEM IC_{50} values and dose-dependent inhibitions are shown in the bar graphs and dose response curves respectively and were calculated from 72 h assays with asynchronous parasites. N≥5, n=2; **p < 0.01; ***p < 0.001; ****p < 0.0001. Mann-Whitney *U* tests compared resistant lines to their respective parent (3D7-A10 or Dd2-B2).

CNVs of ABCI3 only conferred ~2-fold increase in IC_{50} for compound **6**, which closely resembles the CNV-selecting compound **1**, when compared to parental 3D7-A10 values (**Fig. 4.5B, 4.6; Table 4.1**). In contrast, the ABCI3 CNV line had a ~2× to 27× (shift 1 and 2 respectively) increase in IC_{50} compared to the parental line when tested with compound **1** (**Table 4.1**). 3D7-A10 selection studies with compound **6** did not yield resistance, despite using the same conditions as with **1**, indicating a reduced resistance liability with **6**. In a separate assay, neither SNPs nor CNVs of ABCI3 conferred resistance to a panel of seven clinical antimalarials (dihydroartemisinin, CQ, piperaquine, monodesethyl-amodiaquine, quinine, lumefantrine and mefloquine) (**Fig. 4.5A, 4.6; Table 4.1**).

Together, these data suggest that ABCI3 constitutes a resistance pathway that is distinct from that of existing first-line drugs and the tested ABCI3 SNP and CNV-selecting compounds might have different molecular targets. In addition, data from the SNP

susceptibility assays and the cross-resistance results with compound **6** provide evidence that ABCI3 genetic changes confer compound-specific resistance.

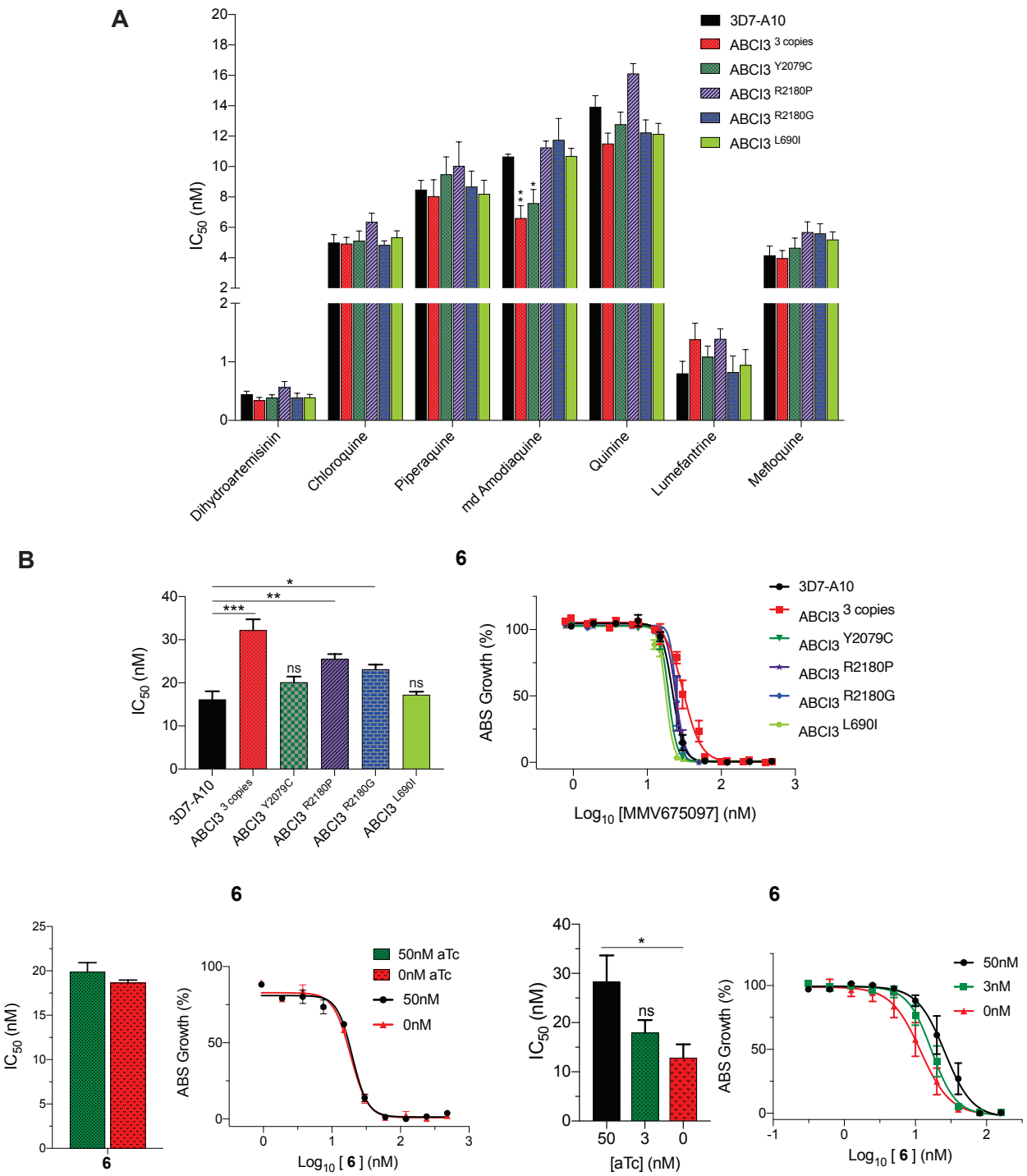

Fig. 4. 5. | Genetic modifications of ABCI3 do not confer cross resistance to first-line antimalarials or to a compound that is structurally similar to compound 1.

(**A**) Dose-response assays of ABCI3 CNV and SNP lines showed no cross-resistance against a panel of clinical antimalarials. Mean ± SEM; N≥4, n=2. Mann-Whitney *U* tests vs. 3D7-A10. (**B**) Compound **6** is structurally similar to the CNV-selecting compound **1** but displays a different dose response profile. The activity of compound **6** was explored with asynchronous ABCI3 edited and selected lines in 72 h dose-response assays (top graphs). The knockdown of ABCI3 showed minimal increase in sensitivity to compound **6** (bottom-right graph) in a 56 h assay. The concentration of anhydrotetracycline (aTc) had no effect on the growth of NF54 control line (bottom-left graph). Mean ± SEM; N≥2, n=2. Mann-Whitney *U* tests compared the different parasite variants to 3D7-A10, and medium or no ABCI3 (3 nM and 0 nM aTc, respectively) to wild-type ABCI3 expression (50nM aTc).

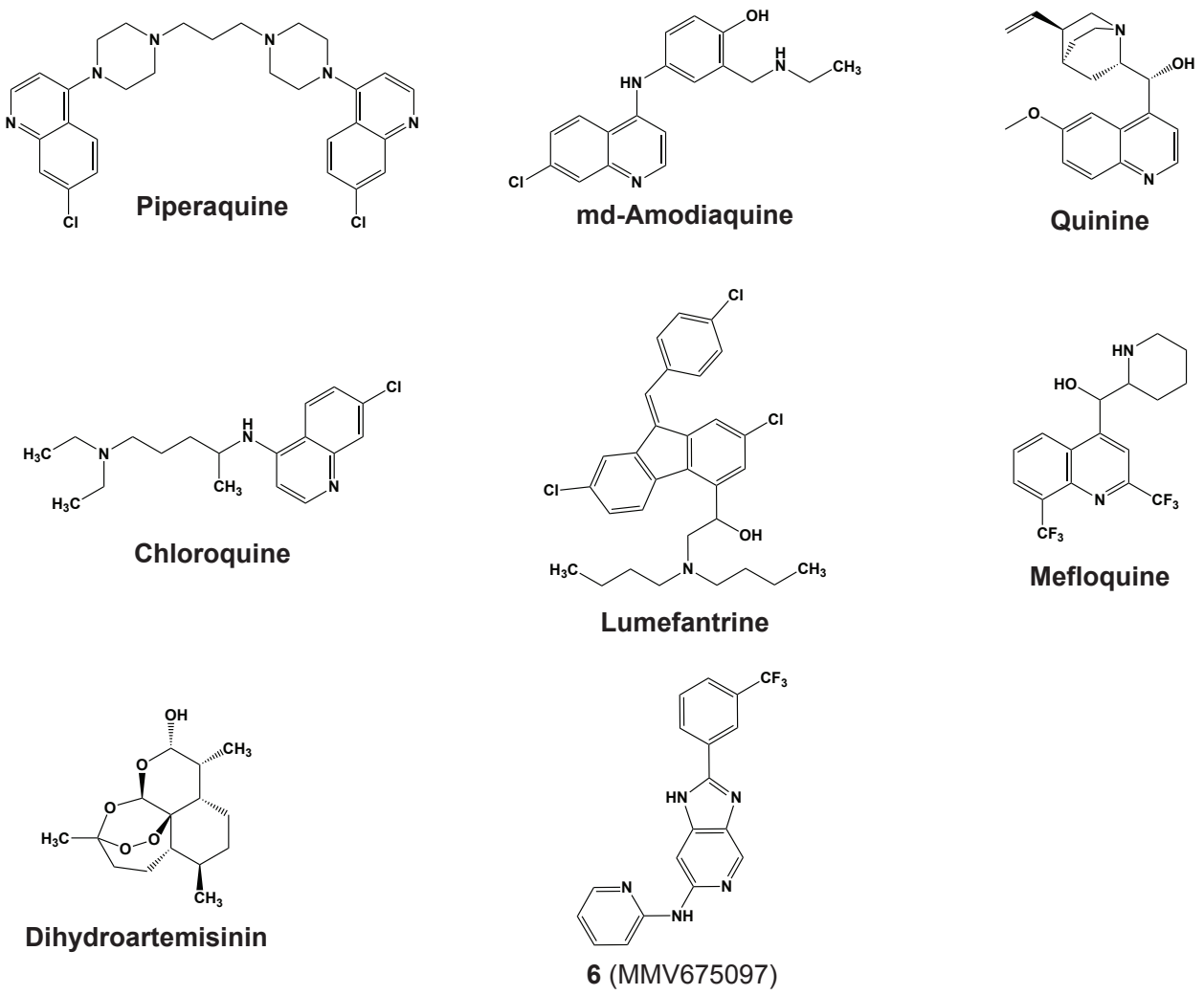

Fig. 4. 6. | Chemical structure of first-line antimalarials and MMV compound 6.
Compound **6** is identical to compound **1** apart from the absence of a $-CF_3$ group in the pyridyl ring.

4.3.2. Evidence for ABCI3 SNP-selecting compounds targeting ABCI3.

To further explore the different interactions between ABCI3 and SNP- or CNV-selecting compounds, we engineered a conditional knockdown (cKD) parasite line in which ABCI3 expression levels were regulated via the TetR-DOZI system [321,322] (**Fig. 4.8A**). In this system, translation of ABCI3 protein occurs in the presence of anhydrotetracycline (aTc), but not in its absence. Wild-type ABCI3 expression levels were maintained by culturing

parasites in the presence of 50 nM aTc. Medium and low ABCI3 expression levels were achieved by culturing the parasites in 3 nM and 0 nM aTc respectively. In the absence of aTc, ABCI3 cKD parasite growth was reduced by ~33% compared to control after the first cell cycle and by ~92% after the second cycle (72 h and 120 h respectively; **Fig. 4.7A**). We used this system to test possible compound inhibition of ABCI3 by conducting 56 h drug susceptibility assays with CQ as a negative control (**Fig. 4.7B-G; Table 4.5**). Compound-target interactions were determined by comparing the IC_{50} of compounds against wild-type versus ABCI3 cKDs parasites. We observed an aTc-dependent increase in parasite sensitivity to the two CNV-selecting compounds **1** and **2**, with 2-3× hypersensitivity at 0 nM aTc (**Fig. 4.7C-D; Table 4.5**). In contrast, under the same conditions we observed a 7-11× increase in sensitivity to the three SNP-selecting compounds **3**, **4** and **5** (**Fig. 4.7E-G; Table 4.5**). cKD parasites were ~2-fold more sensitive to compound **6** in the absence of aTc (**Fig. 4.5B; Table 4.5**). Wild-type parasite susceptibility to the tested compounds was not aTc-dependent (**Fig. 4.8**). The observed increase in cKD sensitivity to the SNP-selecting compounds suggests a stronger inhibitory interaction with ABCI3 that is distinct from that of the CNV-selecting compounds.

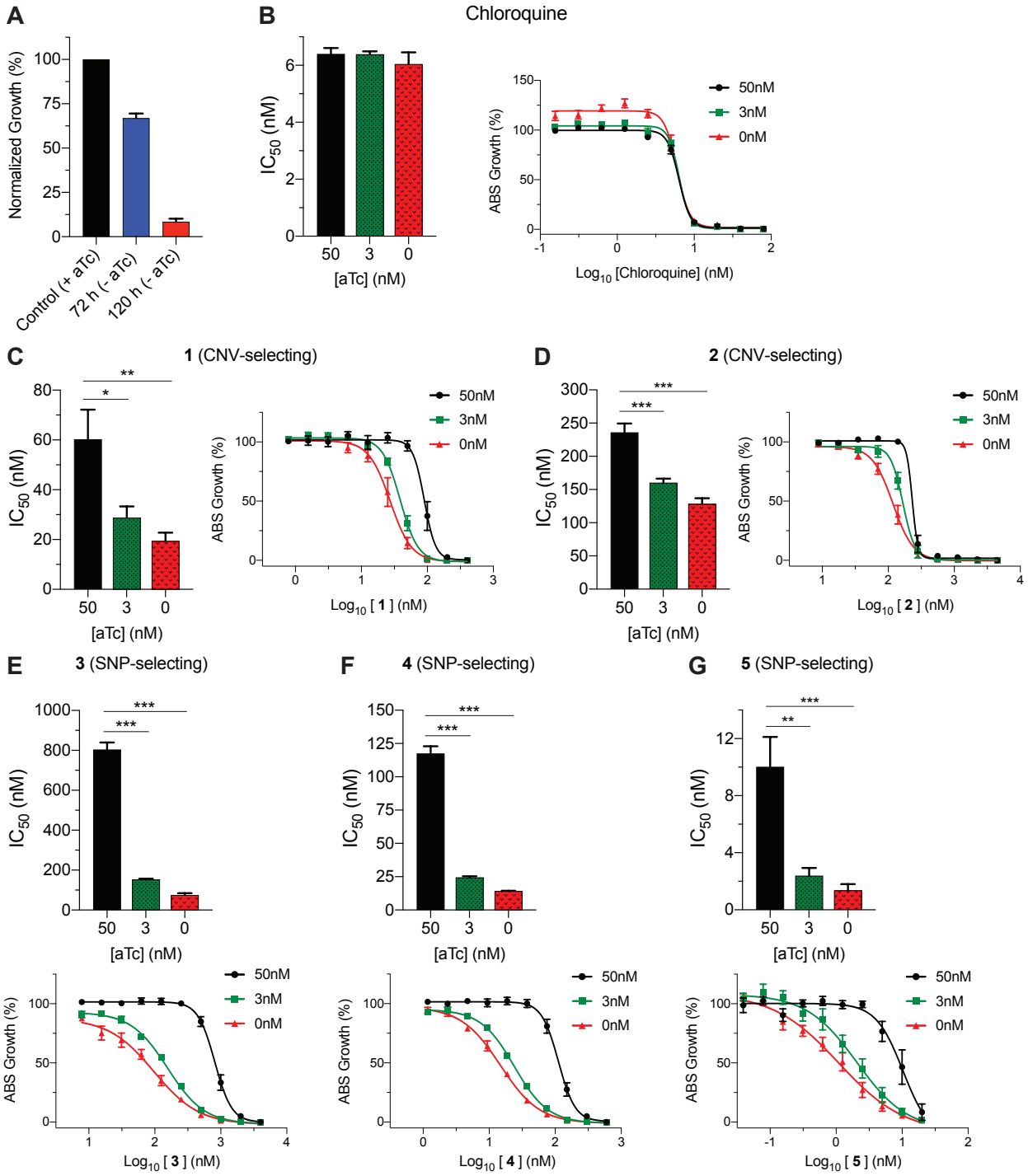

Fig. 4. 7. | Validation of SNP-selecting compound inhibition of ABCI3 using conditional knockdown assays.

(**A**) Down-regulation of ABCI3 (cKD), caused by removing aTc from the culture, reduced parasite viability by ~33% and 92% after one and two complete replication cycles, respectively, providing evidence for ABCI3 essentiality. (**B**) CQ does not inhibit ABCI3

and was used as a negative control. (**C-D**) ABCI3 cKD lines are only 2 to 3-fold sensitized to compounds **1** and **2**. (**E-G**) In the absence of aTc, cKD parasites are ~7 to 11-fold sensitized to SNP-selecting compounds **3**, **4** and **5**, suggesting direct inhibition of ABCI3 as a target. Bar graphs and growth curves indicate mean ± SEM IC_{50} values of 56 h dose-response assays with highly synchronized ring-stage parasites. N, n = 5, 2; *p<0.05, **p<0.01, ***p<0.001. Mann-Whitney *U* tests compared parasites with partially or fully downregulated levels of ABCI3 (achieved with 3 nM and 0 nM aTc, respectively), to parasites with wild-type ABCI3 expression (50 nM aTc).

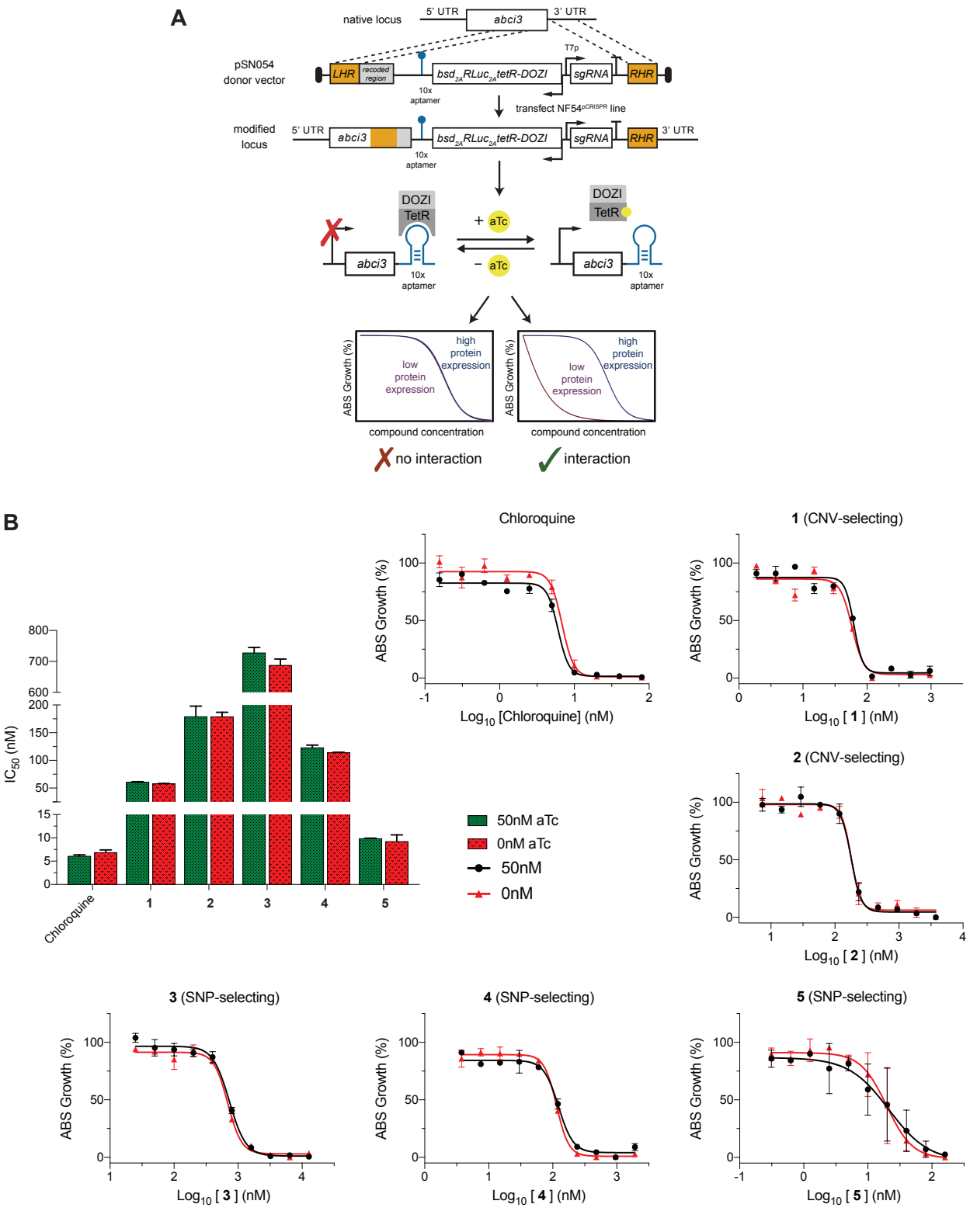
A
native locus
5' UTR
abci3
3' UTR
pSN054
donor vector
T7p
LHR
recoded region
bsd2ARLuc2AtetR-DOZI
sgRNA
RHR
10x aptamer
transfect NF54pCRISPR line
modified locus
DOZI
TetR
+ aTc
– aTc
high protein expression
low protein expression
ABS Growth (%)
compound concentration
no interaction
interaction
B
Chloroquine
1 (CNV-selecting)
2 (CNV-selecting)
3 (SNP-selecting)
4 (SNP-selecting)
5 (SNP-selecting)
IC50 (nM)
50nM aTc
0nM aTc
50nM
0nM
Log10 [Chloroquine] (nM)
Log10 [1] (nM)
Log10 [2] (nM)
Log10 [3] (nM)
Log10 [4] (nM)
Log10 [5] (nM)

Fig. 4. 8. | Regulation of ABCI3 expression using a conditional knock-down line.
(**A**) The pSN054 plasmid was used to transfect NF54^{pCRISPR} parasites to generate a conditional knockdown ABCI3 transgenic line. (**B**) The concentration of aTc had no effect on the growth of NF54 control parasites tested in 56 h assays against the compounds shown. Mean ± SEM; N, n=2.

Table 4. 5. | *Plasmodium falciparum* asexual blood stage IC_{50} data in nM for ABCI3-linked antiplasmodial inhibitors when tested in the presence or absence of aTc in a conditional knockdown cell line.

	50 nM aTc			3 nM aTc				0 nM aTc			
Antimalarials	Mean IC_{50}	SEM	N	Mean IC_{50}	SEM	N	*P* value	Mean IC_{50}	SEM	N	*P* value
Chloroquine	6.4	0.2	4	6.4	0.1	3	>0.9999	6.0	0.4	4	0.69
1	60.2	12.0	7	28.7	4.6	8	0.04	19.4	3.4	7	0.0023
2	236	13.5	8	160	6.2	7	0.0003	128	8.7	8	0.0002
3	804	35.2	7	153	4.2	8	0.0003	74.9	9.6	7	0.0006
4	117	5.5	8	24.5	0.9	7	0.0003	14.1	0.3	8	0.0002
5	10.0	2.1	7	2.4	0.6	7	0.0012	1.4	0.4	8	0.0003
6	28.3	5.4	7	18.0	2.6	8	0.28	12.9	2.7	7	0.03

SEM: standard error of the mean; N: number of biological repeats (with technical duplicates). *P* values were determined by comparing the IC_{50}s of parasites grown under 3 and 0 nM aTc with those grown at 50 nM, using Mann-Whitney *U* tests.

4.3.3. CNV-selecting compound 1 accumulates to high levels in parasites.

We used the parasite inoculum effect on antiplasmodial potency [376] to assess the cellular accumulation of one CNV and two SNP-selecting compounds: **1**, **3** and **4**. The CNV-selecting compound **1** displayed an inoculum-dependent IC_{50} profile similar to that of CQ against parental 3D7-A10 and L690I edited cell lines (**Fig. 4.9A-B**). In contrast, the ABCI3 CNV line had a markedly different profile against **1**, suggesting a difference in this compound's cellular accumulation in the presence of three copies of ABCI3 (**Fig. 4.9B**). We extrapolated the linear relationship between the inoculum size and the measured IC_{50} for CQ and **1** to determine the absolute IC_{50}, which was then used to calculate the cellular accumulation ratio (CAR) (**Fig. 4.9C**) [324]. CAR results predicted that CQ accumulated ~1-2× more in 3D7-A10 and the L690I mutant compared to the CNV line with three copies of ABCI3, whereas compound **1** was predicted to accumulate ~30× more in 3D7-A10 compared to the CNV line. Compound **1** accumulation in the L690I mutant line was estimated to be ~2× less compared to parent 3D7-A10 (**Fig. 4.9C; Table 4.6**). Compounds **3** and **4** did not display an inoculum-dependent concentration response (**Fig. 4.10**). These findings suggest that ABCI3 gene amplification might confer resistance to the CNV-selecting compounds by reducing their concentrations at their site(s) of antiplasmodial action. The lack of cellular accumulation for the SNP-selecting compounds suggests that they might kill parasites through modes of action that differ from those of CNV-selecting compounds.

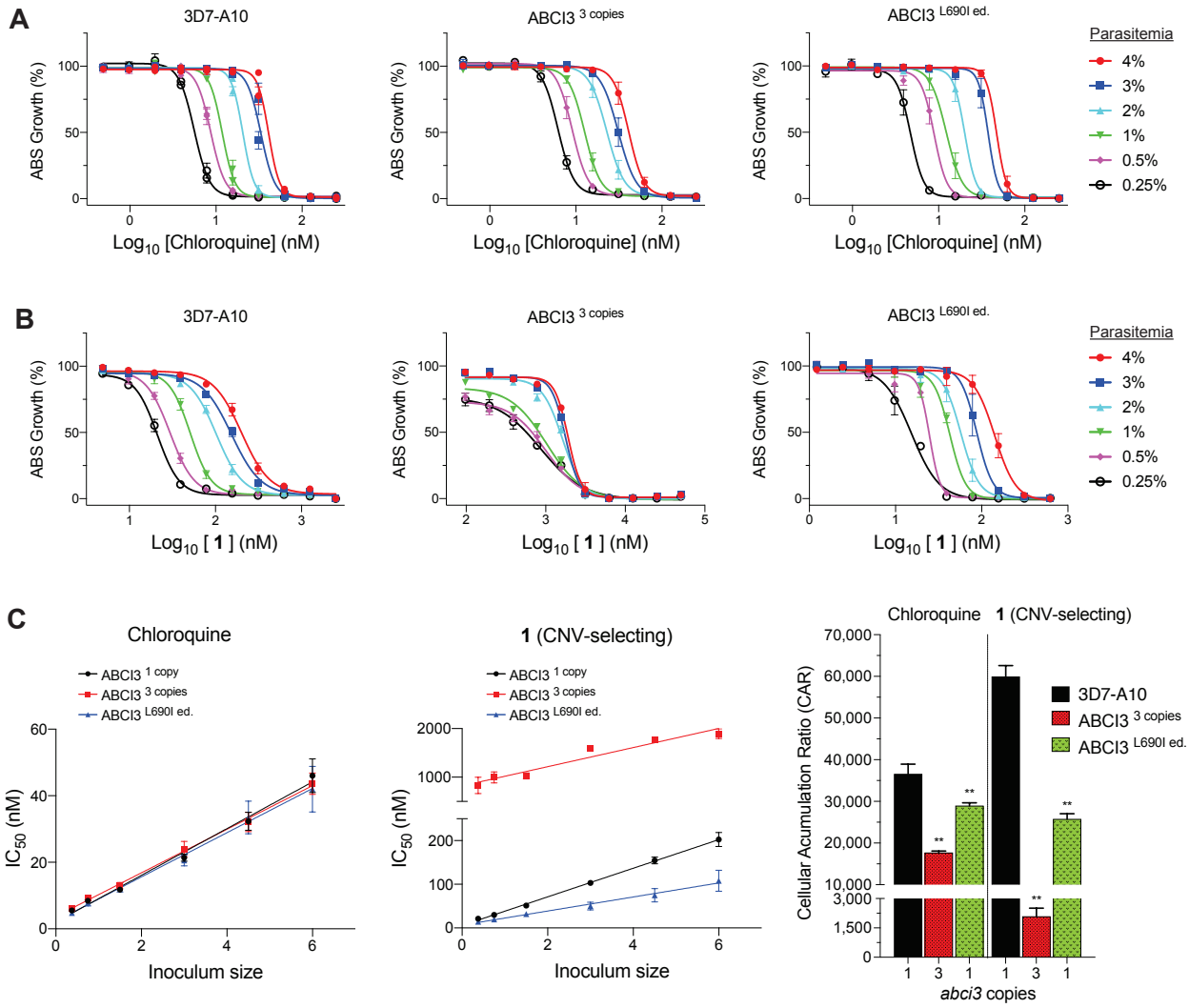

3D7-A10^{WT}-ABCI3-3×Flag

3D7-A10^{WT}-ABCI3-3×HA

Fig. 4. 9. | ABCI3 amplification confers resistance to 1 by potentially effluxing this compound away from its site of action.

(**A**) CQ displays an inoculum effect with a parasitemia-dependent dose-response curve unaffected by amplification or point mutation in ABCI3. Growth was determined 48 h after initiating drug treatment of highly synchronized ring-stage parasites. (**B**) Parental 3D7-A10 and ABCI3 $^{L690I\ ed.}$ parasites also display a parasitemia-dependent dose-response to compound **1**. A reduced inoculum effect was observed with the ABCI3 CNV line treated with **1**. (**C**) The ABCI3 CNV parasite line displays ~30× lower cellular accumulation ratio for compound **1** compared to parental 3D7-A10. CQ was used as a positive control. Mean ± SEM; N, n = 5, 2; **p<0.01. Mann-Whitney *U* tests vs. 3D7-A10. (**D**) ABCI3 foci localize to punctate structures in the parasite cytosol and occasionally with the nucleus and the ER. ABCI3 Flag-tagged parasites were stained with DAPI (nucleus, blue) and antibodies specific to Flag (green), PfCRT (DV membrane, red) and BIP (ER, magenta). Scale bars: 2μm. (**E**) Immuno-EM image of an HA-tagged ABCI3 trophozoite stained with anti-HA antibodies, revealing staining in the cytosol, nucleus, nuclear membrane and ER. Arrowheads highlight organelles of interest. C, cytosol; ER: endoplasmic reticulum; N: nucleus; NM: nuclear membrane; Hz: hemozoin crystals. Scale bar: 500 nm.

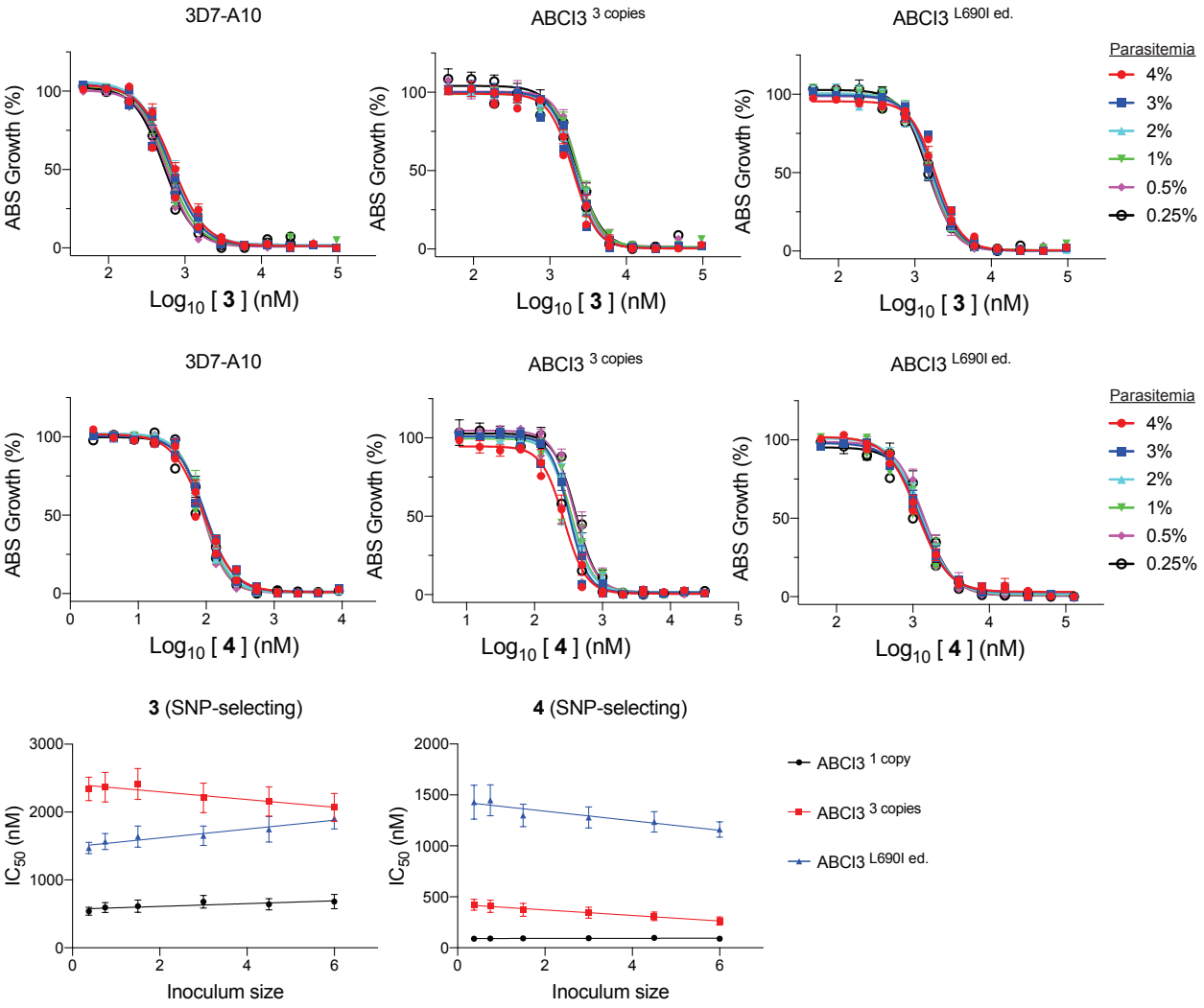

Fig. 4. 10. | ABCI3 mutations and amplifications do not show parasitemia-dependent dose responses against SNP-selecting compounds.

Compounds **3** and **4** had similar dose-response across all the three tested lines regardless of the starting parasite inoculum size. The absolute IC_{50} could therefore not be calculated from extrapolating the linear relationship between starting inoculum size and the measured IC_{50}. Mean ± SEM; N, n = 5, 2.

Table 4. 6. | Cellular accumulation ratio of chloroquine and compound 1 in *Plasmodium falciparum* asexual blood stage parasites.

	3D7-A10			ABCI3 $^{3\ copies}$				ABCI3 $^{L690I\ ed.}$			
Antimalarials	Mean IC_{50}	SEM	N	Mean IC_{50}	SEM	N	*P* value	Mean IC_{50}	SEM	N	*P* value
Chloroquine	36553	2385	6	17658	414	6	0.0022	28916	729	6	0.0043
1	59915	2678	6	2082	426	6	0.0022	25744	1288	6	0.0022

SEM: standard error of the mean; N: number of biological repeats (with technical duplicates). *P* values were determined by comparing accumulation levels between the variant lines and parental 3D7-A10, using Mann-Whitney *U* tests.

4.3.4. ABCI3 shows broad localization to multiple intraparasitic compartments.

We interrogated the subcellular localization of ABCI3 by performing immunofluorescence and immuno-electron microscopy (IEM) assays on tagged ABCI3 parasite lines [193] using 3×HA- or 3×Flag-tagged lines, respectively. We used CRISPR/Cas9 to generate recombinant 3D7-A10 parasite lines that expressed either a 3×Flag or a 3×HA tag at the C-terminal end of the endogenous ABCI3 locus (3D7-A10^{WT}-ABCI3-3×Flag or 3D7-A10^{WT}-ABCI3-3×HA; **Fig. 4.9D, E**).

Immunofluorescence assays (IFA) using an antibody against the Flag tag localized ABCI3 to foci on or around the nucleus as well as in the parasite cytosol (**Fig. 4.9D, 4.11A**). No evident co-localization was observed with the PfCRT digestive vacuole (DV) marker [377], the endoplasmic reticulum (ER) marker binding immunoglobulin protein (Bip) [378] or the cis-Golgi marker ER lumen protein retaining receptor (ERD2) [379] (**Fig. 4.9D, 4.11A**). We observed minimal association with the vesicular transport markers Rab5B and Rab7 [380] (**Fig. 4.11A**). These Rab proteins are thought to contribute in part to endocytosis of host Hb to the DV [193,358,381]. IEM analysis of at least eight parasites cultured independently in triplicate (31 total images) localized ABCI3 49% of the time to the cytosol and 24% to the nucleus and nuclear membrane. Other sites of localization included the DV (8%), the plasma membrane (6%), and the ER and intracellular vesicles (13%) (**Fig. 4.9E, 4.11B, 4.12; Table 4.7**). Parallel processing of untagged parasites revealed no staining with these same labeling conditions. This broad intracellular distribution of ABCI3 mirrors an earlier report of mCherry-3×Myc tagged ABCI3 localizing to intraparasitic structures and surrounding membranes [382].

A

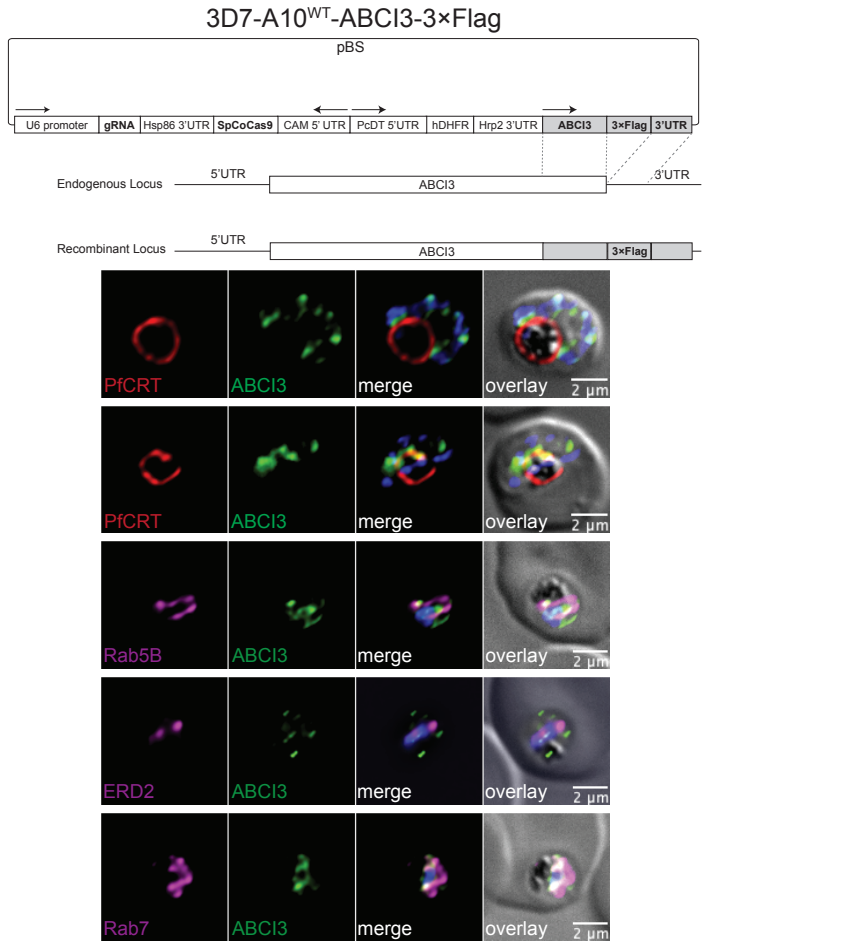
3D7-A10WT-ABCI3-3×Flag
pBS
U6 promoter
gRNA
Hsp86 3'UTR
SpCoCas9
CAM 5' UTR
PcDT 5'UTR
hDHFR
Hrp2 3'UTR
ABCI3
3×Flag
3'UTR
Endogenous Locus
5'UTR
ABCI3
3'UTR
Recombinant Locus
5'UTR
ABCI3
3×Flag
PfCRT
ABCI3
merge
overlay
2 μm
PfCRT
ABCI3
merge
overlay
2 μm
Rab5B
ABCI3
merge
overlay
2 μm
ERD2
ABCI3
merge
overlay
2 μm
Rab7
ABCI3
merge
overlay
2 μm

B

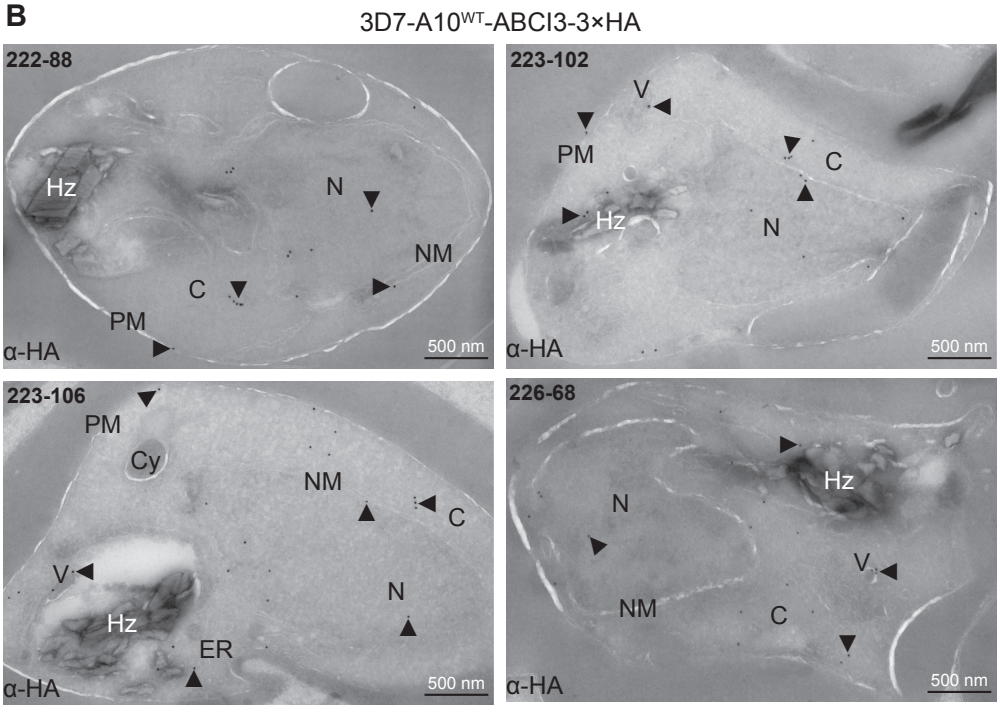
3D7-A10WT-ABCI3-3×HA
222-88
Hz
N
NM
C
PM
α-HA
500 nm
223-102
V
PM
C
Hz
N
α-HA
500 nm
223-106
PM
Cy
NM
C
V
N
Hz
ER
α-HA
500 nm
226-68
Hz
N
V
NM
C
α-HA
500 nm

Fig. 4. 11. | ABCI3 foci localize to vesicles and various cellular organelles.
(**A**) In the fluorescent image, ABCI3 Flag-tagged parasites were stained with anti-Flag (green), DAPI (nuclear, blue), anti-PfCRT (DV membrane, red), anti-ERD2 (cis-golgi), or anti-Rab5B or anti-Rab7 (markers of vesicular transport) antibodies. The plasmid used to generate the tagged lines is illustrated. Scale bars: 2 μm. (**B**) Immuno-EM images of HA-tagged ABCI3 parasites stained with anti-HA antibodies. ER, endoplasmic reticulum; N, nucleus; NM, nuclear membrane; Hz, hemozoin crystals (digestive vacuole); V, vacuole; PM, plasma membrane and C, cytosol. Cy, cytostome. Scale bar: 500 nm.

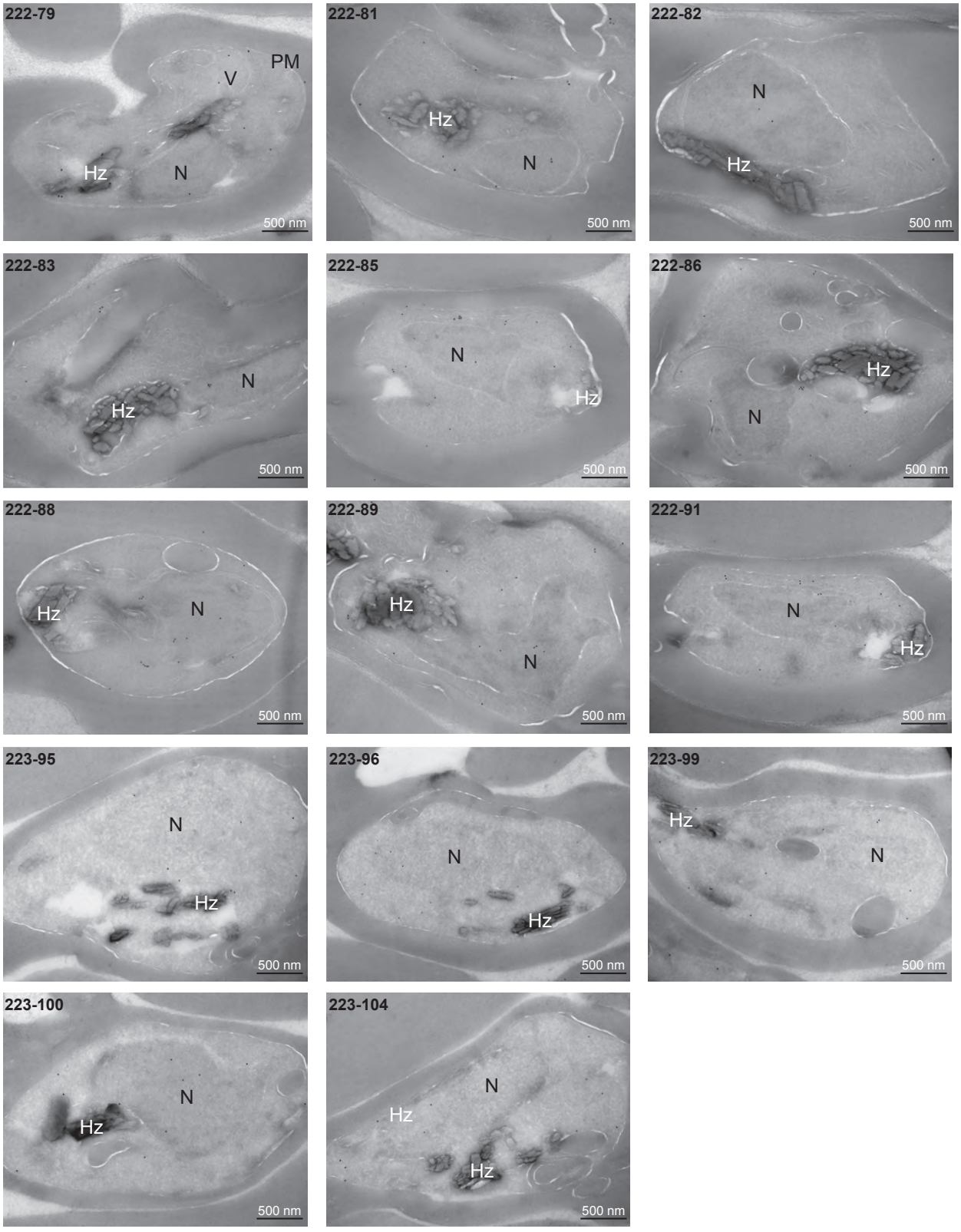
222-79
PM
V
Hz
N
500 nm
222-81
Hz
N
500 nm
222-82
N
Hz
500 nm
222-83
N
Hz
500 nm
222-85
N
Hz
500 nm
222-86
Hz
N
500 nm
222-88
Hz
N
500 nm
222-89
Hz
N
500 nm
222-91
N
Hz
500 nm
223-95
N
Hz
500 nm
223-96
N
Hz
500 nm
223-99
Hz
N
500 nm
223-100
N
Hz
500 nm
223-104
N
Hz
Hz
500 nm

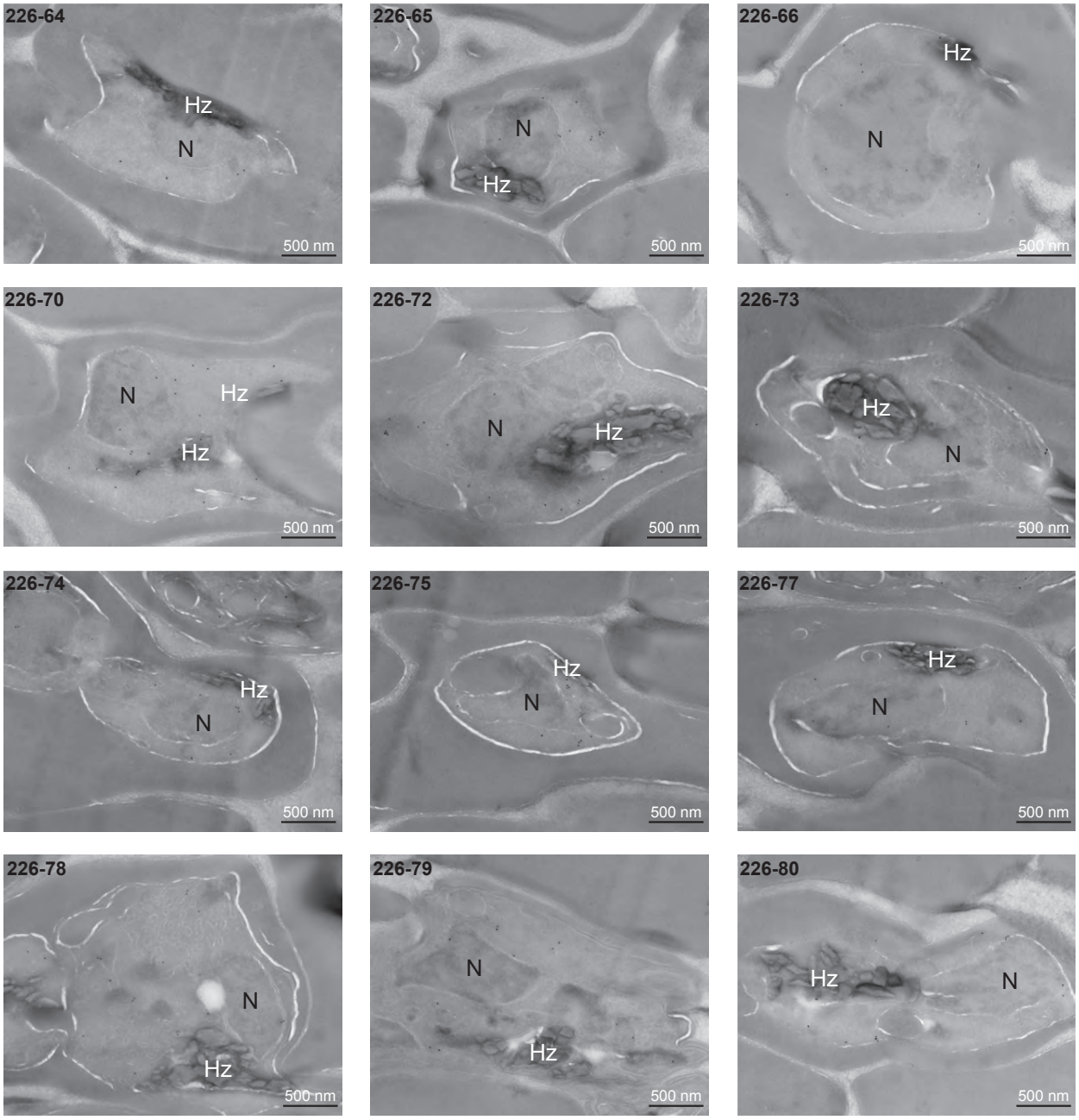

Fig. 4. 12. | (preceding page and this page). Representative immuno-EM images of 3×HA-tagged ABCI3 3D7-A10 parasites show diffuse intracellular localization of ABCI3; N=3.

Table 4. 7. | Transmission electron microscopy image scoring of *Plasmodium falciparum* asexual blood stage parasite subcellular localization of anti-HA stained ABCI3-3×HA.

Sample number	Image number	Plasma membrane	Edoplasmic reticulum	Digestive vacuole	Vesicles	Nucleus	Nuclear membrane	Cytosol	Total ABCI3-3×HA label per sample
222	79	2	0	4	1	1	0	5	13
222	81	2	ND	1	ND	2	1	6	12
222	82	0	ND	1	0	2	0	1	4
222	83	1	0	1	0	4	0	3	9
222	85	3	ND	0	5	2	0	15	26
222	86	0	0	1	2	0	1	10	15
222	88	1	ND	0	0	2	7	6	17
222	89	1	2	2	0	5	0	4	15
222	90	0	3	0	0	5	3	2	13
222	91	1	3	0	1	0	2	5	13
223	95	0	ND	0	ND	2	1	6	9
223	96	0	ND	2	ND	3	0	8	13
223	97	0	ND	0	ND	2	1	4	7
223	99	1	ND	0	1	2	0	8	12
223	100	0	ND	2	0	4	1	3	10
223	102	1	0	3	1	4	1	8	18
223	104	2	2	0	ND	2	0	5	11
223	106	3	1	1	2	5	2	9	23
226	64	0	ND	0	0	0	0	3	3
226	65	0	0	0	0	1	3	7	11
226	66	0	2	1	0	3	0	4	11
226	68	0	0	2	3	3	1	11	20
226	70	0	ND	5	0	2	0	16	23
226	72	1	1	0	0	1	0	14	18
226	73	2	0	1	0	0	0	1	5
226	74	0	1	1	0	3	1	2	8
226	75	0	ND	0	0	0	1	8	9
226	77	1	0	0	1	2	0	4	8
226	78	0	7	3	4	1	1	2	19
226	79	1	ND	0	0	1	1	10	13
226	80	2	0	2	0	1	4	6	15
Total ABCI3-3×HA label per organelle		25	22	33	21	65	32	196	403
% ABCI3-3×HA label per organelle		**6**	**5**	**8**	**5**	**16**	**8**	**49**	

Results were collated from parasites obtained on three separate occasions for electron microscopy processing and imaging. ND: not determined.

4.3.5. CNV-selecting compound 1 inhibits intracellular hemozoin formation.

Given the evidence of its maximal activity against trophozoites [189], partial ABCI3 localization to the DV, and the recent demonstration of inhibition of hemozoin (Hz) formation by an imidazopyridine scaffold [383], we examined the potential of compound **1** to inhibit hemozoin (Hz) formation in *P. falciparum.* As a surrogate for inhibition of heme detoxification in the parasite, we first tested the ability of this compound to inhibit the conversion of hematin to β-hematin (βH), the synthetic equivalent of Hz, in a pyridine-based detergent-mediated assay designed to simulate the DV milieu [384]. Results showed that compound **1** inhibited βH formation (with a mean±SEM IC_{50} of 29±2.2 μM), similar to the two positive control aminoquinolines CQ and amodiaquine (mean±SEM IC_{50}s: 20±1.2 μM and 9±1.3 μM, respectively; **Fig. 4.13J; Table 4.9**). In contrast, SNP-selecting compounds **3-5** failed to block βH formation (IC_{50}: >500 μM), similar to the negative controls pyrimethamine (an antifolate) and doxycycline (a protein synthesis inhibitor; **Fig. 4.13J; Table 4.9**).

To further test whether compound **1** could target intracellular heme detoxification, we performed a cellular heme fractionation assay to test concentration-dependent effects of the compound on the three heme species: hemoglobin (Hb), free heme (i.e. the labile form liberated by Hb proteolysis), and Hz [93,326]. In this experiment, synchronized early ring-stage parasites were incubated with increasing drug concentrations, and the levels of the various heme species were quantified both as proportions of total heme extracted and as absolute amounts of heme iron (Fe) per cell (**Table 4.8**). These amounts were calculated from total amounts of Fe obtained using a heme standard curve. Exposure of parasites to incremental

concentrations of compound **1** led to concentration-dependent increases in the proportions of free heme and a corresponding decrease in Hz compared to untreated controls (**Fig. 4.13E-F**). This profile was statistically significant at 2-4× IC_{50} concentrations and was also observed when the absolute amount of heme per cell, rather than proportions, was analyzed. The mean±SEM amount of free heme present in the untreated control was 2.7±0.3 femtogram (fg) of heme Fe per cell while the amount present at 4×IC_{50} of compound **1** was 6.4±0.3 fg (**Table 4.8**). This mean 2.4-fold increase in toxic free heme directly corresponded to a significant decrease in Hz at the equivalent IC_{50} concentration (**Fig. 4.13F**) and was directly proportional to inhibition of parasite growth (**Fig. 4.13K**). Expectedly, a similar effect was observed upon treating parasites with CQ, a known 4-aminoquinoline inhibitor of the heme detoxification process in the parasite DV (**Fig. 4.13B-C, K**). There was no concentration-related association between the amounts of free heme and Hz in parasites incubated with compounds **3-5** or pyrimethamine, although the amount of Hz Fe appeared to decrease at higher concentrations (**Fig. 4.13H-I, 4.14; Table 4.8**). These decreases, however, did not directly correspond to significant perturbations to free heme Fe levels or correspond to parasite death (**Fig. 4.14J-L**) and might reflect a stress phenotype from inhibition of other unrelated target(s). Treatment with compounds **3** and **4** caused significant increases in Hb levels, with a lesser impact on levels of free heme and Hz, suggesting potential activity of these compounds upstream in the Hb import pathway (**Fig. 4.14A, D, G; Table 4.8**).

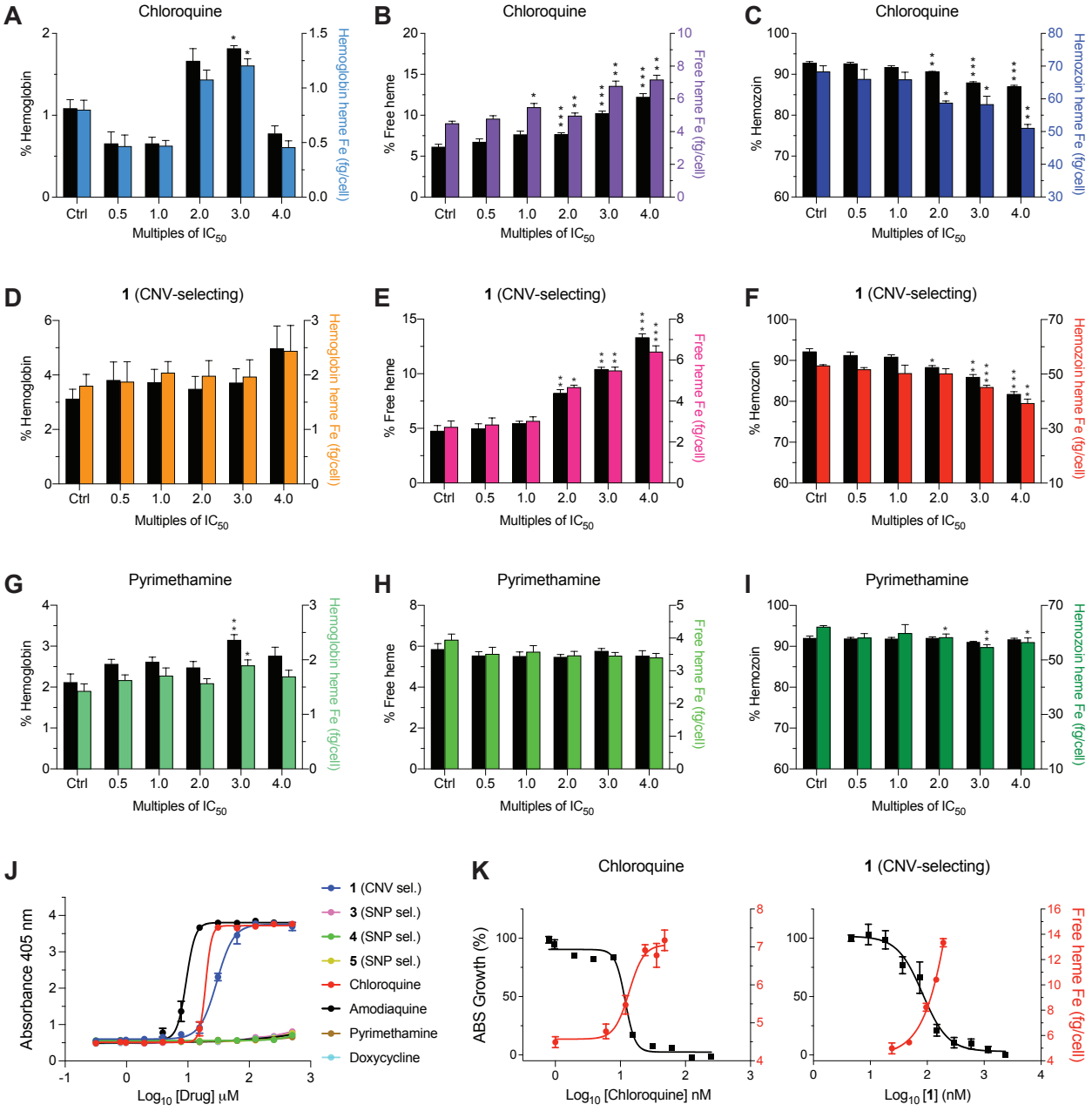

Fig. 4. 13. | Parasites treated with compound 1 display a heme fractionation profile similar to CQ.

(**A-C**) Heme fractionation profile of CQ-treated NF54 parasites showing an increase in free heme and a decrease in Hz, as determined 32 h post drug exposure. (**D-F**) Compound **1** caused a concentration-dependent accumulation of free heme and reduction in Hz levels. (**G-I**) Pyrimethamine treatment did not interfere with heme or Hz accumulation. (**J**) Concentration-dependent inhibition of β-hematin formation by compounds **1**, **3-5** and four clinical antimalarial controls (N=3 independent experiments,

data shown as means±SEM). (**K**) Concentration-dependent inhibition of parasite growth obtained with chloroquine or compound **1** mirrored increasing levels of free heme, with these IC_{50} values intersecting. This result provides evidence that for **1** the inhibition of Hz formation is a primary cause of parasite growth inhibition. Percent levels of heme species are represented on the left y-axis while absolute heme amounts determined from a heme standard curve and measured in femtogram per cell are represented on the right y-axis. Statistical comparisons of the drug-treated lines to their untreated controls were performed using two-tailed Student's tests (with Welch correction). *$p<0.05$; **$p<0.01$; ***$p<0.001$.

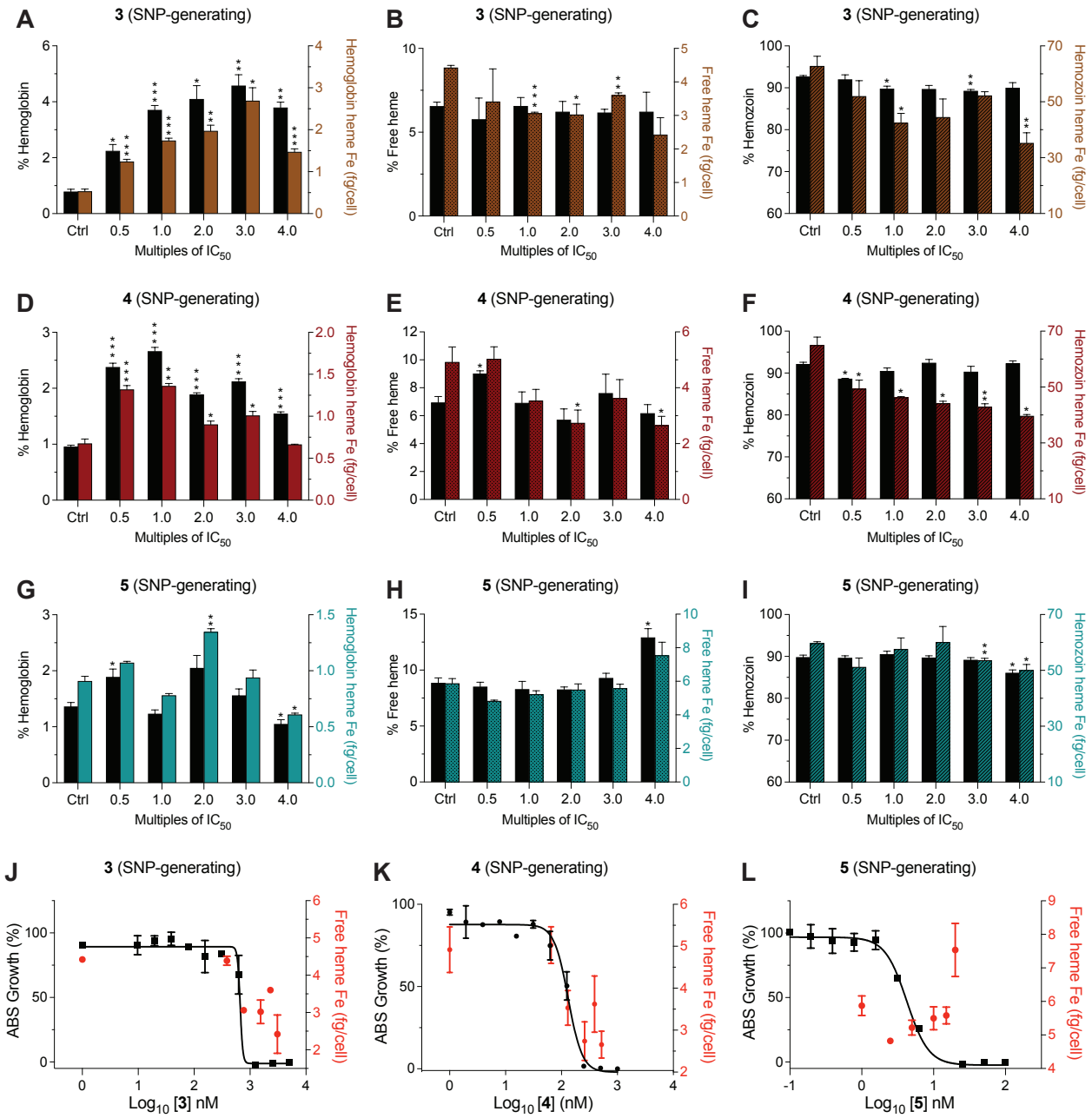

Fig. 4. 14. | Parasites treated with compounds 3-5 do not display a heme fractionation profile similar to CQ.

(**A-I**) Treatment of parasites with compounds **3-5** did not interfere with heme or Hz accumulation. (**J-I**) Concentration-dependent inhibition of parasite growth obtained with compounds **3-5** was independent of free heme levels.

Table 4. 8. | Mean±SEM amount of hemoglobin, free heme and hemozoin in drug-treated parasites represented as percent proportion or absolute amount of heme iron per cell in fg/cell.

Compound	Drug concentration	% Heme species			Heme Fe (fg/cell)		
		Hemoglobin	Free heme	Hemozoin	Hemoglobin	Free heme	Hemozoin
Chloroquine	No drug control	1.08 ± 0.11	6.12 ± 0.34	92.79 ± 0.31	0.80 ± 0.09	4.49 ± 0.14	68.30 ± 1.79
	0.5×IC_{50} (6 nM)	0.65 ± 0.14	6.72 ± 0.40	92.62 ± 0.32	0.47 ± 0.10	4.78 ± 0.19	66.04 ± 2.95
	1.0×IC_{50} (12 nM)	0.65 ± 0.08*	7.63 ± 0.42	91.71 ± 0.38	0.47 ± 0.05*	5.48 ± 0.24*	65.91 ± 2.22
	2.0×IC_{50} (24 nM)	1.12 ± 0.02	11.09 ± 0.35***	87.79 ± 0.35**	0.70 ± 0.01	6.92 ± 0.14**	54.83 ± 1.45*
	3.0×IC_{50} (36 nM)	1.82 ± 0.03*	10.23 ± 0.28***	87.95 ± 0.24***	1.20 ± 0.06*	6.78 ± 0.31**	58.30 ± 2.51*
	4.0×IC_{50} (48 nM)	0.78 ± 0.10	12.23 ± 0.41***	86.99 ± 0.32***	0.46 ± 0.06*	7.17 ± 0.27**	51.05 ± 1.15**
Pyrimethamine	No drug control	2.12 ± 0.11	5.85 ± 0.28	92.04 ± 0.48	1.43 ± 0.13	3.94 ± 0.18	62.11 ± 0.54
	0.5×IC_{50} (12.5 nM	2.56 ± 0.14	5.53 ± 0.20	91.91 ± 0.29	1.61 ± 0.12	3.51 ± 0.21	58.13 ± 1.54
	1.0×IC_{50} (25 nM)	2.61 ± 0.08	5.51 ± 0.21	91.88 ± 0.29	1.64 ± 0.16	3.58 ± 0.19	59.77 ± 3.21
	2.0×IC_{50} (50 nM)	2.48 ± 0.14	5.47 ± 0.13	92.05 ± 0.26	1.57 ± 0.09	3.47 ± 0.13	58.27 ± 1.26*
	3.0×IC_{50} (75 nM)	3.15 ± 0.12**	5.76 ± 0.13	91.09 ± 0.11	1.89 ± 0.11*	3.46 ± 0.11	54.62 ± 1.02**
	4.0×IC_{50} (100 nM)	2.76 ± 0.08	5.53 ± 0.22	91.71 ± 0.27	1.72 ± 0.14	3.40 ± 0.13	56.49 ± 1.56*
1	No drug control	3.12 ± 0.36	4.76 ± 0.50	92.12 ± 0.72	1.80 ± 0.21	2.73 ± 0.29	53.09 ± 0.32
	0.5×IC_{50} (24 nM)	3.81 ± 0.67	4.98 ± 0.43	91.21 ± 0.81	1.87 ± 0.37	2.84 ± 0.33	51.65 ± 0.74
	1.0×IC_{50} (48 nM)	3.73 ± 0.48	5.45 ± 0.21	90.82 ± 0.54	1.84 ± 0.07	3.02 ± 0.21	50.28 ± 3.01
	2.0×IC_{50} (96 nM)	3.48 ± 0.46	8.24 ± 0.31**	88.28 ± 0.45*	1.98 ± 0.28	4.67 ± 0.11*	50.18 ± 1.81
	3.0×IC_{50} (144 nM)	3.71 ± 0.52	10.41 ± 0.18**	85.87 ± 0.64**	1.97 ± 0.31	5.48 ± 0.18**	45.17 ± 0.76***
	4.0×IC_{50} (192 nM)	4.97 ± 0.83	13.32 ± 0.29***	81.71 ± 0.62***	2.83 ± 0.33	6.40 ± 0.29***	39.28 ± 1.55**
3	No drug control	0.78 ± 0.09	6.55 ± 0.25	92.67 ± 0.27	0.53 ± 0.05	4.42 ± 0.07	62.83 ± 3.52
	0.5×IC_{50} (385 nM)	2.24 ± 0.24*	5.77 ± 1.27	92.00 ± 1.13	1.24 ± 0.06***	3.41 ± 0.98	52.01 ± 5.63
	1.0×IC_{50} (770 nM)	3.07 ± 0.17***	6.55 ± 0.52	89.75 ± 0.68*	1.74 ± 0.06***	3.06 ± 0.04***	42.47 ± 3.47*
	2.0×IC_{50} (1540 nM	4.09 ± 0.48*	6.22 ± 0.62	89.69 ± 0.88	1.97 ± 0.14**	3.02 ± 0.32*	44.52 ± 6.56
	3.0×IC_{50} (2310 nM	4.57 ± 0.40**	6.16 ± 0.21	89.27 ± 0.34**	2.69 ± 0.31*	3.60 ± 0.07**	52.27 ± 1.42
	4.0×IC_{50} (3080 nM	3.79 ± 0.20**	6.21 ± 1.17	90.0 ± 1.24	1.47 ± 0.08***	2.42 ± 0.51	35.27 ± 3.72**
4	No drug control	0.95 ± 0.03	6.94 ± 0.44	92.11 ± 0.46	0.67 ± 0.05	4.92 ± 0.54	64.91 ± 2.97
	0.5×IC_{50} (65 nM)	2.38 ± 0.07***	9.00 ± 0.22*	88.62 ± 0.14*	1.32 ± 0.05***	5.03 ± 0.44	49.34 ± 3.13*
	1.0×IC_{50} (130 nM)	2.66 ± 0.07***	6.91 ± 0.80	90.43 ± 0.78	1.36 ± 0.03**	3.53 ± 0.41	46.21 ± 0.37*
	2.0×IC_{50} (260 nM)	1.89 ± 0.03***	5.70 ± 0.79	92.42 ± 0.82	0.90 ± 0.04*	2.74 ± 0.46*	44.10 ± 0.82*
	3.0×IC_{50} (390 nM)	2.12 ± 0.05***	7.60 ± 1.37	90.28 ± 1.35	1.01 ± 0.05*	3.62 ± 0.67	42.89 ± 1.14**
	4.0×IC_{50} (520 nM)	1.54 ± 0.04***	6.16 ± 0.63	92.29 ± 0.61	0.66 ± 0.01	2.65 ± 0.32*	39.60 ± 0.59*
5	No drug control	1.36 ± 0.07	8.84 ± 0.47	89.80 ± 0.50	0.91 ± 0.04	5.87 ± 0.29	59.68 ± 0.57
	0.5×IC_{50} (2.5 nM)	1.89 ± 0.14*	8.50 ± 0.42	89.61 ± 0.56	1.07 ± 0.01	4.82 ± 0.06	51.16 ± 3.26
	1.0×IC_{50} (5 nM)	1.23 ± 0.07	8.29 ± 0.71	90.48 ± 0.77	0.78 ± 0.02	5.22 ± 0.22	57.60 ± 4.04
	2.0×IC_{50} (10 nM)	2.05 ± 0.22	8.26 ± 0.24	89.69 ± 0.46	1.35 ± 0.03**	5.50 ± 0.34	60.09 ± 5.64
	3.0×IC_{50} (15 nM)	1.56 ± 0.12	9.29 ± 0.44	89.15 ± 0.55	0.94 ± 0.07	5.58 ± 0.25	53.59 ± 0.76**
	4.0×IC_{50} (20 nM)	1.05 ± 0.07*	12.90 ± 0.81*	86.04 ± 0.75*	0.61 ± 0.01*	7.54 ± 0.79	50.00 ± 2.10*

Mean±SEM amount of hemoglobin, free heme and hemozoin represented as percent and fg/cell. The amounts of heme in different parasite lines were determined by the heme

fractionation assay (see methods). Parasites were treated with increasing concentrations of chloroquine, pyrimethamine and compounds **1**,**3-5** at different multiples of their IC_{50} values and hemoglobin, free heme and hemozoin amounts measured 30 h later. N, n=1,>3. Statistical comparisons of the drug-treated lines to their untreated controls were performed using two-tailed Student's tests (with Welch correction). *p<0.05; **p<0.01; ***p<0.001.

Table 4. 9. | *In vitro* β-hematin inhibition assay IC_{50} data in µM for the tested antimalarials.

Antimalarials	Mean IC_{50}	SEM	N
1	29.3	2.2	3
3	>500	>500	3
4	>500	>500	3
5	>500	>500	3
Chloroquine	20.0	1.2	3
Amodiaquine	9.4	1.3	3
Pyrimethamine	>500	>500	3
Doxycycline	>500	>500	3

SEM: standard error of the mean; N: number of biological repeats (with technical duplicates). **2** was not tested because of lack of compound.

4.3.6. Mutant PfCRT modulates parasite susceptibility to inhibitors that select for CNVs in ABCI3.

In light of the evidence that part of the mode of action of **1** and **2** involves inhibition of Hz formation and heme detoxification, we next assessed whether PfCRT could affect their activity, as mutations in this DV transporter can protect parasites against Hz formation inhibitors such as CQ. These assays used recombinant Dd2 parasites expressing either the mutant Dd2 PfCRT isoform that mediates CQ resistance, or the wild-type CQ-sensitive 3D7 isoform (Dd2 ^{Dd2} and Dd2 ^{3D7}, respectively). Dose-response assays with the control drug CQ showed the expected 9-fold higher IC_{50} and IC_{90} values in Dd2 ^{Dd2} parasites, compared with isogenic Dd2 ^{3D7} parasites (expressing the Dd2 and 3D7 *pfcrt* alleles, respectively) (**Fig. 4.15A; Table 4.10**). Intriguingly, these isogenic lines implicated Dd2 PfCRT as a mediator of reduced parasite susceptibility to all five inhibitors linked to ABCI3 (**Fig. 4.15B-F; Table 4.10**).

In the case of the two CNV-selecting compounds **1** and **2**, we observed biphasic curves in Dd2 ^{Dd2} parasites, contrasting with a monophasic curve in Dd2 ^{3D7}. IC_{50} values with both lines were similar but Dd2 ^{Dd2} parasites showed substantially higher (14-26 fold) IC_{90} values (**Fig. 4.15B-C; Table 4.10**). In contrast, the SNP-selecting compounds **3**, **4** and **5** showed monophasic curves in both lines with ~2-3× IC_{50} and IC_{90} increases in Dd2 ^{Dd2} parasites compared with Dd2 ^{3D7} (**Fig. 4.15D-F; Table 4.10**). This is similar to the fold IC_{50} increase obtained via mutation in ABCI3 for compound **3** but much lower than the mutant ABCI3-mediated gain of resistance to compounds **4** and **5** (**Table 4.1**, **4.2**). Assays with isogenic parasite lines expressing 1 or 2 copies of *pfmdr1*, which like *pfcrt* encodes a DV-resident

multidrug resistance transporter, showed no effect on the antiplasmodial potency of any ABCI3-associated inhibitor (**Fig. 4.16; Table 4.11**).

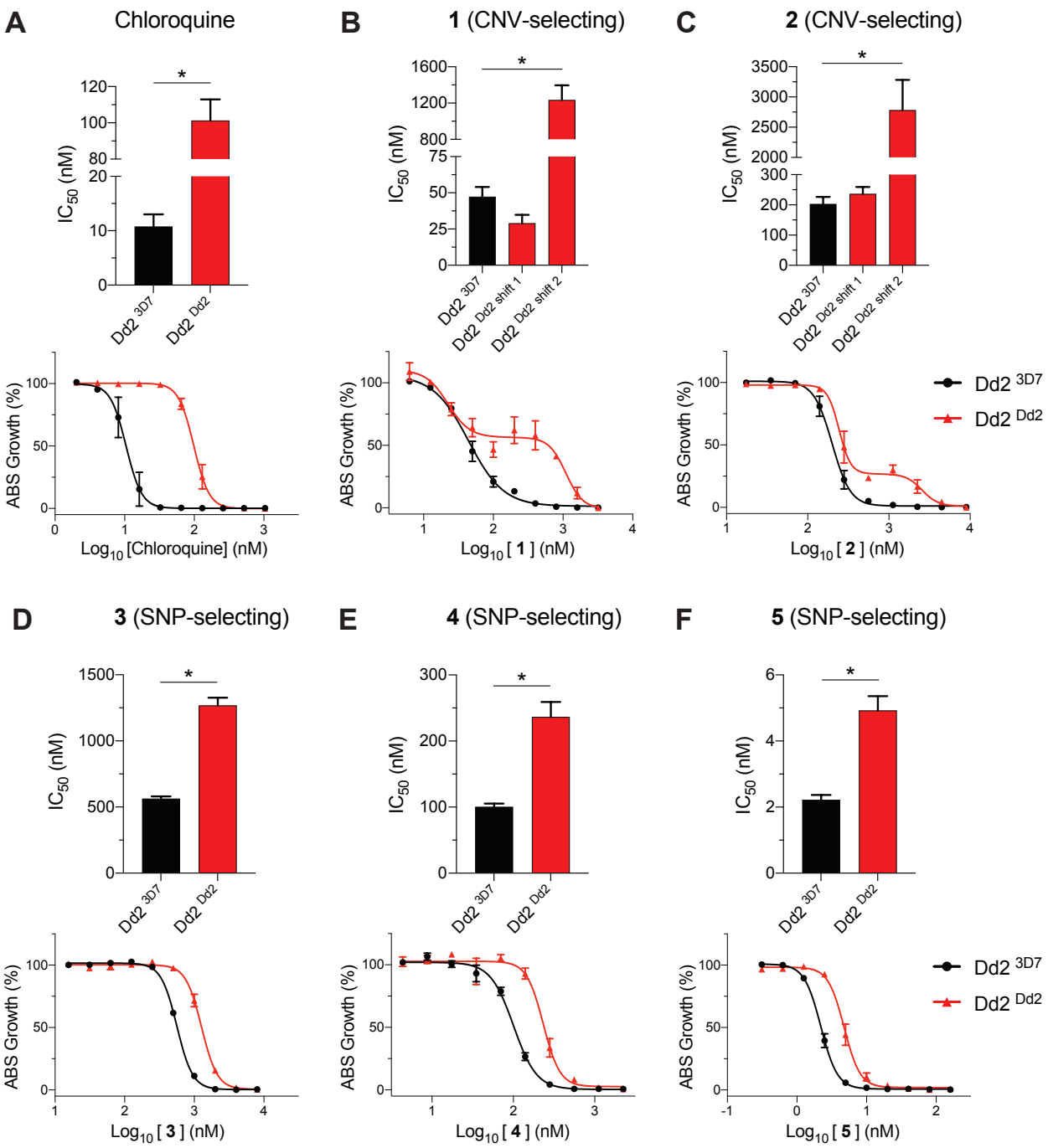

Fig. 4. 15. | Mutant PfCRT in Dd2 parasites plays a role in susceptibility to ABCI3-associated compounds in Dd2 parasites.

(**A**) CQ resistance is conferred by the Dd2 PfCRT isoform (M74I/ N75E/ K76T/ A220S/ Q271E/ N326S/ I356T/ R371I), showing a ~9-fold IC_{50} increase relative to isogenic gene-edited Dd2 parasites expressing the 3D7 wild-type PfCRT isoform. (**B-C**) The mutated PfCRT isoform confers resistance and generates biphasic dose-response curves to compounds **1** and **2**. (**D-F**) Dd2 ^{Dd2} PfCRT isoform confers modest (~2×) resistance to SNP-selecting compounds **3**, **4** and **5**. Mean ± SEM; N, n = 4, 2; *p < 0.05. Mann-Whitney *U* tests compared Dd2 ^{Dd2} to Dd2 ^{3D7}.

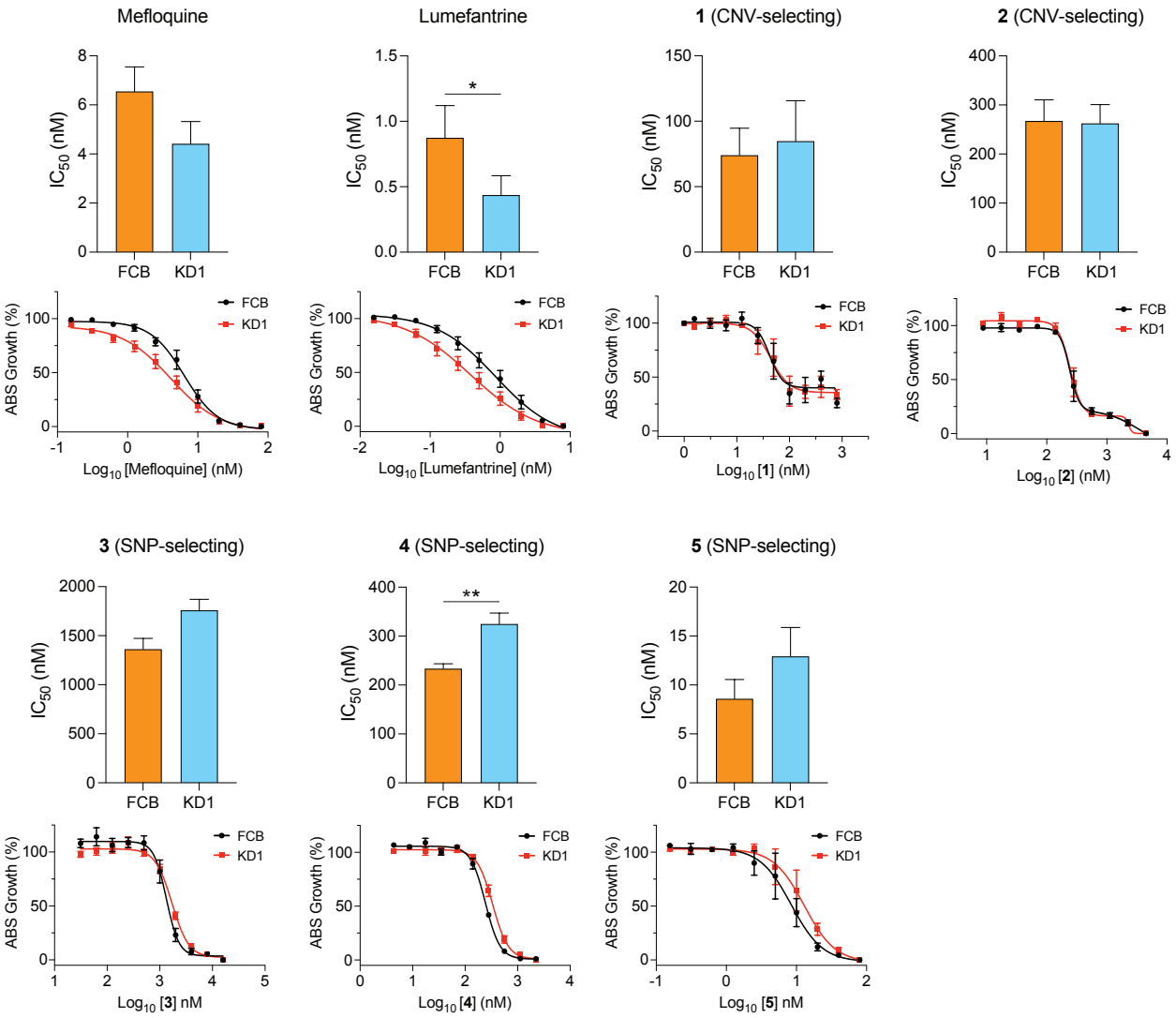

Fig. 4. 16. | PfMDR1 amplifications do not affect parasite susceptibility to ABCI3-associated compounds.

Isogenic parasite lines expressing 1 (KD1) or 2 (FCB) copies of *pfmdr1* were equally susceptible to all five ABCI3-associated inhibitors. Mefloquine and lumefantrine were used as positive controls.

Table 4. 10. | *Plasmodium falciparum* asexual blood stage IC_{50} data in nM for the tested antimalarials against PfCRT isoforms.

	Dd2 ^{3D7}			Dd2 ^{Dd2}			
Antimalarials	Mean IC_{50}	SEM	N	Mean IC_{50}	SEM	N	*P* value
Chloroquine	11.0	2.2	4	101	12	4	0.0286
1	47.0	6.7	4	29.0(1234)	5.8(162)	4	0.1143 (0.0286)
2	203	24.0	4	236(2780)	23.0(504)	4	0.3429 (0.0286)
3	563	18.0	4	1268	58.0	4	0.0286
4	100	4.9	4	236	23.0	4	0.0286
5	2.2	0.2	4	4.9	0.4	4	0.0286

SEM: standard error of the mean; N: number of biological repeats (with technical duplicates); () the IC_{50} and SEM of the second shift of the biphasic curve. *P* values were determined by comparing IC_{50} shift of the Dd2 ^{Dd2} parasite lines compared to Dd2 ^{3D7} using Mann-Whitney *U* tests.

Table 4. 11. | *Plasmodium falciparum* asexual blood stage IC_{50} data in nM for the tested antiplasmodial compounds against PfMDR1 isoforms.

Antimalarials	FCB			KD1			
	Mean IC_{50}	SEM	N	Mean IC_{50}	SEM	N	*P* value
1	74.12	20.6	3	84.86	30.9	3	--
2	278.4	34.9	4	270	33.1	4	0.6857
3	1361	109	5	1760	111	5	0.0556
4	233.5	10.1	5	324.8	22.4	5	0.0079
5	8.592	1.96	4	12.93	2.94	4	0.2
Mefloquine	6.549	1	4	4.416	0.91	4	0.2
Lumefantrine	0.639	0.1	4	0.295	0.05	4	0.0286

--: not determined

4.4. Discussion

Our data identify ABCI3 as a pleiotropic modulator of *P. falciparum* asexual blood stage parasite susceptibility to a range of antiplasmodial chemotypes represented by compounds **1-5**, with resistance associated with ABCI3 amplifications or point mutations. Intriguingly, this member of the *P. falciparum* ATP-binding cassette transporters appears to be broadly distributed within the parasite, mostly to punctate structures in the cytosol, with additional staining of the nucleus, nuclear membrane, DV, and plasma membrane. *In vitro* resistance selection assays using **1** and **2** generated parasites with three copies of *abci3* that conferred varying levels of resistance to all five compounds. In contrast, selections with **3**-**5** generated SNPs in *abci3* that did not alter parasite susceptibility to either of the CNV-selecting compounds. None of these SNPs: Y2079C and R2180P (compound **3**), L690I and R2180G (**4**), and F689C and S696Y (**5**), have been observed in parasite genome data sets (reported in malariagen.net and plasmoDB.org) from field isolates, suggesting that these compounds have modes of action unrelated to antimalarials in clinical use.

We confirmed that ABCI3 L690I, F689C and S696Y were the primary drivers of parasite resistance to compounds **4** and **5** using CRISPR/Cas9 gene editing. Cross-resistance studies showed that unlike CNVs, these mutations sometimes conferred no resistance or even hypersensitized parasites to other SNP-selecting compounds. The L690I and F689C mutations, while adjacent, produced distinct phenotypes when profiled against the three SNP-selecting compounds. L690I, selected with compound **4**, conferred resistance to both this compound and **3** but not **5**. In contrast, F689C, selected with **5**, only conferred resistance to this agent but sensitized parasites to both **3** and **4**. Strikingly, S696Y, located

in the same transmembrane 5 helix as residues 689 and 690, conferred high levels of resistance (≥180-fold) to all three SNP-selecting compounds. These data provide evidence that ABCI3 SNP-mediated drug resistance is compound specific and suggest that this transporter interacts differently with the SNP and CNV-selecting compounds. These results also suggest that like the CNVs, some ABCI3 mutations can confer resistance to a broad set of chemotypes.

To explore differences in cellular accumulation between compounds and the impact of genetic changes in ABCI3, we assayed compounds **1** (CNV), **3** (Y2079C and R2180P) and **4** (L690I and R2180G) in parental 3D7-A10, ABCI3 $^{3\ copies}$ and ABCI3 $^{L690I\ ed.}$ parasites using an inoculum effect assay [376]. These assays extrapolated linear relationships between the IC_{50} and the parasite inoculum size to quantify the cellular drug accumulation ratio (CAR), defined as the ratio of the amount of drug in a parasitized red blood cell versus the amount in a similar volume of medium [324,325,376,385]. Results showed that the CNV-selecting compound **1** accumulated ~30× and ~2× less in the ABCI3 CNV line and in the L690I mutant line respectively, relative to the 3D7-A10 parent. The difference in CQ accumulation between the three lines was only ~2-fold. No cellular accumulation was observed for the two SNP-selecting compounds **3** and **4**. The decreased cellular accumulation of **1** in the ABCI3 $^{3\ copies}$ line suggests that ABCI3 might potentially mediate parasite resistance to this compound **1** by effluxing it from its primary site of action.

Based on results from our cellular accumulation experiments that hinted at different targets/modes of action for the SNP and CNV-selecting compounds, and the ABCI3

localization assays that showed partial DV localization, we tested the ability of select compounds to inhibit biomineralization of heme to Hz as a potential mode of action. Compound **1** appeared to interfere with the heme detoxification pathway in a CQ-like pattern, leading to the accumulation of free heme and a corresponding decrease in Hz levels consistent with recent observations of similar effect by 2,4-disubstituted imidazopyridine series [383]. In contrast, none of the tested ABCI3 SNP-selecting compounds showed any activity on the heme-Hz detoxification pathway, pointing to alternative modes of action. These findings corroborate the βH inhibition results and flag inhibition of heme detoxification by compound **1** as it's likely mode of action. Recent studies have reported that the *Plasmodium* cGMP-dependent kinase, PfPKG, might be a potential target for imidazopyridine-based derivatives [386]. However, our observation of optimal compound **1** activity against trophozoites [189] does not collaborate with the ring and schizont peak expression of PfPKG, making the latter an unlikely target and further supporting Hz inhibition as the mode of action model of this compound. We also observed that compound **1** had no effect on Hb levels, suggesting that it does not target endocytosis of this host factor.

Our observation of an unusual biphasic dose-response curves with compounds **1** and **2,** tested in growth inhibition assays against the 3D7-based ABCI3 CNV parasite line (selected with **1**) and the non-drug-pressured Dd2-B2 line, recalls the biphasic responses to piperaquine (PPQ) seen in PPQ-resistant parasites [201,292,387]. These biphasic relationships have been attributed to either the presence of multiple parasite stages that differ in their susceptibility, polypharmacology with multiple modes of actions,

concentration-dependent off-target activity (that can sometimes be overcome with subtle chemical changes), or concentration-dependent activation of drug efflux mechanisms [207,311,388,389].

For **1** and **2**, we also identified mutant PfCRT as a contributor to susceptibility in Dd2 parasites. Growth inhibition assays with these compounds and isogenic Dd2 ^{Dd2} (CQ-resistant) and Dd2 ^{3D7} (CQ-sensitive) lines [310] revealed biphasic dose-response curves in the former line, as opposed to the monophasic profile obtained with Dd2 ^{3D7}. This shift to a biphasic curve in the edited *pfcrt*-mutant line mirrors the observation with non-edited Dd2, suggesting that mutant *pfcrt* is the major driver of this biphasic response in Dd2 parasites (that harbor a sole copy of *abci3*), as opposed to 3D7 that shows a classic monophasic curve. Of note, *pfcrt*-edited Dd2 ^{Dd2} differs from Dd2 ^{3D7} by 8 amino acid substitutions in this transporter (M74I/ N75E/ K76T/ A220S/ Q271E/ N326S/ I356T/ R371I), which collectively mediate resistance via a gain of CQ transport [377,390,391]. These data suggest that the biphasic gain of resistance observed with Dd2 PfCRT might reflect its ability to transport **1** and **2**. A similar biphasic dose-response profile was earlier observed with the PfCRT variants Dd2+F145I and Dd2+T93S that confer PPQ resistance, also via a gain of transport [202,377].

Both CQ and PPQ accumulate by up to several thousand fold in drug-sensitive parasites, driven presumably by their gain of protonation (to PPQ^{4+} or CQ^{2+}) in the highly acidic DV and their binding to Hz, combined with the absence of an appropriately mutated PfCRT transporter that can efflux them back into the parasite cytosol [207,377,392]. Our studies

revealed even higher levels of compound **1** accumulation in drug-sensitive 3D7 parasites compared with CQ, and **1** and **2** both harbor multiple sites for protonation. Conceivably, these two ABCI3 CNV-selecting compounds might act primarily in the DV, with the CQ-resistant Dd2 PfCRT isoform able to efflux them out of the vacuole into the parasite cytosol. This proposed mode of action is consistent with our observation that compound **1** inhibited Hz formation and parasite growth at equivalent IC_{50} values.

Selection studies with **1** and **2** in initially fully-sensitive 3D7 parasites revealed a different path to resistance. This line harbors wild-type PfCRT that transports less CQ than the Dd2 isoform and presumably also transports little or no compounds **1** and **2**. Selection with these compounds resulted in ABCI3 amplification, which we hypothesize results in their lack of accumulation in the DV. Indeed, we observed significantly less cellular accumulation of **1** in 3D7 parasites that had acquired 3 copies of *abci3*. This transporter was observed mostly in the parasite cytosol, presumably associated with membrane-bound structures, and to only a minor extent with the parasite DV. These data suggest that multicopy ABCI3 might be able to efflux compound out of the parasite or perhaps, as a result of increased levels on the DV, might enable efflux from this site of drug action. Interestingly, *abci3* amplification in 3D7 parasites created a biphasic dose-response curve, phenocopying the dose-response obtained via mutant PfCRT in Dd2 parasites. To our knowledge, this is the first instance where the resistance determinant to a particular compound with antiplasmodial activity differs depending on the parasite genetic background.

Our studies point to a separate mode of action of compounds **3-5** compared with **1** and **2**, based on their differences in dose response, cellular accumulation, heme fractionation, and genetic changes causing resistance. These results collectively suggest that **3-5** act outside the DV. Intriguingly, Dd2 mutants resistant to **5** (harboring the ABCI3 mutations F689C or S696Y) lost their biphasic dose-response with the heme-inhibiting compounds **1** and **2**, providing evidence that these SNPs reversed mutant PfCRT-mediated resistance. Results with our ABCI3 cKD lines (generated in NF54, the parent of 3D7) were informative in showing that reduced levels of ABCI3 caused increased parasite sensitivity to all five tested compounds. This susceptibility profile, however, differed markedly between the SNP (**3**, **4** and **5**)- and CNV (**1** and **2**)-selecting compounds. While the cKD parasites were ~7-11-fold more sensitive to **3**-**5** in the absence of aTc, they were only ~2 to 3-fold more sensitive to **1** and **2**. We conjecture that ABCI3 itself might therefore be a target of **3-5**. This distinction between the modes of action between the SNP- and CNV-selecting compounds is consistent with our recent observations of differences in their timing of action, with **1** showing a peak of activity in trophozoites (the stage of maximal heme detoxification) versus **3** and **4** that showed cumulative activity across all stages [189]. We note that ABCI3 was also observed in proteomic studies to be abundant throughout all asexual blood stages [393]. For compounds **3-5**, Dd2 PfCRT caused a minor (2-fold) increase in the IC_{50}. These data suggest an intricate connection between PfCRT and ABCI3 in dictating parasite susceptibility to these compounds. We note that both transporters are apparently essential for asexual blood stage parasite growth, as previously demonstrated for PCfRT and evidenced herein with our cKD studies showing a loss of growth upon depletion of ABCI3 [382,394,395]. In contrast, we found no evidence for

a role of *pfmdr1* amplification, which can modulate parasite susceptibility to the first-line drugs lumefantrine and mefloquine and which like *pfcrt* encodes a DV-resident transporter [207].

ABCI3 belongs to the AAA+ superfamily of ATPases that are found in all kingdoms of living organisms, where they participate in diverse cellular processes including membrane fusion, proteolysis and DNA replication. Other potential functions for members of this superfamily include protein folding and unfolding, assembly or disassembly of protein complexes, protein transport and degradation, replication, recombination, repair and transcription [396,397]. The diffuse localization of ABCI3 suggests that in *P. falciparum*, the endogenous functions of this protein involve some of these essential processes in parasites. However, more research, including solving the structure of the protein and solute and drug transport assays, is required to narrow down the list of potential endogenous functions of ABCI3 in intra-erythrocytic *P. falciparum* parasites and to better understand how this function is coopted through amplification or point mutations to mediate antiplasmodial drug resistance.

Chapter 5. The antimalarial MMV688533 provides single-dose cures with a high barrier to *Plasmodium falciparum* parasite resistance

James M. Murithi[1§], Cécile Pascal[2§¶], Jade Bath[1], Xavier Boulenc[3¶], Nina F. Gnädig[1], Charisse F.A. Pasaje[4], Kelly Rubiano[1], Tomas Yeo[1], Sachel Mok[1], Sylvie Klieber[2], Paul Desert[3], Maria Belen Jimenez-Diaz[5], Jutta Marfurt[6], Mélanie Rouillier[7], Mohammed Cherkaoui[7], Nathalie Gobeau[7], Sergio Wittlin[8,9], Anne-Catrin Uhlemann[10], Ric N. Price[6,11,12], Grennady Wirjanata[13], Rintis Noviyanti[14], Patrick Tumwebaze[15], Roland A. Cooper[16], Philip J. Rosenthal[17], Laura M. Sanz[18], Francisco Javier Gamo[18], Jayan Joseph[19], Shivendra Singh[19], Sridevi Bashyam[19], Jean Michel Augereau[2], Elie Giraud[2¶], Tanguy Bozec[2¶], Thierry Vermat[2¶], Gilles Tuffal[2], Jean-Michel Guillon[2], Jérôme Menegotto[2¶], Laurent Sallé[2], Guillaume Louit[2], Marie-José Cabanis[2], Marie Françoise Nicolas[2], Michel Doubovetzky[2], Rita Merino[2†], Nadir Bessila[2¶], Iñigo Angulo-Barturen[5], Delphine Baud[7], Lidiya Bebrevska[7], Fanny Escudié[7ʃ], Jacquin C. Niles[4], Benjamin Blasco[7$], Simon Campbell[7], Gilles Courtemanche[20], Laurent Fraisse[2ʃ], Alain Pellet[2¶], David A. Fidock[1,10*], Didier Leroy[7*]

[1]Department of Microbiology and Immunology, Columbia University Irving Medical Center, New York, NY, USA. [2]Sanofi, Infectious Diseases Therapeutic Area, Marcy l'Etoile, France. [3]Sanofi Pasteur, Lyon, France. [4]Department of Biological Engineering, Massachusetts Institute of Technology, Cambridge, MA, USA. [5]GSK, Tres Cantos Medicines Development Campus, Madrid, Spain. [6]Global and Tropical Health Division, Menzies School of Health Research and Charles Darwin University, Darwin, Australia. [7]Medicines for Malaria Venture, Geneva, Switzerland. [8]Department of Medical Parasitology and Infection Biology, Swiss Tropical and Public Health Institute, CH-4002 Basel, Switzerland. [9]Universität Basel, CH-4003 Basel, Switzerland. [10]Division of Infectious Diseases, Department of Medicine, Columbia University Irving Medical Center, New York, NY 10032, USA. [11]Centre for Tropical Medicine and Global Health, Nuffield Department of Medicine, University of Oxford, Oxford, United Kingdom. [12]Mahidol-Oxford Tropical Medicine Research Unit, Faculty of Tropical Medicine, Mahidol University, Bangkok, Thailand. [13] Global Health and Tropical Medicine Division, Menzies School of Health Research, Charles Darwin University, Darwin, Northern Territory, Australia. [14]Eijkman Institute for Molecular Biology, Jakarta, Indonesia.

[15]Infectious Diseases Research Collaboration, Kampala, Uganda. [16]Department of Natural Sciences and Mathematics, Dominican University of California, San Rafael, CA, USA. [17]Department of Medicine, University of California, San Francisco, CA, USA. [18]Global Health Pharma Research Unit, GSK, Tres Cantos, Madrid, Spain. [19]Syngene International Ltd. Bangalore, India. [20]Bioaster, Paris, France.
Current addresses: [¶]Evotec Infectious Diseases Lyon, France. [ʃ]Drugs for Neglected Diseases initiative, Geneva, Switzerland. [$]Global Antibiotic Research and Development Partnership, Geneva, Switzerland.
[†]In memoriam.
*Co-corresponding

Author contributions

J.M.M., C.P., I.A.-B., G.C., L.F., A.P., D.A.F. and D.L. designed the study; J.M.M., J.B., N.F.G., C.F.A.P., K.R., P.D., M.B.J.-D., J.M., G.W., R.N. and P.T. generated data; J.M.M., C.P., J.B., X.B., N.F.G., C.F.A.P., K.R., T.Y., S.M., S.K., P.D., M.B.J.-D., J.M., D.B., M.C., N.G., S.W., R.N.P., G.W., R.N., P.T., R.A.C., P.J.R., L.M.S., F.J.G., J.M.A., E.G., T.B., T.V., G.T., J.-M.G., M.F.N., N.B., I.A.-B., F.E., D.A.F. and D.L. analyzed data; C.P., X.B., A.-C.U., R.A.C., J.J., S.S., S.B., J.M., L.S., G.L., M.-J.C., I.A.-B., B.B. and J.C.N. provided reagents or expertise; M.R., M.D., R.M., L.B., B.B., S.C., G.C., L.F., A.P., D.A.F. and D.L. were the project managers; J.M.M., D.A.F. and D.L. wrote the manuscript, with input from all the authors.

Note: This chapter is reproduced and adapted from: **James M. Murithi**, Cécile Pascal, Jade Bath, Xavier Boulenc, Nina F. Gnädig, Charisse F.A. Pasaje, Kelly Rubiano, Tomas Yeo, Sachel Mok, Sylvie Klieber *et al*. “The antimalarial MMV688533 provides single-dose cures with a high barrier to *Plasmodium falciparum* parasite resistance” (2021). Accepted (pending minor textual revisions) in ***Science Translational Medicine***.

I generated: **60%** of the data in **Fig. 5.2, 100%** in **Fig. 5.5**, **20%** in **Figs. 5.6-5.9** and **20%** in **Table 5.23 and 100% in Table 5.25**. All other data were generated by colleagues in the Fidock Lab, MalDA and MMV.

5.1. Abstract

The emergence and spread of *Plasmodium falciparum* resistance to first line antimalarials creates an imperative to identify and develop novel potent chemotypes. Here we report the identification of MMV688533, an acylguanidine discovered using an orthology-based screen that displays fast parasite clearance *in vitro* and is not cross-resistant with known antimalarials. In a *P. falciparum* SCID mouse model, MMV688533 displays a long-lasting pharmacokinetic profile and excellent safety. Selection studies revealed a very low propensity for resistance, with modest loss of potency mediated via point mutations in PfACG1 and PfEHD. These proteins are implicated in intracellular trafficking, lipid utilization and endocytosis, suggesting interference with these pathways as a novel mode of action. This declared preclinical candidate offers the potential for a single low-dose cure in patients.

5.2. Introduction

Worldwide, malaria mortality and incidence were estimated to decrease by 60% and 37% respectively from 2000 to 2015. This positive trend came to an end in 2016, with cases and deaths plateauing and 229 million cases and 409,000 deaths estimated in 2019 [2]. *P. falciparum* parasite resistance to first-line Artemisinin-based Combination Therapies (ACTs) continues to be on the rise in Southeast Asia and now threatens Africa [371-373]. Despite extensive worldwide efforts, malaria drug discovery and development efforts have encountered major obstacles to identifying new agents with novel modes of antiplasmodial action that do not readily succumb to parasite resistance [339].

To address these barriers, we applied a novel drug discovery approach leveraging research and development programs on human diseases at Sanofi. While classic approaches rely on the identification of compounds that are both potent and specific against *Plasmodium* parasites, our strategy first identified *Plasmodium*-active compounds from a library of chemical matter with known activity against human targets selected from discovery programs through to Phase III clinical trials. Compounds active against *P. falciparum* asexual blood-stage parasites were then chemically optimized to increase antiplasmodial specificity and reduce host toxicity. Our approach led to the identification of several highly potent new chemical series, including the acylguanidines ultimately exemplified by MMV688533. This molecule was shown to act via a novel mode of action that only allowed *P. falciparum* parasites to acquire low-grade resistance under drug pressure.

5.3. Results

5.3.1. Identification of acylguanidines as a potent antiplasmodial chemical series with promising physicochemical properties.

A bioinformatics-mediated analysis of Sanofi drug discovery programs led to the selection of 450 compounds active against one of 33 human targets for which putative orthologs were found in *P. falciparum, Trypanosoma brucei*, *Trypanosoma cruzi*, and/or *Leishamania donovani*. We also included 350 compounds active against any one of 28 Sanofi high-priority human targets. Screening of these 800 compounds against cultured *P. falciparum* asexual blood stage parasites identified 120 compounds whose half-maximal growth inhibition concentration (IC_{50}) was ≤1 mM, corresponding to a 15% hit rate. As a comparison, classical random screening approaches have earlier yielded 0.35-0.68% hit

rates [234-236], highlighting the benefit of our drug discovery strategy. We then applied hit selection criteria including suitable physicochemical properties (https://www.mmv.org/research-development/information-scientists) and IC_{50} values <1 mM against a panel of drug-sensitive or -resistant *P. falciparum* strains, and screened an additional set of 800 analogs of preferred hits to expand Structure-Activity Relationships (SAR) [398]. This work yielded six chemical scaffolds for medicinal chemistry optimization. Here we describe the acylguanidine series, which includes the initial hit MMV668603 that was exquisitely potent against *P. falciparum* NF54 asexual blood stages, with an IC_{50} of 1.7 nM. This hit originated from the dimerization of a compound chemically related to Cariporide, an inhibitor of human Na^+/H^+ exchanger isoform 1 (NHE1) that has anticancer and cardioprotective properties [399,400]. A hit to lead optimization program, including SAR studies, led to the intermediate compound MMV669851 and the eventual preclinical candidate MMV688533 (**Fig. 5.1A**). Compared to MMV668603, the candidate MMV688533 does not contain a diazo moiety, shows improved solubility (from <10 µg/mL to >1,000 µg/mL at pH 1) and intestinal permeability, and retains potent antiplasmodial activity (**Fig. 5.1A; Tables 5.1, 5.2**).

5.3.2. MMV688533 displayed fast parasite killing rate and high potency against *P. falciparum* and *P. vivax* strains *in vitro* and *ex vivo*.

MMV688533 was highly potent against multiple *P. falciparum* strains, with IC_{50} values in the low nanomolar range and no evidence of reduced potency against parasite lines resistant to antimalarials currently in the clinic or in development (**Table 5.3**). These data suggest that MMV688533 might have a distinct mode of antiplasmodial action.

MMV688533 also showed excellent *ex vivo* activity against asexual blood stage parasites from fresh *P. falciparum* isolates from Ugandan patients (median IC_{50} = 1.3 nM, range 0.02 – 6.3 nM, N=143). In Papua Indonesia, where both *P. falciparum* and *P. vivax* are endemic, MMV688533 remained potent in *ex vivo* assays, with similar IC_{50} values against both parasite species (medians of 18.9 and 12.0 nM respectively; **Table 5.4**). MMV688533 was as potent if not more so than either chloroquine or piperaquine against *P. falciparum* and *P. vivax* clinical field isolates (**Table 5.4**).

MMV688533 displayed a fast-killing profile in the parasite reduction rate (PRR) assay [332], as demonstrated by a $\log_{10}$ PRR of nearly 5, corresponding to a decrease of parasitemia by nearly 5 orders of magnitude during a single 48 h intra-erythrocytic developmental cycle (**Fig. 5.1B**). This profile is similar to dihydroartemisinin, the active metabolite of artemisinins that constitute the fastest-acting class of antimalarials available to date [182]. This compound displayed very rapid parasite killing when tested over the range of 1-30× IC_{50} (**Fig. 5.1C**), as well as very low cytotoxicity (**Table 5.5**).

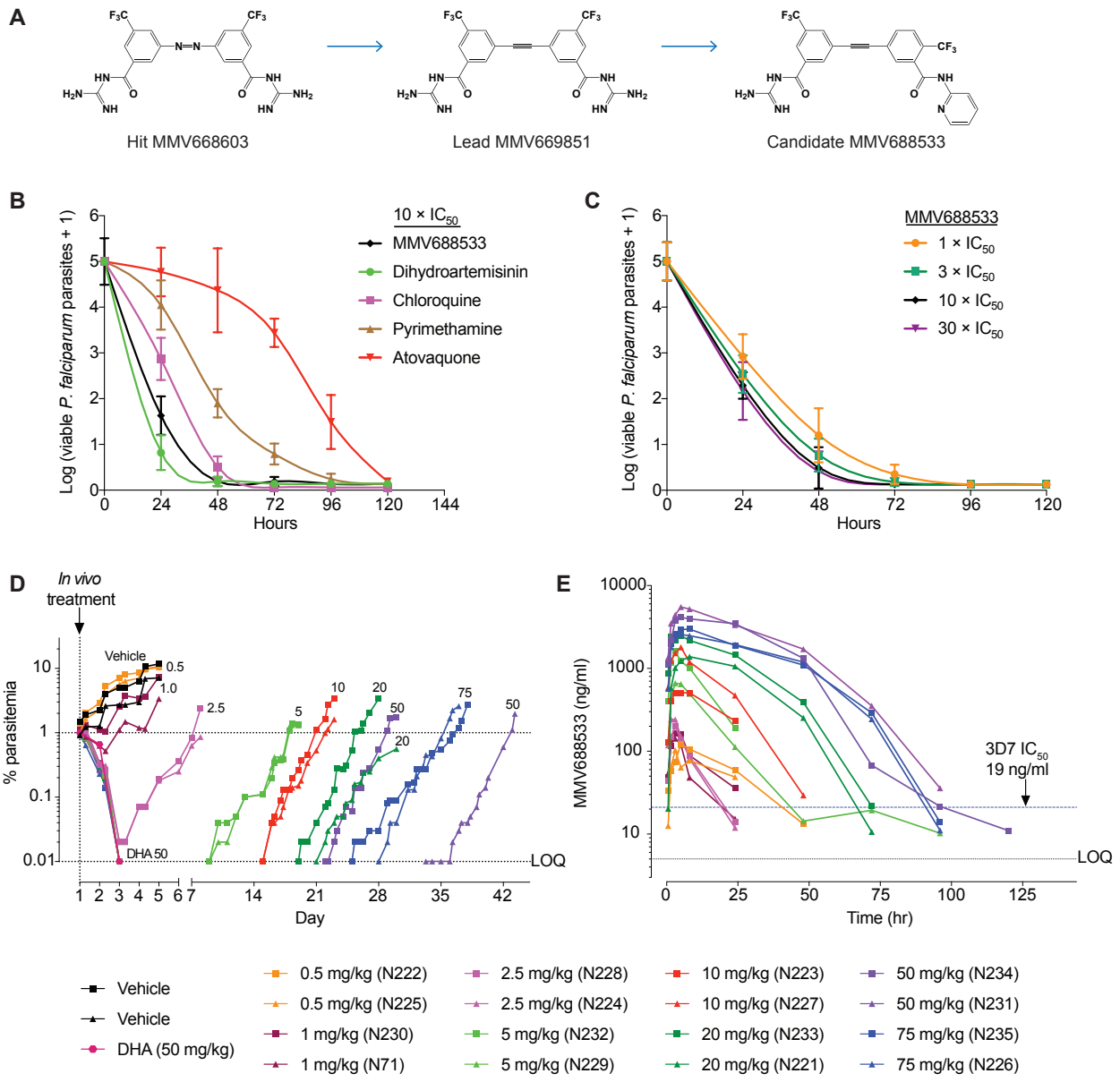

Fig. 5. 1. | The preclinical antimalarial candidate MMV688533 has a fast rate of antiplasmodial activity that offers single-dose cure of *P. falciparum* infection in a humanized mouse model.

(**A**) Structural representation showing the optimization of the acylguanidine series from the initial hit MMV668603 and the lead MMV669851 to the candidate MMV688533. (**B**) Mean ± SD values of viable *P. falciparum* parasites determined daily for 5 days after *in vitro* with MMV688533 at 10× the IC_{50}. Dihydroartemisinin, Chloroquine, pyrimethamine and atovaquone were included as reference antimalarial drugs. (**C**) Mean ± SD values of *P. falciparum* viability determined daily for 5 days following MMV688533 treatment at doses corresponding to 1×, 3×, 10× or 30× the IC_{50}.

(**D**) Compound efficacy was assessed by measuring the initial clearance and time of recrudescence of *P. falciparum* in the peripheral blood of humanized mice administered single doses of MMV688533 ranging from 0.5 mg/kg to 75 mg/kg (two mice per dose). DHA (50 mg/kg) and vehicles were included as controls. (**E**) Concentration of MMV688533 in serial blood samples obtained after administering different doses to *P. falciparum*-infected humanized mice assayed in (**D**). LOQ: Limit Of Quantification.

5.3.3. MMV688533 displayed fast and potent *in vivo* efficacy and favorable *in vitro* ADME and *in vivo* PK properties.

MMV688533 was highly efficacious in the NOD-SCID IL2Rγ^{null} mouse model of *P. falciparum* asexual blood-stage infection [333], with a single oral dose of 5 mg/kg resulting in a rapid reduction in parasitemia to below the limit of detection within 48 h, followed by recrudescence to 1% by day 18. By comparison, vehicle-treated mice attained a lethal parasitemia of 8-10% by day 5 (**Fig. 5.1D**). These data predicted an ED_{90} of 2 mg/kg, corresponding to the single dose required to reduce parasitemia by >90% by day 7 compared to vehicle-treated mice (**Table 5.6**). Four consecutive daily doses of 0.9 mg/kg produced >90% reduction in parasitemia by day 7 (data not shown). Importantly, one dose of at least 5 mg/kg MMV688533 cleared parasites as rapidly as 50 mg/kg dihydroartemisinin **(Fig. 5.1D**). Pharmacokinetic-pharmacodynamic (PK/PD) modeling predicted an *in vivo* minimal parasiticidal concentration of 20.3 ng/mL (**Table 5.7**).

PK studies indicated a low plasma clearance (C_L) in mice, rats and dogs (**Table 5.8**). When tested on purified cytochrome P450 enzymes, MMV688533 did not show high inhibitory potency (**Table 5.9**). MMV688533 also displayed a moderate to high volume of distribution (V_{ss}: 1.4 L/kg in mice, 4.7 L/kg in Beagle dogs), and a moderate to long half-life in all species

(3.2 h in mice, 50.7 h in dogs) (**Table 5.10; Table 5.14**). The oral bioavailability of MMV688533 was >70% in rodent species (**Table 5.10**). Human C_L and V_{ss} parameters calculated from rat and dog allometry were predicted to be inferior to 5% of the hepatic blood flow using two methods (see Methods section) and 5.0 L for a 70 kg patient, respectively. The predicted half-life of MMV688533 in humans was greater than 100 h (**Table 5.16**).

We then predicted the efficacious single dose in humans based on: (i) the minimal parasiticidal concentration derived from PK/PD modeling of the *Pf* NOD-SCID data (**Tables 5.6; 5.7**); (ii) the K_{kill} derived from *in vitro* PRR studies (**Fig. 5.1B**); (iii) the PK in mouse, rat and dog used in allometric scaling (**Tables 5.10-15**); and (iv) a biopharmaceutical model (GastroPlus). This latter model predicted that at least 50% of a 500 mg dose was absorbed when administered in fed conditions. A 100 mg dose is absorbed up to 70% in fasted conditions while at this dose, the food effect is less than 30% (data not shown). Using these parameters, a single oral administration of 30 mg MMV688533 in humans was predicted to maintain its concentration above the minimal parasiticidal concentration over a period of 96 h, which covers two *P. falciparum* erythrocytic replication cycles, and to reduce parasitemia by at least 6 logs when a conservative *in vitro* log PRR value was capped at 3. Similarly, a dose of 24 mg was predicted to reduce parasitemia when the *in vitro* log PRR value of 5 was used. A single-dose treatment with 66 mg of MMV688533 was predicted to reduce parasitemia by 12 logs, suggesting very favorable characteristics for future clinical studies.

5.3.4. MMV688533 revealed a favorable tolerability profile.

In silico toxicity predictions did not raise any safety alerts other than a moderate phototoxic risk (**Table 5.17**), which proved minimal when tested in MMV688533-treated BALB/c 3T3 mouse fibroblasts exposed to UV light. Genotoxicity testing with MMV688533, including preliminary Ames and micronucleus assay were negative. Profiled on a receptor/enzyme panel, MMV688533 displayed micromolar affinity for calcium and chloride channels as well as for benzodiazepine and dopamine receptors (**Table 5.18**). Considering its similarity with cariporide, cardiovascular parameters were assessed in detail. MMV688533 had a modest effect on the hERG channel with an IC_{50} of 30 µM (data not shown) and 4.6 µM when measured by automatic and manual Patch-Clamp (**Table 5.19**), respectively. Inhibition studies with Nav1.5 and Cav1.1 ion channels yielded IC_{50} values of 14 µM and 2.1 µM, respectively (**Table 5.19**). When tested in the Pukinje fiber assay, MMV688533 induced mild effects that were not suggestive of a torsadogenic profile. However, because of the limited solubility of the compound in the conditions of this study, a full cardio-safety *in vitro* evaluation at higher concentrations was not possible. Therefore, *in vivo* studies were conducted to better assess potential cardiovascular safety risks. Continuous intravenous administration of MMV688533 (at 10, 20 and 30 mg/kg) to anesthetized guinea pigs did not affect blood pressure, heart rate, the ECG RR or QT intervals, or the QRS complex (data not shown). In summary, in silico, *in vitro* and *in vivo* safety studies with MMV688533 did not raise any measurable cardiotoxicity alerts.

Preliminary safety was assessed in rats and dogs via oral treatment and drug exposure measurements (Toxicokinetics: **Tables 5.20, 5.21**). In a non-GLP 2-week toxicity study in

Sprague-Dawley rats, no clinically apparent changes were observed at 12.5, 25 and 50 mg/kg dose levels. 12.5 mg/kg/day exposure was considered the No-Observed Effect Level (NOEL) in this study due to an increase of liver biomarkers and microscopic changes (foamy macrophages, microscopic changes) at the two highest doses. In a non-GLP 2-week toxicity study in beagle dogs, (0.5 and 1 mg/kg/day once daily and 2 mg/kg/day every other day), only minimal transient changes of no safety concern were detected. In conclusion, the no-observed-adverse-effect level (NOAEL) was declared at 1 mg/kg and the corresponding cumulated exposure over 14 days was 14-fold higher than that predicted for a 30 mg single dose in humans (**Table 5.22**). Such a predicted safety margin was judged promising enough to progress MMV688533 to more detailed regulatory preclinical studies before first-in-human clinical trials.

5.3.5. MMV688533 is maximally potent against *P. falciparum* rings and early trophozoite stages.

To assess the timing of MMV688533 action, we employed an *in vitro* asexual blood stage susceptibility assay that measures compound activity against early and late rings, early and late trophozoites, and schizonts [189]. The assay was validated by the stage-specific susceptibility profiles of dihydroartemisinin, chloroquine and the PI4K inhibitor KAI407 [61], which showed the expected peak activities on early rings, rings and trophozoites, and schizonts, respectively [189]. MMV688533 and dihydroartemisinin shared a similar activity profile, with early rings to early trophozoites being the most susceptible, whereas schizonts were the least affected (**Fig. 5.2A**).

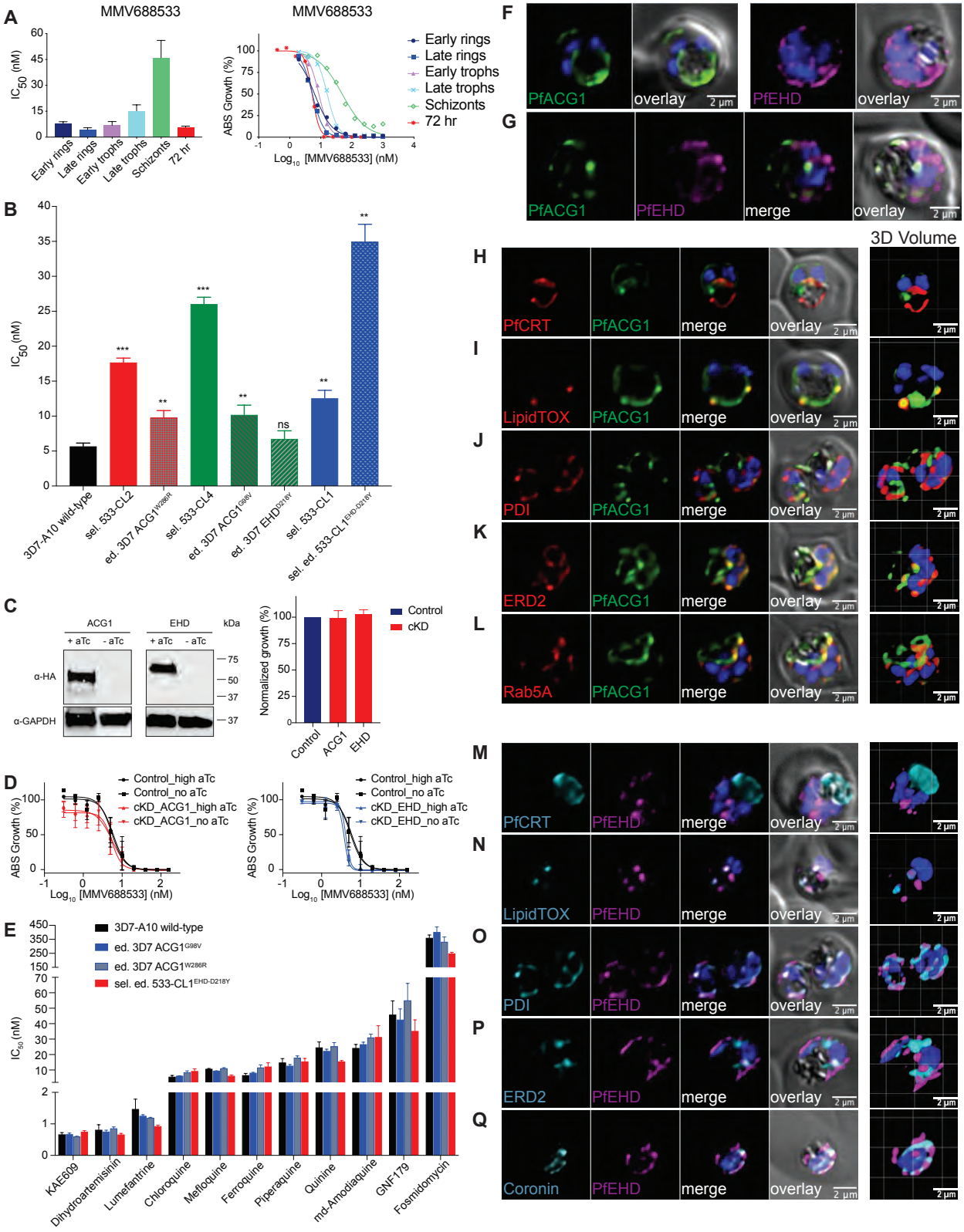

Fig. 5. 2. | MMV688533 antiplasmodial activity is unrelated to existing antimalarials and selects for low-grade resistance mediated in part by mutations in PfACG1 and PfEHD.

(**A**) *In vitro* asexual blood stage susceptibility assay showing MMV688533 activity in early and late rings, early and late trophozoites, and schizonts. IC_{50} values are shown as means ± SEM (N>3, n = 2). (**B**) Mean ± SEM IC_{50} values of selected (sel.) (533-CL1, 533-CL2 and 533-CL4), edited (ed.) (PfACG1^{G98V}, PfACG1^{W286R}, PfEHD^{D218Y}) lines and the sel. ed. line 533-CL1$^{EHD\text{-}D218Y}$ compared to the 3D7-A10 parental line. N>6, n = 2; ***P* <0.01, ****P* <0.0005; ns: not significant. (**C**) Western blot data showing effective reduction in PfACG1 and PfEHD protein levels upon removal of aTc, as detected using antibodies specific to the 2×HA tag added to the C-terminus of each protein. Parasite survival was measured by quantifying expression of the integrated RLuc cassette (Fig. 5.3), in the presence (50 nM) or absence of aTc. Data represent the mean of three biological replicates and are normalized to a fully inhibitory concentration of chloroquine (200 nM). (**D**) Dose-response curves for MMV688533 against PfACG1 and PfEHD conditional knockdown (ckD) parasites expressing wild-type or substantially reduced levels of each protein upon culturing with 500 nM aTc or no aTc, respectively. (**E**) G98V and W286R mutations in PfACG1 and a combination of both G98V in PfACG1 and D218Y in PfEHD in sel. ed. 533-CL1$^{EHD\text{-}D218Y}$ did not confer cross-resistance to a panel of known antimalarial drugs compared to the 3D7-A10 parent. Mean ± SEM; N>3, n = 2. (**F**) Fluorescence microscopy images of fixed NF54$^{3\times HA\text{-}EHD}$attB-ACG1-eGFP parasites either stained with anti-GFP (green) antibodies or anti-HA (magenta) antibodies. Nuclei were stained with DAPI (blue). Scale bars: 2 µm. (**G**) Fluorescence microscopy image of fixed and doubly stained NF54$^{3\times HA\text{-}EHD}$attB-ACG1-eGFP parasites using anti-GFP (green) and anti-HA (magenta) antibodies. Nuclei were stained with DAPI (blue). Scale bars: 2 µm. (**H-L**) Fluorescence microscopy images and 3D reconstructions of fixed NF54$^{3\times HA\text{-}EHD}$attB-ACG1-eGFP parasites co-stained with antibodies to anti-GFP (green) and (**H**) anti-PfCRT antibodies, (**I**) LipidTOX neutral lipid stain, (**J**) anti-PDI, (**K**) anti-ERD2 or (**L**) anti-Rab5A (red) antibodies. Nuclei were stained with DAPI (blue). Scale bars: 2 µm. (M-Q) Fluorescence microscopy images and 3D reconstructions of fixed NF54$^{3\times HA\text{-}EHD}$attB-ACG1-eGFP parasites co-stained with antibodies to anti-HA (magenta) and (**M**) anti-PFCRT antibodies, (**N**) LipidTOX neutral lipid stain, (**O**) anti-PDI, (**P**) anti-ERD2 or (**Q**) anti-coronin (cyan) antibodies. Nuclei were stained with DAPI (blue). Scale bars: 2 µm.

5.3.6. Ramping selections with *P. falciparum* asexual blood stage parasites yield low-grade resistance to MMV688533.

To identify possible resistance mechanisms to MMV688533, we performed single-step *in vitro* resistance selections by exposing triplicate flasks of 2×10^9 wild-type Dd2-B2 parasites to $3\times IC_{50}$ of MMV688533. These single-step selections did not yield resistant parasites after 60 days, suggesting a low propensity for resistance development for this compound. This was further confirmed in ramping selections, which entailed gradually increasing the drug pressure from 1 to $11\times$ IC_{50} on triplicate flasks of 2×10^8 3D7-A10 parasites each over a six-month period. This selection yielded only very low-grade resistance, with a 2 to 5-fold IC_{50} increase in each of the three drug-pressured lines (**Fig. 5.2B; Table 5.23**). Whole-genome sequencing (WGS) of four resistant clones obtained from across the three pressured lines identified single nucleotide polymorphisms (SNPs) in five genes: a conserved *Plasmodium* protein of unknown function (PF3D7_0910300); an EH domain-containing protein (EHD; PF3D7_0304200); a conserved *Plasmodium* protein of unknown function (PF3D7_0510100); a putative RNA pseudouridylate synthase (PF3D7_0511500); and the putative ATP synthase (C/AC39) subunit (PF3D7_1464700) (**Table 5.23; 5.24**).

Of significance, all four clones (sel. 533-CL1 – CL4, named after the last three digits of the selecting compound MMV688533 followed by the clone name), carried G98V (clones sel. 533-CL1 and sel. 533-CL4), W286R (clone sel. 533-CL2) or T92* stop codon (clone sel. 533-CL3) mutations in PF3D7_0910300, suggesting a key role for this protein in conferring resistance to MMV688533. PF3D7_0910300, which we herein have named *Plasmodium falciparum* acylguanidine 1 (PfACG1) after the chemical series that generated MMV688533,

is a conserved *Plasmodium* protein of unknown function. Clone sel. 533-CL4, which also has a D218Y mutation in gene PF3D7_0304200 (PfEHD), displayed the highest level of resistance to MMV688533 (4.6-fold IC_{50} shift) (**Fig. 5.2B; Table 5.23**). This points to an additional role for PfEHD in enhancing parasite resistance to the compound. Based on these observations, the presence of PfACG1 mutations in all the selected clones and the boost in resistance conveyed by an additional PfEHD D218Y mutation in sel. 533-CL4, we hypothesized that these two proteins, out of the five proteins identified using WGS, play a crucial role in mediating resistance to MMV688533.

To test this hypothesis, we introduced the G98V and W286R mutations in PfACG1 and the D218Y mutation in PfEHD individually into wild-type 3D7-A10 parasites using a CRISPR/Cas9 gene-editing strategy. This yielded the edited lines ed. 3D7 $ACG1^{G98V}$, ed. 3D7 $ACG1^{W286R}$ and ed. 3D7 EHD^{D218Y} lines respectively. The G98V mutation in the ed. 3D7 $ACG1^{G98V}$ line conferred comparable levels of resistance to the corresponding selected clone sel. 533-CL1, whereas the W286R mutation in ed. 3D7 $ACG1^{W286R}$ line only contributed around half of the resistance observed in sel. 533-CL2 (**Fig. 5.2B; Table 5.23)**. The D218Y mutation in PfEHD alone was insufficient to confer resistance. To test whether SNPs in PfACG1 are needed to obtain higher grade resistance to MMV688533 we introduced the D218Y mutation into the background of the clone sel. 533-CL1, using a CRISPR/Cas9 strategy. This clone harbors the G98V mutation in PfACG1. The resulting sel. ed. 533-$CL1^{EHD\text{-}D218Y}$ line showed a 6.2-fold shift in IC_{50} compared to wild-type parasites, comparable to the 4.6-fold shift in clone sel. 533-CL4. These results provide

evidence that the D218Y mutation in PfEHD enhances resistance to MMV688533 only when the G98V mutation is already present in PfACG1.

5.3.7. Conditional knockdown of the resistance determinants PfACG1 and PfEHD does not affect *in vitro* parasite growth.

To further explore the role of PfACG1 and PfEHD, we engineered conditional knockdown parasite lines in which we could regulate protein expression levels via the TetR-DOZI system [322]. Normal protein levels were maintained by culturing parasites in the presence of anhydrotetracycline (aTc) (**Fig. 5.3**). Western blot analysis of these lines, which harbored a C-terminal 2×HA epitope tag fused to each gene product, confirmed the expression of PfACG1 and PfEHD in the presence of aTc (**Fig. 5.2C; Fig. 5.3B)**. aTc withdrawal resulted in the loss of protein expression, confirming efficient knockdown of the proteins. Despite the significant knockdown observed from the Western blots, assessment of growth over two replicative cycles revealed that PfACG1 and PfEHD parasite lines, maintained in the absence of aTc, were able to progress through the intra-erythrocytic stage life cycle similar to controls, suggesting that loss of function of both proteins does not affect viability under normal culture conditions (**Fig. 5.2C**). To test for *ex vivo* compound-target interactions, we determined the IC_{50} of MMV688533 against wild-type versus knockdown conditions of PfACG1 and PfEHD. Similar to an unrelated control line, knockdown of PfACG1 and PfEHD did not result in differential susceptibility to MMV688533 (**Fig. 5.2D**), pointing to a non-inhibitory interaction between MMV688533 and these two proteins.

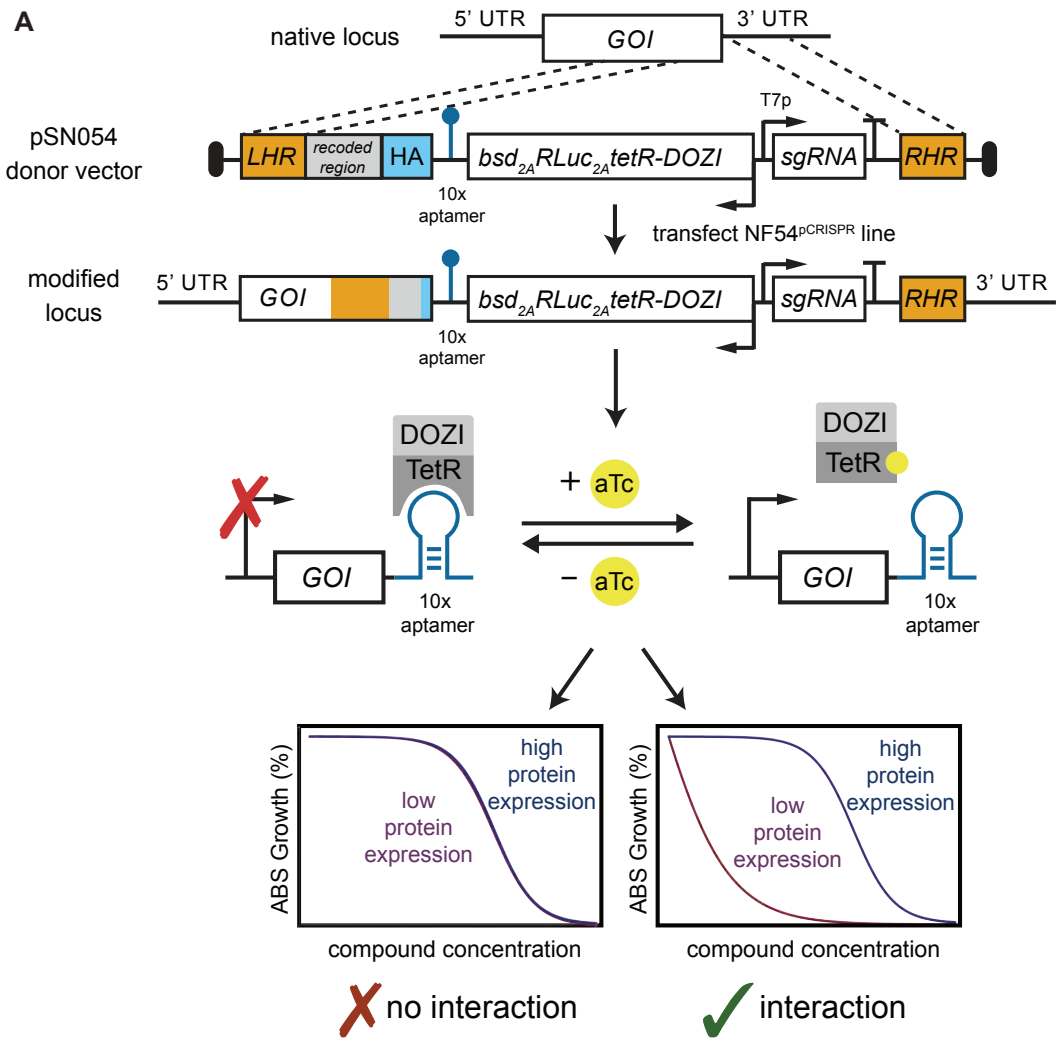
A
native locus
5' UTR
GOI
3' UTR
pSN054
donor vector
LHR
recoded region
HA
bsd2ARLuc2AtetR-DOZI
T7p
sgRNA
RHR
10x aptamer
transfect NF54pCRISPR line
modified locus
5' UTR
GOI
bsd2ARLuc2AtetR-DOZI
sgRNA
RHR
3' UTR
10x aptamer
DOZI
TetR
+ aTc
– aTc
GOI
10x aptamer
DOZI
TetR
GOI
10x aptamer
ABS Growth (%)
high protein expression
low protein expression
compound concentration
ABS Growth (%)
high protein expression
low protein expression
compound concentration
no interaction
interaction

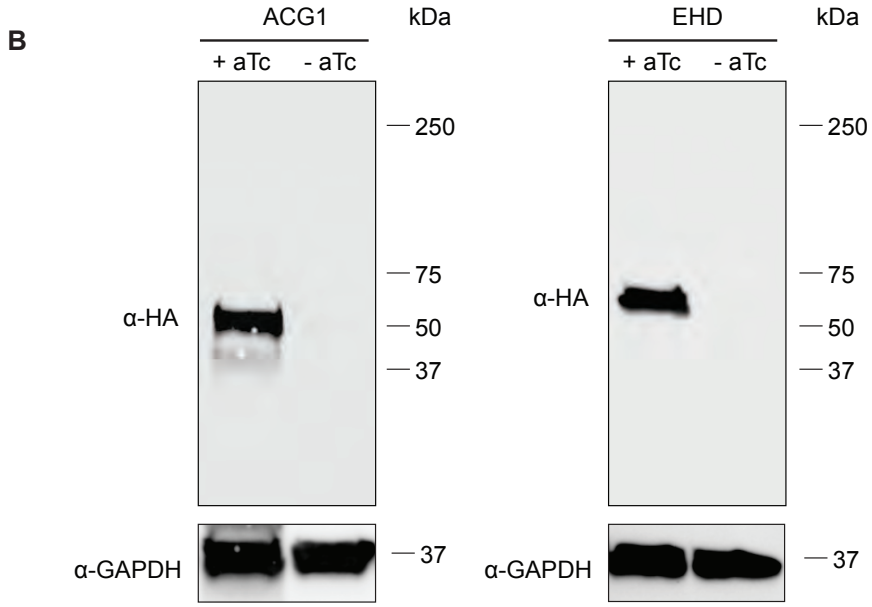
B
ACG1
kDa
+ aTc
- aTc
250
75
50
37
α-HA
37
α-GAPDH
EHD
kDa
+ aTc
- aTc
250
75
50
37
α-HA
37
α-GAPDH

Fig. 5. 3. | Conditional knockdown (cKD) strategy for PfACG1 and PfEHD.
(**A**) Schematic representation of the generation of PfACG1 and PfEHD cKD lines. (**B**) Western blot-based assessment of PfACG1 and PfEHD translational regulation via the TetR-DOZI-RNA aptamer module. The expected mass of the PfACG1-2×HA and EHD-2×HA proteins are 55.7 kDa and 66.4 kDa, respectively. Results show maintenance of protein expression in the presence of aTc, contrasting with undetectable levels of either protein upon removal of aTc. GAPDH was used as a loading control.

5.3.8. MMV688533-resistant parasites do not show cross resistance to current antimalarials.

To test whether resistance to MMV688533 might impact the efficacy of clinical antimalarials, we tested the 3D7 ACG1^{G98V} and 3D7 ACG1^{W286R} edited lines as well as the high-grade resistant clone sel. ed. 533-CL1$^{EHD\text{-}D218Y}$ for cross-resistance against a diverse panel of eleven known antimalarials. This study employed 72 h asexual blood stage parasite susceptibility assays across a range of drug concentrations (**Fig. 5.2E, 5.4; Table 5.25**). Neither the individual G98V and W286R mutations in PfACG1 nor the multiple SNPs in sel. ed. 533-CL1$^{EHD\text{-}D218Y}$ conferred cross-resistance to these drugs, implying that MMV688533 has a novel mode of action against *P. falciparum*.

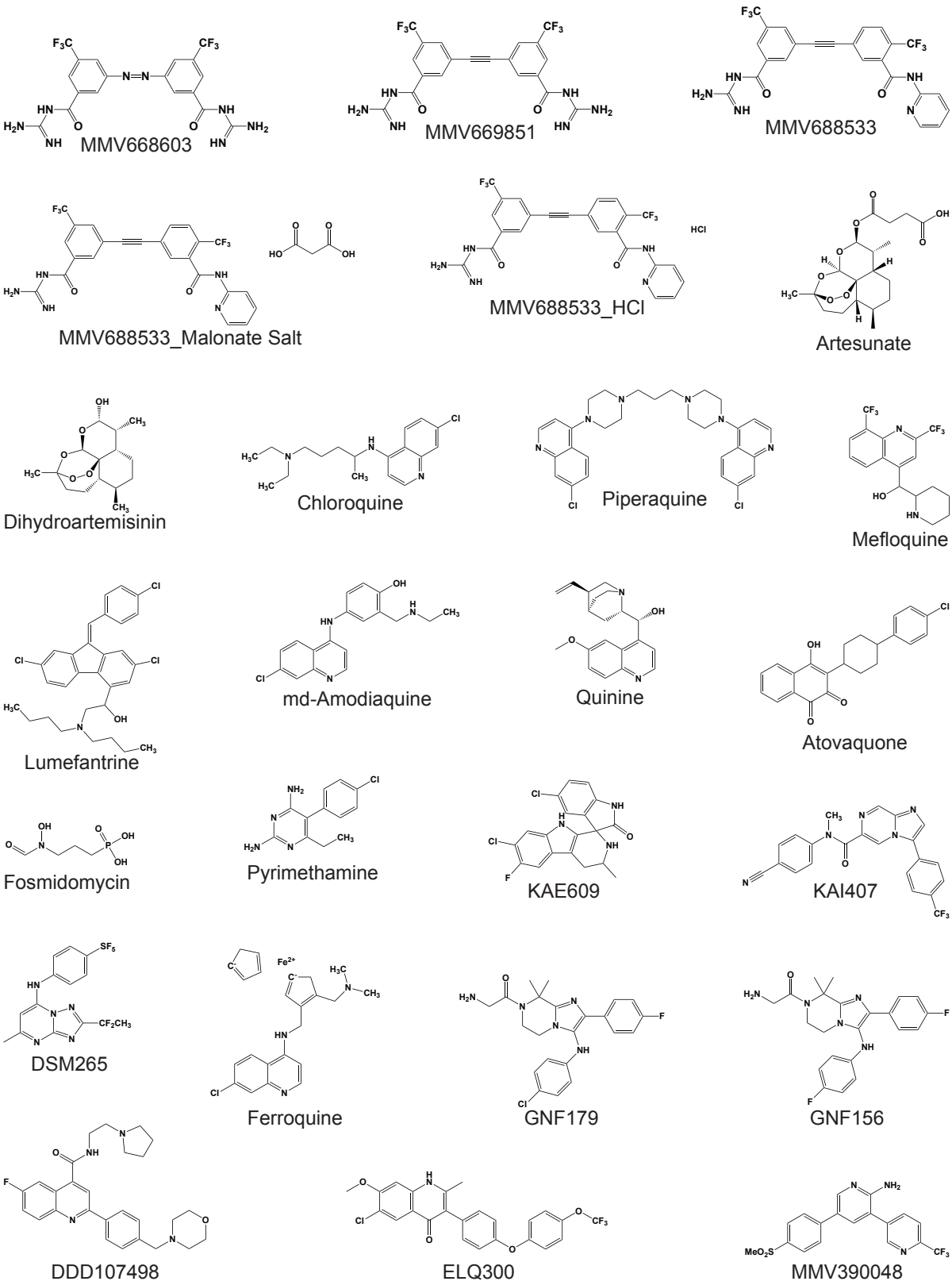

Fig. 5. 4. | Chemical structures of antimalarial compounds tested herein.

5.3.9. PfACG1 and PfEHD localize primarily to distinct intracellular parasite vesicles.

To interrogate the subcellular localization of PfACG1 and PfEHD we performed immunofluorescence studies with a variety of cellular co-markers. We generated a doubly tagged recombinant NF54attB parasite line expressing a 3×HA tag at the C-terminus of the PfEHD endogenous locus as well as a stably-integrated transgenic copy of PfACG1 that was C-terminally tagged with eGFP (NF54$^{3\times HA\text{-}EHD}$attB-ACG1-eGFP) (**Fig 5.5**).

PfACG1-eGFP mainly localized to foci around the digestive vacuole (DV) of the parasite with residual labeling observed around the parasite nucleus (**Fig. 5.2F; Fig. 5.6, 5.7**). PfEHD likewise appeared in foci that localized mostly to the parasite periphery as well as close to the DV; other foci were also other observed, although to a lesser extent, throughout the parasite cytoplasm (**Fig. 5.2F; Fig. 5.8, 5.9**). Co-labeling using anti-HA and anti-GFP antibodies to assess co-localization of PfACG1 with PfEHD showed no overlap between the two fluorophores (**Fig. 5.2G**).

Since most of the eGFP signal for the PfACG1-fusion protein was observed adjacent to the DV we performed co-stains using antibodies directed to PfCRT, PfMDR1 or Plasmepsin II, which are known to localize to the DV (**Fig. 5.2H; Fig. 5.6A-B, 5.7B-C**). This confirmed proximity to the DV, but only showed infrequent, seemingly random overlap between PfACG1 and either of the DV transmembrane proteins PfCRT and PfMDR1. To investigate whether PfACG1 could overlap with neutral lipid bodies, which are often localized adjacent to the parasite DV [401], we carried out co-stains using LipidTOX and Nile Red (**Fig. 5.2I; Fig.**

5.6C-F, 5.7D-G). Although not all eGFP positive foci exclusively overlapped with these lipid bodies we observed very frequent juxtaposition. These observations point to the possibility that PfACG1 partially associates with lipid storage bodies localized close to the DV. Despite our detection of an eGFP signal close to the nucleus, no overlap was detected when co-staining for the parasite endoplasmic reticulum (ER) using antibodies specific for PDI (protein disulfide isomerase; **Fig. 5.2J; Fig. 5.7H-I**). Instead, the eGFP signal showed some overlap with antibodies to ERD2 and PMT (phosphoethanolamine N-methyltransferase), which represent markers for the cis- and trans-Golgi [378,379], respectively (**Fig. 5.2K; Fig. 5.6G-J, 5.7J-K**). To test whether PfACG1 localized to Rab-positive vesicles that are known mediators of vesicular traffic, we co-stained with Rab5A, 5B and Rab7 antibodies. We only observed infrequent overlap, similarly to co-stains performed with antibodies against K13, a marker for hemoglobin endocytosis [193,402] (**Fig. 5.2L; Fig. 5.6K-N, 5.7L-O**). Along these lines no colocalization was observed for PfACG1 and coronin, a protein involved in F-actin organization that has recently been associated with *in vitro* resistance of early ring stages to artemisinins [403] (**Fig. 5.6O**). Lastly, we assessed co-localization to the parasite mitochondrion using MitoTracker Deep Red, as well as to the apicoplast as visualized with anti-ACP antibodies. No overlap was observed between PfACG1-eGFP and those organelles (**Fig. 5.6P,Q**).

Similar to our observations with PfACG1, we detected PfEHD-positive foci that were close to the DV but did not co-localize with PfCRT (**Fig. 5.2M; Fig. 5.9B-C**). Co-stains using LipidTOX occasionally co-localized some of the HA-labeled PfEHD vesicles with neutral lipid bodies (**Fig. 5.2N; Fig. 5.8A-B, 5.9D**). To investigate PfEHD association with the

parasite ER as well as the Golgi apparatus we used anti-PDI antibodies or anti-ERD2 and anti-PMT antibodies respectively. Frequent proximity and partial overlap were observed between PfEHD positive foci and the ER-resident markers PDI and BIP, whereas the Golgi stains revealed no obvious association between PfEHD and this organelle (**Fig. 5.2O-P; Fig. 5.8C-F, 5.9E-H**). In mammalian cells, EH domain (EHD)-containing proteins, serving as protein interaction platforms, are known to primarily function as key regulators in endocytosis [404]. To explore whether PfEHD could play a similar role in protein and lipid trafficking processes in parasites we performed immunofluorescence (IFA) studies using antibodies to coronin and Rab proteins. We found that PfEHD vesicles that localized close to the parasite membrane frequently overlapped with coronin, hinting at a possible interaction between the two proteins (**Fig. 5.2Q; Fig. 5.8G-J, 5.9I-J**). Immunofluorescence assays carried out with the panel of Rab antibodies (anti-Rab5A, 5B, 5C, Rab7 and Rab11A) as well as antibodies to K13 revealed some juxtaposition of Rab-positive vesicles and K13-positive foci with PfEHD (**Fig. 5.8K-P, 5.9K**). In contrast, when assessing potential PfEHD association with the apicoplast using anti-ACP antibodies, we did not observe overlap between the fluorophores (**Fig. 5.8Q**).

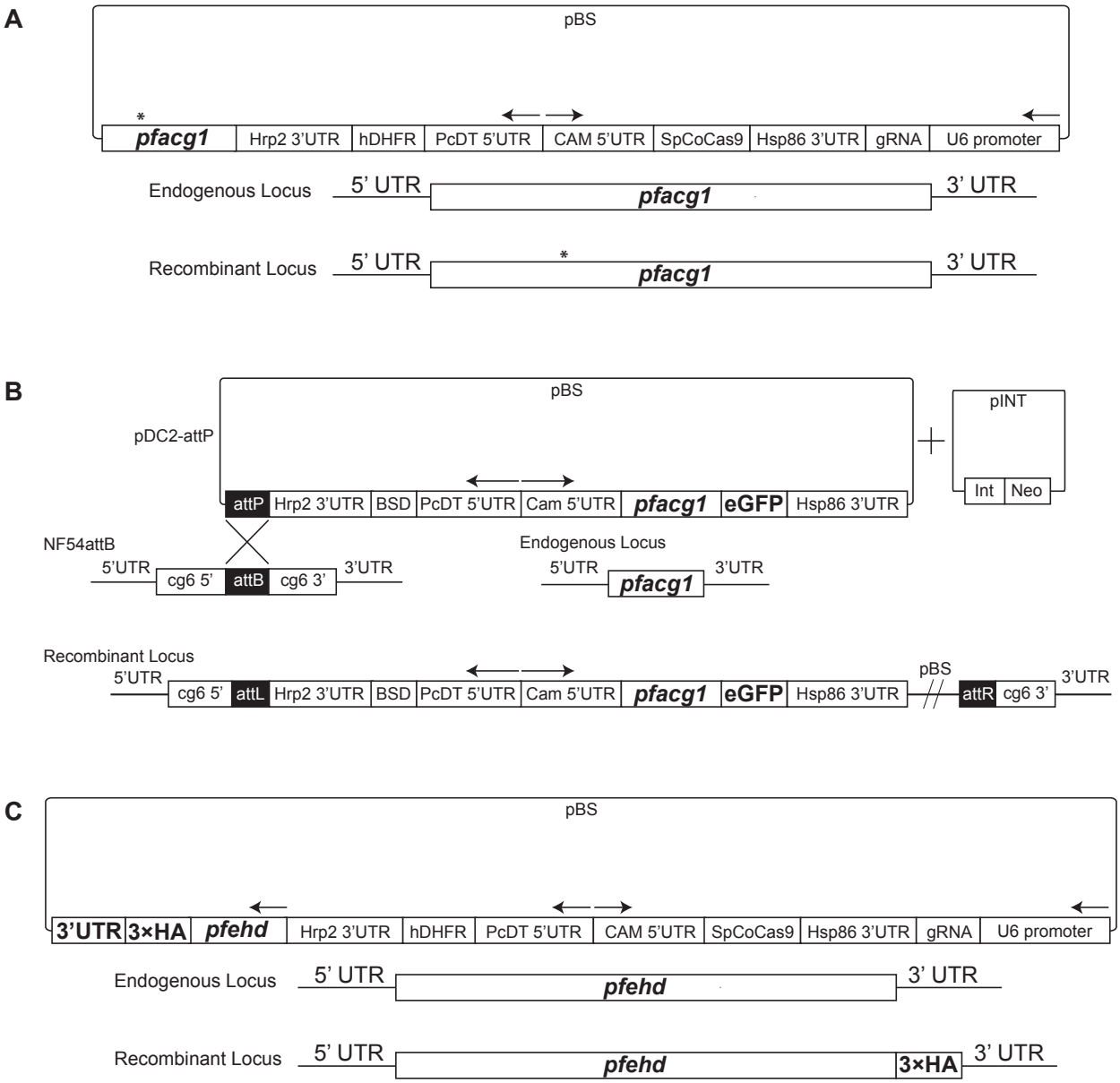

Fig. 5. 5. | Genetic manipulation strategies for PfACG1 and PfEHD.

(A) CRISPR/Cas9 strategy to edit SNPs into the endogenous *pfacg1* locus. Cas9 was derived from *Streptococcus pyogenes* and codon optimized for *P. falciparum*; transcription was regulated from a *P. falciparum* calmodulin promoter. The plasmid also contains a hDHFR selectable marker under the PcDT promoter and a sequence encoding the guide RNA (gRNA) under a U6 promoter. The *pfacg1* donor has >300bp of homology flanking the mutation of interest (G96V or W286R). **(B)** attB×attP based strategy to integrate *pfacg1*-eGFP as a transgene into the *cg6* locus of NF54attB parasites. *pfacg1*-eGFP and the BSD selectable marker are transcribed from a calmodulin and a PcDT promoter, respectively. **(C)**

CRISPR/Cas9 strategy to introduce a 3×HA into the 3' end of the endogenous *pfehd* locus in NF54attB parasites expressing the *pfacg1*-eGFP transgene. The plasmid also contains a hDHFR selectable marker and a sequence encoding the guide RNA (gRNA), under a PcDT and a U6 promoter, respectively. The donor fragment has two regions of *pfehd* homology flanking the 3×HA tag. attL: attB left junction segment; attR: attB right junction segment. BSD: Blasticidin-S deaminase; CAM: Calmodulin; eGFP: enhanced Green Fluorescent Protein; gRNA: guide RNA. hDHFR: human dihydrofolate reductase; Hrp2: histidine-rich protein 2; Int: Mycobacteriophage Bxb1 serine integrase; Neo: Neomycin; pBS: BlueScript plasmid; Hsp86: Heat shock protein 86; PcDT: *Plasmodium chabaudi* dihydrofolate reductase-thymidylate synthase; *pfacg1*: *Plasmodium falciparum* acylguanidine 1 gene; *pfehd: Plasmodium falciparum* Eps15 homology domain containing gene; SpCoCas9: *Streptococcus pyogenes-Plasmodium falciparum* codon-optimized Cas9; UTR: Untranslated region.

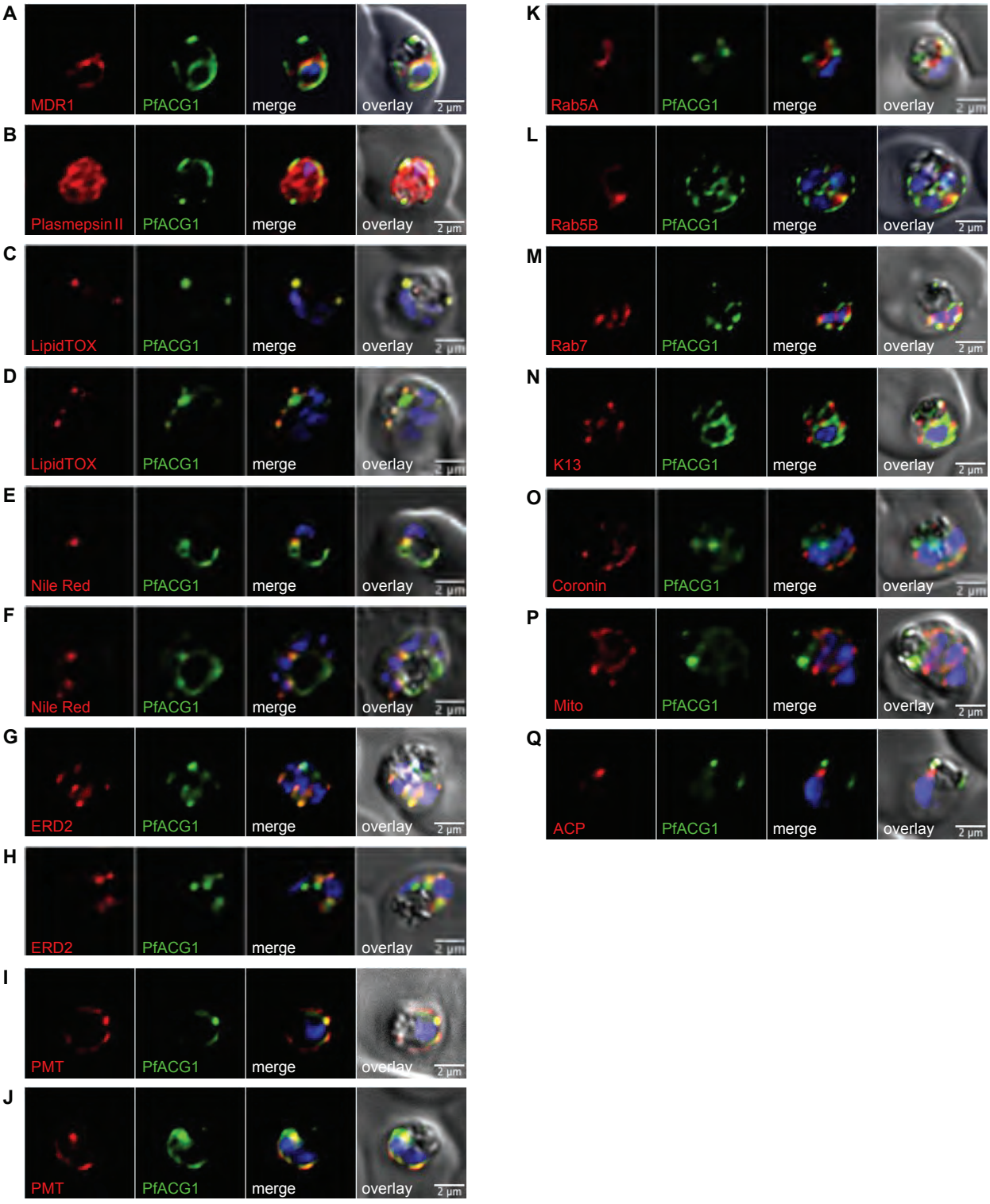

Fig. 5. 6. | Fluorescence microscopy images of fixed and labeled NF54$^{3\times HA\text{-}EHD}$attB-ACG1-eGFP parasites.

PfACG1 was detected using antibodies specific to eGFP. Costaining used **(A)** anti-PfMDR1 antibodies that label the digestive vacuole membrane [405,406]; **(B)** anti-plasmepsin II antibodies that label the digestive vacuole lumen [407]; **(C, D)** LipidTOX neutral lipid stain that stains lipid bodies [408]; **(E, F)** Nile Red that also stains lipid bodies [409]; **(G, H)** anti-ERD2 antibodies that label the cis-golgi [379]; **(I, J)** anti-PMT that labels phosphoethanolamine N-methyltransferase present in trans-Golgi structures [378]; **(K-M)** anti-Rab5A, anti-Rab5B and anti-Rab7 that labels vesicles [193]; **(N)** anti-K13 that labels the ER, vesicles and cytostomes [193]; **(O)** anti-coronin antibodies that stain compartments with F-actin [410]; **(P)** MitoTracker Red that labels mitochondria; or **(Q)** anti-ACP antibodies that label the acyl carrier protein present in the apicoplast [411]. Nuclei were stained with DAPI (blue). Scale bars: 2 μm.

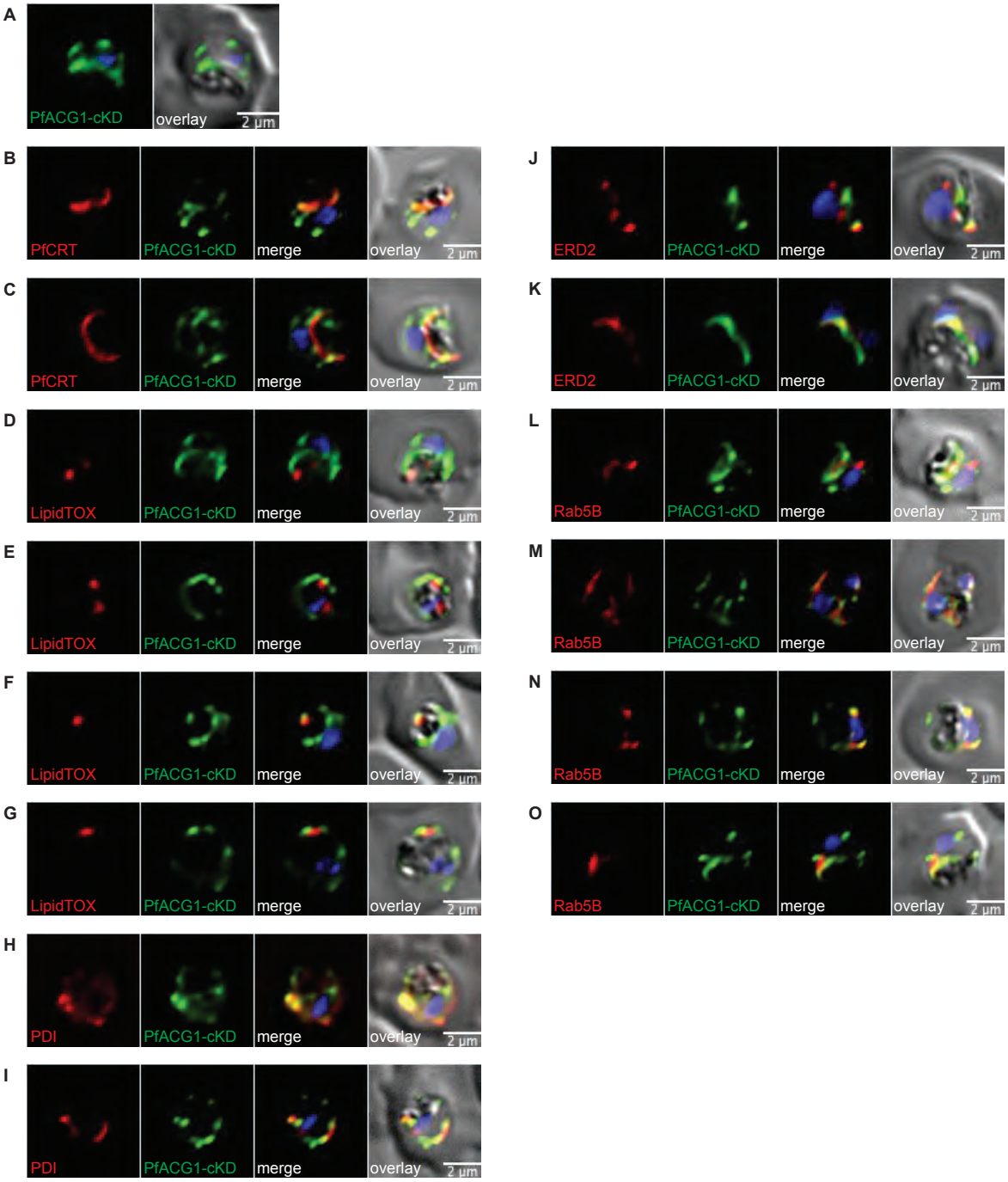

Fig. 5. 7. | Fluorescence microscopy images of fixed and labeled NF54^{pCRISPR}TetR-DOZI-ACG1-2×HA parasites.

PfACG1 was detected using antibodies specific to HA (green). Costaining used **(A)** anti-HA stain; **(B-C)** anti-PfCRT antibodies that label the digestive vacuole membrane [377]; **(D-G)** LipidTOX neutral lipid stain; **(H-I)** anti-PDI; **(J-K)** anti-ERD2; **(L-0)** anti-Rab5B. Nuclei were stained with DAPI (blue). Scale bars: 2 µm.

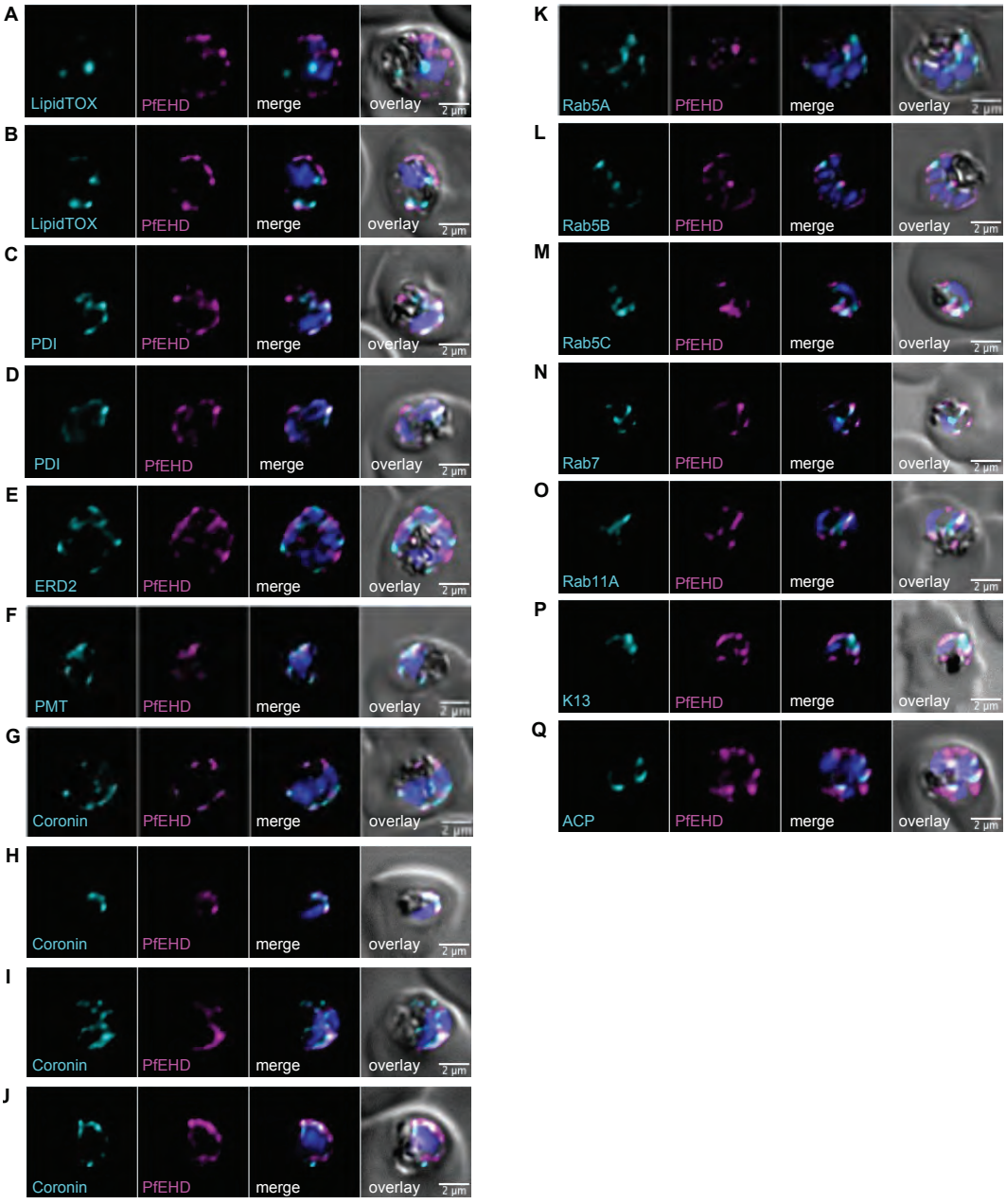

Fig. 5. 8. | Fluorescence microscopy images of fixed and labeled NF54$^{3\times HA\text{-}EHD}$attB-ACG1-eGFP parasites.

PfEHD was detected using antibodies specific to HA (magenta). Costaining used **(A, B)** LipidTOX neutral lipid stain; **(C, D)** anti-PDI that labels the plasmodial protein disulfide isomerase that is localized in the ER [412]; **(E)** anti-ERD2; **(F)** anti-PMT; **(G-J)** anti-coronin; **(K-0)** anti-Rab5A, anti-Rab5B, anti-Rab5C, anti-Rab7 and anti-Rab11A that label vesicles involved in trafficking [413,414]; **(P)** anti-K13; or **(Q)** anti-ACP antibodies (cyan). Nuclei were stained with DAPI (blue). Scale bars: 2 µm.

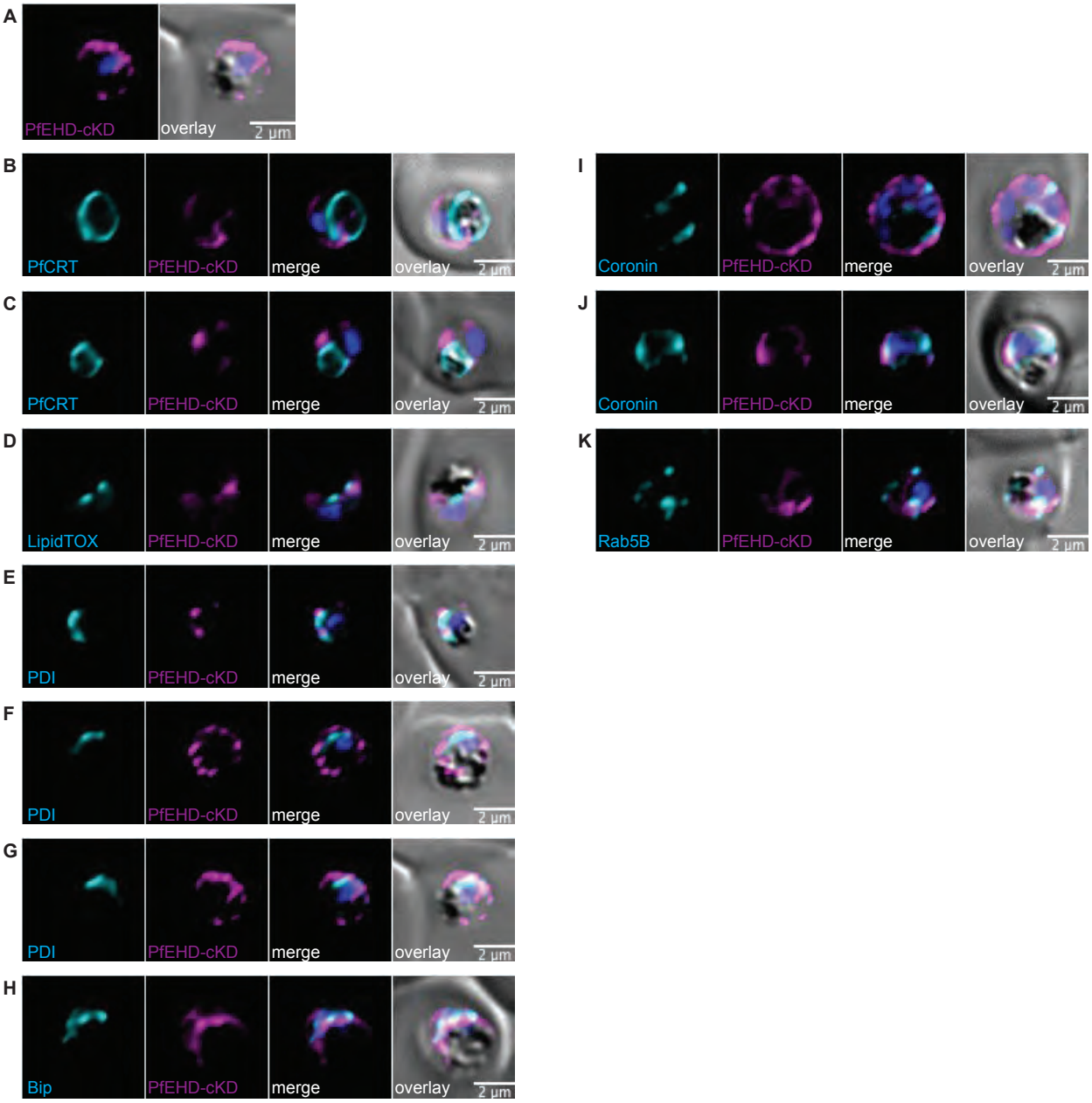

Fig. 5. 9. | Fluorescence microscopy images of fixed and labeled NF54^{pCRISPR}TetR-DOZI-EHD-2×HA parasites.

PfEHD was detected using antibodies specific to HA (magenta). Costaining used **(A)** anti-HA stain; **(B-C)** anti-PfCRT; **(D)** LipidTOX neutral lipid stain; **(E-G)** anti-PDI; **(H)** Bip antibodies that stain the ER [415]; **(I-J)** anti-coronin; **(K)** anti-Rab5B. Nuclei were stained with DAPI (blue). Scale bars: 2 µm.

5.4. Discussion

Here, we report an exquisitely potent antimalarial, MMV688533, discovered among Sanofi compounds active on defined human targets and that were assayed for potency against *P. falciparum* asexual blood stage parasites. Our screen of 800 compounds yielded a high hit rate, with 120 showing submicromolar antiplasmodial activity. Physicochemical analysis identified acylguanidines as the most promising series, with subsequent structure analysis relationship (SAR)-based lead optimization yielding MMV688533. Parasite reduction ratio assays revealed exceptionally fast killing, with MMV688533 reducing the parasite load by >3 log within 24 h after drug addition, similar to dihydroartemisinin and considerably faster than the comparator first-line drugs chloroquine and pyrimethamine. MMV688533 also displayed minimal toxicity against mammalian cells, slow clearance, and a long half-life predicted at 100 h in humans. Single-dose efficacy in the *P. falciparum*-infected SCID mouse model was excellent, with parasite clearance and delayed recrudescence observed at doses as low as 5 mg/kg. These data highlight the therapeutic potential of this novel class of antimalarials.

Whole-cell screens for antimalarials have in recent years yielded multiple potent antimalarials that despite their promise have encountered parasite resistance at frequencies and levels that pose an important concern for their further development as curative drugs [41]. For example, inhibitors of the drug targets PfATP4 or PfeEF2 can select for resistance from as a few as 10^6-10^7 parasites, with SNPs causing IC_{50} increases of up to several hundred-fold [251,264,416]; unpublished results). In contrast, using these same selection procedures [417], MMV688533 yielded no resistance when used to pressure even

large parasite inocula (6×10^9). Low-grade resistance could only be achieved using a ramping method of gradually increasing drug concentrations over a 6-month period. Parasite clones from these selections showed 2- to 5-fold higher IC_{50} values against MMV688533. Whole-genome sequencing identified two distinct point mutations or a stop codon in the PfACG1 gene in all clones assayed from three independent selections. Upon gene editing, both point mutations afforded only a 2-fold IC_{50} increase. One clone also harbored a point mutation in PfEHD, which upon editing into a PfACG1 mutant line resulted in a 6-fold higher IC_{50} relative to the drug-sensitive 3D7 line. Other editing results showed that this PfEHD mutation on its own was insufficient to mediate parasite resistance. We note that three other genes were observed to each harbor a single non-synonymous mutation. These mutations occurred separately in only one of the three flasks and may be attributable to stochastic events that arise naturally at low frequency during extended *in vitro* culture [418,419].

PfACG1 and PfEHD are both considered to be dispensable for *P. falciparum* asexual blood stage *in vitro* growth [395], consistent with our cKD data in which no significant growth inhibition occurred despite virtually complete protein knockdown (**Fig. 5.2C**). PfACG1, previously annotated as conserved protein of unknown function, is only conserved among Apicomplexan parasites of the genus *Plasmodium*, with minimal (~ 20%) amino acid identity to *Cryptotosporidium andersoni* and *C. muris*. Protein sequence analysis shows a signal peptide at the N-terminus and a single transmembrane domain at the C-terminal end. Little else is known about this protein. PfEHD contains a highly-conserved Eps15 homology domain (EHD) involved in protein-protein interactions and found in proteins that play a key

role in endocytosis [404]. PfEHD has previously been linked to vesicular trafficking in *P. falciparum* parasites [420].

PfACG1 and PfEHD did not co-localize in our immunofluorescence assays. Nonetheless, PfACG1 co-localized with the neutral lipid markers LipidTOX and Nile Red, as well as the Golgi markers ERD2 that mediates protein retention in the ER and PMT that plays a critical role in phosphatidylcholine synthesis, suggesting its role in vesicular trafficking or storage of lipids. In contrast, PfEHD showed some co-localization with the ER markers ERD2 and PDI as well as the actin-binding protein coronin. PfEHD has previously been shown to be an interacting partner of AP-2μ, an adapter protein that is essential for endocytosis and intracellular trafficking [421]. Taken together, these data suggest that PfACG1 and PfEHD might be involved in related intracellular trafficking pathway(s) acted upon by MMV688533, which would be consistent with our observation that mutations in both proteins contributed to higher-grade resistance to this compound. These results, along with lack of chemical-genetic interaction observed using the cKD lines (**Fig. 5.2C**), suggest that neither of these two proteins is the actual target of MMV688533 and function instead as resistance mediators. Finally, these data suggest that the MMV688533 mode of action involves inhibition of vesicular trafficking and/or lipid storage pathways.

In conclusion, we report the novel acylguanidine MMV688533 with favorable fast-acting and long-lasting pharmacokinetic/pharmacodynamic properties. Drug selection studies showed that parasites could only acquire low-grade resistance with large inocula, and no cross-resistance was observed with established antimalarials or advanced preclinical candidates.

These data suggest a novel mode of action for MMV688533, which appears to involve lipid-associated intracellular trafficking of essential components. The promising preclinical therapeutic margin and very low single doses predicted to be efficacious in humans should significantly improve compliance and enable a low cost of goods. Further safety and pharmacological preclinical evaluations are currently ongoing to support the initiation of human clinical trials.

Table 5. 1. | MMV688533 chemical formula and calculated /experimental properties of malonate salt.

Chemical name	5-[2-[3-(carbamimidoylcarbamoyl)-5-(trifluoromethyl)phenyl]ethynyl]-N-(2-pyridyl)-2-(trifluoromethyl)benzamide, malonate salt
Molecular weight	623.47 g/mol (free base: 519.41 g/mol)
Molecular formula	$C_{27}H_{19}F_6N_5O_6$ (free base: $C_{24}H_{15}F_6N_5O_2$)
Rings	3
Hydrogen bond donor	5
Hydrogen bond acceptor	7
tPSA (Å)	195.03 (free base: 120.43)
Number of chiral centers	0
pK_a (measured)	2.4 (base) /5.8 (base)
LogP (calculated/measured)	3.93 / No value (> 3)*
LogD (pH.4)	3.79
Polymorphism	All batches synthetized so far are under the same crystalline form (anhydrous form)
Melting point	180°C

* Technical limit of the Syrius T3 apparatus. tPSA: Topological polar surface area (the sum of the surface of all polar atoms, primarily oxygen and nitrogen including hydrogen atoms). Compounds with tPSA >140 Å suffer from poor cell permeability. pK_a: Dissociation constant. LogP: Partition coefficient. LogD: Distribution coefficient. LogP is expressed as a $\log_{10}$ of the concentration ratio between non-aqueous organic (n-octanol) and aqueous (pH-buffered water). Ideally, compounds should possess a LogP value not greater than 5 (otherwise too lipophilic, thereby creating solubility issues). LogD is a distribution coefficient related to the lipophilicity of ionizable compounds (pH dependent).

Table 5. 2. | MMV688533 (malonate salt) solubilization profile against time.

MMV688533	Solubility µg/mL Room temperature						pH		X-Ray diffraction results at 24 hr	Predicted solubility of malonate salt
Time (hours)	0.25	0.5	1	2	4	24	Medium	Supernatant (24h)		
pH 1.0 (0.1N HCl)	1750	2480	2870	2670	3770	4780	1.1	1.1	Malonate form1	≥ 4.7 mg/ml
pH 3.0	2.8	5.4	6.5	7.6	7.2	14.2	2.8	2.9	Malonate form1	≥ 14 µg/ml
pH 4.5	1.6	2.1	2.72	3	2.8	0.96	4.3	4.3	Malonate form1	≤ 3 µg/ml
pH 7.4	<LOQ	<LOQ	<LOQ	<LOQ	<LOQ	<LOQ	7.4	6.5	Base form 2	≤ 3 µg/ml
Water	1	2	4.3	7.6	10	14.4	N/A	3.1	Malonate form1	
	37°C									
Gastric fasted state	4220	3540	1890	1670	1010	420	1.3	1.5	Salt probably monohydrochloride	≥ 4.2 mg/ml
Gastric fed state	11	12	14	15	18	27	3.1	3.1	Malonate form1	27 µg/ml
Fasted state simulated intestinal fluid	107	154	15	11	13	20	6.7	4.7	Base form2	≥ 150 µg/ml
Fed state simulated intestinal fluid	3980	3540	1760	1990	2180	150	5	4.8	Base form2	≥ 3.9 mg/ml

The equilibrium solubility of MMV688533 malonate salt in buffered solutions (room temperature) and physiological relevant aqueous buffers (37°C) is pH dependent. Good solubility was observed in acidic conditions and poor solubility under more neutral conditions. Because the solubility of malonate salt is difficult to assess in some media due to its conversion into the free base form 2 (hydrated form of free base), we determined the concentration of solubilized compound as a function of time. LOQ: Limit Of Quantification. Low solubility is < 10 µg/mL; moderate solubility is between 10 µg/mL and 1000 µg/mL; high solubility is > 1000 µg/mL.

Table 5. 3. | MMV688533 *in vitro* IC_{50} (nM) of culture-adapted lab and field *P. falciparum* isolates.

Salt	NF54	3D7	K1	Dd2	HB3	7G8	TM90C2B	D6	V1/S	FCB	Cam3.1	PFeEF2 Y186N	PFDXR CNV	PFPI4K S743T	PFCARL I1139K	PFDHOD H G181C	PFCYTB I22L
HCl	9.0	8.6	7.3	7.8	2.5	5.5	4.1	4.4	7.1	8.5	-	7.5	8.7	7.2	7.3	-	-
Malonate	16	31*	-	-	-	-	15	-	-	-	16	-	-	15	-	21	18

MMV688533 potency on chloroquine-sensitive (NF54, 3D7) and chloroquine-resistant (K1, Dd2) parasites, as determined from dose-response assays and IC_{50} analyses, was below 10 nM. This compound showed no cross-resistance with other known antimalarials as determined using a diverse panel of lab-adapted field isolates: HB3, 7G8, TM90C2B, D6, V1/S, FCB and Cam3.1. No cross resistance was observed with Dd2 mutant parasites selected for resistance to DDD107498, fosmidomycin, MMV390048, GNF156, DSM265 or ELQ300 and which acquired resistance via amino acid substitutions or copy number variation (CNV) in eEF2, PFDXR, PFPI4K, PFACRL, PFDHODH and PFCYTB respectively. HCl: Hydrochloric acid; *SYBR Green assay; PFEF2: *P. falciparum* translation elongation factor 2; PFDXR: *P. falciparum* 1-deoxy-D-xylulose-5-phosphate reductoisomerase; PFPI4K: *P. falciparum* phosphatidylinositol 4-kinase; PFCARL: *P. falciparum* cyclic amine resistance locus; PFDHODH: *P. falciparum* dihydroorotate dehydrogenase; PFCYTB: *P. falciparum* cytochrome b.

Table 5. 4. | MMV688533 activity against *Plasmodium* parasite lines and field isolates.

	Laboratory lines				Clinical field isolates (Uganda)	Clinical field isolates (Papua, Indonesia)	
	P. falciparum				*P. falciparum*	*P. falciparum*	*P. vivax*
Antimalarial	(Median, N)	(Median, N)	FC27 (Mean, N)	K1 (Mean, N)	Median (N; range)	Median (N; range)	Median (N; range)
MMV688533	1.9 (4)	3.0 (4)	9.7 (2)	19 (2)	1.3 (143; 0.02 - 6.3)	18.9 (15; 5.3-39.2)	12.0 (6; 5.4-19.9)
Chloroquine	11 (11)	347 (10)	10.9 (2)	100.3 (2)	17*** (143; 2.1 - 346)	64.8*** (15; 38.3-283)	36.4* (6; 11.6-114)
Piperaquine	4.4 (11)	7.9 (10)	25.8 (2)	111.2 (2)	5.1*** (140; 0.3 - 26)	60.8*** (15; 17.6-130)	46.6* (6; 15.0-135)
Mefloquine	4.8 (11)	6.6 (10)	37.2 (2)	8 (2)	8.3*** (120; 0.5 - 24)	10.0 (15; 4.9-41.9)	11.2 (6; 8.1-20.7)
DHA/artesunate[a]	1.9 (9)	1.7 (9)	0.6 (2)	1.1 (2)	1.5 (142; 0.1 - 9.0)	1.2*** (15; 0.4-4.3)	0.6* (6; 0.3-2.4)

In vitro activity against *Plasmodium* culture-adapted lines or field isolates was calculated from dose-response curves and is shown as median or mean half-maximal growth inhibition concentrations (IC_{50} values) in nM. For the laboratory lines, numbers of independent repeats are shown in brackets. 3D7 and FC27 are chloroquine-sensitive whereas Dd2 and K1 are chloroquine-resistant. Potency of the other antimalarials was compared to MMV688533 using a Wilcoxon rank sum test. *p<0.05; ***p<0.001. aDHA was tested on 3D7, Dd2 and Ugandan parasites, whereas artesunate was tested on FC27, K1 and Papua/Indonesian parasites.

Table 5. 5. | MMV688533 *in vitro* cytotoxicity IC_{50} (µM) on human cell lines and rat hepatocytes.

Salt	HL60	HepG2	Rat hepatocytes
HCl	13.1	> 15.6	15.0 (18.0 w/o BSA)

MMV688533 showed a selectivity of >1,000 against the three designated cell lines tested. There was also no swelling or depolarization on rat liver-isolated mitochondria at 62.5 µM. HCl: Hydrochloric acid; HL60: Human leukemia cell line; HepG2: Human liver carcinoma cells; w/o: without; BSA: Bovine Serum Albumin.

Table 5. 6. | Summary of efficacy parameters from the *P. falciparum*-infected human red blood cell SCID mouse model study performed in recrudescence mode.

Assay	Parameter	Mean	95% Interval of confidence	Units
Non-standard 1-day	ED_{90}	2.0	1.9 - 2.1	mg/kg
Non-standard 1-day	AUC_{ED90}	3,097	2,335 - 4,484	ng.h/ml
Non-standard 1-day	AUC_{PCC}	8,046	3,802 - 12,511	ng.h/ml
Non-standard 1-day	C_{maxPCC}	382	231 - 576	ng/ml
Non-standard 1-day	AUC_{CURE}	> 193,123	-	ng.h/ml
Non-standard 1-day	$C_{maxCURE}$	> 5,506	-	ng/ml

Effective dose 90% (ED_{90}) and area under the curve 90% (AUC_{ED90}) are defined as the dose in mg/kg and the estimated average daily exposure, respectively, that reduce parasitemia by 90% on day 7 post-infection as compared to vehicle-treated mice. In this assay, this level of reduction implies no net parasite growth in blood. AUC_{PCC} and C_{maxPCC} is defined as the minimum average daily exposure (PCC, parasite clearance concentration) and maximal blood concentration (C_{max}) necessary to achieve maximum parasite clearance from peripheral blood. AUC_{CURE} and $C_{maxCURE}$ are defined as the minimum drug exposure and C_{max} in blood associated with cure of *P. falciparum*-infected SCID mice infused with human red blood cells.

Table 5. 7. | Minimal parasiticidal concentration of MMV688533 in the *P. falciparum* infected NSG mouse model.

EC_{50} origin	EC_{50} (ng/mL)	MPC (EC_{90}) (ng/mL)
Final run #79865 (population estimate)	1.63	14.7
Bootstrap analysis: median [25,75% quantile] from n= 504 successful runs	2.25 [1.59;3.44]	20.3 [14.3;30.9][a]

The minimal parasiticidal concentration (MPC), was determined from the IC_{90} value of the killing curve plotted as a function of the circulating drug concentration and calculated from IC_{50} and the Hill coefficient. The MPC determined from either the IC_{50} estimate of the final PK/PD run or from the median IC_{50} of its related bootstrap analysis ranged between 14.7 and 20.2 ng/ml. a [25,75% quantile] for MPC deduced from [25,75% quantile] for IC_{50}.

Table 5. 8. | MMV688533 *in vitro* metabolic clearances in microsomes and hepatocytes from different species.

Species	Liver microsomes CL_{int} (µL/min/mg)	Hepatocytes CL_{int} (µL/h/10^6cells)
Mouse	13	0-9
Rat	6.5	6-9
Dog	0	6
Macaque	0	15
Human	0	2

In vitro metabolic stability studies were performed using liver microsomes and cryopreserved hepatocytes of mouse, rat, dog, macaque or human origin. Results indicate low metabolic clearances in all species. CL_{int}: *in vivo* intrinsic clearance. Low liver microsome CL_{int} values are < 10 µL/min/mg, moderate values are between 10 and 50 µL/min/mg, and high values are > 50 µL/min/mg. Low hepatocyte CL_{int} values are < 4 mL/h/10^6 cells; moderate values are between 4 and 20 mL/h/10^6 cells; and high values are > 20 mL/h/10^6 cells.

Table 5. 9. | MMV688533 inhibition of cytochromes P450 (CYP).

CYP enzyme	Selective substrate	IC_{50} (μM)	Mode of inhibition	K_i (μM)
CYP1A2	Phenacetin	no inhibition		
CYP2B6	Bupropion	56.4	Mixed	12.6
CYP2C8	Amodiaquine	1.6	Mixed	0.8
CYP2C9	Diclofenac	3.3	Mixed	2.4
CYP2C19	S-Mephenytoin	13.7	Mixed	9.0
CYP2D6	Dextromethorphan	10.6	Competitive	4.0
CYP3A4/5	Midazolam	8.2	Mixed	15.3
CYP3A4/5	Testosterone	27.3	Mixed	11.1

Data shown above were generated with purified CYP enzymes. When tested *in vitro* with human liver microsomes, MMV688533 did not inhibit CYP1A2, CYP2C9, CYP2C19, CYP2D6, and CYP3A at concentrations up to 10 μM (data not shown).

Table 5. 10. | MMV688533 pharmacokinetic parameters in male Swiss mice and male Sprague Dawley rats after intravenous and oral route administration.

Route	Dose (mg/kg)	Matrix	C_{max} (µg/mL)	AUC_{0-24} (µg.h/mL)	CL (L/h/kg)	V_{ss} (L/kg)	$T_{1/2}$ (h)	T_{max} (h)	F (%)	B/P
Male Swiss mice										
Intravenous	3	Plasma	6.14	10.3	0.29	1.36	3.2	-	-	-
Per os	3	Blood	0.86	11.7	-	-	4	8	-	-
Per os	10	Plasma	2.24	33	-	-	-	4	96	-
Per os	10	Blood	2.21	30	-	-	16	8	-	1.2
Per os	30	Blood	8.13	152	ND	ND	26	4	ND	ND
Male Sprague Dawley rats										
Intravenous	3	Blood	5.65	9.5	0.30	2.09	7.5	-	-	
Per os	10	Blood	1.14	22.8	-	-	9.6	4	71	

MMV688533 was administered by oral gavage (po, with compound suspended in methylcellulose/Tween 80 0.6%/0.5% in water) and by IV route as a solution using PEG200/ solutol/ G5% (20/5/75; w/w/v) to male Swiss mice (PKS10191-VA) and male Sprague Dawley rats respectively. Compound concentrations were determined by LC-MS/MS, with a Limit of Quantification (LOQ) of 2 ng/mL for plasma and 5 ng/mL for blood. (-) below the LOQ. In both species, the clearance (CL) is equivalent to the relatively low value of 0.005 µL/min/mg. In rodents, a $T_{1/2}$ value (po) > 8h is considered as a long half-life when translated into humans. F (%), percent bioavailability. B/P, blood to plasma ratio. ND, not done.

Table 5. 11. | MMV688533 pharmacokinetic parameters in male Sprague Dawley rats after oral administration.

Salt	Route	Dose (mg/kg)	Matrix	C_{max} (µg/mL)	T_{max} (h)	AUC_{0-168} (µg.h/mL)	AUC (µg.h/mL)	$T_{1/2}$ (h)	AUC ratio 300/30
Malonate	Per os	30	Blood	6.0	6	310	310	16	-
Malonate	Per os	300	Blood	30	48	2800	2800	38	9.1
Malonate	Per os	30	Brain	3.2	4	140	160	24	0.5*
Malonate	Per os	30	Liver	246	6	11000	11000	21	35*
Malonate	Per os	30	Heart	81	6	3200	3200	19	10*
Malonate	Per os	30	Kidney	182	4	7500	7500	16	24*
Malonate	Per os	30	Lung	439	24	17000	17000	16	55*

MMV688533 malonate salt was administered at 30 and 300 mg/kg by oral gavage (methylcellulose/Tween 80 0.6%/0.5% in water) to male Sprague Dawley rats. Concentrations were determined using LC-MS/MS, with a limit of quantification of 25 ng/ml for blood and 125 ng/g for tissues. At the 30 mg/kg dose level, the highest concentrations were reached at 6 h post-dosing and the exposures increased roughly proportionally with dose between 30 and 300 mg/kg for AUC exposure while C_{max} increased sub-proportionally with dose. The quantitative tissue distribution was also evaluated in brain, liver, lung, heart and kidney at the 30 mg/kg dose level after oral administration. Broad distribution of MMV688533 was observed with tissue/blood concentration ratios above 1 in all tissues except the brain. The T_{max} ranged mostly between 4 and 24 hours. The highest levels (tissue/blood concentration ratio = 55) were observed in lung > liver > kidney > heart > brain. Penetration into brain was significantly lower compared to penetration into other tissues. *Tissue:blood AUC ratio.

Table 5. 12. | MMV688533 blood toxicokinetic parameters in male and female Sprague Dawley rats.

Sex	Dose (mg/kg/day)	Matrix	C_{max} (µg/mL)		T_{max} (h)		AUC_{0-24} (µg.h/mL)	
			Day 1	Day 4	Day 1	Day 4	Day 1	Day 4
Male	25	Blood	-	3.0	-	-	-	57.6
Male	50	Blood	-	8.9	-	-	-	188
Male	100	Blood	8.6	20.4	8	24	163	413
Female	25	Blood	-	5.2	-	-	-	99.4
Female	50	Blood	-	16.0	-	-	-	335
Female	100	Blood	10.1	17.9	24	24	195	355

MMV688533 maximal blood concentrations (C_{max}) were reached in females at 24 h post-dosing (last sampling time) and in males at 8 h post-dosing on Day 1 at 100 mg/kg. In females, MMV688533 Day 4 dose proportionality (C_{max} and AUC_{0-24}) over the 25-50 mg/kg/day dose range increased slightly supra-proportionally and were similar to the 50-100 mg/kg/day dose range. A 2-fold increase in dose (50 mg/kg/day vs 25 mg/kg/day) led to a 3.1-fold increase in C_{max} and a 3.4–fold increase in AUC_{0-24} and a further 2-fold increase in dose (100 mg/kg/day vs 50 mg/kg/day) led to a 1.1-fold increase in C_{max} and a 1.1–fold increase in AUC_{0-24}. In males, a slightly sub-proportional increase was observed. MMV688533 exposures increased in proportion over the 50-100 mg/kg/day dose range. A 2-fold increase in dose (50 mg/kg/day vs 25 mg/kg/day) led to a 3.0-fold increase in C_{max} and a 3.3–fold increase in AUC_{0-24}. A further 2-fold increase in dose (100 mg/kg/day vs 50 mg/kg/day) yielded a 2.3-fold increase in C_{max} and a 2.2–fold increase in AUC_{0-24}. At 100 mg/kg/day, MMV688533 mean accumulation ratios (D4/D1) in blood were 1.8 for both AUC_{0-24} and C_{max} in females and 2.5 AUC_{0-24} and 2.4 C_{max} in males. Based on MMV688533 C_{max} and AUC_{0-24} in blood, no gender effect was observed on Day 1. On Day 4, exposure in females was slightly higher with a female to male ratio ranging from 1.7 to 1.8 after dosing with 25 mg/kg/day or 50 mg/kg/day. No gender effect was observed at 100 mg/kg/day on Day 4, with a female to male ratio of 0.86 to 0.88. -, not determined. Two rats (one male and one female) were used per dose.

Table 5. 13. | MMV688533 mean biliary and urinary excretion parameters in male Sprague Dawley rats.

	Excreted drug cumulated over 24 hours (% of administered dose)	
Period (h)	Bile	Urine
0-4	1.36 ± 0.28 (12)	-
0-8	1.48 ± 0.28 (19)	-
0-24	2.05 ± 0.38 (18)	2.22 ± 1.13 (51)

Biliary and urinary excretion was evaluated over 24 h after intravenous administration of 10 mg/kg MMV688533 as a solution of 40% Captisol in water to dual cannulated (bile duct and duodenum) male Sprague Dawley rats. An exploratory LC-MS/MS method with a limit of quantification of 1 ng/ml was used to quantify urine and bile samples. Data are shown as mean ± SD (CV%), from three rats. Low biliary and urine excretions were observed with around 2% of the administered dose being recovered after 24 h.

Table 5. 14. | MMV688533 mean pharmacokinetic parameters in female Beagle dogs after intravenous injection.

Route	Dose (mg/kg)	Matrix	C_0 (µg/mL)	AUC_{0-72} (µg.h/mL)	AUC (µg.h/mL)	CL (L/h/kg)	V_{ss} (L/kg)	$T_{1/2}$ (h)
Intravenous	2	Blood	1.8	19.8	> 30%	0.07	4.74	50.7

MMV688533 was administered to 3 female Beagle dogs via intravenous route as a solution using PEG400/Ethanol/Solutol HS15/G5% (20/5/5/75) pH 3.0. Compound concentration was determined using LC-MS/MS. The limit of quantification was 5 ng/ml for blood. CL is equivalent to 0.011 µL/min/mg and is indicative of low clearance. In humans, compounds with a volume of distribution (V_{ss}) < 4 L are expected to be found exclusively in plasma. When V_{ss} is > 40 L, compounds are distributed in all tissues of the body and are almost absent in the plasma.

Table 5. 15. | Mean blood pharmacokinetic parameters of MMV688533 and its metabolite RA14677213 following a single oral administration as capsule or oral solution to pentagastrin-induced male Beagle dogs.

Compound	Formulation	C_{max} (ng/mL)	T_{max} (min-max) (h)	AUC_{0-24} (µg.h/mL)	AUC_{0-168} (µg.h/mL)	AUC (µg.h/mL)	T_{last} (h)	$T_{1/2}$ (h)
MMV688533	Capsule	89.7	10.7 (2-24)	1.55	4.58	4.85	168	41
MMV688533	Solution	99.6	2.67 (2-4)	1.99	6.09	6.49	168	42.8
RA14677213	Capsule	19.9	3.33 (2-4)	0.36	1.13	1.24	168	51.5
RA14677213	Solution	22	5.33 (4-6)	0.405	1.38	1.54	168	51.6

The pharmacokinetics of MMV688533 and its metabolite RA14677213 were investigated in blood after a single 0.5 mg/kg dose that was orally administered to male Beagle pentagastrin-induced dogs. The solution formulation was at 0.25 mg/mL in PEG400/Ethanol/Solutol/G5% (20/5/7.5/67.5). The capsule formulation [MMV688533 /microcrystalline cellulose/croscarmellose sodium (5/91.67/3.33)] was followed by 50 ml water. 30 minutes before oral administration, the dogs were treated with pentagastrin (intra-muscular injection, 6 µg/kg, 0.25 mL/kg). The gastric pH was measured before dosing and was found to be < 3.0. MMV688533 and RA14677213 were quantified using LC-MS/MS with limits of quantification of 0.83 ng/ml and 1.0 ng/ml, respectively. Maximal MMV688533 blood concentrations were observed between 2-24 h for the capsule and between 2-4 h for the solution. MV688533 exposure observed after oral administration as capsule was around 25% lower compared to exposure observed after oral administration as solution. For RA14677213, the maximal blood concentrations were observed between 2-4 h for the capsule and between 4-6 h for the solution. Similar pharmacokinetic profiles were observed between MMV688533 and its metabolite. The elimination half-life for both capsule and solution formulations was ~40 h for MMV688533 and ~50 h for its metabolite. On average, RA14677213 represented around 22% of parent exposure for both formulations.

Table 5. 16. | MMV688533 predicted human parameters.

Clearance (L/h)	$T_{1/2}$ (h)	V_{dss} (L)
Low: 3.6	103	5.0
Very low: 1.4	277	5.0

Mahmood rules and Fixed exponent method of allometric scaling of clearance from animal data predicted a low to a very low MMV688533 clearance (3.6 and 1.4 L/h (< 5%) of hepatic blood flow) in humans. This corresponded to a predicted half-life of 103 and 277 h respectively. The volume of distribution relying on allometry method with an exponent of 1 was predicted to be as high as 5.0L for a 70 kg individual.

Table 5. 17. | MMV688533 in silico prediction of genotoxicity/organ toxicity.

Toxicity	Derek	Leadscope	Internal toxicity results
Mutagenicity	No alert	No alert	No alert
Clastogenicity	No alert	No alert	No alert
Hepatotoxicty	No alert	Not relevant	To be monitored
Nephrotoxicity	No alert	Not applicable	To be monitored
Cardiac toxicity	No alert	Not applicable	To be monitored
Phototoxicity	No alert	moderate/low risks*	No alert

Knowledge-based approach using the software Derek and QSAR based (Leadscope) were used to predict in silico genotoxicity, hepatotoxicity, nephrotoxicity, cardiotoxicity and phototoxicity. (* moderate *in vitro* and low *in vivo*).

Table 5. 18. | MMV688533 off-target activities.

Assay	IC_{50} (μM)
BZD (peripheral) (antagonist radioligand)	0.9
Ca^{2+} channel (L, dihydropyridine site) (antagonist radioligand)	1.1
Cl^- channel (GABA-gated) (antagonist radioligand)	4.3
Dopamine transporter (h) (antagonist radioligand)	9.4
Sigma (non-selective (h) (agonist radioligand)	4.8

Off target potential pharmacological activities of MMV688533 were assessed in a full CEREP profile on 19 enzymes (uptake assays), 88 receptors (binding assays), ion channels and amine transporters at 1 μM inhibition activity. The criterion for dose-response determination was "greater than 60% inhibition of activity or displacement of the labeled ligand". MMV688533 was found inactive at 1 μM on a panel of 315 kinases. Interactions of MMV688533 with receptors – although at very high concentrations – carry an alert for central nervous system and cardiovascular effects. These alerts have not been confirmed when assessed through *in vivo* experiments and GLP safety pharmacology testing prior to human clinical trials.

Table 5. 19. | MMV688533 *in vitro* activity in µM on different cardiac ion channels.

Channel	Conc. (µM)
Potassium channel (hERG)	4.6
Sodium channel (Nav1.5)	14
Calcium channel (Cav1.1)	2.1

No cardiotoxicity alert was identified with MMV688533 from all the evaluated *in vitro* endpoints.

Table 5. 20. | MMV688533 non-compartmental analysis of exposure in male Sprague Dawley rats.

Dose (mg/kg)	Mean male and Female $AUC_{0\text{-}24h}$ (ng.h/mL)	Cumulated AUC (ng.h/mL)
12.5	53,400	747,600
25	108,500	1,519,000

The steady-state $AUC_{0\text{-}24h}$ and cumulated AUC in 2-week toxicity studies were calculated using a non-compartmental analysis. Five animals per dose and sex were used to determine the concentration of MMV688533 in whole blood.

Table 5. 21. | MMV688533 cumulated exposure over 14 days of treatment in Beagle dogs.

Dose (mg/kg)	Regimen	Total dose over 15 days (mg/kg)	$AUC_{0\text{-}360h}$ individual values from non-parametric superposition (ng.h/mL)						Mean male + female (min-max) $AUC_{0\text{-}360h}$
			Male		mean	Female		mean	Male & Female
0.5	once daily	7.5	30,000	27,400	28,700	52,000	32,300	42,200	35,400 (27,400-52,000)
1.0	(QD)	15	76,600	87,700	82,200	67,400	86,000	76,700	79,400 (67,400-87,700)
2.0	once every 2 days (Q2D)	14	73,300	76,200	74,800	41,100	69,100	55,100	64,900 (41,100-76,200)

Cumulated AUC was calculated from 2-week toxicity studies using a population pharmacokinetic model.

Table 5. 22. | Calculation of MMV688533 safety margin based on cumulative AUC over 14 days at the NOAEL dose in rats and dogs.

Species	Dose (mg/kg)	Mean AUC_{cum} (µg.h/mL)	Exposure ($AUC_{0\text{-}inf}$, µg.h/mL) of the human single dose (30 mg)	Therapeutic Index
Rat	12.5	747	5.7	>20
Dog	1.0	79	5.7	13.8

For rats the therapeutic index based on the cumulative AUC over 14 days at the NOAEL (No Observed Adverse Effect Level) dose of 12.5 mg/kg in rats, as compared with the AUC from an estimated single oral dose of 30 mg in humans, was estimated to be >20. For dogs the therapeutic index calculated based on the cumulative AUC over 14 days at the NOAEL dose of 1 mg/kg in dogs, compared with the AUC from an estimated single oral dose of 30 mg in humans, was estimated to be 14. Whole blood exposure in humans was predicted based on compound efficacy in the Pf SCID mouse model and the calculated *in vitro* PRR of 3.0.

Table 5. 23. | Mutations identified in MMV688533-selected resistant *P. falciparum* clones and validated using CRISPR/Cas9 gene editing.

		Amino acid substitution							
		sel. 533-CL2	ed. 3D7 ACG1^{W286R}	sel. 533-CL3	sel. 533-CL4	ed. 3D7 ACG1^{G98V}	ed. 3D7 EHD^{D218Y}	sel. 533-CL1	sel. ed. 533-CL1$^{EHD-D218Y}$
Gene product	Gene ID	3.1× IC_{50}	1.7× IC_{50}	2.5× IC_{50}	4.6× IC_{50}	1.8× IC_{50}	1.2× IC_{50}	2.2× IC_{50}	6.2× IC_{50}
Conserved *Plasmodium* protein (PfACG1)	PF3D7_0910300	W286R	W286R	T92*	G98V	G98V	wt	G98V	G98V
EH domain-containing protein (PfEHD)	PF3D7_0304200	wt	wt	wt	D218Y	wt	D218Y	wt	D218Y
Conserved *Plasmodium* protein	PF3D7_0510100	wt	wt	wt	wt	wt	wt	N1042H	N1042H
RNA pseudouridylate synthase, putative	PF3D7_0511500	wt	wt	K2762E	wt	wt	wt	wt	wt
ATP synthase (C/AC39) subunit, putative	PF3D7_1464700	L260I	wt	wt	wt	wt	wt	wt	wt

Four parasite clones (sel. 533-CL1 from flask 1, sel. 533-CL2 and 533-CL3 from flask 2, and sel. 533-CL4 from flask 3) were generated from selections (sel.), and named after the last 3 digits of the selecting compound (MMV688533) followed by the clone number. These clones were then chosen for whole-genome sequencing. Fold IC_{50} increases compared to the parent 3D7-A10 are indicated below the clone names. *P. falciparum* ACG1^{W286R}, ACG1^{G98V} and EHD^{D218Y} strains were gene edited (ed.) using CRISPR/Cas9 to introduce the designated mutation into 3D7-A10 parasites. The sel. ed. 533-CL1$^{EHD-D218Y}$ clone was generated by CRISPR/Cas9 editing the EHD D218Y mutation into the selected 533-CL1 clone. wt: wild-type, *: stop mutation resulting from a deletion-induced frameshift.

Table 5. 24. | Protein functional pathway relationships.

Gene product	Gene ID	Protein ID	GO_component	GO_process	GO_function1	GO_function2
Conserved *Plasmodium* protein (PfACG1)	PF3D7_0910300	Q8I349_PLAF7	-	-	-	-
EH domain-containing protein (PfEHD)	PF3D7_0304200	Q9NLB8_PLAF7	vesicle	transport	heterocyclic compound	-
Conserved *Plasmodium* protein	PF3D7_0510100	Q8I403_PLAF7	-	-	heterocyclic compound	RNA binding
RNA pseudouridylate synthase, putative	PF3D7_0511500	Q8I3Z1_PLAF7	-	-	heterocyclic compound	RNA binding
ATP synthase (C/AC39) subunit, putative	PF3D7_1464700	Q8IKJ0_PLAF7	-	transport	heterocyclic compound	-

GO: Gene Ontology

Table 5. 25. | Asexual blood stage IC_{50} data in nM of MMV688533-resistant parasite lines against common antimalarials.

	3D7-A10 wild type			ed. 3D7 ACG1^{G98V}			ed. 3D7 ACG1^{W286R}			sel. ed. 533-CL1$^{EHD-D218Y}$		
Compound	Mean IC_{50}	SEM	N	Mean IC_{50}	SEM	N	Mean IC_{50}	SEM	N	Mean IC_{50}	SEM	N
KAE609	0.7	0.1	3	0.7	0.0	3	0.6	0.02	3	0.7	0.04	3
Dihydroartemisinin	0.8	0.2	3	0.7	0.1	3	0.9	0.1	3	0.7	0.04	3
Lumefantrine	1.5	0.3	3	1.2	0.04	3	1.2	0.02	3	0.9	0.04	3
Chloroquine	5.5	1.0	3	6.2	0.1	3	8.3	1.1	3	9.2	1.5	3
Mefloquine	10.6	0.4	3	9.3	0.1	3	11.0	0.5	3	6.1	0.7	3
Ferroquine	6.5	1.3	3	8.1	0.4	3	11.5	1.9	3	12.1	2.6	3
Piperaquine	14.8	2.6	3	12.6	1.0	3	17.8	1.4	3	15.4	2.1	3
Quinine	24.5	3.7	3	22.2	1.3	3	25.2	2.6	3	15.4	0.8	3
md-amodiaquine	24.1	2.4	3	26.5	1.5	3	30.9	2.2	3	31.2	7.4	3
GNF179	45.7	9.1	3	42.4	7.1	3	55.0	11.2	3	35.1	7.4	3
Fosmidomycin	359	22	3	401	38	3	331	37	3	248	9.7	3

SEM: standard error of the mean; N: number of biological repeats (with technical duplicates). ed., gene edited. sel., selected under drug pressure.

Chapter 6. Concluding Remarks and Future Directions

6.1. Overview

The advancement of next generation antimalarials hinges on the identification of new *Plasmodium* drug targets and innovative drug discovery approaches. Presented herein are three independent projects that cover both of these areas. The experimental tools used in these studies provide a basis for new research avenues into protein-drug interactions and compound structure-activity relationships and constitute a foundation on which to build on the progress made thus far in the fight against malaria.

6.2. Chapter 3. Combining stage specificity and metabolomic profiling to advance antimalarial drug discovery.

With the increasing spread of *P. falciparum* resistance to artemisinins and their partner drugs, the development of antimalarials with new mode of actions is more critical than ever. High-throughput screens are able to identify potent chemical scaffolds, but not knowing their target often hampers their further development. Malaria drug discovery pipelines would thus greatly benefit from new assays that interrogate the mode of action and activity profile of screening hits. We designed an approach that provides more resolution into the different modes of action of clinical and experimental antimalarials by identifying the specific moment of asexual blood stage development against which these compounds are most active and combining this with a metabolomics assessment of pathway perturbations. This identified several stage specificity profiles that correlated well with inhibition of particular metabolic pathways. Interestingly, we also identified

compounds that act on similar pathways albeit through different targets, based on their shared metabolomics profile but differential stage specificity profile. Aside from the insight that this approach provided into the tested clinical antimalarials, the results also offered a rationale for the prioritization of experimental compounds. As such, we identified several hits from the MMV Malaria Box and the Malaria Drug Accelerator consortium with promising antimalarial profiles for further development, especially in the context of combination therapies. Importantly, this approach can also be adopted for other pathogens that undergo multiple differentiation steps within their host.

As earlier stated, it is important to note that the metabolomics experiments in this study were exploratory and involved only one to two biological replicates to screen for known and novel candidate mode of actions within a large set of compounds. Further targeted and in-depth follow-up experiments should be conducted once compounds are selected and prioritized for further discovery or development studies. Moving forward, and given the time- and resource-commitment required to generate robust data sets for these experiments, compounds should go through additional screenings and only be proposed for these assays after meeting set criteria. Benchmarks include but are not limited to compound propensity for resistance (minimum inoculum of resistance), speed of kill, activity against multiple life cycle stages, and structural and target novelty. These pre-screenings would inevitably reduce the number of compounds for the asexual blood stage-specificity and metabolomics analyses, which would in turn allow for a more robust analysis of metabolomic pathways targeted by the said compounds.

6.3. Chapter 4. The *Plasmodium falciparum* ABC transporter ABCI3 confers parasite strain-dependent pleiotropic antimalarial drug resistance.

The persistent threat of multidrug resistance mediated by *P. falciparum* transporters makes it imperative to identify their interactions with first-line drugs and antiplasmodial compounds in the discovery and development pipeline. Here we report on *P. falciparum* ABCI3, an ATP-binding cassette transporter with broad cellular localization that can confer antiplasmodial drug resistance through gene amplifications or point mutations. Results from *in vitro* selections, validated through gene editing, conditional knockdown and cellular accumulation studies, provide evidence that ABCI3 might be the primary target of point mutation-selecting carboxamide-containing compounds **3-5**. We also observed that the gene amplification-selecting imidazopyridine-containing compound **1** targets the heme detoxification pathway, supporting the hypothesis that although ABCI3 is a resistance mediator to both SNP and CNV-generating compounds, the latter have a separate mode of action.

The unusual biphasic dose-response curves observed with compounds **1** and **2** against a 3D7-A10-based ABCI3 CNV line and a Dd2-B2 line revealed intriguing insights into parasite biology. ABCI3 amplifications in 3D7-A10 resulted in decreased intracellular accumulation of compound **1**, presumably via drug being effluxed away from its site of action. Growth inhibition data for **1** and **2** assayed against isogenic Dd2 ^{Dd2} (CQ-resistant) and Dd2 ^{3D7} (CQ-sensitive) lines suggested a different mode of parasite resistance in Dd2-B2 parasites with the CQ-resistant Dd2 PfCRT isoform able to confer resistance,

also presumably through gain of transport properties resulting from PfCRT mutations. Intriguingly, point mutations in ABCI3 neutralized this PfCRT-driven resistance.

This study highlights unique ways in which *P. falciparum* is able to evade antiplasmodial drug action and underscores the complexity of antimalarial drug discovery efforts. This study also identifies ABCI3 as a pleiotropic drug transporter to consider when assessing the risk of resistance arising to new antimalarials in the discovery and development pipeline.

Future work on this project should focus on experiments to elucidate the intriguing mediation of resistance to compounds **1** and **2** by ABCI3 and PfCRT. An example of one such experiment that is already underway involves using recombinant PfCRT (in proteoliposomes) to conduct competition transport assays of compounds **1**, **4** and **5** and known DV-acting ^{3}H-CQ. Based on the Dd2 ^{Dd2} and Dd2 ^{3D7} cross-resistance dataset, we hypothesize that mutations in PfCRT confer resistance to compound **1** by effluxing it from the DV (proteoliposomes) and that this competes with CQ transport *in vitro*. It would also be interesting to test whether these ABCI3 inhibitors and CQ might show drug-drug interactions such as a gain of synergy with certain combinations of these loci.

A second and equally important set of experiments would be a more detailed co-staining of 3'-tagged ABCI3-3×Flag/HA parasite with antibodies against various vesicular makers to better establish the membrane structures contributing to the ~50% cytosolic localization of ABCI3. Ideally, this set of experiments would also encompass multiple asexual blood

stages to show how the location of these vesicles changes throughout this developmental cycle. Lastly, solving the structure of ABCI3 using cryo-EM would be an important advance in further understanding the structure/function relationship of this protein, which would in turn allow for the development of more targeted compounds. Parasites with the relevant ABCI3 tags for protein extraction from cultures have already been generated and validated.

6.4. Chapter 5. The antimalarial MMV688533 provides single-dose cures with a high barrier to *Plasmodium falciparum* parasite resistance

The rise and spread of artemisinin resistance in Southeast Asia has compromised the use of some of the first-line ACT therapies, including AS-MQ and more recently DHA-PPQ. The threat posed by the spread of this multidrug resistance to Africa has been exacerbated by the identification of mutant K13 strains in Rwanda. This necessitates the discovery of novel antiplasmodial compounds that may one day replace the artemisinins. Here we present on acylguanidines, a novel class of compounds that was discovered using an innovative phenotypic screening of the Sanofi chemical library of compounds with known activity on human targets. The candidate compound MMV688533 is a potent antimalarial with fast antiplasmodial killing kinetics, excellent *in vivo* activity, and safety and pharmacokinetic/ADME standards that allow for advancement to preclinical development. In addition, *in vitro* evolution assays with large parasite inocula using this compound only yielded low-grade resistance, and no cross-resistance was observed with established antimalarials or advanced preclinical candidates. These findings suggest a novel mode of

compound antiplasmodial action involving vesicular trafficking and neutral lipid storage pathways.

Future work on this project should focus on the identification of the actual compound target. While PF3D7_0910300, PF3D7_0304200, PF3D7_0510100, PF3D7_0511500 and PF3D7_1464700 gene products were implicated as targets from the *in vitro* evolution assays, their polymorphisms only conferred marginal resistance compared to the parental line. In addition, cKDs of the putative resistance mediators PF3D7_0910300 and PF3D7_0304200 revealed these to be non-essential for parasite *in vitro* survival. These findings imply that the aforementioned gene products are merely resistance mediators and not the actual targets of MMV688533. This conclusion has recently been reinforced by unpublished data from cellular thermal shift assays (CETSA) performed by our collaborators at the University of Dundee, Scotland.

CETSA is an innovative target identification assay that can be used to assess whether a protein binds a drug in *in vitro* or *in vivo* experiments by measuring its melting point changes in the presence of drug compared to an untreated control [422-424]. Protein(s) complexed to a ligand (compound) tends to become more resistant against heat-induced unfolding and this has been used successfully to screen recombinant proteins against potential inhibitors in a thermal shift assays in the past [425]. Compounds that alter the melting point of a protein are considered binders of the protein under investigation.

CETSA experiments using MMV688533 on *P. falciparum* cell lysate identified several putative targets: a hydroxyethylthiazole kinase (PF3D7_1239600); a *Plasmodium* protein of unknown function (PF3D7_0707200); the U6 snRNA-associated Sm-like protein LSm5 (PF3D7_1443300); the photo-sensitized INA-labelled protein PHIL1 (PF3D7_0109000); the 40S ribosomal protein S21 (PF3D7_1144000); and an AP2 domain transcription factor (AP2-EXP; PF3D7_1466400). Of these, only PF3D7_0707200, PF3D7_1443300 and PF3D7_0109000 gene products are essential for parasite survival [395]. Of those three, only PF3D7_0707200 gene product had a positive melting temperature in the presence of MMV688533, making it the most likely target. In addition, the PF3D7_0707200 gene product is expressed at the ring stage of parasite development when MMV688533 is most active as determined by the stage-specificity assays presented herein [73,393]. All these positive factors notwithstanding, it is worth noting that the parasite lysates for these CETSA experiments were prepared from synchronized late trophozoites and schizonts. As a result, more repeats, ideally using lysate from rings, will need to be conducted before any definitive conclusions can be made. Conditional knockdown experiments are also scheduled and the results from these two datasets will be key to test whether the PF3D7_0707200 gene product could be the primary target of MMV688533.

References

1. Carter R and Mendis KN (2002). Evolutionary and historical aspects of the burden of malaria. *Clin Microbiol Rev,* 15: 564-94.
2. WHO (2019). World Health Organization. World malaria report 2020. https://www.who.int/teams/global-malaria-programme/reports/world-malaria-report-2020:
3. Miller RL, Ikram S, Armelagos GJ, Walker R, Harer WB*, et al.* (1994). Diagnosis of *Plasmodium falciparum* infections in mummies using the rapid manual ParaSight-F test. *Trans R Soc Trop Med Hyg,* 88: 31-2.
4. Lopez C, Saravia C, Gomez A, Hoebeke J and Patarroyo MA (2010). Mechanisms of genetically-based resistance to malaria. *Gene,* 467: 1-12.
5. Piel FB (2016). The Present and Future Global Burden of the Inherited Disorders of Hemoglobin. *Hematol Oncol Clin North Am,* 30: 327-41.
6. Bayoumi RA (1987). The sickle-cell trait modifies the intensity and specificity of the immune response against *P. falciparum* malaria and leads to acquired protective immunity. *Med Hypotheses,* 22: 287-98.
7. Kwiatkowski DP (2005). How malaria has affected the human genome and what human genetics can teach us about malaria. *Am J Hum Genet,* 77: 171-92.
8. Elguero E, Delicat-Loembet LM, Rougeron V, Arnathau C, Roche B*, et al.* (2015). Malaria continues to select for sickle cell trait in Central Africa. *Proc Natl Acad Sci U S A,* 112: 7051-4.
9. Makani J, Williams TN and Marsh K (2007). Sickle cell disease in Africa: burden and research priorities. *Ann Trop Med Parasitol,* 101: 3-14.
10. Paul AS, Egan ES and Duraisingh MT (2015). Host-parasite interactions that guide red blood cell invasion by malaria parasites. *Curr Opin Hematol,* 22: 220-6.
11. Cheng Y, Lu F, Wang B, Li J, Han JH*, et al.* (2016). Plasmodium vivax GPI-anchored micronemal antigen (PvGAMA) binds human erythrocytes independent of Duffy antigen status. *Sci Rep,* 6: 35581.
12. Gunalan K, Lo E, Hostetler JB, Yewhalaw D, Mu J*, et al.* (2016). Role of Plasmodium vivax Duffy-binding protein 1 in invasion of Duffy-null Africans. *Proc Natl Acad Sci U S A,* 113: 6271-6.
13. Guindo A, Fairhurst RM, Doumbo OK, Wellems TE and Diallo DA (2007). X-linked G6PD deficiency protects hemizygous males but not heterozygous females against severe malaria. *PLoS Med,* 4: e66.
14. Laveran CL (1982). Classics in infectious diseases: A newly discovered parasite in the blood of patients suffering from malaria. Parasitic etiology of attacks of malaria: Charles Louis Alphonse Laveran (1845-1922). *Rev Infect Dis,* 4: 908-11.

15. Ross R (1897). On some peculiar pigmented cells found in two mosquitos fed on malarial blood. *Br Med J,* 2: 1786-8.

16. Martin N (1999). Surgeon-Major Ronald Ross, IMS Nobel laureate in medicine (1902) for his work on malaria. *J R Army Med Corps,* 145: 40-1.

17. Cox FE (2010). History of the discovery of the malaria parasites and their vectors. *Parasit Vectors,* 3: 5.

18. Shortt HE and Garnham PC (1948). Pre-erythrocytic stage in mammalian malaria parasites. *Nature,* 161: 126.

19. Shortt HE and Garnham PC (1948). The pre-erythrocytic development of Plasmodium cynomolgi and Plasmodium vivax. *Trans R Soc Trop Med Hyg,* 41: 785-95.

20. Shortt HE, Garnham PC and et al. (1948). The pre-erythrocytic stage of human malaria, Plasmodium vivax. *Br Med J,* 1: 547.

21. Shortt HE, Fairley NH and et al. (1949). The pre-erythrocytic stage of Plasmodium falciparum; a preliminary note. *Br Med J,* 2: 1006-8, illust.

22. Garnham PC, Bray RS, Cooper W, Lainson R, Awad FI*, et al.* (1954). Pre-erythrocytic Stages of Human Malaria: Plasmodium Ovale. *Br Med J,* 1: 257.

23. Sinka ME, Bangs MJ, Manguin S, Coetzee M, Mbogo CM*, et al.* (2010). The dominant Anopheles vectors of human malaria in Africa, Europe and the Middle East: occurrence data, distribution maps and bionomic precis. *Parasit Vectors,* 3: 117.

24. Florens L, Washburn MP, Raine JD, Anthony RM, Grainger M*, et al.* (2002). A proteomic view of the Plasmodium falciparum life cycle. *Nature,* 419: 520-6.

25. Gardner MJ, Hall N, Fung E, White O, Berriman M*, et al.* (2002). Genome sequence of the human malaria parasite Plasmodium falciparum. *Nature,* 419: 498-511.

26. Winzeler EA (2009). Advances in parasite genomics: from sequences to regulatory networks. *PLoS Pathog,* 5: e1000649.

27. Anstey NM, Douglas NM, Poespoprodjo JR and Price RN (2012). Plasmodium vivax: clinical spectrum, risk factors and pathogenesis. *Adv Parasitol,* 80: 151-201.

28. Sutherland CJ, Tanomsing N, Nolder D, Oguike M, Jennison C*, et al.* (2010). Two nonrecombining sympatric forms of the human malaria parasite Plasmodium ovale occur globally. *J Infect Dis,* 201: 1544-50.

29. Cox-Singh J, Davis TM, Lee KS, Shamsul SS, Matusop A*, et al.* (2008). Plasmodium knowlesi malaria in humans is widely distributed and potentially life threatening. *Clin Infect Dis,* 46: 165-71.

30. Singh B, Kim Sung L, Matusop A, Radhakrishnan A, Shamsul SS*, et al.* (2004). A large focus of naturally acquired Plasmodium knowlesi infections in human beings. *Lancet,* 363: 1017-24.

31. Wassmer SC, Taylor TE, Rathod PK, Mishra SK, Mohanty S*, et al.* (2015). Investigating the Pathogenesis of Severe Malaria: A Multidisciplinary and Cross-Geographical Approach. *Am J Trop Med Hyg,* 93: 42-56.

32. Ataide R, Mayor A and Rogerson SJ (2014). Malaria, primigravidae, and antibodies: knowledge gained and future perspectives. *Trends Parasitol,* 30: 85-94.

33. Desai M, ter Kuile FO, Nosten F, McGready R, Asamoa K*, et al.* (2007). Epidemiology and burden of malaria in pregnancy. *Lancet Infect Dis,* 7: 93-104.

34. McGready R, Lee SJ, Wiladphaingern J, Ashley EA, Rijken MJ*, et al.* (2012). Adverse effects of falciparum and vivax malaria and the safety of antimalarial treatment in early pregnancy: a population-based study. *Lancet Infect Dis,* 12: 388-96.

35. Tilley L, Straimer J, Gnadig NF, Ralph SA and Fidock DA (2016). Artemisinin Action and Resistance in Plasmodium falciparum. *Trends Parasitol,* 32: 682-96.

36. Douglas RG, Amino R, Sinnis P and Frischknecht F (2015). Active migration and passive transport of malaria parasites. *Trends Parasitol,* 31: 357-62.

37. Cowman AF, Healer J, Marapana D and Marsh K (2016). Malaria: Biology and Disease. *Cell,* 167: 610-24.

38. Prudencio M, Rodriguez A and Mota MM (2006). The silent path to thousands of merozoites: the *Plasmodium* liver stage. *Nat Rev Microbiol,* 4: 849-56.

39. Shin SC, Vanderberg JP and Terzakis JA (1982). Direct infection of hepatocytes by sporozoites of *Plasmodium berghei*. *J Protozool,* 29: 448-54.

40. Tavares J, Formaglio P, Thiberge S, Mordelet E, Van Rooijen N*, et al.* (2013). Role of host cell traversal by the malaria sporozoite during liver infection. *J Exp Med,* 210: 905-15.

41. Blasco B, Leroy D and Fidock DA (2017). Antimalarial drug resistance: linking *Plasmodium falciparum* parasite biology to the clinic. *Nat Med,* 23: 917-28.

42. Sturm A, Amino R, van de Sand C, Regen T, Retzlaff S*, et al.* (2006). Manipulation of host hepatocytes by the malaria parasite for delivery into liver sinusoids. *Science,* 313: 1287-90.

43. Venugopal K, Hentzschel F, Valkiunas G and Marti M (2020). *Plasmodium* asexual growth and sexual development in the haematopoietic niche of the host. *Nat Rev Microbiol,* 18: 177-89.

44. Lim C, Pereira L, Saliba KS, Mascarenhas A, Maki JN*, et al.* (2016). Reticulocyte preference and stage development of *Plasmodium vivax* isolates. *J Infect Dis,* 214: 1081-4.

45. Weiss GE, Gilson PR, Taechalertpaisarn T, Tham WH, de Jong NW*, et al.* (2015). Revealing the sequence and resulting cellular morphology of receptor-ligand interactions during *Plasmodium falciparum* invasion of erythrocytes. *PLoS Pathog,* 11: e1004670.

46. Holder AA (1994). Proteins on the surface of the malaria parasite and cell invasion. *Parasitology,* 108 Suppl: S5-18.

47. Lin CS, Uboldi AD, Epp C, Bujard H, Tsuboi T*, et al.* (2016). Multiple *Plasmodium falciparum* merozoite surface protein 1 complexes mediate merozoite binding to human erythrocytes. *J Biol Chem,* 291: 7703-15.

48. Das S, Hertrich N, Perrin AJ, Withers-Martinez C, Collins CR*, et al.* (2015). Processing of *Plasmodium falciparum* merozoite surface protein MSP1 activates a spectrin-binding function enabling parasite egress from RBCs. *Cell Host Microbe,* 18: 433-44.

49. Tham WH, Healer J and Cowman AF (2012). Erythrocyte and reticulocyte binding-like proteins of *Plasmodium falciparum*. *Trends Parasitol,* 28: 23-30.

50. Crosnier C, Bustamante LY, Bartholdson SJ, Bei AK, Theron M*, et al.* (2011). Basigin is a receptor essential for erythrocyte invasion by Plasmodium falciparum. *Nature,* 480: 534-7.

51. Besteiro S, Dubremetz JF and Lebrun M (2011). The moving junction of apicomplexan parasites: a key structure for invasion. *Cell Microbiol,* 13: 797-805.

52. Riglar DT, Richard D, Wilson DW, Boyle MJ, Dekiwadia C*, et al.* (2011). Super-resolution dissection of coordinated events during malaria parasite invasion of the human erythrocyte. *Cell Host Microbe,* 9: 9-20.

53. Boddey JA and Cowman AF (2013). Plasmodium nesting: remaking the erythrocyte from the inside out. *Annu Rev Microbiol,* 67: 243-69.

54. Spillman NJ, Beck JR and Goldberg DE (2015). Protein export into malaria parasite-infected erythrocytes: mechanisms and functional consequences. *Annu Rev Biochem,* 84: 813-41.

55. Dvorin JD, Martyn DC, Patel SD, Grimley JS, Collins CR*, et al.* (2010). A plant-like kinase in *Plasmodium falciparum* regulates parasite egress from erythrocytes. *Science,* 328: 910-2.

56. Collins CR, Hackett F, Strath M, Penzo M, Withers-Martinez C*, et al.* (2013). Malaria parasite cGMP-dependent protein kinase regulates blood stage merozoite secretory organelle discharge and egress. *PLoS Pathog,* 9: e1003344.

57. Vanaerschot M, Murithi JM, Pasaje CFA, Ghidelli-Disse S, Dwomoh L*, et al.* (2020). Inhibition of resistance-refractory *P. falciparum* kinase PKG delivers prophylactic, blood stage, and transmission-blocking antiplasmodial activity. *Cell Chem Biol,* 27: 806-16 e8.

58. Istvan ES, Dharia NV, Bopp SE, Gluzman I, Winzeler EA*, et al.* (2011). Validation of isoleucine utilization targets in Plasmodium falciparum. *Proc Natl Acad Sci U S A,* 108: 1627-32.

59. Spillman NJ, Allen RJ, McNamara CW, Yeung BK, Winzeler EA*, et al.* (2013). Na(+) regulation in the malaria parasite Plasmodium falciparum involves the cation

ATPase PfATP4 and is a target of the spiroindolone antimalarials. *Cell Host Microbe,* 13: 227-37.

60. Jimenez-Diaz MB, Ebert D, Salinas Y, Pradhan A, Lehane AM*, et al.* (2014). (+)-SJ733, a clinical candidate for malaria that acts through ATP4 to induce rapid host-mediated clearance of Plasmodium. *Proc Natl Acad Sci U S A,* 111: E5455-62.

61. McNamara CW, Lee MC, Lim CS, Lim SH, Roland J*, et al.* (2013). Targeting *Plasmodium* PI(4)K to eliminate malaria. *Nature,* 504: 248-53.

62. Kafsack BF, Rovira-Graells N, Clark TG, Bancells C, Crowley VM*, et al.* (2014). A transcriptional switch underlies commitment to sexual development in malaria parasites. *Nature,* 507: 248-52.

63. Hawking F, Wilson ME and Gammage K (1971). Evidence for cyclic development and short-lived maturity in the gametocytes of *Plasmodium falciparum*. *Trans R Soc Trop Med Hyg,* 65: 549-59.

64. Sinden RE (1982). Gametocytogenesis of *Plasmodium falciparum in vitro*: an electron microscopic study. *Parasitology,* 84: 1-11.

65. Meibalan E and Marti M (2017). Biology of Malaria Transmission. *Cold Spring Harb Perspect Med,* 7:

66. Billker O, Lindo V, Panico M, Etienne AE, Paxton T*, et al.* (1998). Identification of xanthurenic acid as the putative inducer of malaria development in the mosquito. *Nature,* 392: 289-92.

67. Billker O, Shaw MK, Margos G and Sinden RE (1997). The roles of temperature, pH and mosquito factors as triggers of male and female gametogenesis of *Plasmodium berghei in vitro*. *Parasitology,* 115 (Pt 1): 1-7.

68. Kawamoto F, Alejo-Blanco R, Fleck SL and Sinden RE (1991). Plasmodium berghei: ionic regulation and the induction of gametogenesis. *Exp Parasitol,* 72: 33-42.

69. Aly AS, Vaughan AM and Kappe SH (2009). Malaria parasite development in the mosquito and infection of the mammalian host. *Annu Rev Microbiol,* 63: 195-221.

70. Bennink S, Kiesow MJ and Pradel G (2016). The development of malaria parasites in the mosquito midgut. *Cell Microbiol,* 18: 905-18.

71. Carlton JM, Adams JH, Silva JC, Bidwell SL, Lorenzi H*, et al.* (2008). Comparative genomics of the neglected human malaria parasite Plasmodium vivax. *Nature,* 455: 757-63.

72. Pain A, Bohme U, Berry AE, Mungall K, Finn RD*, et al.* (2008). The genome of the simian and human malaria parasite Plasmodium knowlesi. *Nature,* 455: 799-803.

73. Bozdech Z, Llinas M, Pulliam BL, Wong ED, Zhu J*, et al.* (2003). The transcriptome of the intraerythrocytic developmental cycle of *Plasmodium falciparum*. *PLoS Biol,* 1: E5.

74. Le Roch KG, Zhou Y, Blair PL, Grainger M, Moch JK*, et al.* (2003). Discovery of gene function by expression profiling of the malaria parasite life cycle. *Science,* 301: 1503-8.

75. Young JA, Fivelman QL, Blair PL, de la Vega P, Le Roch KG*, et al.* (2005). The Plasmodium falciparum sexual development transcriptome: a microarray analysis using ontology-based pattern identification. *Mol Biochem Parasitol,* 143: 67-79.

76. Vembar SS, Droll D and Scherf A (2016). Translational regulation in blood stages of the malaria parasite Plasmodium spp.: systems-wide studies pave the way. *Wiley Interdiscip Rev RNA,* 7: 772-92.

77. Gissot M, Kim K, Schaap D and Ajioka JW (2009). New eukaryotic systematics: a phylogenetic perspective of developmental gene expression in the Apicomplexa. *Int J Parasitol,* 39: 145-51.

78. Gopalakrishnan AM, Nyindodo LA, Ross Fergus M and Lopez-Estrano C (2009). Plasmodium falciparum: Preinitiation complex occupancy of active and inactive promoters during erythrocytic stage. *Exp Parasitol,* 121: 46-54.

79. Su XZ and Wellems TE (1999). Plasmodium falciparum: assignment of microsatellite markers to chromosomes by PFG-PCR. *Exp Parasitol,* 91: 367-9.

80. Su X and Wellems TE (1996). Toward a high-resolution Plasmodium falciparum linkage map: polymorphic markers from hundreds of simple sequence repeats. *Genomics,* 33: 430-44.

81. Tyagi S, Pande V and Das A (2014). Whole mitochondrial genome sequence of an Indian Plasmodium falciparum field isolate. *Korean J Parasitol,* 52: 99-103.

82. Feagin JE, Harrell MI, Lee JC, Coe KJ, Sands BH*, et al.* (2012). The fragmented mitochondrial ribosomal RNAs of Plasmodium falciparum. *PLoS One,* 7: e38320.

83. Milton ME and Nelson SW (2016). Replication and maintenance of the Plasmodium falciparum apicoplast genome. *Mol Biochem Parasitol,* 208: 56-64.

84. McFadden GI, Reith ME, Munholland J and Lang-Unnasch N (1996). Plastid in human parasites. *Nature,* 381: 482.

85. Lanzer M, de Bruin D and Ravetch JV (1992). Transcription mapping of a 100 kb locus of Plasmodium falciparum identifies an intergenic region in which transcription terminates and reinitiates. *EMBO J,* 11: 1949-55.

86. Balu B, Blair PL and Adams JH (2009). Identification of the transcription initiation site reveals a novel transcript structure for Plasmodium falciparum maebl. *Exp Parasitol,* 121: 110-4.

87. DeBarry JD and Kissinger JC (2011). Jumbled genomes: missing Apicomplexan synteny. *Mol Biol Evol,* 28: 2855-71.

88. Lee AH, Symington LS and Fidock DA (2014). DNA repair mechanisms and their biological roles in the malaria parasite Plasmodium falciparum. *Microbiol Mol Biol Rev,* 78: 469-86.

89. Yayon A, Timberg R, Friedman S and Ginsburg H (1984). Effects of chloroquine on the feeding mechanism of the intraerythrocytic human malarial parasite Plasmodium falciparum. *J Protozool,* 31: 367-72.

90. Saliba KJ, Allen RJ, Zissis S, Bray PG, Ward SA*, et al.* (2003). Acidification of the malaria parasite's digestive vacuole by a H+-ATPase and a H+-pyrophosphatase. *J Biol Chem,* 278: 5605-12.

91. Klonis N, Tan O, Jackson K, Goldberg D, Klemba M*, et al.* (2007). Evaluation of pH during cytostomal endocytosis and vacuolar catabolism of haemoglobin in Plasmodium falciparum. *Biochem J,* 407: 343-54.

92. Gavigan CS, Dalton JP and Bell A (2001). The role of aminopeptidases in haemoglobin degradation in Plasmodium falciparum-infected erythrocytes. *Mol Biochem Parasitol,* 117: 37-48.

93. Combrinck JM, Mabotha TE, Ncokazi KK, Ambele MA, Taylor D*, et al.* (2013). Insights into the role of heme in the mechanism of action of antimalarials. *ACS Chem Biol,* 8: 133-7.

94. Lopez-Estrano C, Bhattacharjee S, Harrison T and Haldar K (2003). Cooperative domains define a unique host cell-targeting signal in Plasmodium falciparum-infected erythrocytes. *Proc Natl Acad Sci U S A,* 100: 12402-7.

95. Sullivan DJ, Jr., Gluzman IY and Goldberg DE (1996). Plasmodium hemozoin formation mediated by histidine-rich proteins. *Science,* 271: 219-22.

96. Pandey AV, Babbarwal VK, Okoyeh JN, Joshi RM, Puri SK*, et al.* (2003). Hemozoin formation in malaria: a two-step process involving histidine-rich proteins and lipids. *Biochem Biophys Res Commun,* 308: 736-43.

97. Jani D, Nagarkatti R, Beatty W, Angel R, Slebodnick C*, et al.* (2008). HDP-a novel heme detoxification protein from the malaria parasite. *PLoS Pathog,* 4: e1000053.

98. Zhang J, Krugliak M and Ginsburg H (1999). The fate of ferriprotorphyrin IX in malaria infected erythrocytes in conjunction with the mode of action of antimalarial drugs. *Mol Biochem Parasitol,* 99: 129-41.

99. Hanssen E, Knoechel C, Dearnley M, Dixon MW, Le Gros M*, et al.* (2012). Soft X-ray microscopy analysis of cell volume and hemoglobin content in erythrocytes infected with asexual and sexual stages of Plasmodium falciparum. *J Struct Biol,* 177: 224-32.

100. Krugliak M, Zhang J and Ginsburg H (2002). Intraerythrocytic Plasmodium falciparum utilizes only a fraction of the amino acids derived from the digestion of host cell cytosol for the biosynthesis of its proteins. *Mol Biochem Parasitol,* 119: 249-56.

101. Mauritz JM, Seear R, Esposito A, Kaminski CF, Skepper JN*, et al.* (2011). X-ray microanalysis investigation of the changes in Na, K, and hemoglobin concentration in plasmodium falciparum-infected red blood cells. *Biophys J,* 100: 1438-45.

102. Mauritz JM, Esposito A, Ginsburg H, Kaminski CF, Tiffert T*, et al.* (2009). The homeostasis of Plasmodium falciparum-infected red blood cells. *PLoS Comput Biol,* 5: e1000339.

103. Lew VL, Macdonald L, Ginsburg H, Krugliak M and Tiffert T (2004). Excess haemoglobin digestion by malaria parasites: a strategy to prevent premature host cell lysis. *Blood Cells Mol Dis,* 32: 353-9.

104. WHO (2014). Severe malaria. *Tropical Medicine and International Health 19, Supplement 1,*

105. Lover AA, Baird JK, Gosling R and Price RN (2018). Malaria elimination: Time to target all species. *Am J Trop Med Hyg,* 99: 17-23.

106. Phiri K, Kimani J, Mtove GA, Zhao Q, Rojo R*, et al.* (2016). Parasitological Clearance Rates and Drug Concentrations of a Fixed Dose Combination of Azithromycin-Chloroquine in Asymptomatic Pregnant Women with Plasmodium Falciparum Parasitemia: An Open-Label, Non-Comparative Study in Sub-Saharan Africa. *PLoS One,* 11: e0165692.

107. Worldwide Antimalarial Resistance Network ALDISG (2015). The effect of dose on the antimalarial efficacy of artemether-lumefantrine: a systematic review and pooled analysis of individual patient data. *Lancet Infect Dis,* 15: 692-702.

108. Joanny F, Lohr SJ, Engleitner T, Lell B and Mordmuller B (2014). Limit of blank and limit of detection of Plasmodium falciparum thick blood smear microscopy in a routine setting in Central Africa. *Malar J,* 13: 234.

109. Azikiwe CC, Ifezulike CC, Siminialayi IM, Amazu LU, Enye JC*, et al.* (2012). A comparative laboratory diagnosis of malaria: microscopy versus rapid diagnostic test kits. *Asian Pac J Trop Biomed,* 2: 307-10.

110. McCarthy JS, Sekuloski S, Griffin PM, Elliott S, Douglas N*, et al.* (2011). A pilot randomised trial of induced blood-stage Plasmodium falciparum infections in healthy volunteers for testing efficacy of new antimalarial drugs. *PLoS One,* 6: e21914.

111. Imwong M, Stepniewska K, Tripura R, Peto TJ, Lwin KM*, et al.* (2016). Numerical Distributions of Parasite Densities During Asymptomatic Malaria. *J Infect Dis,* 213: 1322-9.

112. Notomi T, Okayama H, Masubuchi H, Yonekawa T, Watanabe K*, et al.* (2000). Loop-mediated isothermal amplification of DNA. *Nucleic Acids Res,* 28: E63.

113. Sema M, Alemu A, Bayih AG, Getie S, Getnet G*, et al.* (2015). Evaluation of non-instrumented nucleic acid amplification by loop-mediated isothermal amplification (NINA-LAMP) for the diagnosis of malaria in Northwest Ethiopia. *Malar J,* 14: 44.

114. Gamboa D, Ho MF, Bendezu J, Torres K, Chiodini PL*, et al.* (2010). A large proportion of P. falciparum isolates in the Amazon region of Peru lack pfhrp2 and pfhrp3: implications for malaria rapid diagnostic tests. *PLoS One,* 5: e8091.

115. Cheng Q, Gatton ML, Barnwell J, Chiodini P, McCarthy J*, et al.* (2014). Plasmodium falciparum parasites lacking histidine-rich protein 2 and 3: a review and recommendations for accurate reporting. *Malar J,* 13: 283.

116. Mouatcho JC and Goldring JPD (2013). Malaria rapid diagnostic tests: challenges and prospects. *J Med Microbiol,* 62: 1491-505.

117. Parroche P, Lauw FN, Goutagny N, Latz E, Monks BG*, et al.* (2007). Malaria hemozoin is immunologically inert but radically enhances innate responses by presenting malaria DNA to Toll-like receptor 9. *Proc Natl Acad Sci U S A,* 104: 1919-24.

118. Karunaweera ND, Grau GE, Gamage P, Carter R and Mendis KN (1992). Dynamics of fever and serum levels of tumor necrosis factor are closely associated during clinical paroxysms in Plasmodium vivax malaria. *Proc Natl Acad Sci U S A,* 89: 3200-3.

119. Vijaykumar M, Naik RS and Gowda DC (2001). Plasmodium falciparum glycosylphosphatidylinositol-induced TNF-alpha secretion by macrophages is mediated without membrane insertion or endocytosis. *J Biol Chem,* 276: 6909-12.

120. Wijesekera SK, Carter R, Rathnayaka L and Mendis KN (1996). A malaria parasite toxin associated with Plasmodium vivax paroxysms. *Clin Exp Immunol,* 104: 221-7.

121. Hosseini SM and Feng JJ (2012). How malaria parasites reduce the deformability of infected red blood cells. *Biophys J,* 103: 1-10.

122. Bernabeu M and Smith JD (2017). EPCR and Malaria Severity: The Center of a Perfect Storm. *Trends Parasitol,* 33: 295-308.

123. Duraisingh MT and Horn D (2016). Epigenetic Regulation of Virulence Gene Expression in Parasitic Protozoa. *Cell Host Microbe,* 19: 629-40.

124. Smith JD (2014). The role of PfEMP1 adhesion domain classification in Plasmodium falciparum pathogenesis research. *Mol Biochem Parasitol,* 195: 82-7.

125. Storm J, Jespersen JS, Seydel KB, Szestak T, Mbewe M*, et al.* (2019). Cerebral malaria is associated with differential cytoadherence to brain endothelial cells. *EMBO Mol Med,* 11:

126. Moxon CA, Gibbins MP, McGuinness D, Milner DA, Jr. and Marti M (2020). New insights into malaria pathogenesis. *Annu Rev Pathol,* 15: 315-43.

127. Bernabeu M, Danziger SA, Avril M, Vaz M, Babar PH*, et al.* (2016). Severe adult malaria is associated with specific PfEMP1 adhesion types and high parasite biomass. *Proc Natl Acad Sci U S A,* 113: E3270-9.

128. Fox LL, Taylor TE, Pensulo P, Liomba A, Mpakiza A*, et al.* (2013). Histidine-rich protein 2 plasma levels predict progression to cerebral malaria in Malawian children with Plasmodium falciparum infection. *J Infect Dis,* 208: 500-3.

129. Rosenberg R, Wirtz RA, Schneider I and Burge R (1990). An estimation of the number of malaria sporozoites ejected by a feeding mosquito. *Trans R Soc Trop Med Hyg,* 84: 209-12.

130. Vanderberg JP and Frevert U (2004). Intravital microscopy demonstrating antibody-mediated immobilisation of *Plasmodium berghei* sporozoites injected into skin by mosquitoes. *Int J Parasitol,* 34: 991-6.

131. Sinnis P and Zavala F (2012). The skin: where malaria infection and the host immune response begin. *Semin Immunopathol,* 34: 787-92.

132. Frischknecht F, Baldacci P, Martin B, Zimmer C, Thiberge S*, et al.* (2004). Imaging movement of malaria parasites during transmission by Anopheles mosquitoes. *Cell Microbiol,* 6: 687-94.

133. Zheng H, Tan Z and Xu W (2014). Immune evasion strategies of pre-erythrocytic malaria parasites. *Mediators Inflamm,* 2014: 362605.

134. Dobbs KR and Dent AE (2016). Plasmodium malaria and antimalarial antibodies in the first year of life. *Parasitology,* 143: 129-38.

135. Fowkes FJ, Boeuf P and Beeson JG (2016). Immunity to malaria in an era of declining malaria transmission. *Parasitology,* 143: 139-53.

136. Teo A, Feng G, Brown GV, Beeson JG and Rogerson SJ (2016). Functional Antibodies and Protection against Blood-stage Malaria. *Trends Parasitol,* 32: 887-98.

137. Marsh K and Kinyanjui S (2006). Immune effector mechanisms in malaria. *Parasite Immunol,* 28: 51-60.

138. Bhatt S, Weiss DJ, Cameron E, Bisanzio D, Mappin B*, et al.* (2015). The effect of malaria control on Plasmodium falciparum in Africa between 2000 and 2015. *Nature,* 526: 207-11.

139. Chanda E, Remijo CD, Pasquale H, Baba SP and Lako RL (2014). Scale-up of a programme for malaria vector control using long-lasting insecticide-treated nets: lessons from South Sudan. *Bull World Health Organ,* 92: 290-6.

140. Ojuka P, Boum Y, 2nd, Denoeud-Ndam L, Nabasumba C, Muller Y*, et al.* (2015). Early biting and insecticide resistance in the malaria vector Anopheles might compromise the effectiveness of vector control intervention in Southwestern Uganda. *Malar J,* 14: 148.

141. Knapp J, Macdonald M, Malone D, Hamon N and Richardson JH (2015). Disruptive technology for vector control: the Innovative Vector Control Consortium and the US Military join forces to explore transformative insecticide application technology for mosquito control programmes. *Malar J,* 14: 371.

142. Madzorera T, Sibanda M, Focke W, Madito M and Manyala N (2019). Malathion-filled trilayer polyolefin film for malaria vector control. *Mater Sci Eng C Mater Biol Appl,* 96: 419-25.

143. Kruger T, Sibanda MM, Focke WW, Bornman MS and de Jager C (2015). Acceptability and effectiveness of a monofilament, polyethylene insecticide-treated wall lining for malaria control after six months in dwellings in Vhembe District, Limpopo Province, South Africa. *Malar J,* 14: 485.

144. Burt A (2014). Heritable strategies for controlling insect vectors of disease. *Philos Trans R Soc Lond B Biol Sci,* 369: 20130432.

145. Oliva CF, Vreysen MJ, Dupe S, Lees RS, Gilles JR*, et al.* (2014). Current status and future challenges for controlling malaria with the sterile insect technique: technical and social perspectives. *Acta Trop,* 132 Suppl: S130-9.

146. Bourtzis K, Lees RS, Hendrichs J and Vreysen MJ (2016). More than one rabbit out of the hat: Radiation, transgenic and symbiont-based approaches for sustainable management of mosquito and tsetse fly populations. *Acta Trop,* 157: 115-30.

147. Black WCt, Alphey L and James AA (2011). Why RIDL is not SIT. *Trends Parasitol,* 27: 362-70.

148. Windbichler N, Menichelli M, Papathanos PA, Thyme SB, Li H*, et al.* (2011). A synthetic homing endonuclease-based gene drive system in the human malaria mosquito. *Nature,* 473: 212-5.

149. Esvelt KM, Smidler AL, Catteruccia F and Church GM (2014). Concerning RNA-guided gene drives for the alteration of wild populations. *Elife,* 3:

150. Hammond A, Galizi R, Kyrou K, Simoni A, Siniscalchi C*, et al.* (2016). A CRISPR-Cas9 gene drive system targeting female reproduction in the malaria mosquito vector Anopheles gambiae. *Nat Biotechnol,* 34: 78-83.

151. Gantz VM, Jasinskiene N, Tatarenkova O, Fazekas A, Macias VM*, et al.* (2015). Highly efficient Cas9-mediated gene drive for population modification of the malaria vector mosquito Anopheles stephensi. *Proc Natl Acad Sci U S A,* 112: E6736-43.

152. Bull JJ and Turelli M (2013). Wolbachia versus dengue: Evolutionary forecasts. *Evol Med Public Health,* 2013: 197-207.

153. Wilke AB and Marrelli MT (2015). Paratransgenesis: a promising new strategy for mosquito vector control. *Parasit Vectors,* 8: 342.

154. Wang S, Ghosh AK, Bongio N, Stebbings KA, Lampe DJ*, et al.* (2012). Fighting malaria with engineered symbiotic bacteria from vector mosquitoes. *Proc Natl Acad Sci U S A,* 109: 12734-9.

155. Berman JD (2019). Approval of Tafenoquine for Malaria Chemoprophylaxis. *Am J Trop Med Hyg,* 100: 1301-4.

156. Cairns M, Roca-Feltrer A, Garske T, Wilson AL, Diallo D*, et al.* (2012). Estimating the potential public health impact of seasonal malaria chemoprevention in African children. *Nat Commun,* 3: 881.

157. Noor AM, Kibuchi E, Mitto B, Coulibaly D, Doumbo OK*, et al.* (2015). Sub-National Targeting of Seasonal Malaria Chemoprevention in the Sahelian Countries of the Nouakchott Initiative. *PLoS One,* 10: e0136919.

158. Tagbor H, Antwi GD, Acheampong PR, Bart Plange C, Chandramohan D*, et al.* (2016). Seasonal malaria chemoprevention in an area of extended seasonal transmission in Ashanti, Ghana: an individually randomised clinical trial. *Trop Med Int Health,* 21: 224-35.

159. Tine RC, Ndour CT, Faye B, Cairns M, Sylla K*, et al.* (2014). Feasibility, safety and effectiveness of combining home based malaria management and seasonal malaria chemoprevention in children less than 10 years in Senegal: a cluster-randomised trial. *Trans R Soc Trop Med Hyg,* 108: 13-21.

160. Zongo I, Milligan P, Compaore YD, Some AF, Greenwood B*, et al.* (2015). Randomized Noninferiority Trial of Dihydroartemisinin-Piperaquine Compared with Sulfadoxine-Pyrimethamine plus Amodiaquine for Seasonal Malaria Chemoprevention in Burkina Faso. *Antimicrob Agents Chemother,* 59: 4387-96.

161. Wilson AL and Taskforce IP (2011). A systematic review and meta-analysis of the efficacy and safety of intermittent preventive treatment of malaria in children (IPTc). *PLoS One,* 6: e16976.

162. Matondo SI, Temba GS, Kavishe AA, Kauki JS, Kalinga A*, et al.* (2014). High levels of sulphadoxine-pyrimethamine resistance Pfdhfr-Pfdhps quintuple mutations: a cross sectional survey of six regions in Tanzania. *Malar J,* 13: 152.

163. Gutman J, Kovacs S, Dorsey G, Stergachis A and Ter Kuile FO (2017). Safety, tolerability, and efficacy of repeated doses of dihydroartemisinin-piperaquine for prevention and treatment of malaria: a systematic review and meta-analysis. *Lancet Infect Dis,* 17: 184-93.

164. Keegan LT and Dushoff J (2013). Population-level effects of clinical immunity to malaria. *BMC Infect Dis,* 13: 428.

165. Doolan DL, Dobano C and Baird JK (2009). Acquired immunity to malaria. *Clin Microbiol Rev,* 22: 13-36, Table of Contents.

166. Hoffman SL, Vekemans J, Richie TL and Duffy PE (2015). The March Toward Malaria Vaccines. *Am J Prev Med,* 49: S319-33.

167. McCarthy JS, Griffin PM, Sekuloski S, Bright AT, Rockett R*, et al.* (2013). Experimentally induced blood-stage Plasmodium vivax infection in healthy volunteers. *J Infect Dis,* 208: 1688-94.

168. Engwerda CR, Minigo G, Amante FH and McCarthy JS (2012). Experimentally induced blood stage malaria infection as a tool for clinical research. *Trends Parasitol,* 28: 515-21.

169. Roestenberg M, Teirlinck AC, McCall MB, Teelen K, Makamdop KN*, et al.* (2011). Long-term protection against malaria after experimental sporozoite inoculation: an open-label follow-up study. *Lancet,* 377: 1770-6.

170. Wykes MN, Horne-Debets JM, Leow CY and Karunarathne DS (2014). Malaria drives T cells to exhaustion. *Front Microbiol,* 5: 249.

171. Rts SCTP (2015). Efficacy and safety of RTS,S/AS01 malaria vaccine with or without a booster dose in infants and children in Africa: final results of a phase 3, individually randomised, controlled trial. *Lancet,* 386: 31-45.

172. Penny MA, Verity R, Bever CA, Sauboin C, Galactionova K*, et al.* (2016). Public health impact and cost-effectiveness of the RTS,S/AS01 malaria vaccine: a systematic comparison of predictions from four mathematical models. *Lancet,* 387: 367-75.

173. Hollingdale MR and Sedegah M (2017). Development of whole sporozoite malaria vaccines. *Expert Rev Vaccines,* 16: 45-54.

174. Itsara LS, Zhou Y, Do J, Grieser AM, Vaughan AM*, et al.* (2018). The Development of Whole Sporozoite Vaccines for Plasmodium falciparum Malaria. *Front Immunol,* 9: 2748.

175. Sissoko MS, Healy SA, Katile A, Omaswa F, Zaidi I*, et al.* (2017). Safety and efficacy of PfSPZ Vaccine against Plasmodium falciparum via direct venous inoculation in healthy malaria-exposed adults in Mali: a randomised, double-blind phase 1 trial. *Lancet Infect Dis,* 17: 498-509.

176. Gosling R and von Seidlein L (2016). The Future of the RTS,S/AS01 Malaria Vaccine: An Alternative Development Plan. *PLoS Med,* 13: e1001994.

177. Mengesha T and Makonnen E (1999). Comparative efficacy and safety of chloroquine and alternative antimalarial drugs: a meta-analysis from six African countries. *East Afr Med J,* 76: 314-9.

178. Chekem L and Wierucki S (2006). [Extraction of artemisinin and synthesis of its derivates artesunate and artemether]. *Med Trop (Mars),* 66: 602-5.

179. Cohen J and Saran I (2018). The impact of packaging and messaging on adherence to malaria treatment: Evidence from a randomized controlled trial in Uganda. *J Dev Econ,* 134: 68-95.

180. Llanos-Cuentas A, Lacerda MV, Rueangweerayut R, Krudsood S, Gupta SK*, et al.* (2014). Tafenoquine plus chloroquine for the treatment and relapse prevention of Plasmodium vivax malaria (DETECTIVE): a multicentre, double-blind, randomised, phase 2b dose-selection study. *Lancet,* 383: 1049-58.

181. Tu Y (2011). The discovery of artemisinin (qinghaosu) and gifts from Chinese medicine. *Nat Med,* 17: 1217-20.

182. White NJ (2008). Qinghaosu (artemisinin): the price of success. *Science,* 320: 330-4.

183. Eastman RT and Fidock DA (2009). Artemisinin-based combination therapies: a vital tool in efforts to eliminate malaria. *Nat Rev Microbiol,* 7: 864-74.

184. Dondorp AM, Nosten F, Yi P, Das D, Phyo AP*, et al.* (2009). Artemisinin resistance in Plasmodium falciparum malaria. *N Engl J Med,* 361: 455-67.

185. White NJ, Pukrittayakamee S, Hien TT, Faiz MA, Mokuolu OA*, et al.* (2014). Malaria. *Lancet,* 383: 723-35.

186. Wang J, Zhang CJ, Chia WN, Loh CC, Li Z*, et al.* (2015). Haem-activated promiscuous targeting of artemisinin in Plasmodium falciparum. *Nat Commun,* 6: 10111.

187. Mok S, Ashley EA, Ferreira PE, Zhu L, Lin Z*, et al.* (2015). Drug resistance. Population transcriptomics of human malaria parasites reveals the mechanism of artemisinin resistance. *Science,* 347: 431-5.

188. Mbengue A, Bhattacharjee S, Pandharkar T, Liu H, Estiu G*, et al.* (2015). A molecular mechanism of artemisinin resistance in Plasmodium falciparum malaria. *Nature,* 520: 683-7.

189. Murithi JM, Owen ES, Istvan ES, Lee MCS, Ottilie S*, et al.* (2020). Combining stage specificity and metabolomic profiling to advance antimalarial drug discovery. *Cell Chem Biol,* 27: 158-71 e3.

190. Noedl H, Se Y, Schaecher K, Smith BL, Socheat D*, et al.* (2008). Evidence of artemisinin-resistant malaria in western Cambodia. *N Engl J Med,* 359: 2619-20.

191. Amato R, Pearson RD, Almagro-Garcia J, Amaratunga C, Lim P*, et al.* (2018). Origins of the current outbreak of multidrug-resistant malaria in southeast Asia: a retrospective genetic study. *Lancet Infect Dis,* 18: 337-45.

192. Straimer J, Gnadig NF, Witkowski B, Amaratunga C, Duru V*, et al.* (2015). Drug resistance. K13-propeller mutations confer artemisinin resistance in *Plasmodium falciparum* clinical isolates. *Science,* 347: 428-31.

193. Gnadig NF, Stokes BH, Edwards RL, Kalantarov GF, Heimsch KC*, et al.* (2020). Insights into the intracellular localization, protein associations and artemisinin resistance properties of *Plasmodium falciparum* K13. *PLoS Pathog,* 16: e1008482.

194. F. L (1946). Activity of a new antimalarial agent, chloroquine (SN 7618). *JAMA,* 130: 1069–70.

195. Ecker A, Lehane AM, Clain J and Fidock DA (2012). PfCRT and its role in antimalarial drug resistance. *Trends Parasitol,* 28: 504-14.

196. Berliner RW, Earle DP, Taggart JV, Zubrod CG, Welch WJ*, et al.* (1948). Studies on the Chemotherapy of the Human Malarias. Vi. The Physiological Disposition, Antimalarial Activity, and Toxicity of Several Derivatives of 4-Aminoquinoline. *J Clin Invest,* 27: 98-107.

197. Bompart F, Kiechel JR, Sebbag R and Pecoul B (2011). Innovative public-private partnerships to maximize the delivery of anti-malarial medicines: lessons learned from the ASAQ Winthrop experience. *Malar J,* 10: 143.

198. Aninagyei E, Tetteh CD, Oppong M, Boye A and Acheampong DO (2020). Efficacy of Artemether-Lumefantrine on various Plasmodium falciparum Kelch 13 and Pfmdr1 genes isolated in Ghana. *Parasite Epidemiol Control,* 11: e00190.

199. Chen L, Qu FY and Zhou YC (1982). Field observations on the antimalarial piperaquine. *Chin Med J (Engl),* 95: 281-6.

200. Spring MD, Lin JT, Manning JE, Vanachayangkul P, Somethy S*, et al.* (2015). Dihydroartemisinin-piperaquine failure associated with a triple mutant including kelch13 C580Y in Cambodia: an observational cohort study. *Lancet Infect Dis,* 15: 683-91.

201. Ross LS, Dhingra SK, Mok S, Yeo T, Wicht KJ*, et al.* (2018). Emerging Southeast Asian PfCRT mutations confer *Plasmodium falciparum* resistance to the first-line antimalarial piperaquine. *Nat Commun,* 9: 3314.

202. Dhingra SK, Small-Saunders JL, Menard D and Fidock DA (2019). *Plasmodium falciparum* resistance to piperaquine driven by PfCRT. *Lancet Infect Dis,* 19: 1168-9.

203. van der Pluijm RW, Imwong M, Chau NH, Hoa NT, Thuy-Nhien NT*, et al.* (2019). Determinants of dihydroartemisinin-piperaquine treatment failure in Plasmodium falciparum malaria in Cambodia, Thailand, and Vietnam: a prospective clinical, pharmacological, and genetic study. *Lancet Infect Dis,* 19: 952-61.

204. Amato R, Lim P, Miotto O, Amaratunga C, Dek D*, et al.* (2017). Genetic markers associated with dihydroartemisinin-piperaquine failure in Plasmodium falciparum malaria in Cambodia: a genotype-phenotype association study. *Lancet Infect Dis,* 17: 164-73.

205. Witkowski B, Duru V, Khim N, Ross LS, Saintpierre B*, et al.* (2017). A surrogate marker of piperaquine-resistant Plasmodium falciparum malaria: a phenotype-genotype association study. *Lancet Infect Dis,* 17: 174-83.

206. Dhingra SK, Redhi D, Combrinck JM, Yeo T, Okombo J*, et al.* (2017). A variant PfCRT isoform can contribute to *Plasmodium falciparum* resistance to the first-line partner drug piperaquine. *mBio,* 8:

207. Wicht KJ, Mok S and Fidock DA (2020). Molecular Mechanisms of Drug Resistance in Plasmodium falciparum Malaria. *Annu Rev Microbiol,* 74: 431-54.

208. Zheng XY, Xia Y, Gao FH and Chen C (1979). [Synthesis of 7351, a new antimalarial drug (author's transl)]. *Yao Xue Xue Bao,* 14: 736-7.

209. Chang C, Lin-Hua T and Jantanavivat C (1992). Studies on a new antimalarial compound: pyronaridine. *Trans R Soc Trop Med Hyg,* 86: 7-10.

210. Okombo J and Fidock DA (2020). Pyronaridine-artesunate Shows Promise as an Effective and Well-tolerated Treatment for Artemisinin-resistant Plasmodium falciparum Malaria. *Clin Infect Dis,* 70: 2196-8.

211. Wani WA, Jameel E, Baig U, Mumtazuddin S and Hun LT (2015). Ferroquine and its derivatives: new generation of antimalarial agents. *Eur J Med Chem,* 101: 534-51.

212. Ashley EA and Phyo AP (2018). Drugs in development for malaria. *Drugs,* 78: 861-79.

213. McCarthy JS, Ruckle T, Djeriou E, Cantalloube C, Ter-Minassian D*, et al.* (2016). A Phase II pilot trial to evaluate safety and efficacy of ferroquine against early Plasmodium falciparum in an induced blood-stage malaria infection study. *Malar J,* 15: 469.

214. Berman J, Brown T, Dow G and Toovey S (2018). Tafenoquine and primaquine do not exhibit clinical neurologic signs associated with central nervous system lesions in the same manner as earlier 8-aminoquinolines. *Malar J,* 17: 407.

215. Flannery EL, Chatterjee AK and Winzeler EA (2013). Antimalarial drug discovery - approaches and progress towards new medicines. *Nat Rev Microbiol,* 11: 849-62.

216. Baird JK (2018). Tafenoquine for travelers' malaria: evidence, rationale and recommendations. *J Travel Med,* 25:

217. Ebstie YA, Abay SM, Tadesse WT and Ejigu DA (2016). Tafenoquine and its potential in the treatment and relapse prevention of Plasmodium vivax malaria: the evidence to date. *Drug Des Devel Ther,* 10: 2387-99.

218. Achan J, Talisuna AO, Erhart A, Yeka A, Tibenderana JK*, et al.* (2011). Quinine, an old anti-malarial drug in a modern world: role in the treatment of malaria. *Malar J,* 10: 144.

219. Kovacs SD, Rijken MJ and Stergachis A (2015). Treating severe malaria in pregnancy: a review of the evidence. *Drug Saf,* 38: 165-81.

220. Bohorquez EB, Chua M and Meshnick SR (2012). Quinine localizes to a non-acidic compartment within the food vacuole of the malaria parasite Plasmodium falciparum. *Malar J,* 11: 350.

221. Cui L and Su XZ (2009). Discovery, mechanisms of action and combination therapy of artemisinin. *Expert Rev Anti Infect Ther,* 7: 999-1013.

222. Trenholme CM, Williams RL, Desjardins RE, Frischer H, Carson PE*, et al.* (1975). Mefloquine (WR 142,490) in the treatment of human malaria. *Science,* 190: 792-4.

223. Brasseur P, Druilhe P, Kouamouo J, Brandicourt O, Danis M*, et al.* (1986). High level of sensitivity to chloroquine of 72 Plasmodium falciparum isolates from southern Cameroon in January 1985. *Am J Trop Med Hyg,* 35: 711-6.

224. Nevin RL and Croft AM (2016). Psychiatric effects of malaria and anti-malarial drugs: historical and modern perspectives. *Malar J,* 15: 332.

225. Araujo FG, Huskinson J and Remington JS (1991). Remarkable in vitro and in vivo activities of the hydroxynaphthoquinone 566C80 against tachyzoites and tissue cysts of Toxoplasma gondii. *Antimicrob Agents Chemother,* 35: 293-9.

226. Curd FH, Davey DG and Rose FL (1945). Studies on synthetic antimalarial drugs; some biguanide derivatives as new types of antimalarial substances with both therapeutic and causal prophylactic activity. *Ann Trop Med Parasitol,* 39: 208-16.

227. Fry M and Pudney M (1992). Site of action of the antimalarial hydroxynaphthoquinone, 2-[trans-4-(4'-chlorophenyl) cyclohexyl]-3-hydroxy-1,4-naphthoquinone. *Biochem Pharmacol,* 43: 1545-53.

228. Patel SN and Kain KC (2005). Atovaquone/proguanil for the prophylaxis and treatment of malaria. *Expert Rev Anti Infect Ther,* 3: 849-61.

229. Laing AB (1965). Treatment of Acute Falciparum Malaria with Sulphorthodimethoxine (Fanasil). *Br Med J,* 1: 905-7.

230. Tse EG, Korsik M and Todd MH (2019). The past, present and future of anti-malarial medicines. *Malar J,* 18: 93.

231. Lumb V, Das MK, Singh N, Dev V, Khan W*, et al.* (2011). Multiple origins of Plasmodium falciparum dihydropteroate synthetase mutant alleles associated with sulfadoxine resistance in India. *Antimicrob Agents Chemother,* 55: 2813-7.

232. Zhao L, Pi L, Qin Y, Lu Y, Zeng W*, et al.* (2020). Widespread resistance mutations to sulfadoxine-pyrimethamine in malaria parasites imported to China from Central and Western Africa. *Int J Parasitol Drugs Drug Resist,* 12: 1-6.

233. Cowell AN, Istvan ES, Lukens AK, Gomez-Lorenzo MG, Vanaerschot M*, et al.* (2018). Mapping the malaria parasite druggable genome by using *in vitro* evolution and chemogenomics. *Science,* 359: 191-9.

234. Gamo FJ, Sanz LM, Vidal J, de Cozar C, Alvarez E*, et al.* (2010). Thousands of chemical starting points for antimalarial lead identification. *Nature,* 465: 305-10.

235. Guiguemde WA, Shelat AA, Bouck D, Duffy S, Crowther GJ*, et al.* (2010). Chemical genetics of *Plasmodium falciparum*. *Nature,* 465: 311-5.

236. Plouffe D, Brinker A, McNamara C, Henson K, Kato N*, et al.* (2008). *In silico* activity profiling reveals the mechanism of action of antimalarials discovered in a high-throughput screen. *Proc Natl Acad Sci U S A,* 105: 9059-64.

237. Macarron R, Banks MN, Bojanic D, Burns DJ, Cirovic DA*, et al.* (2011). Impact of high-throughput screening in biomedical research. *Nat Rev Drug Discov,* 10: 188-95.

238. Spillman NJ and Kirk K (2015). The malaria parasite cation ATPase PfATP4 and its role in the mechanism of action of a new arsenal of antimalarial drugs. *Int J Parasitol Drugs Drug Resist,* 5: 149-62.

239. Ashton TD, Devine SM, Mohrle JJ, Laleu B, Burrows JN*, et al.* (2019). The Development Process for Discovery and Clinical Advancement of Modern Antimalarials. *J Med Chem,* 62: 10526-62.

240. Siciliano G, Santha Kumar TR, Bona R, Camarda G, Calabretta MM*, et al.* (2017). A high susceptibility to redox imbalance of the transmissible stages of *Plasmodium falciparum* revealed with a luciferase-based mature gametocyte assay. *Mol Microbiol,* 104: 306-18.

241. D'Alessandro S, Camarda G, Corbett Y, Siciliano G, Parapini S*, et al.* (2016). A chemical susceptibility profile of the Plasmodium falciparum transmission stages

by complementary cell-based gametocyte assays. *J Antimicrob Chemother,* 71: 1148-58.

242. Plouffe DM, Wree M, Du AY, Meister S, Li F*, et al.* (2016). High-Throughput Assay and Discovery of Small Molecules that Interrupt Malaria Transmission. *Cell Host Microbe,* 19: 114-26.

243. Sinden RE (2017). Targeting the Parasite to Suppress Malaria Transmission. *Adv Parasitol,* 97: 147-85.

244. Lucantoni L, Fidock DA and Avery VM (2016). Luciferase-based, high-throughput assay for screening and profiling transmission-blocking compounds against *Plasmodium falciparum* gametocytes. *Antimicrob Agents Chemother,* 60: 2097-107.

245. Gunsaru B, Burgess SJ, Morrill W, Kelly JX, Shomloo S*, et al.* (2017). Simplified Reversed Chloroquines To Overcome Malaria Resistance to Quinoline-Based Drugs. *Antimicrob Agents Chemother,* 61:

246. Kelly JX, Smilkstein MJ, Brun R, Wittlin S, Cooper RA*, et al.* (2009). Discovery of dual function acridones as a new antimalarial chemotype. *Nature,* 459: 270-3.

247. Kesely KR, Pantaleo A, Turrini FM, Olupot-Olupot P and Low PS (2016). Inhibition of an Erythrocyte Tyrosine Kinase with Imatinib Prevents Plasmodium falciparum Egress and Terminates Parasitemia. *PLoS One,* 11: e0164895.

248. Zumla A, Rao M, Wallis RS, Kaufmann SH, Rustomjee R*, et al.* (2016). Host-directed therapies for infectious diseases: current status, recent progress, and future prospects. *Lancet Infect Dis,* 16: e47-63.

249. Smith CM, Jerkovic A, Puy H, Winship I, Deybach JC*, et al.* (2015). Red cells from ferrochelatase-deficient erythropoietic protoporphyria patients are resistant to growth of malarial parasites. *Blood,* 125: 534-41.

250. Vial H, Taramelli D, Boulton IC, Ward SA, Doerig C*, et al.* (2013). CRIMALDDI: platform technologies and novel anti-malarial drug targets. *Malar J,* 12: 396.

251. Baragana B, Hallyburton I, Lee MC, Norcross NR, Grimaldi R*, et al.* (2015). A novel multiple-stage antimalarial agent that inhibits protein synthesis. *Nature,* 522: 315-20.

252. Baragana B, Norcross NR, Wilson C, Porzelle A, Hallyburton I*, et al.* (2016). Discovery of a Quinoline-4-carboxamide Derivative with a Novel Mechanism of Action, Multistage Antimalarial Activity, and Potent in Vivo Efficacy. *J Med Chem,* 59: 9672-85.

253. Burgess SJ, Selzer A, Kelly JX, Smilkstein MJ, Riscoe MK*, et al.* (2006). A chloroquine-like molecule designed to reverse resistance in Plasmodium falciparum. *J Med Chem,* 49: 5623-5.

254. Wirjanata G, Sebayang BF, Chalfein F, Prayoga, Handayuni I*, et al.* (2015). Contrasting ex vivo efficacies of "reversed chloroquine" compounds in

chloroquine-resistant Plasmodium falciparum and P. vivax isolates. *Antimicrob Agents Chemother,* 59: 5721-6.

255. Yuthavong Y, Tarnchompoo B, Vilaivan T, Chitnumsub P, Kamchonwongpaisan S*, et al.* (2012). Malarial dihydrofolate reductase as a paradigm for drug development against a resistance-compromised target. *Proc Natl Acad Sci U S A,* 109: 16823-8.

256. Floyd DM, Stein P, Wang Z, Liu J, Castro S*, et al.* (2016). Hit-to-Lead Studies for the Antimalarial Tetrahydroisoquinolone Carboxanilides. *J Med Chem,* 59: 7950-62.

257. Le Bihan A, de Kanter R, Angulo-Barturen I, Binkert C, Boss C*, et al.* (2016). Characterization of Novel Antimalarial Compound ACT-451840: Preclinical Assessment of Activity and Dose-Efficacy Modeling. *PLoS Med,* 13: e1002138.

258. Boss C, Aissaoui H, Amaral N, Bauer A, Bazire S*, et al.* (2016). Discovery and Characterization of ACT-451840: an Antimalarial Drug with a Novel Mechanism of Action. *ChemMedChem,* 11: 1995-2014.

259. Dong Y, Wang X, Kamaraj S, Bulbule VJ, Chiu FC*, et al.* (2017). Structure-Activity Relationship of the Antimalarial Ozonide Artefenomel (OZ439). *J Med Chem,* 60: 2654-68.

260. Allman EL, Painter HJ, Samra J, Carrasquilla M and Llinas M (2016). Metabolomic Profiling of the Malaria Box Reveals Antimalarial Target Pathways. *Antimicrob Agents Chemother,* 60: 6635-49.

261. Kuhen KL, Chatterjee AK, Rottmann M, Gagaring K, Borboa R*, et al.* (2014). KAF156 is an antimalarial clinical candidate with potential for use in prophylaxis, treatment, and prevention of disease transmission. *Antimicrob Agents Chemother,* 58: 5060-7.

262. Nagle A, Wu T, Kuhen K, Gagaring K, Borboa R*, et al.* (2012). Imidazolopiperazines: lead optimization of the second-generation antimalarial agents. *J Med Chem,* 55: 4244-73.

263. White NJ, Pukrittayakamee S, Phyo AP, Rueangweerayut R, Nosten F*, et al.* (2014). Spiroindolone KAE609 for falciparum and vivax malaria. *N Engl J Med,* 371: 403-10.

264. Rottmann M, McNamara C, Yeung BK, Lee MC, Zou B*, et al.* (2010). Spiroindolones, a potent compound class for the treatment of malaria. *Science,* 329: 1175-80.

265. McCarthy JS, Lotharius J, Ruckle T, Chalon S, Phillips MA*, et al.* (2017). Safety, tolerability, pharmacokinetics, and activity of the novel long-acting antimalarial DSM265: a two-part first-in-human phase 1a/1b randomised study. *Lancet Infect Dis,* 17: 626-35.

266. Coteron JM, Marco M, Esquivias J, Deng X, White KL*, et al.* (2011). Structure-guided lead optimization of triazolopyrimidine-ring substituents identifies potent

Plasmodium falciparum dihydroorotate dehydrogenase inhibitors with clinical candidate potential. *J Med Chem,* 54: 5540-61.

267. Younis Y, Douelle F, Feng TS, Gonzalez Cabrera D, Le Manach C*, et al.* (2012). 3,5-Diaryl-2-aminopyridines as a novel class of orally active antimalarials demonstrating single dose cure in mice and clinical candidate potential. *J Med Chem,* 55: 3479-87.

268. Xie SC, Gillett DL, Spillman NJ, Tsu C, Luth MR*, et al.* (2018). Target Validation and Identification of Novel Boronate Inhibitors of the Plasmodium falciparum Proteasome. *J Med Chem,* 61: 10053-66.

269. Li H, O'Donoghue AJ, van der Linden WA, Xie SC, Yoo E*, et al.* (2016). Structure- and function-based design of *Plasmodium*-selective proteasome inhibitors. *Nature,* 530: 233-6.

270. Stokes BH, Yoo E, Murithi JM, Luth MR, Afanasyev P*, et al.* (2019). Covalent *Plasmodium falciparum*-selective proteasome inhibitors exhibit a low propensity for generating resistance *in vitro* and synergize with multiple antimalarial agents. *PLoS Pathog,* 15: e1007722.

271. Vanaerschot M, Lucantoni L, Li T, Combrinck JM, Ruecker A*, et al.* (2017). Hexahydroquinolines are antimalarial candidates with potent blood-stage and transmission-blocking activity. *Nat Microbiol,* 2: 1403-14.

272. Gilson PR, Kumarasingha R, Thompson J, Zhang X, Penington JS*, et al.* (2019). A 4-cyano-3-methylisoquinoline inhibitor of Plasmodium falciparum growth targets the sodium efflux pump PfATP4. *Sci Rep,* 9: 10292.

273. Zhang YK, Plattner JJ, Easom EE, Jacobs RT, Guo D*, et al.* (2017). Benzoxaborole Antimalarial Agents. Part 5. Lead Optimization of Novel Amide Pyrazinyloxy Benzoxaboroles and Identification of a Preclinical Candidate. *J Med Chem,* 60: 5889-908.

274. Zhang YK, Plattner JJ, Easom EE, Jacobs RT, Guo D*, et al.* (2015). Benzoxaborole antimalarial agents. Part 4. Discovery of potent 6-(2-(alkoxycarbonyl)pyrazinyl-5-oxy)-1,3-dihydro-1-hydroxy-2,1-benzoxaboroles. *J Med Chem,* 58: 5344-54.

275. Hameed PS, Solapure S, Patil V, Henrich PP, Magistrado PA*, et al.* (2015). Triaminopyrimidine is a fast-killing and long-acting antimalarial clinical candidate. *Nat Commun,* 6: 6715.

276. Duffey M, Sanchez CP and Lanzer M (2018). Profiling of the anti-malarial drug candidate SC83288 against artemisinins in Plasmodium falciparum. *Malar J,* 17: 121.

277. Pegoraro S, Duffey M, Otto TD, Wang Y, Rosemann R*, et al.* (2017). SC83288 is a clinical development candidate for the treatment of severe malaria. *Nat Commun,* 8: 14193.

278. Younis Y, Douelle F, Gonzalez Cabrera D, Le Manach C, Nchinda AT*, et al.* (2013). Structure-activity-relationship studies around the 2-amino group and pyridine core

of antimalarial 3,5-diarylaminopyridines lead to a novel series of pyrazine analogues with oral in vivo activity. *J Med Chem,* 56: 8860-71.

279. Gonzalez Cabrera D, Douelle F, Younis Y, Feng TS, Le Manach C*, et al.* (2012). Structure-activity relationship studies of orally active antimalarial 3,5-substituted 2-aminopyridines. *J Med Chem,* 55: 11022-30.

280. Jorgensen R, Merrill AR and Andersen GR (2006). The life and death of translation elongation factor 2. *Biochem Soc Trans,* 34: 1-6.

281. Burrows JN, van Huijsduijnen RH, Mohrle JJ, Oeuvray C and Wells TN (2013). Designing the next generation of medicines for malaria control and eradication. *Malar J,* 12: 187.

282. Saliba KJ and Kirk K (1999). pH regulation in the intracellular malaria parasite, Plasmodium falciparum. H(+) extrusion via a V-type H(+)-ATPase. *J Biol Chem,* 274: 33213-9.

283. van Schalkwyk DA, Chan XW, Misiano P, Gagliardi S, Farina C*, et al.* (2010). Inhibition of Plasmodium falciparum pH regulation by small molecule indole derivatives results in rapid parasite death. *Biochem Pharmacol,* 79: 1291-9.

284. Hoelz LV, Calil FA, Nonato MC, Pinheiro LC and Boechat N (2018). Plasmodium falciparum dihydroorotate dehydrogenase: a drug target against malaria. *Future Med Chem,* 10: 1853-74.

285. Baldwin J, Farajallah AM, Malmquist NA, Rathod PK and Phillips MA (2002). Malarial dihydroorotate dehydrogenase. Substrate and inhibitor specificity. *J Biol Chem,* 277: 41827-34.

286. Yuthavong Y, Yuvaniyama J, Chitnumsub P, Vanichtanankul J, Chusacultanachai S*, et al.* (2005). Malarial (Plasmodium falciparum) dihydrofolate reductase-thymidylate synthase: structural basis for antifolate resistance and development of effective inhibitors. *Parasitology,* 130: 249-59.

287. Uhlemann AC, McGready R, Ashley EA, Brockman A, Singhasivanon P*, et al.* (2007). Intrahost selection of Plasmodium falciparum pfmdr1 alleles after antimalarial treatment on the northwestern border of Thailand. *J Infect Dis,* 195: 134-41.

288. Sidhu AB, Uhlemann AC, Valderramos SG, Valderramos JC, Krishna S*, et al.* (2006). Decreasing pfmdr1 copy number in plasmodium falciparum malaria heightens susceptibility to mefloquine, lumefantrine, halofantrine, quinine, and artemisinin. *J Infect Dis,* 194: 528-35.

289. Petersen I, Gabryszewski SJ, Johnston GL, Dhingra SK, Ecker A*, et al.* (2015). Balancing drug resistance and growth rates via compensatory mutations in the Plasmodium falciparum chloroquine resistance transporter. *Mol Microbiol,* 97: 381-95.

290. Pascual A, Madamet M, Bertaux L, Amalvict R, Benoit N*, et al.* (2013). In vitro piperaquine susceptibility is not associated with the Plasmodium falciparum chloroquine resistance transporter gene. *Malar J,* 12: 431.

291. Amaratunga C, Lim P, Suon S, Sreng S, Mao S*, et al.* (2016). Dihydroartemisinin-piperaquine resistance in Plasmodium falciparum malaria in Cambodia: a multisite prospective cohort study. *Lancet Infect Dis,* 16: 357-65.

292. Duru V, Khim N, Leang R, Kim S, Domergue A*, et al.* (2015). Plasmodium falciparum dihydroartemisinin-piperaquine failures in Cambodia are associated with mutant K13 parasites presenting high survival rates in novel piperaquine in vitro assays: retrospective and prospective investigations. *BMC Med,* 13: 305.

293. Saunders DL, Vanachayangkul P, Lon C, Program USAMMR, National Center for Parasitology E*, et al.* (2014). Dihydroartemisinin-piperaquine failure in Cambodia. *N Engl J Med,* 371: 484-5.

294. Ross LS and Fidock DA (2019). Elucidating mechanisms of drug-resistant *Plasmodium falciparum*. *Cell Host Microbe,* 26: 35-47.

295. Uwimana A, Legrand E, Stokes BH, Ndikumana JM, Warsame M*, et al.* (2020). Emergence and clonal expansion of in vitro artemisinin-resistant Plasmodium falciparum kelch13 R561H mutant parasites in Rwanda. *Nat Med,* 26: 1602-8.

296. Venkatesan M, Gadalla NB, Stepniewska K, Dahal P, Nsanzabana C*, et al.* (2014). Polymorphisms in Plasmodium falciparum chloroquine resistance transporter and multidrug resistance 1 genes: parasite risk factors that affect treatment outcomes for P. falciparum malaria after artemether-lumefantrine and artesunate-amodiaquine. *Am J Trop Med Hyg,* 91: 833-43.

297. Veiga MI, Dhingra SK, Henrich PP, Straimer J, Gnadig N*, et al.* (2016). Globally prevalent PfMDR1 mutations modulate Plasmodium falciparum susceptibility to artemisinin-based combination therapies. *Nat Commun,* 7: 11553.

298. Cheeseman IH, Miller B, Tan JC, Tan A, Nair S*, et al.* (2016). Population Structure Shapes Copy Number Variation in Malaria Parasites. *Mol Biol Evol,* 33: 603-20.

299. Rosenthal PJ (2013). The interplay between drug resistance and fitness in malaria parasites. *Mol Microbiol,* 89: 1025-38.

300. Malaria GENPfCP (2016). Genomic epidemiology of artemisinin resistant malaria. *Elife,* 5:

301. Anderson TJ and Roper C (2005). The origins and spread of antimalarial drug resistance: lessons for policy makers. *Acta Trop,* 94: 269-80.

302. Trape JF (2001). The public health impact of chloroquine resistance in Africa. *Am J Trop Med Hyg,* 64: 12-7.

303. Woodrow CJ and White NJ (2017). The clinical impact of artemisinin resistance in Southeast Asia and the potential for future spread. *FEMS Microbiol Rev,* 41: 34-48.

304. Packard RM (2014). The origins of antimalarial-drug resistance. *N Engl J Med,* 371: 397-9.

305. Djimde AA, Doumbo OK, Traore O, Guindo AB, Kayentao K*, et al.* (2003). Clearance of drug-resistant parasites as a model for protective immunity in Plasmodium falciparum malaria. *Am J Trop Med Hyg,* 69: 558-63.

306. Ekland EH, Schneider J and Fidock DA (2011). Identifying apicoplast-targeting antimalarials using high-throughput compatible approaches. *FASEB J,* 25: 3583-93.

307. Agrawal S, Kumar S, Sehgal R, George S, Gupta R*, et al.* (2019). El-MAVEN: a fast, robust, and user-friendly mass spectrometry data processing engine for metabolomics. *Methods Mol Biol,* 1978: 301-21.

308. Chong J, Soufan O, Li C, Caraus I, Li S*, et al.* (2018). MetaboAnalyst 4.0: towards more transparent and integrative metabolomics analysis. *Nucleic Acids Res,* 46: W486-W94.

309. Ponnudurai T, Meuwissen JH, Leeuwenberg AD, Verhave JP and Lensen AH (1982). The production of mature gametocytes of Plasmodium falciparum in continuous cultures of different isolates infective to mosquitoes. *Trans R Soc Trop Med Hyg,* 76: 242-50.

310. Dhingra SK, Gabryszewski SJ, Small-Saunders JL, Yeo T, Henrich PP*, et al.* (2019). Global Spread of Mutant PfCRT and Its Pleiotropic Impact on Plasmodium falciparum Multidrug Resistance and Fitness. *mBio,* 10:

311. Le Manach C, Paquet T, Wicht K, Nchinda AT, Brunschwig C*, et al.* (2018). Antimalarial lead-optimization studies on a 2,6-Imidazopyridine series within a constrained chemical space to circumvent atypical dose-response curves against multidrug resistant parasite strains. *J Med Chem,* 61: 9371-85.

312. Nchinda AT, Le Manach C, Paquet T, Gonzalez Cabrera D, Wicht KJ*, et al.* (2018). Identification of fast-acting 2,6-disubstituted imidazopyridines that are efficacious in the *in vivo* humanized *plasmodium falciparum* NODscidIL2Rgamma (null) mouse model of malaria. *J Med Chem,* 61: 4213-27.

313. Fisher GM, Cobbold SA, Jezewski A, Carpenter EF, Arnold M*, et al.* (2020). The key glycolytic enzyme phosphofructokinase is involved in resistance to antiplasmodial glycosides. *mBio,* 11:

314. Dorjsuren D, Eastman RT, Wicht KJ, Jansen D, Talley DC*, et al.* (2021). Chemoprotective antimalarials identified through quantitative high-throughput screening of *Plasmodium* blood and liver stage parasites. *Sci Rep,* 11: 2121.

315. Manary MJ, Singhakul SS, Flannery EL, Bopp SE, Corey VC*, et al.* (2014). Identification of pathogen genomic variants through an integrated pipeline. *BMC Bioinformatics,* 15: 63.

316. Gujjar R, Marwaha A, El Mazouni F, White J, White KL*, et al.* (2009). Identification of a metabolically stable triazolopyrimidine-based dihydroorotate dehydrogenase inhibitor with antimalarial activity in mice. *J Med Chem,* 52: 1864-72.

317. Janse CJ, Ramesar J and Waters AP (2006). High-efficiency transfection and drug selection of genetically transformed blood stages of the rodent malaria parasite Plasmodium berghei. *Nat Protoc,* 1: 346-56.

318. Fidock DA, Nomura T and Wellems TE (1998). Cycloguanil and its parent compound proguanil demonstrate distinct activities against *Plasmodium falciparum* malaria parasites transformed with human dihydrofolate reductase. *Mol Pharmacol,* 54: 1140-7.

319. Adjalley SH, Lee MC and Fidock DA (2010). A method for rapid genetic integration into *Plasmodium falciparum* utilizing mycobacteriophage Bxb1 integrase. *Methods Mol Biol,* 634: 87-100.

320. Fidock DA and Wellems TE (1997). Transformation with human dihydrofolate reductase renders malaria parasites insensitive to WR99210 but does not affect the intrinsic activity of proguanil. *Proc Natl Acad Sci U S A,* 94: 10931-6.

321. Nasamu AS, Falla A, Pasaje CFA, Wall BA, Wagner JC*, et al.* (2021). An integrated platform for genome engineering and gene expression perturbation in *Plasmodium falciparum*. *Sci Rep,* 11: 342.

322. Ganesan SM, Falla A, Goldfless SJ, Nasamu AS and Niles JC (2016). Synthetic RNA-protein modules integrated with native translation mechanisms to control gene expression in malaria parasites. *Nat Commun,* 7: 10727.

323. Deitsch K, Driskill C and Wellems T (2001). Transformation of malaria parasites by the spontaneous uptake and expression of DNA from human erythrocytes. *Nucleic Acids Res,* 29: 850-3.

324. Geary TG, Divo AD, Jensen JB, Zangwill M and Ginsburg H (1990). Kinetic modelling of the response of *Plasmodium falciparum* to chloroquine and its experimental testing in vitro. Implications for mechanism of action of and resistance to the drug. *Biochem Pharmacol,* 40: 685-91.

325. Bray PG, Hawley SR and Ward SA (1996). 4-Aminoquinoline resistance of *Plasmodium falciparum*: insights from the study of amodiaquine uptake. *Mol Pharmacol,* 50: 1551-8.

326. Combrinck JM, Fong KY, Gibhard L, Smith PJ, Wright DW*, et al.* (2015). Optimization of a multi-well colorimetric assay to determine haem species in *Plasmodium falciparum* in the presence of anti-malarials. *Malar J,* 14: 253.

327. Snyder C, Chollet J, Santo-Tomas J, Scheurer C and Wittlin S (2007). In vitro and in vivo interaction of synthetic peroxide RBx11160 (OZ277) with piperaquine in *Plasmodium* models. *Exp Parasitol,* 115: 296-300.

328. Karyana M, Burdarm L, Yeung S, Kenangalem E, Wariker N*, et al.* (2008). Malaria morbidity in Papua Indonesia, an area with multidrug resistant Plasmodium vivax and Plasmodium falciparum. *Malar J,* 7: 148.

329. Russell B, Chalfein F, Prasetyorini B, Kenangalem E, Piera K*, et al.* (2008). Determinants of in vitro drug susceptibility testing of Plasmodium vivax. *Antimicrob Agents Chemother,* 52: 1040-5.

330. Marfurt J, Chalfein F, Prayoga P, Wabiser F, Kenangalem E*, et al.* (2011). Ex vivo drug susceptibility of ferroquine against chloroquine-resistant isolates of Plasmodium falciparum and P. vivax. *Antimicrob Agents Chemother,* 55: 4461-4.

331. Smilkstein M, Sriwilaijaroen N, Kelly JX, Wilairat P and Riscoe M (2004). Simple and inexpensive fluorescence-based technique for high-throughput antimalarial drug screening. *Antimicrob Agents Chemother,* 48: 1803-6.

332. Sanz LM, Crespo B, De-Cozar C, Ding XC, Llergo JL*, et al.* (2012). *P. falciparum in vitro k*illing rates allow to discriminate between different antimalarial mode-of-action. *PLoS One,* 7: e30949.

333. Angulo-Barturen I, Jimenez-Diaz MB, Mulet T, Rullas J, Herreros E*, et al.* (2008). A murine model of falciparum-malaria by in vivo selection of competent strains in non-myelodepleted mice engrafted with human erythrocytes. *PLoS One,* 3: e2252.

334. Adjalley SH, Johnston GL, Li T, Eastman RT, Ekland EH*, et al.* (2011). Quantitative assessment of *Plasmodium falciparum* sexual development reveals potent transmission-blocking activity by methylene blue. *Proc Natl Acad Sci USA,* 108: E1214-23.

335. Yoo E, Schulze CJ, Stokes BH, Onguka O, Yeo T*, et al.* (2020). The Antimalarial Natural Product Salinipostin A Identifies Essential alpha/beta Serine Hydrolases Involved in Lipid Metabolism in P. falciparum Parasites. *Cell Chem Biol,* 27: 143-57 e5.

336. Mamoun CB, Gluzman IY, Goyard S, Beverley SM and Goldberg DE (1999). A set of independent selectable markers for transfection of the human malaria parasite *Plasmodium falciparum*. *Proc Natl Acad Sci USA,* 96: 8716-20.

337. Wang P, Wang Q, Sims PF and Hyde JE (2002). Rapid positive selection of stable integrants following transfection of *Plasmodium falciparum*. *Mol Biochem Parasitol,* 123: 1-10.

338. WHO. World malaria report 2018. (World Health Organization, 2018).

339. Phillips MA, Burrows JN, Manyando C, van Huijsduijnen RH, Van Voorhis WC*, et al.* (2017). Malaria. *Nat Rev Dis Primers,* 3: 17050.

340. Miller LH, Baruch DI, Marsh K and Doumbo OK (2002). The pathogenic basis of malaria. *Nature,* 415: 673-9.

341. Menard D and Dondorp A (2017). Antimalarial drug resistance: A threat to malaria elimination. *Cold Spring Harb Perspect Med,* 7:

342. Delves MJ, Miguel-Blanco C, Matthews H, Molina I, Ruecker A*, et al.* (2018). A high throughput screen for next-generation leads targeting malaria parasite transmission. *Nat Commun,* 9: 3805.

343. Antonova-Koch Y, Meister S, Abraham M, Luth MR, Ottilie S*, et al.* (2018). Open-source discovery of chemical leads for next-generation chemoprotective antimalarials. *Science,* 362: aat9446.

344. Wu W, Herrera Z, Ebert D, Baska K, Cho SH*, et al.* (2015). A chemical rescue screen identifies a *Plasmodium falciparum* apicoplast inhibitor targeting MEP isoprenoid precursor biosynthesis. *Antimicrob Agents Chemother,* 59: 356-64.

345. Raphemot R, Lafuente-Monasterio MJ, Gamo-Benito FJ, Clardy J and Derbyshire ER (2015). Discovery of dual-stage malaria inhibitors with new targets. *Antimicrob Agents Chemother,* 60: 1430-7.

346. Okombo J and Chibale K (2017). Insights into integrated lead generation and target identification in malaria and tuberculosis drug discovery. *Acc Chem Res,* 50: 1606-16.

347. Zhang Y, Asante KS and Jung A (1986). Stage-dependent inhibition of chloroquine on Plasmodium falciparum in vitro. *J Parasitol,* 72: 830-6.

348. Jomaa H, Wiesner J, Sanderbrand S, Altincicek B, Weidemeyer C*, et al.* (1999). Inhibitors of the nonmevalonate pathway of isoprenoid biosynthesis as antimalarial drugs. *Science,* 285: 1573-6.

349. Duffy S and Avery VM (2017). *Plasmodium falciparum in vitro* continuous culture conditions: A comparison of parasite susceptibility and tolerance to anti-malarial drugs throughout the asexual intra-erythrocytic life cycle. *Int J Parasitol Drugs Drug Resist,* 7: 295-302.

350. Wilson DW, Langer C, Goodman CD, McFadden GI and Beeson JG (2013). Defining the timing of action of antimalarial drugs against *Plasmodium falciparum*. *Antimicrob Agents Chemother,* 57: 1455-67.

351. Paguio MF, Bogle KL and Roepe PD (2011). *Plasmodium falciparum* resistance to cytocidal versus cytostatic effects of chloroquine. *Mol Biochem Parasitol,* 178: 1-6.

352. Painter HJ, Morrisey JM and Vaidya AB (2010). Mitochondrial electron transport inhibition and viability of intraerythrocytic *Plasmodium falciparum*. *Antimicrob Agents Chemother,* 54: 5281-7.

353. Phillips MA, Lotharius J, Marsh K, White J, Dayan A*, et al.* (2015). A long-duration dihydroorotate dehydrogenase inhibitor (DSM265) for prevention and treatment of malaria. *Sci Transl Med,* 7: 296ra111.

354. Cassera MB, Zhang Y, Hazleton KZ and Schramm VL (2011). Purine and pyrimidine pathways as targets in *Plasmodium falciparum*. *Curr Top Med Chem,* 11: 2103-15.

355. Gomez-Lorenzo MG, Rodriguez-Alejandre A, Moliner-Cubel S, Martinez-Hoyos M, Bahamontes-Rosa N*, et al.* (2018). Functional screening of selective mitochondrial inhibitors of *Plasmodium*. *Int J Parasitol Drugs Drug Resist,* 8: 295-303.

356. Linares M, Viera S, Crespo B, Franco V, Gomez-Lorenzo MG*, et al.* (2015). Identifying rapidly parasiticidal anti-malarial drugs using a simple and reliable in vitro parasite viability fast assay. *Malar J,* 14: 441.

357. Painter HJ, Chung NC, Sebastian A, Albert I, Storey JD*, et al.* (2018). Genome-wide real-time in vivo transcriptional dynamics during *Plasmodium falciparum* blood-stage development. *Nat Commun,* 9: 2656.

358. Elliott DA, McIntosh MT, Hosgood HD, 3rd, Chen S, Zhang G*, et al.* (2008). Four distinct pathways of hemoglobin uptake in the malaria parasite Plasmodium falciparum. *Proc Natl Acad Sci U S A,* 105: 2463-8.

359. Xie SC, Dogovski C, Hanssen E, Chiu F, Yang T*, et al.* (2016). Haemoglobin degradation underpins the sensitivity of early ring stage *Plasmodium falciparum* to artemisinins. *J Cell Sci,* 129: 406-16.

360. Blank O, Davioud-Charvet E and Elhabiri M (2012). Interactions of the antimalarial drug methylene blue with methemoglobin and heme targets in *Plasmodium falciparum*: a physico-biochemical study. *Antioxid Redox Signal,* 17: 544-54.

361. Supan C, Mombo-Ngoma G, Kombila M, Ospina Salazar CL, Held J*, et al.* (2017). Phase 2a, open-label, 4-escalating-dose, randomized multicenter study evaluating the safety and activity of ferroquine (SSR97193) plus artesunate, versus amodiaquine plus artesunate, in African adult men with uncomplicated *Plasmodium falciparum* malaria. *Am J Trop Med Hyg,* 97: 514-25.

362. Isba R, Zani B, Gathu M and Sinclair D (2015). Artemisinin-naphthoquine for treating uncomplicated *Plasmodium falciparum* malaria. *Cochrane Database Syst Rev,* CD011547.

363. Chavain N, Vezin H, Dive D, Touati N, Paul JF*, et al.* (2008). Investigation of the redox behavior of ferroquine, a new antimalarial. *Mol Pharm,* 5: 710-6.

364. Dubar F, Khalife J, Brocard J, Dive D and Biot C (2008). Ferroquine, an ingenious antimalarial drug: thoughts on the mechanism of action. *Molecules,* 13: 2900-7.

365. Atamna H and Ginsburg H (1993). Origin of reactive oxygen species in erythrocytes infected with *Plasmodium falciparum*. *Mol Biochem Parasitol,* 61: 231-41.

366. Goodman CD, Buchanan HD and McFadden GI (2017). Is the mitochondrion a good malaria drug target? *Trends Parasitol,* 33: 185-93.

367. Llanos-Cuentas A, Casapia M, Chuquiyauri R, Hinojosa JC, Kerr N*, et al.* (2018). Antimalarial activity of single-dose DSM265, a novel *Plasmodium* dihydroorotate dehydrogenase inhibitor, in patients with uncomplicated *Plasmodium falciparum* or *Plasmodium vivax* malaria infection: a proof-of-concept, open-label, phase 2a study. *Lancet Infect Dis,* 18: 874-83.

368. Musset L, Le Bras J and Clain J (2007). Parallel evolution of adaptive mutations in *Plasmodium falciparum* mitochondrial DNA during atovaquone-proguanil treatment. *Mol Biol Evol,* 24: 1582-5.

369. Schalkwijk J, Allman EL, Jansen PAM, de Vries LE, Verhoef JMJ*, et al.* (2019). Antimalarial pantothenamide metabolites target acetyl-coenzyme A biosynthesis in Plasmodium falciparum. *Sci Transl Med,* 11:

370. Yoo E, Stokes BH, de Jong H, Vanaerschot M, Kumar T*, et al.* (2018). Defining the determinants of specificity of *Plasmodium* proteasome inhibitors. *J Am Chem Soc,* 140: 11424-37.

371. Conrad MD and Rosenthal PJ (2019). Antimalarial drug resistance in Africa: the calm before the storm? *Lancet Infect Dis,* 19: e338-e51.

372. Imwong M, Dhorda M, Myo Tun K, Thu AM, Phyo AP*, et al.* (2020). Molecular epidemiology of resistance to antimalarial drugs in the Greater Mekong subregion: an observational study. *Lancet Infect Dis,* 20: 1470-80.

373. Uwimana A, Legrand E, Stokes BH, Ndikumana JM, Warsame M*, et al.* (2020). Emergence and clonal expansion of *in vitro* artemisinin-resistant *Plasmodium falciparum* kelch13 R561H mutant parasites in Rwanda. *Nat Med,* 26: 1602-8.

374. Tuo Yang SO, Eva S. Istvan, Karla P. Godinez-Macias, Amanda K. Lukens, Beatriz Baragaña, Brice Campo, Chris Walpole, Jacquin C. Niles, Kelly Chibale, Koen J. Dechering, Manuel Llinás, Marcus C.S. Lee, Nobutaka Kato, Susan Wyllie, Case W. McNamara, Francisco Javier Gamo, Jeremy Burrows, David A. Fidock, Daniel E. Goldberg, Ian H. Gilbert, Dyann F. Wirth, Elizabeth A. Winzeler, the Malaria Drug Accelerator Consortium (2021). MalDA, Accelerating Malaria Drug Discovery. *Trends in Parasitology,*

375. Ng CL and Fidock DA (2019). *Plasmodium falciparum in vitro* drug resistance selections and gene editing. *Methods Mol Biol,* 2013: 123-40.

376. Brook I (1989). Inoculum effect. *Rev Infect Dis,* 11: 361-8.

377. Kim J, Tan YZ, Wicht KJ, Erramilli SK, Dhingra SK*, et al.* (2019). Structure and drug resistance of the *Plasmodium falciparum* transporter PfCRT. *Nature,* 576: 315-20.

378. Witola WH, Pessi G, El Bissati K, Reynolds JM and Mamoun CB (2006). Localization of the phosphoethanolamine methyltransferase of the human malaria parasite *Plasmodium falciparum* to the golgi apparatus. *J Biol Chem,* 281: 21305-11.

379. Elmendorf HG and Haldar K (1993). Identification and localization of ERD2 in the malaria parasite *Plasmodium falciparum*: separation from sites of sphingomyelin synthesis and implications for organization of the golgi. *EMBO J,* 12: 4763-73.

380. Stenmark H (2009). Rab GTPases as coordinators of vesicle traffic. *Nat Rev Mol Cell Biol,* 10: 513-25.

381. Howe R, Kelly M, Jimah J, Hodge D and Odom AR (2013). Isoprenoid biosynthesis inhibition disrupts Rab5 localization and food vacuolar integrity in Plasmodium falciparum. *Eukaryot Cell,* 12: 215-23.

382. Kenthirapalan S, Waters AP, Matuschewski K and Kooij TW (2016). Functional profiles of orphan membrane transporters in the life cycle of the malaria parasite. *Nat Commun,* 7: 10519.

383. Horatscheck A, Andrijevic A, Nchinda AT, Le Manach C, Paquet T*, et al.* (2020). Identification of 2,4-Disubstituted Imidazopyridines as Hemozoin Formation Inhibitors with Fast-Killing Kinetics and In Vivo Efficacy in the Plasmodium falciparum NSG Mouse Model. *J Med Chem,* 63: 13013-30.

384. Carter MD, Phelan VV, Sandlin RD, Bachmann BO and Wright DW (2010). Lipophilic mediated assays for beta-hematin inhibitors. *Comb Chem High Throughput Screen,* 13: 285-92.

385. Gluzman IY, Schlesinger PH and Krogstad DJ (1987). Inoculum effect with chloroquine and *Plasmodium falciparum*. *Antimicrob Agents Chemother,* 31: 32-6.

386. Large JM, Birchall K, Bouloc NS, Merritt AT, Smiljanic-Hurley E*, et al.* (2019). Potent bicyclic inhibitors of malarial cGMP-dependent protein kinase: approaches to combining improvements in cell potency, selectivity and structural novelty. *Bioorg Med Chem Lett,* 29: 126610.

387. Bopp S, Magistrado P, Wong W, Schaffner SF, Mukherjee A*, et al.* (2018). Plasmepsin II-III copy number accounts for bimodal piperaquine resistance among Cambodian *Plasmodium falciparum*. *Nat Commun,* 9: 1769.

388. Co EM, Dennull RA, Reinbold DD, Waters NC and Johnson JD (2009). Assessment of malaria *in vitro* drug combination screening and mixed-strain infections using the malaria Sybr green I-based fluorescence assay. *Antimicrob Agents Chemother,* 53: 2557-63.

389. Patel V, Booker M, Kramer M, Ross L, Celatka CA*, et al.* (2008). Identification and characterization of small molecule inhibitors of *Plasmodium falciparum* dihydroorotate dehydrogenase. *J Biol Chem,* 283: 35078-85.

390. Shafik SH, Cobbold SA, Barkat K, Richards SN, Lancaster NS*, et al.* (2020). The natural function of the malaria parasite's chloroquine resistance transporter. *Nat Commun,* 11: 3922.

391. Riegel B and Roepe PD (2020). Altered drug transport by *Plasmodium falciparum* chloroquine resistance transporter isoforms harboring mutations associated with piperaquine resistance. *Biochemistry,* 59: 2484-93.

392. Bray PG, Mungthin M, Ridley RG and Ward SA (1998). Access to hematin: the basis of chloroquine resistance. *Mol Pharmacol,* 54: 170-9.

393. Pease BN, Huttlin EL, Jedrychowski MP, Talevich E, Harmon J*, et al.* (2013). Global analysis of protein expression and phosphorylation of three stages of *Plasmodium falciparum* intraerythrocytic development. *J Proteome Res,* 12: 4028-45.

394. Waller KL, Muhle RA, Ursos LM, Horrocks P, Verdier-Pinard D*, et al.* (2003). Chloroquine resistance modulated in vitro by expression levels of the Plasmodium falciparum chloroquine resistance transporter. *J Biol Chem,* 278: 33593-601.

395. Zhang M, Wang C, Otto TD, Oberstaller J, Liao X*, et al.* (2018). Uncovering the essential genes of the human malaria parasite *Plasmodium falciparum* by saturation mutagenesis. *Science,* 360:

396. Borst P (2020). Looking back at multidrug resistance (MDR) research and ten mistakes to be avoided when writing about ABC transporters in MDR. *FEBS Lett,* 594: 4001-11.

397. Thomas C and Tampe R (2020). Structural and Mechanistic Principles of ABC Transporters. *Annu Rev Biochem,* 89: 605-36.

398. Katsuno K, Burrows JN, Duncan K, Hooft van Huijsduijnen R, Kaneko T*, et al.* (2015). Hit and lead criteria in drug discovery for infectious diseases of the developing world. *Nat Rev Drug Discov,* 14: 751-8.

399. Rupprecht HJ, vom Dahl J, Terres W, Seyfarth KM, Richardt G*, et al.* (2000). Cardioprotective effects of the Na(+)/H(+) exchange inhibitor cariporide in patients with acute anterior myocardial infarction undergoing direct PTCA. *Circulation,* 101: 2902-8.

400. Chen Q, Liu Y, Zhu XL, Feng F, Yang H*, et al.* (2019). Increased NHE1 expression is targeted by specific inhibitor cariporide to sensitize resistant breast cancer cells to doxorubicin in vitro and in vivo. *BMC Cancer,* 19: 211.

401. Jackson KE, Klonis N, Ferguson DJ, Adisa A, Dogovski C*, et al.* (2004). Food vacuole-associated lipid bodies and heterogeneous lipid environments in the malaria parasite, *Plasmodium falciparum*. *Mol Microbiol,* 54: 109-22.

402. Birnbaum J, Scharf S, Schmidt S, Jonscher E, Hoeijmakers WAM*, et al.* (2020). A Kelch13-defined endocytosis pathway mediates artemisinin resistance in malaria parasites. *Science,* 367: 51-9.

403. Demas AR, Sharma AI, Wong W, Early AM, Redmond S*, et al.* (2018). Mutations in Plasmodium falciparum actin-binding protein coronin confer reduced artemisinin susceptibility. *Proc Natl Acad Sci U S A,* 115: 12799-804.

404. Miliaras NB and Wendland B (2004). EH proteins: multivalent regulators of endocytosis (and other pathways). *Cell Biochem Biophys,* 41: 295-318.

405. Cowman AF, Karcz S, Galatis D and Culvenor JG (1991). A P-glycoprotein homologue of *Plasmodium falciparum* is localized on the digestive vacuole. *J Cell Biol,* 113: 1033-42.

406. Cremer G, Basco LK, Le Bras J, Camus D and Slomianny C (1995). *Plasmodium falciparum*: detection of P-glycoprotein in chloroquine-susceptible and chloroquine-resistant clones and isolates. *Exp Parasitol,* 81: 1-8.

407. Klemba M, Beatty W, Gluzman I and Goldberg DE (2004). Trafficking of plasmepsin II to the food vacuole of the malaria parasite *Plasmodium falciparum*. *J Cell Biol,* 164: 47-56.

408. Tran PN, Brown SH, Rug M, Ridgway MC, Mitchell TW*, et al.* (2016). Changes in lipid composition during sexual development of the malaria parasite *Plasmodium falciparum*. *Malar J,* 15: 73.

409. Palacpac NM, Hiramine Y, Mi-ichi F, Torii M, Kita K*, et al.* (2004). Developmental-stage-specific triacylglycerol biosynthesis, degradation and trafficking as lipid bodies in *Plasmodium falciparum*-infected erythrocytes. *J Cell Sci,* 117: 1469-80.

410. Bane KS, Lepper S, Kehrer J, Sattler JM, Singer M*, et al.* (2016). The actin filament-binding protein coronin regulates motility in *Plasmodium* sporozoites. *PLoS Pathog,* 12: e1005710.

411. Gallagher JR and Prigge ST (2010). *Plasmodium falciparum* acyl carrier protein crystal structures in disulfide-linked and reduced states and their prevalence during blood stage growth. *Proteins,* 78: 575-88.

412. Mouray E, Moutiez M, Girault S, Sergheraert C, Florent I*, et al.* (2007). Biochemical properties and cellular localization of *Plasmodium falciparum* protein disulfide isomerase. *Biochimie,* 89: 337-46.

413. Wandinger-Ness A and Zerial M (2014). Rab proteins and the compartmentalization of the endosomal system. *Cold Spring Harb Perspect Biol,* 6: a022616.

414. Stenmark H (2009). Rab GTPases as coordinators of vesicle traffic. *Nat Rev Mol Cell Biol,* 10: 513-25.

415. Witola WH, Pessi G, El Bissati K, Reynolds JM and Mamoun CB (2006). Localization of the phosphoethanolamine methyltransferase of the human malaria parasite *Plasmodium falciparum* to the Golgi apparatus. *J Biol Chem,* 281: 21305-11.

416. Lee AH and Fidock DA (2016). Evidence of a Mild Mutator Phenotype in Cambodian Plasmodium falciparum Malaria Parasites. *PLoS One,* 11: e0154166.

417. Ding H and Li D (2015). Identification of mitochondrial proteins of malaria parasite using analysis of variance. *Amino Acids,* 47: 329-33.

418. Bopp SE, Manary MJ, Bright AT, Johnston GL, Dharia NV*, et al.* (2013). Mitotic evolution of Plasmodium falciparum shows a stable core genome but recombination in antigen families. *PLoS Genet,* 9: e1003293.

419. Claessens A, Hamilton WL, Kekre M, Otto TD, Faizullabhoy A*, et al.* (2014). Generation of antigenic diversity in Plasmodium falciparum by structured rearrangement of Var genes during mitosis. *PLoS Genet,* 10: e1004812.

420. Thakur V, Asad M, Jain S, Hossain ME, Gupta A*, et al.* (2015). Eps15 homology domain containing protein of *Plasmodium falciparum* (PfEHD) associates with endocytosis and vesicular trafficking towards neutral lipid storage site. *Biochim Biophys Acta,* 1853: 2856-69.

421. Henrici RC, Edwards RL, Zoltner M, van Schalkwyk DA, Hart MN*, et al.* (2020). The *Plasmodium falciparum* artemisinin susceptibility-associated AP-2 adaptin mu subunit is clathrin independent and essential for schizont maturation. *mBio,* 11: e02918-19.

422. Jafari R, Almqvist H, Axelsson H, Ignatushchenko M, Lundback T*, et al.* (2014). The cellular thermal shift assay for evaluating drug target interactions in cells. *Nat Protoc,* 9: 2100-22.

423. Martinez Molina D, Jafari R, Ignatushchenko M, Seki T, Larsson EA*, et al.* (2013). Monitoring drug target engagement in cells and tissues using the cellular thermal shift assay. *Science,* 341: 84-7.

424. Dziekan JM, Wirjanata G, Dai L, Go KD, Yu H*, et al.* (2020). Cellular thermal shift assay for the identification of drug-target interactions in the Plasmodium falciparum proteome. *Nat Protoc,* 15: 1881-921.

425. Pantoliano MW, Petrella EC, Kwasnoski JD, Lobanov VS, Myslik J*, et al.* (2001). High-density miniaturized thermal shift assays as a general strategy for drug discovery. *J Biomol Screen,* 6: 429-40.